Investigation of an Intraoral Scanner and Analysis Workflows for Measuring Surface Loss on Planar and Freeform Surfaces in vitro

Charalambous, Polyvios

Awarding institution:
King's College London

Investigation of an Intraoral Scanner and Analysis Workflows for Measuring Surface Loss on Planar and Freeform Surfaces *in vitro*

Thesis submitted for the degree of Doctor of Philosophy (PhD)

Polyvios Charalambous

BDS MFDS RCPS (Glasg)

KING'S COLLEGE LONDON

FACULTY OF DENTISTRY, ORAL AND CRANIOFACIAL SCIENCES

Centre for Oral, Clinical and Translational Sciences

London SE1 9RT

November 2022

Abstract

Objective – The aim of this thesis was to determine the accuracy and measurement thresholds of an intraoral scanner, IOS-TD (True Definition, Midmark Corp., Ohio, USA) for measuring surface change on planar and freeform surfaces such as seen in polished and natural enamel.

Methods – The IOS-TD's accuracy for measuring a groove on polished enamel was investigated using two handling techniques (handheld Vs jig-guided scanning) at different surface-to-camera distances (3, 4, 5, and 7 mm), and its titanium dioxide scanning powder was characterised. Thereafter, the IOS-TD was tested for measuring *Sq* roughness on flat textured surfaces (*Sq* range: 1.2 – 269.0 µm) and for measuring step heights and XY areas of grooves (0.0 - 86.5 µm depth range) on polished enamel, as well as surface skewness and kurtosis. Moreover, two techniques (surface-subtraction and surface-registration) were compared to the gold standard single-scan analysis for measuring enamel grooves (2 - 19 µm depth). Consequently, the errors of four bi-scan analyses were investigated, namely: best-fit surface-registration (BF-Reg), reference-based surface-registration (Ref-Reg), a combination of best-fit surface-registration and surface-subtraction (BF-Sub) and reference-based surface registration and surface subtraction (Ref-Sub), using freeform softgauges with craters of known depths. Using the Ref-Sub analysis thereafter, step height and XY areas of craters (11 – 81 µm depth) on natural enamel were measured by the IOS-TD. Finally, the effect of different scan sizes (cusp/tooth/sextant/quadrant/full-arch) on the accuracy of the IOS-TD for measuring different crater depths was investigated. Throughout the thesis, the IOS-TD measurements were compared to a gold standard non-contacting laser profilometer, NCLP (TaiCaan Technologies™, XYRIS 2000CL, UK).

Results – No statistically significant differences were observed between handheld and jig-guided scanning at any surface-to-camera distances 3-, 4-, 5-, and 7-mm (p=0.8946-0.9999). Scanning

powder application increased surface roughness significantly ($p<0.0001$); however, the change in surface form was < 1 µm. The IOS-TD demonstrated significantly different roughness measurements than the NCLP ($p<0.0001$). It also demonstrated significant XY area measurement differences compared to NCLP below 44 µm ($p<0.05$). Enamel groove depths ≥ 44 µm were reliably measured by the IOS-TD whilst no significant differences were observed compared to NCLP for step heights and XY area measurements above this depth. The bi-scan surface subtraction and single-scan analyses were not statistically different; whilst the bi-scan surface-registration analysis resulted in significant overestimation ($p=0.0001 – 0.0119$) of groove depths. The methods of BF-Sub and Ref-Sub resulted in a significant reduction of errors, achieving 0.0 to -0.3% error, compared to -29.7 – -32.5% for the BF-Reg and -2.4 – -3.6 % for the Ref-Reg ($p < 0.0001$). Using the Ref-Reg, the IOS-TD measurements were significantly different than the NCLP for crater depths below 73 µm ($p=0.0001$-0.0005), whilst above this threshold the IOS-TD could reliably measure all craters. Finally, the highest accuracy (±5% error) was observed using scan sizes restricted to single teeth, even at the smallest crater depth of 83 µm. This decreased significantly ($p<0.0001$) as the scan size increased to a sextant, quadrant and full-arch. Using full-arch scanning, the accuracy plateaued to approximately 10-12% underestimation for crater depths ≥195µm.

Conclusions – This thesis demonstrated the accuracy, thresholds and limitations of the IOS-TD in combination with software analysis workflows for measuring change on planar and freeform surfaces. The limitations are linked to the scanner's lower spatial resolution and propagation of image-stitching errors as well as errors arising during surface alignment. The findings showed potential for intraoral scanners to measure surface loss in the order of ≥ 80 µm when using datasets of single-teeth. However, the accuracy decreased using full arch scanning even up to depths ≤195µm. Further research is needed to optimise the resolution and accuracy of intraoral scanners and software workflows.

Acknowledgements

Undertaking this doctoral studentship at King's College London has been one of the most unforgettable experiences in my life. I have been blessed with the friendship of many wonderful people, whose assistance and encouragement have helped me keep going until the very end. I am very grateful to all those people, the unsung heroes of this thesis, who have given me so much of their time, love, and energy.

First and foremost, I would like to thank my dearest parents, Anastasia and Panayiotis, as well as my siblings, Maria and Michalis, without whom I would not have started, continued, or finished this PhD. Their unconditional love and guidance have defined me as a person and have always helped me endure difficult moments in life. This work is dedicated to them.

I would like to thank my esteemed supervisor and research mentor, Professor David Bartlett, for his invaluable supervision and tutelage during the course of the last four years. Your persistent energy and leadership have been inspirational and helped me become a better researcher.

I am also forever grateful to, Dr. Rupert Austin, who has not only been my supervisor but also a dear friend. You have showed trust in me and allowed me to flourish as a young scientist; whilst your ability to combine work and fun has made this a truly enjoyable journey. I am immensely proud to have been your first PhD student, acting as a co-first supervisor.

To my industrial supervisor, Dr. Jon Creeth, thank you ever so much for the continuous support, offering an added valuable perspective to my research. My gratitude extends to GSK and the Medical Research Council for financially supporting this endeavour.

I would like to thank Dr. Tom Bull whose profound understanding in surface metrology has provided a level of insight that has been invaluable for this process.

Mrs Fiona Warburton for her statistical training and sound advice throughout the course, always making herself available when needed.

Professor Owen Addison, Dr. Saoirse O'Toole, and Dr. Petros Mylonas for their friendly chats, brainstorms, and advice. To the rest of the tooth wear team for being such a great company and making this journey worthwhile.

To Mr. Peter Pilecki whose insight of the laboratory armamentarium and equipment has made life a lot more practical.

To my close friends, near and afar, for making life so special and meaningful, and never stopping believing in me.

Declarations

Professor David Bartlett and Dr Rupert Austin contributed to the design, analysis, and discussion of all Chapters within this thesis.

Dr Tom Bull contributed to the design, analysis, and discussion of Chapter 3 and Dr. Saoirse O'Toole contributed to the design and discussion of Chapters 3 and 5.

I am grateful for the collaborative help and support received in this Thesis.

I herewith certify that all material in this dissertation which is not my own work has been properly acknowledged and cited accordingly.

Polyvios Charalambous

06 June 2023~~29 April 2023~~

Publications and Presentations

Listed below are the publications, presentations, and prizes obtained as a result of the work conducted during the PhD.

Publications [peer-reviewed research papers]:

1. **Charalambous, P**., O'Toole, S., Austin, R., & Bartlett, D. (2022). The threshold of an intra oral scanner to measure lesion depth on natural unpolished teeth. Dental Materials, 38(8), 1354–1361. https://doi.org/10.1016/j.dental.2022.06.022
2. **Charalambous, P**., Saoirse, O., Thomas, B., Bartlett, D., & Austin, R. (2021). The measurement threshold and limitations of an intra-oral scanner on polished human enamel. Dental Materials, 1–7. https://doi.org/10.1016/j.dental.2021.01.006
3. O'Toole, S., **Charalambous, P**., Almatrafi, A., Mukar, S., Elsharkawy, S., & Bartlett, D. (2021). Progress and limitations of current surface registration methods when measuring natural enamel wear. Journal of Dentistry, 112, 103738. https://doi.org/10.1016/j.jdent.2021.103738

Media Publications:

1. **Charalambous, P**. (2021). Intra-oral scanners for tooth wear quantification. Surface Newsletter, Summer, 4–5.

Presentations:

1. International Association of Dental Research (IADR), Marseille, France (2022). Depth measuring accuracy of a Cusp-to-Arch intraoral scanning workflow. Oral presentation. First author.

2. British Society of Dental Research (BSODR), Birmingham, United Kingdom (2021). High-precision surface metrology of sub-80 µm enamel lesions using intraoral scanning. Oral presentation. First author.
3. British Society of Dental Research (BSODR), Birmingham, United Kingdom (2021). Analysing early wear lesions on curved surfaces using novel methods. Poster presentation. Co-author
4. British Society of Dental Research (BSODR), Leeds, United Kingdom (2019). Preliminary results of intraoral scanning in measuring tooth wear. Poster presentation. First author

Contents

List of Figures

List of Tables

Chapter 1 Literature review

1.1 Scope and delimitations of this thesis

This thesis was originally intended to investigate the measurement threshold of a clinical intraoral scanner for measuring erosive tooth wear (ETW). Through experimentation, it was determined that the performance and limitations of the intraoral scanner prohibited it from characterising early ETW i.e., any loss of tooth tissue below 5 µm (Mylonas et al., 2018). Furthermore, for ease of experimentation the *in vitro* modelling used throughout this thesis was conducted using different surface substrates with simulated bulk surface loss. As such, although measuring and monitoring erosive tooth wear is the underlying aim for the future, it is beyond the scope of this thesis's experiments to investigate the mechanisms of progression and histopathology of ETW. Instead, it aims to explore surface metrology using gold standard devices and analysis techniques in relation to ETW and the potential use of intraoral scanning technologies for *in vivo* wear measurements.

1.2 Erosive Tooth wear

1.2.1 Definitions

Tooth wear is defined as the cumulative surface loss of mineralised dental tissue as a result of chemo-physical processes (Schlueter et al., 2020). It has a multi-factorial complex aetiology which can be categorised into three main processes: erosion, attrition, and abrasion. Dental erosion is the chemical dissolution and loss of mineralised tooth tissue by exposure to acids of non-bacterial origin from extrinsic or intrinsic sources (Lussi and Ganss, 2014), whilst dental attrition and abrasion are the physical loss of mineralised tooth tissue caused by tooth-to-tooth and tooth-to-foreign-body contacts, respectively (Schlueter et al., 2020). These processes often occur simultaneously making it difficult to distinguish between each aetiology. The importance of erosion has become

increasingly recognised as it is rare for tooth wear to occur without erosion as the primary aetiological factor; therefore, there has been a recent move towards using the term 'erosive tooth wear' (Bartlett, 2016), which is the preferred term which will be used throughout this thesis.

Erosive tooth wear (ETW) occurs as an underlying natural process during life; indeed, anthropological schools of thought have considered it a normal physiological phenomenon due to abrasive wear from diets (Kaidonis, 2008). Currently, there is a shift towards classifying ETW pathological in nature. ETW is believed to have active phases in the presence of risk factors resulting in unacceptable (pathological) levels of ETW (Bartlett and Dugmore, 2008). Several studies have shown relatively low progression rates in patients with physiological ETW, with reported annual height losses between 11 and 29 µm (Lambrechts et al., 1989; Pintado et al., 1997). In patients with advanced ETW or existing parafunctional habits, progression rates can be much higher, between 73 and 140 µm per year (Ahmed et al., 2017; Bartlett et al., 1997).

It is important to be able to distinguish between these physiological and pathological states of ETW as this would determine whether to intervene or not. Smith and Knight (1984) proposed to discriminate between physiological and pathological wear based on loss of function, serious aesthetic deterioration and longevity of teeth. Pain can be another major consideration for determining the pathological nature of ETW as dentine hypersensitivity and pulpal complications can be observed in ETW cases (Ganss and Lussi, 2014).

1.2.2 Prevalence of ETW

Epidemiological data suggests that ETW is a common oral condition with an increasing prevalence over the last decades; therefore, it is imperative to identify early erosive changes to improve diagnosis, prevention and patient outcomes (Bartlett, 2016; Van't Spijker et al., 2009). According to an epidemiological study, nearly a third of European young adults presented with moderate (26.1%)

or severe (3.3%) ETW (Bartlett et al., 2013). It was also shown that the prevalence of ETW is higher in the UK compared to six other European countries (Bartlett et al., 2013); this may be attributed to wider developments such as changes in our diet and increased consumption of acidic foods and beverages (O'Toole and Mullan, 2018). Furthermore, it has been estimated that the percentage of adults with severe ETW increases from 3% at 20 years to 17% at 70 years of age, signifying the cumulative nature of ETW damage with age (Van't Spijker et al., 2009). The Adult Dental Health Survey in 2009 suggested that 77% of dentate adults experienced ETW in their anterior teeth consistent with ageing; however, 15% showed moderate and 2% severe wear that extended as far as secondary dentine. Additionally, it was observed that compared to the previous survey in 1998 the proportion of adults with moderate ETW increased from 11% to 15%; highlighting the increasing prevalence and the urgent need for early clinical diagnosis and monitoring (White et al., 2012).

ETW is not only a concern for adults but can also affect younger populations. A systematic review investigating its prevalence in permanent teeth of children and adolescents across the globe estimated it to be 30.4% (95% CI: 23.8% – 37.0%) (Salas et al., 2015). More recently, a systematic review and meta-analysis estimated the overall prevalence of dental erosion among preschool children below 7 years old to be 39.64% (95% CI: 27.62%, 51.65%) worldwide and that children with a higher frequency of consumption of soft drinks and fruit juices presented with more severe ETW (Yip et al., 2022).

1.2.3 Structure of human enamel

Human enamel is the outer layer of teeth and the hardest biological tissue. It is a non-vital densely packed mineralised structure, primarily consisting of calcium (Ca^{2+}) and phosphate (PO_4^{3-}) in the form of calcium hydroxyapatite $Ca_{10}(PO_4)_6(OH)_2$. Although its exact composition differs slightly among different people, types of teeth, and areas of teeth; generally, enamel consists of 95% w/w

calcium hydroxyapatite, 4% w/w water, and 1% w/w organic matrix (i.e., lipids and proteins) (Beniash et al., 2019; Ganss et al., 2014).

Enamel has a hierarchical ultrastructure with an intricate organisation of prisms, each approximately 3 – 6 μm in diameter, separated by a thin organic prism sheath and by an interprismatic area (Berkovitz et al., 2009; Cui and Ge, 2007; Cuy et al., 2002). These enamel prisms form the building block of enamel which themselves are made of millions of hydroxyapatite hexagonal crystallites assembled into a thin rod or prism formation. These crystallites forming the prisms are about 50 - 70 nm in height, 20 - 25 nm width and of great length, generally extending across the full thickness of the enamel tissue. The cores of the crystallites differ slightly in composition from the periphery which contains more magnesium and carbonate making them more soluble (Berkovitz et al., 2009). The orientation of the crystallites is not entirely uniform with the greatest variation seen at the occlusal surface which makes it stronger and more durable (Al-Jawad et al., 2007). The orientation and alignment of prisms also varies in different regions of enamel. At the dentino-enamel junction (DEJ), the prisms have a random orientation, in outer enamel the prisms run longitudinally and emerge perpendicular to the occlusal plane, whilst in cusps the prisms cross between each other creating decussation patterns (Berkovitz et al., 2009; Raue et al., 2012; West and Joiner, 2014)

The concentration of minerals varies according to the distance from the DEJ. Moving from the DEJ towards the outer layers of enamel, the concentration of calcium, fluoride and phosphate increases reaching the highest concentration in the outermost layers whilst the concentration of impurities such as carbonate and magnesium decreases (Berkovitz et al., 2009).

The chemical composition and hierarchical organisation of prisms determine the physicochemical properties of enamel (West and Joiner, 2014). Surface enamel is considered the most significant region as it is here that the tooth is in direct contact with the oral environment. It is markedly harder,

less porous and less soluble than subsurface enamel (Berkovitz et al., 2009). Indeed, previous studies have shown that surface enamel is more resistant to erosive ETW than enamel which has the outer surface polished down (Francesca Mullan et al., 2017; Zheng et al., 2010).

Surface enamel features a variable appearance, exhibiting topographies such as perikymata grooves and ridges, prism-end markings, cracks, pits, and elevations. It also contains areas which appear devoid of prisms (aprismatic enamel) as the junctions and orientation of prisms is often highly complex that is difficult to observe a clear prism structure (Whittaker, 1982). The complex nature of outer enamel topography makes it more difficult for characterisation and measurement of surface changes caused by ETW. Additionally, the optical properties of outer enamel in terms of light scattering and absorption differ throughout its surface which complicate its assessment with optical instruments (Darling et al., 2006). Therefore, most *in vitro* experimentation has been based on polished flat enamel samples by removing the natural outer layer which makes wear lesions more uniform and identifiable. However, to fully understand and optimise the measurement of enamel wear it is preferable for investigations to be carried out on natural unpolished enamel as it is considered more clinically relevant.

1.2.4 Chemical and histopathological mechanisms of erosive tooth wear

ETW is typically initiated by erosive dissolution of enamel. Whilst enamel is highly resistant to physiological oral impacts, being exposed to an acidic environment, results in hydroxyapatite demineralisation and alteration of its physical and chemical characteristics, a process known as ‘softening' (Shellis and Addy, 2014). Short-duration acid attacks may result in the formation of a softened enamel layer, varying between 0.2 and 5 µm in thickness (Lussi et al., 2011). This partial loss of surface minerals, such as calcium, phosphate and fluoride, results in decreased microhardness and increased surface roughness, leaving the tissue susceptible to mechanical wear

(Cheng et al., 2009). Eisenburger et al., (2001) have previously demonstrated the weakness of this softened layer by performing 5 secs of ultrasonication which led to the removal of this layer and to further enamel loss. This process can be modified according to the type of acid, duration of exposure, and saliva quality (Eisenburger and Addy, 2002; Hughes et al., 2000). Repeated erosive attacks will lead to irreversible bulk tissue loss (Shellis and Addy, 2014) which can be accentuated in the presence of attritive and abrasive factors (Voronets and Lussi, 2010).

During the erosive challenge, there is a continuous exchange of calcium, phosphate and hydroxide ions between the enamel surface and saliva. When saliva becomes saturated, with a higher concentration of calcium and phosphate ions than enamel, remineralisation starts occurring on the enamel surface; however, the opposite occurs if saliva is undersaturated leading to a higher rate of demineralisation (Shellis et al., 2014).

In the case of caries, enamel has been described to have a critical pH 5.5 – 5.7 i.e., the pH of the plaque acidic solution surrounding the enamel below which demineralisation occurs. However, there is no fixed critical pH associated with dental erosion as this will vary according to the type of erosive solution, its concentration of calcium, phosphate and fluoride ions, and flow characteristics (Lussi and Ganss, 2014; West and Joiner, 2014).

1.2.5 The signs and symptoms of ETW

Signs of ETW include cupping or dished out lesions on the occlusal surfaces of molars and premolars or anterior teeth appearing translucent (shining through) due to thinning of enamel or darker due to exposed dentine. Anterior teeth may chip or fracture, and restorations may stand proud from the surrounding tooth surface (Hemmings et al., 2018). Attritional wear is characterised by flattening of the cusp tips and incisal edges of teeth that inter-digitate during static and dynamic occlusions (Hemmings et al., 2018). Abrasion presents itself as lesions with a shape pattern fitting the shape of

the object causing the wear and is usually seen on the incisors, canine and premolars (Hemmings et al., 2018).

Patients may be unaware of the presence of ETW, especially in the early stages; however, at later stages they can often complain of unsatisfactory aesthetics attributed to the changing shape, optical properties, and colour of their teeth (Hemmings et al., 2018). ETW has also been associated with dentine hypersensitivity as erosive challenges can remove the smear layer on the teeth's exposed dentine surface, opening the dentinal tubules (West et al., 2013). At more advanced stages, ETW can cause mobility of teeth, impaired function or even lead to loss of teeth. Pathological attrition resulting from clenching or bruxism habits, might affect the temporomandibular joints and result in temporomandibular disorders (Van't Spijker et al., 2009).

The clinical diagnosis of ETW is still derived from a visual examination (Hemmings et al., 2018; Lussi and Ganss, 2014); as such, early surface changes are very difficult to detect with the naked eye. Considering the possible effects of pathological ETW, a treatment plan should be sought at the moment of diagnosis. However, it not easy to discriminate between physiological and pathological ETW due to the variety in clinical appearances and the range in symptoms that patient report. Additionally, the rate of ETW over time would need to be established, for dentists to have an indication as to monitor or treat severe cases (Van't Spijker et al., 2009).

1.2.6 Clinical recording of ETW

There is a continuous clinical and scientific drive to be able to measure ETW and monitor its progression. Determining the rate of wear can help the clinician decide when and how to restore the teeth (Carvalho et al., 2015).

Several qualitative means for measuring ETW have been developed and reported in the literature. Currently, ETW indices, study casts, and photography are used to monitor ETW in the clinical setting; however, each method comes with their own inherent limitations.

1.2.6.1 Tooth wear indices

A review of the literature carried out by López-Frías et al., (2012) revealed an array of ETW indices that were developed for both clinical and research use. These are tools that utilise a grading or scoring system designed to identify increasing severity or progression of ETW. Some of the most popular indices include the tooth wear index, TWI (Smith and Knight, 1984), the Eccles Index (Eccles, 1979) and the simpler and increasingly adopted Basic Erosive Wear Examination (BEWE) (Bartlett et al., 2008). This plethora of indices offers little standardisation among different international working groups, making it difficult to compare data. Furthermore, these indices traditionally concentrate on a single aetiological factor, on different surfaces, or use different terminologies which generates further confusion (Lopez-Frias et al., 2012).

Measuring ETW *in vivo* is difficult as there is no natural baseline surface that can reliably remain unaffected from wear factors and act as a reference between periodic assessments. In most cases, the severity of ETW is determined based on visual inspection and recorded numerically. Indices have low sensitivity to small surface changes, are highly subjective (Mehta et al., 2012), and can lead to dissimilar opinions among clinicians (Hemmings et al., 2018).

1.2.6.2 Articulated study casts

Sequential study casts at approximately 6-12 monthly intervals are helpful in observing three-dimensional morphological changes in teeth (Mehta et al., 2012). The assessment of ETW can be performed repeatedly, under optimal conditions, outside the mouth, without time pressure (Ganss et al., 2001). They are also excellent for examining the occlusal surfaces of anterior teeth and their

occlusal relationship (Johansson et al., 1996). However, the difficulty in assessing ETW on study casts without the advantage of direct clinical observation remains an issue (Bartlett, 2003). The optical properties of enamel (Ganss et al., 2001) and the extent of dentine exposure (Bartlett, 2003) cannot be assessed on study casts, losing valuable information. Furthermore, dimensional changes of impression materials (Kim et al., 2001) and dental stones (Heshmati et al., 2002) contribute to measurement uncertainty.

1.2.6.3 Clinical photographs

Periodic high quality clinical photographs can also be used in monitoring ETW; however, similarly to study casts, photographs are not very sensitive and are subject to each clinician's interpretation (Mehta et al., 2012). In addition, the difficulty in achieving the same effects of camera angle and lightning on the tooth surfaces each time make it less repeatable and reproducible method.

1.3 Surface metrology

1.3.1 Terminology of surface metrology

According to the Oxford English Dictionary, (2022), a surface is defined as 'the outermost part of a solid object considered with respect to its form, texture, or extent'. ISO 17450-1 (2011) differentiates between a real surface as the "set of features which physically exist and separate the entire workpiece from the surrounding medium" and the model surface as the "model representing the set of physical limits of the virtual or the real workpiece". The measurement of the real surface of a material can be recorded by application of different techniques using physical phenomena such as mechanical contact, electromagnetic reflection/transmission (See Section 1.3.3 below) among others; therefore, a surface is a property that can have different values depending on the type of measurement technique and the applied scale.

In precision engineering and manufacturing, control of the areal nature of the surface allows the manufacturer to alter the tribological, biological, fluidic and many other properties of manufactured components. For example, control of surface texture is important for surface structuring to facilitate binding of biological molecules or for surfaces of microfluidic channels for flow control (Leach, 2014). Surface measurement and characterisation are critical elements for quality control, diagnosis and monitoring during the manufacturing process as well as predicting a manufactured component's functional properties in order to prevent engineering component failures that can be explained through tribological (wear, lubrication, and friction) mechanisms (Leach, 2014; Zheng et al., 2022). In dental research, this knowledge can be applied for various purposes such as investigating interacting surfaces among teeth, restorative materials, implants in the presence of saliva, food slurry and other external lubricants (Zheng et al., 2022); comparing surface textures (Field et al., 2010) and measuring bulk enamel and dentine tissue loss due to wear (Almohefer et al., 2021; Paepegaey et al., 2013).

A surface profile measurement is defined as the measurement of line across the surface that can be represented mathematically as a height function in the Z axis, with lateral displacement, in the X or Y axes (Leach, 2014). A single 2D profile provides limited information about the investigated surface. Instead, multiple profile measurements can be measured and juxtaposed using software to generate a three-dimensional (3D) areal topography which would have far more bearing on the function and properties of the surface being investigated (Leach, 2014).

Understanding the measuring capability of the equipment enables the operator to better understand the value of the results. Accuracy is defined by a combination of two necessary and complimentary elements: trueness and precision (ISO, 1994). In metrology, accuracy is defined as the "closeness of agreement between a measured quantity value and a true quantity value of a

measurand", trueness as the "closeness of agreement between the average of an infinite number of replicate measured quantity values and a reference quantity value", and precision as the "closeness of agreement between indications or measured quantity values obtained by replicate measurements on the same or similar objects under specified conditions" (JCGM, 2012). A system can have a bias i.e., poor accuracy but good precision, which can be corrected by calibrating the device. An accurate system with poor precision can also exist, in which case the mean of multiple measurements can be taken (DeLong, 2006). Ideally, both trueness and precision should be high.

Resolution is the smallest change in a measured quantity that causes a perceptible change in the corresponding indication (JCGM, 2012). For example, the spatial resolution of a non-contacting laser profilometer (NCLP) would be the minimum distance between two adjacent features on a surface that can be differentiated (Leach, 2011). This is determined by the NCLP sensor, the step over distance (X, Y axis), and the sensor spot size (Boltryk et al., 2008; F. Mullan et al., 2017). Discrimination threshold of a measuring system is the largest change in a value of quantity being measured that causes no detectable change in the corresponding indication; the sensitivity of the instrument which is the smallest absolute amount of change that can be detected should be above the discrimination threshold. The noise floor (i.e., the sum of all unwanted signals) of a measurement system is a combination of the instrument's internal noise (instability in the instrument electronics); environmental noise (temperature, floor vibrations) and the noise of the X and Y drive units in the measurement along the Z-axis when scanning (Leach, 2014).

1.3.2 Surface topography characterisation

A surface can be represented as a superimposition of different geometrical structures with different scales or wavelengths, from a large-scale component to a small-scale one. For example, the surface of a road is made up of features of many different wavelengths, ranging from the large hills and

valleys (long wavelengths) to the texture of the gravel and asphalt (short wavelengths). These components composing a surface are differentiated into form, waviness and roughness (DigitalSurf, 2022a). Form has a large scale and represents the underlying shape of the surface. In dentistry, It is used for measurement of wear of dental tissues and materials measurements which will be described further below. Waviness is an intermediate-scale texture component, whilst roughness has a small scale and represents the fine structure of the surface and texture (Figure 1-1) (Leach, 2013).

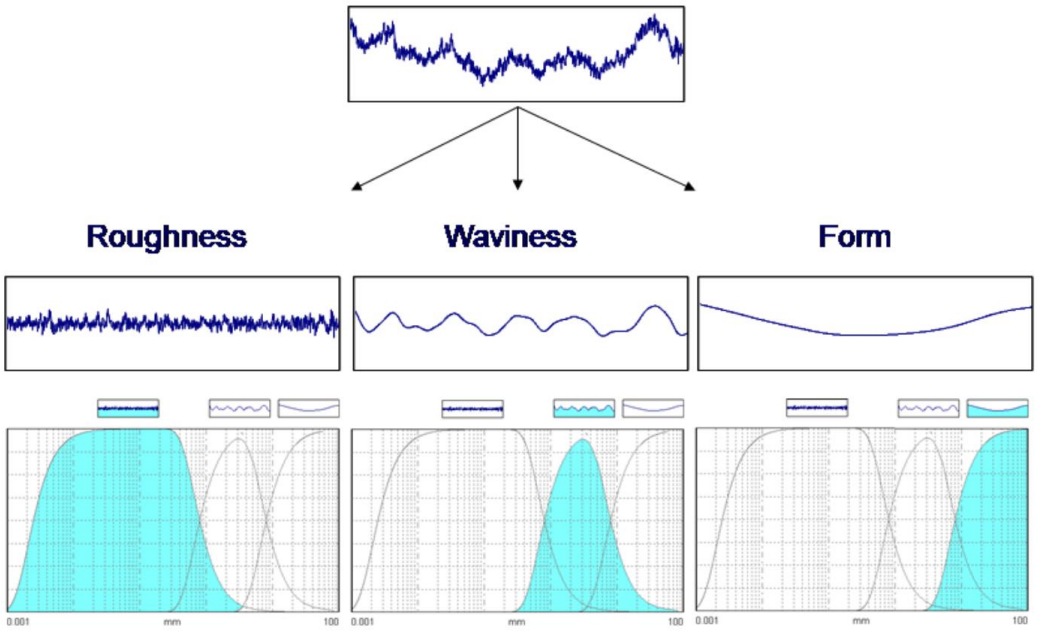

Figure 1-1 – The topography of a surface profile consisting of three components (form, waviness, and roughness).

Filters select (or reject) structure, according to their scale in the X axis, in order to separate long-scale components from short-scale components within the extracted profile (the digital form generated from a surface measuring instrument) which are judged to be of significance in a particular situation. Removing the form is fundamental for analysing surface texture which is considered the 'fingerprint' of a surface. A low-pass filter preserves (allows to pass) the lowest frequencies (retains the longer wavelengths) and therefore is applied to remove the shortest

wavelength components which usually signal the presence of noise and should not be considered for a roughness measurement. The result of low-pass filtering on a measured profile is called the primary profile. A high-pass filter preserves the high frequency features (retains the shorter wavelengths) while rejecting the longer ones to create surface roughness. A band-pass filter (combination of a low-pass and high-pass filter) is applied to create the surface waviness (DigitalSurf, 2022a; Leach, 2014, 2013).

A filter is defined by two things, a cutoff wavelength and a filter type. The cutoff wavelength defines the intersection between long and short wavelengths and can be described as the 'amount of smoothing'. Figure 1-2 shows the impact of the cutoff wavelength selection of filters on a primary profile (DigitalMetrology, 2019). A 0.8 mm cutoff separates a waviness profile with many peaks and valleys and a roughness profile. On the other hand, an 8.0 mm cutoff creates a smoother waviness profile and what remains is an increased roughness profile. The filter type defines the way the smoothing occurs. One of the most common filters is the Gaussian filter which is based on the weighted moving average that runs through the primary profile, accounting for any outliers, to create a smoother one (DigitalMetrology, 2019; Leach, 2013).

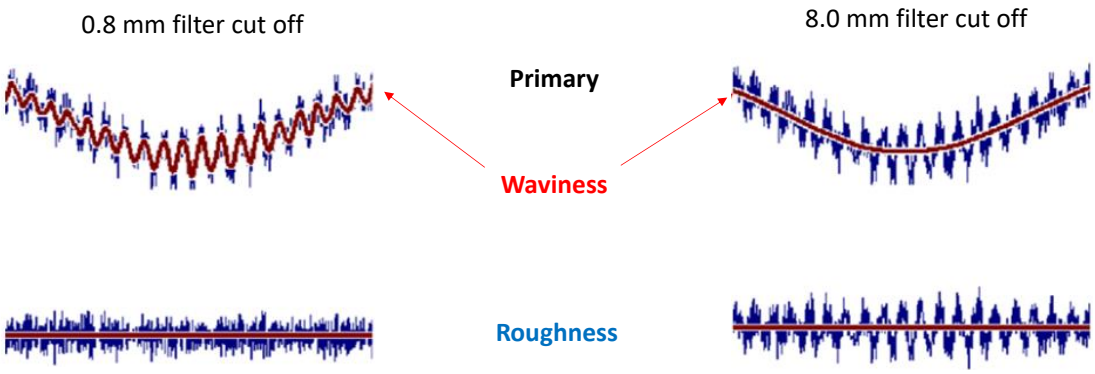

Figure 1-2 – The impact of the cutoff wavelength selection of filters (adapted from DigitalMetrology, 2019).

1.3.3 Surface profilometry

Surface profilometry is a technique that measures the vertical displacement across a surface of material by traversing a physical or light-based stylus across a line on the surface to produce a 2D topographical measurement, i.e., a surface profile (Leach, 2014). By accumulating vertical displacement data as a height function, together with its XY lateral displacement $Z(x)$ for a series of juxta-positioned profiles, it is possible to analyse the 3D areal surface topography and characterise its surface texture features (Leach, 2013). Surface profilometers can be divided into two categories, according to the type of stylus being used; contact and non-contact (optical) profilometers which will be described in further detail below. These techniques have been utilised in several applications within dental research such as characterisation of tooth tissue and restorative material surfaces *in vitro* (Beleidy and Ziada, 2022; Özkan Karaca and Tunar, 2021; Saleeva et al., 2022); this literature review will concentrate on its applications in evaluating ETW.

1.3.3.1 Contact Profilometry

Contact profilometry utilises a diamond or metal stylus in direct contact with the sample surface to capture data. The stylus tip diameter usually ranges between 1.5 - 20 µm and the loading force can vary between 0.05 - 100 mg; however, styli tips of varying geometry have been developed for specialist applications such as determination of tribological characteristics including friction, rheology and wear. (Barbour and Rees, 2004; Field et al., 2010; Lu et al., 2022). As the stylus is dragged across the surface at a constant speed, the vertical displacement of the stylus is converted into an electrical signal by a transducer which is then used for 2D and 3D measurements.

There are many potential sources of measurement error from contacting surface profilometry which may also apply for optical profilometers described in Section 1.3.3.2 below. These are derived from environmental factors such as temperature, air pressure, mechanical vibrations and humidity;

software factors such as parameter definitions, filters and reference plane; object factors such as fixturing, relocation, deformation, cleanliness; instrument/hardware factors such as friction, electronic noise, quantisation, filters, zero-point drift, Abbe-offset, resolution, sensitivity, and tracking error and finally stylus errors such as hysteresis, shape, damage, load, wear and tip size (Leach, 2014; Leach et al., 2008).

Owing to their finite shape, styli may not be able to penetrate intro valleys smaller than their diameter resulting in a distorted or filtered measure of the surface (Figure 1-3~~Figure 1-3~~) (Field et al., 2010; Leach, 2014). The lateral resolution (shortest wavelength) of a stylus instrument, λ, of a sinusoidal profile where the stylus can reach the bottom of the surface can be defined by the equation $\lambda = 2\pi\sqrt{\alpha r}$, where α is the amplitude of the surface and r is the radius of the stylus tip. Its axial (height resolution) is determined by the noise floor of the instrument (Leach, 2014). For smooth surfaces, contact profilometers can have vertical resolution as low as 0.1 nm and up to 1 nm for rough surfaces or large steps (Field et al., 2010).

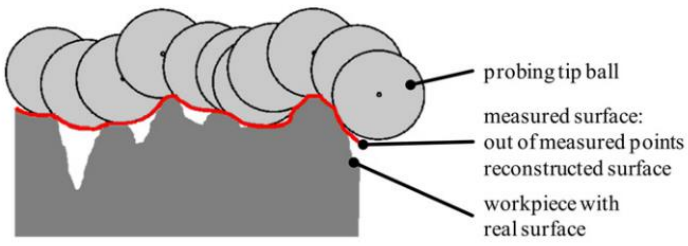

Figure 1-3 – Contact profilometry on a mechanical surface to produce a 2D profile topography.
A physical stylus modelled as a ball of finite diameter, defining the mechanical surface of the sample by moving across the real surface of the sample (adapted from R. Leach et al., 2014).

If the force is too high, the stylus can cause damage to the surface being measured. On the other hand, smaller forces limit the measurement speed due to the risk of 'stylus flight' (Leach, 2014). Paepegaey et al., (2013) showed that the stylus used in contact profilometers was able to penetrate and damage the fragile softened layer of eroded enamel and thus it should be avoided when

investigating ETW, especially when *in vitro* longitudinal assessments are required. Another drawback of contact profilometry is the length of time required to take a measurement when 3D areal scanning is required (Leach, 2014), which is an area that optical instruments may offer an advantage over contact profilometry. Furthermore, the drag of the stylus in contact profilometers may lead to surface contamination (Boltryk et al., 2008).

1.3.3.2 Non-contacting laser profilometry

Similar to the operation of contact profilometry, non-contacting laser profilometers (NCLP), or also known as optical profilometers, measure surface topography by physically scanning a light spot across a surface and taking a point of measurement at set intervals in the X axis (usually 5 - 50 µm step over distance), in a raster or rectilinear pattern to create a 3D surface topography (F. Mullan et al., 2017; J.M. Rodriguez et al., 2012). This optical stylus (beam) is typically below 100 µm in spot diameter (Rodriguez et al., 2009), and can be in the form of a polychromatic (white) or monochromatic light source. The sensor of the NCLP captures information from the light deflected from the sample surface, it is analysed by a spectrometer or a charge-coupled device (CCD) array and then a measurement point is plotted on a digital XYZ grid. When the point measurement sensor is set up with a controllable XY stage platform, 3D topographical maps of the scanned surface can be created consisting of numerous individually measured points on the digital XYZ grid (Austin et al., 2015; Boltryk et al., 2008; Leach, 2014). Anything which can affect the reflection of light back to the sensor may have an impact on the NCLP measurement capability (Leach, 2014).

One of the biggest advantages of using an NCLP for measuring surfaces is that unlike contact profilometers, there is no direct contact between a stylus and the sample surface eliminating the risks of surface damage (Barbour and Rees, 2004). This allows for longitudinal assessment of the same surface over time. Additionally, NCLPs can be programmed to scan a batch of samples, placed

on its XY stage, thereby increasing time efficiency of experimentation, unlike contact profilometers which can only scan one sample at time.

A common limitation of NCLPs is that the optical stylus used to measure complex surfaces, such as human enamel, can be distorted resulting in sensor drop out and data loss due to the inability of the sensor to detect the reflected light (Boltryk et al., 2009; J.M. Rodriguez et al., 2012). Similarly, the spot size of the optical stylus must be sufficiently small to accurately measure troughs, and its gauge range (the range of surface heights over which the sensor will operate) sufficiently large to detect valleys and peaks (Boltryk et al., 2009; Field et al., 2010).

The two most commonly used optical techniques that profilometers use to measure surface topography are either by measuring the displacement of the laser beam using triangulation principles or, by using confocal imaging principles; therefore, these techniques will be reviewed below. Different displacement sensors that have been previously utilised to measure ETW include confocal white light (WL) (Mistry et al., 2015; O'Toole et al., 2016), confocal laser (CL) (F. Mullan et al., 2018; F Mullan et al., 2018), and triangulation laser (TL) (J M Rodriguez et al., 2012; J.M. Rodriguez et al., 2012; Rodriguez and Bartlett, 2010).

1.3.3.2.1 Triangulation laser profilometry

Triangulation laser profilometry can be classified as a light scattering optical profiling technique and is used for a wide variety of industrial applications. Figure 1-4~~Figure 1-4~~ below shows a schematic set-up of optical triangulation in its simplest form. Light generated from a laser source is projected on to the target surface. A camera composed of a lens, focuses the scattered light to a spot on a position-sensitive photodetector, which measures the location of the illuminated point on the object. As the topography of the surface changes, this causes the spot to be displaced (d) so that the laser spot now appears at different places in the camera's field of view. As the distance between

the laser source and inspection point changes, so changes the location on the detector. Changes from the nominal vertical distance will produce proportional changes in position (d') at the detector. Using trigonometry, it is possible to calculate the X, Y, Z coordinates of the spot on the surface (Leach, 2014).

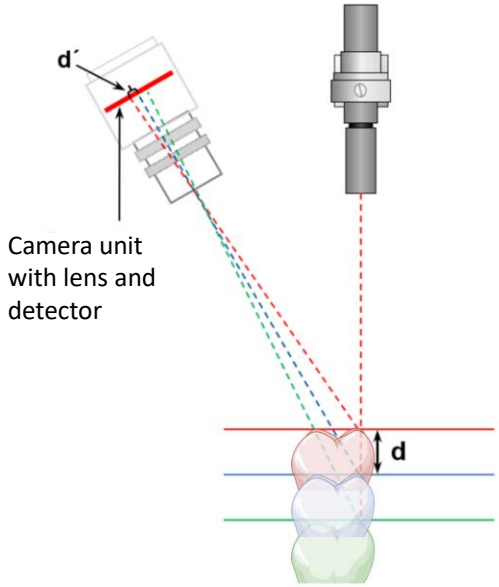

Figure 1-4 – Optical Triangulation
This technique uses principles of trigonometry to determine the distance to the object using the angles and positions of two points of view, in this case the laser source and the camera (Created with BioRender.com).

Laser triangulation profilometry would typically have a 1 µm axial resolution and, compared to confocal profilometry (see Section 1.3.3.2.2 below), an increased gauge range of 10 000 µm (Boltryk et al., 2008) which is useful in dental research for measuring the macro geometry of entire teeth in vitro that have been reproduced in dental stone or impression material (Rodriguez et al., 2009). Such systems are optimised for measurement of diffuse surfaces, such as dental stone, which scatter and reflect incident rays at many angles rather than at just one angle (Rodriguez et al., 2009). The accuracy and repeatability of a triangulation laser profilometer was reported to be 1.3 µm and 1.6 µm, respectively, for scanning plaster models (J M Rodriguez et al., 2012).

Triangulation sensors suffer from a number of disadvantages. Firstly, the spot diameter of the focused laser beam on the surface varies throughout the vertical measuring range, which can be important when measuring relatively small features; the size of the spot will act as an averaging filter near the beginning and the end of the measuring range (Leach, 2014). Secondly, an uninterrupted line of sight between the laser, surface, and camera/detector, without occlusions, is required for measurement. Therefore, the sensor must be in the correct orientation so that the laser spot is not hidden by any complex morphologies/high curvatures/undercuts (Boltryk et al., 2008; Leach, 2014; Logozzo et al., 2014; Richert et al., 2017). The presence of two or more detectors at different positions reduces the risk of these complex morphologies potentially blocking the return path of the reflected light (Boltryk et al., 2009; Leach, 2014). Thirdly, problems may arise from smooth, highly reflective specular surfaces that allow mirror-like reflection of light from a surface, in which light from a single incoming direction is reflected into a single outgoing direction. The lack of scattering means that triangulation lasers are least suited for directly measuring enamel and dentine; unlike other optical surface measurements such as confocal profilometers.

1.3.3.2.2 Confocal profilometry

Confocal profilometers use a sensor that operates on the confocal chromatic length aberration principle. Figure 1-5~~Figure 1-5~~ shows a commonly described configuration of a confocal profilometer. A polychromatic (i.e., white) light is emitted from a light source and projected to a lens with high chromatic aberration. The aberration lens separates the polychromatic light into its constituent wavelengths and the resulting dispersed light is projected onto the sample surface. The different wavelengths are now focused at different distances from the lens. Surface areas closer to the sensor (i.e., at a higher Z position) are exposed to the blue end of the light spectrum whilst surface areas further from the sensor are exposed to the red end of the spectrum. The resulting

reflected light from the focal area is therefore mostly monochromatic with all other wavelengths out of focus. The reflected light is transmitted back through the chromatic lens via a beam splitter, through a pinhole to a spectrometer with a charged coupled sensor (CCD). The purpose of the confocal pinhole is to filter the reflected light even further, isolating one single wavelength in perfect focus. The CCD detects this light and converts it to digital data. The spectrometer analyses the spectral distribution of the reflected light by determining the position of maximum intensity on the CCD signal (i.e., the maximum wavelength peak of the received signal). Therefore, the wavelength of peak intensity represents the average Z axis position, within the area of the light spot projected onto the sample surface (JYFEL, 2022; Leach, 2014).

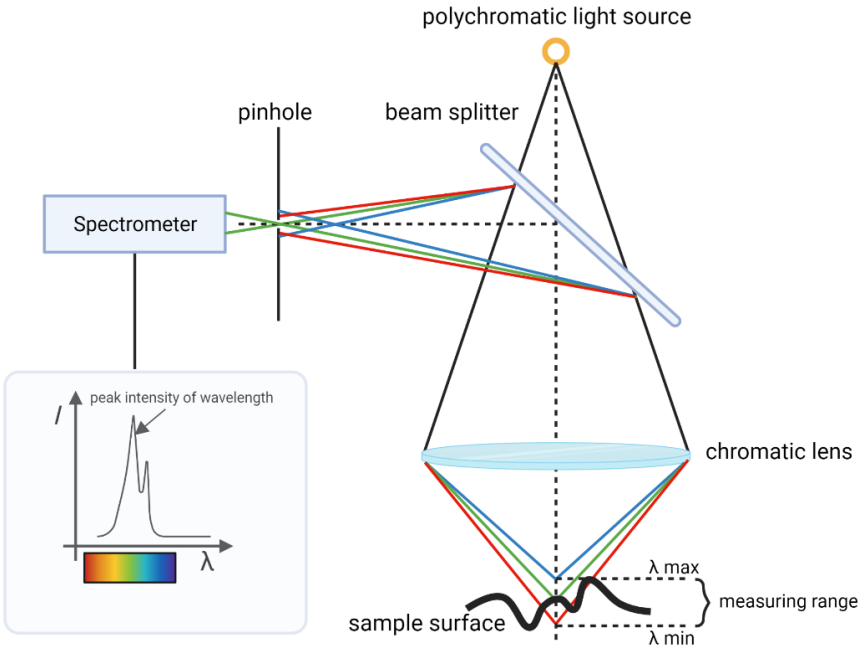

Figure 1-5 – Schematic of the optical principles of confocal chromatic profilometry (Created with BioRender.com)

Confocal profilometers that utilise monochromatic light also operate based on the confocal principle and therefore utilise a similar optical configuration (see Figure 1-6 below). Light is emitted from the light source through a pinhole before it passes through an objective lens. The Z height position of the lens can be adjusted so that the monochromatic light is focused on the surface. The reflected

light is transmitted back via a beam splitter, through another pinhole to the sensor. The sensor detects the heightened light intensity when the sample surface is in focus; whilst it detects no light intensity when the sample surface is out of focus. In confocal monochromatic profilometers, there is no need for an objective lens with longitudinal chromatic aberration as the light is filtered by the use of multiple pinholes (Boltryk et al., 2009; NanoFocus, 2022).

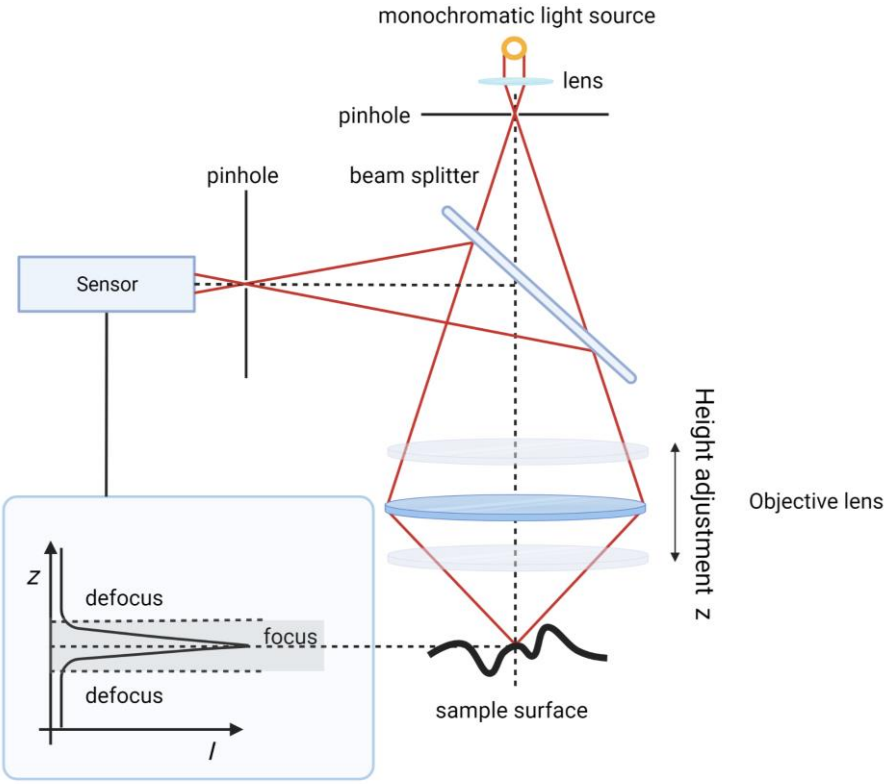

Figure 1-6 – Schematic of the optical principles of confocal monochromatic profilometry (Created with BioRender.com)

The advantages of confocal profilometers in general include rapid scanning time, high vertical resolution of ~1 nm and a small spot size that optimises lateral resolution. Due to the principle of confocal imaging, such profilometers exhibit a high spatial resolution, regardless of any ambient illumination, which means less environmental light noise. The chromatic configuration enables the device to be less sensitive to reflectivity variations in the sample enabling the measurement of varying types of materials, transparent and opaque, specular or scattering, polished or not.

Therefore, any need of sample surface treatment is eliminated. The use of polychromatic light and not of a coherent source laser eliminates the rise of issues associated with speckle and artefacts such as batwings often seen with confocal laser (monochromatic) profilometry (Boltryk et al., 2009; Leach, 2014). On the other hand, chromatic profilometers have been reported to be limited when measuring features with steep angulations greater than 30°, resulting in loss of data (Boltryk et al., 2009). Furthermore, monochromatic profilometer systems can have greater gauge range of 600 µm compared to its chromatic equivalent that was limited to 350 µm. Therefore, the monochromatic confocal sensor is more suitable for measurement of curved surfaces with steep angulations and vertically larger features whilst the polychromatic sensor is best suited for relatively flat surfaces with micro features (Boltryk et al., 2009).

1.3.3.2.3 Confocal laser scanning microscopy

Confocal laser scanning microscopy (CLSM) is a non-destructive 3D imaging technique utilising a light or laser source to scan the surface of an object using principles of confocal imaging to obtain high-resolution images (Field et al., 2010). It differs from conventional microscopy in that its optical configuration has additional pinhole apertures, in front of the light source and in front of the detector which help to increase the lateral optical resolution (super-resolution). It operates using the confocal principle i.e., only surface points in focus are bright, while out of focus points remain dark (Leach, 2014). Although this technique has a limited vertical (Z) range between 4 and 50 µm, with the removal of out-of-focus light and 3D image reconstruction, it can produce high quality images, one depth level at a time. Surface images of samples can be similar in character to scanning electron microscopy (SEM), but without many of its issues associated with specimen preparation (Maia et al., 2014). The potential benefits of CLSM in comparison to the other techniques are the smaller laser spot size resulting in improved lateral resolution and thus potentially higher quality

measurement for the key features of the 4–6 µm enamel prism (Leach, 2011). However, as with other microscopy techniques, CLSM is limited in its application to record surface texture.

1.3.4 Profile and areal field parameters

There are several different parameters that can be used to calculate the different components within a surface. Currently, profile (ISO 4287) and areal (ISO 25178) parameters are defined by international standards. Profile parameters are divided into three groups depending on the type of profile from which they are calculated. *P* parameters are calculated on the primary profile whilst *W* and *R* parameters are calculated on the waviness and roughness profiles, respectively (DigitalSurf, 2022a). Height (or amplitude) profile parameters measure the vertical deviations from the mean line which is used as a reference and is calculated as the mean value of all heights (Leach, 2014). Two of the most common profile parameters for roughness are *Ra* and *Rq* (Figure 1-7).

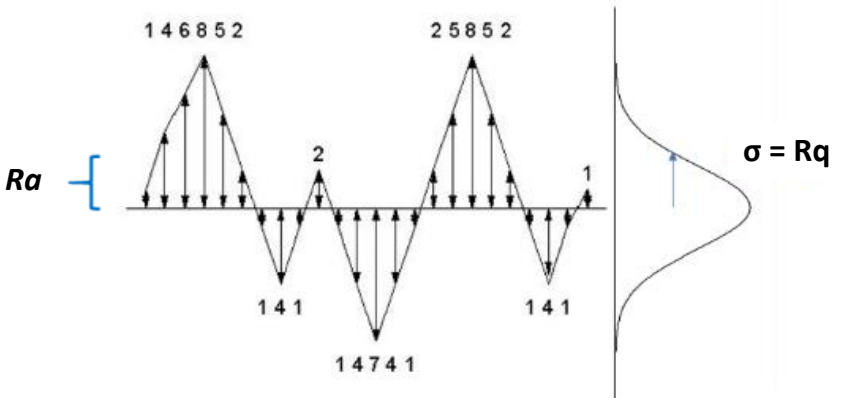

Figure 1-7 – *Ra* and *Rq* roughness parameters (adapted from DigitalMetrology, 2019).

The *Ra* (average roughness) parameter is the arithmetic mean of the absolute ordinate height values, $Z(x)$ within the sampling length, l,

$$Ra = \frac{1}{l}\int_0^l |z(x)| dx.$$

Rq is another parameter that is gaining popularity and corresponds to the standard deviation (root mean square deviation) of the height distribution, Z(x), within the sampling length, l,

$$Rq = \sqrt{\frac{1}{l}\int_0^l z^2(x) dx}\,.$$

The skewness of the extracted roughness profile, *Rsk*, is a measurement of the asymmetry of the height distribution about the mean reference line, within the sampling length. Figure 1-8 shows profiles with positive, zero, and negative *Rsk* values. Positive values correspond to high peaks spread on a regular surface (positively skewed, while negative values correspond to surfaces with valleys. For a surface with a random (or Gaussian) height distribution that has symmetrical topography the skewness is zero. Therefore, this parameter represents the degree of bias of a height distribution curve. Using *Rsk,* we can distinguish two surfaces having the same *Ra* value (Leach, 2014, 2001).

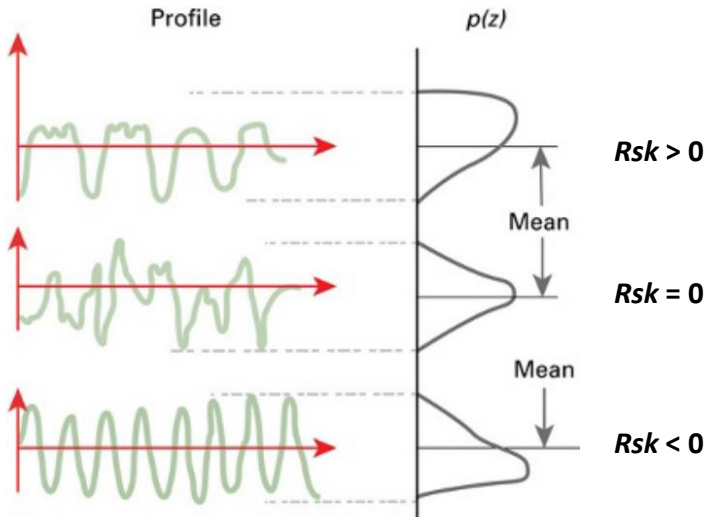

Figure 1-8 – Profiles with positive, zero, and negative *Rsk* values (adapted from R. Leach, 2014).

The kurtosis of the assessed profile, *Rku*, is a measure of the sharpness of the surface height distribution, within the sampling length. A surface with a perfectly random (or Gaussian) distribution

has a *Rku* value of three. The farther the result is from three, the less random and more repetitive the surface is. A spiky surface will have a high kurtosis value and a bumpy surface will have a low kurtosis value (Figure 1-9) (DigitalSurf, 2022a; Leach, 2014, 2001; Zygo, 2018).

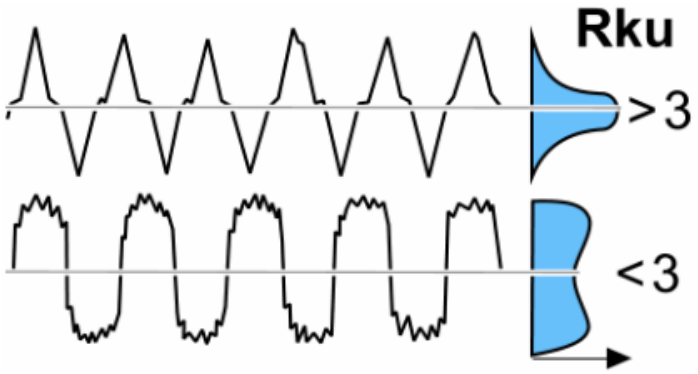

Figure 1-9 – Profiles with high and low values of Rku (Zygo, 2018).

There are inherent limitations with 2D surface measurements as a 2D profile does not necessarily indicate the exact nature of any topographical features and the functional properties of the 3D surface. Furthermore, two profiles with dissimilar features may yield similar *Ra* and *Rq* values. For this reason, areal field parameters have been developed for characterisation of the 3D surface. Unlike profile parameters, prefixes of areal (surface) parameters do not require three different groups distinguishing between profile, waviness, and roughness; therefore, they always start with the upper-case letter *S*. These areal parameters are the extension of the mathematical expressions of profile parameters that can be applied to the whole surface. For example, *Sa* and *Sq* are simply the extension to a plane of the equations of *Ra* and *Rq* that are defined for a line, respectively, (DigitalSurf, 2022a; Leach, 2014).

These parameters have been extensively used in dental research, especially within the field of tooth and material wear. Ghazal & Kern, (2009) investigated the correlation of wear of human enamel and nanofilled composite resin teeth against increasing surface roughness of antagonistic zirconia ceramic balls using the *Ra* values measured with a laser scanner. They showed that ceramic with

increased *Ra* roughness resulted in increased wear of human enamel and composite resin. Derceli et al., (2020) reported no statistical differences in *Ra* roughness on bovine and human enamel after erosive wear by exposure to gaseous hydrochloric acid. Another study using the *Rq* roughness parameter showed an increase in enamel softening and hence wear after ten 1-min cycles of wine exposure (Kwek et al., 2015). Rodriguez et al., (2009) showed that there were statistically significant differences between *Ra* and *Rq* roughness of three type IV dental stones and 15 impression materials digitised which can be used for the monitoring of ETW. More recently, Meireles et al., (2015) used *Sa*, *Sq*, *Ssk,* and *Sku* parameters to characterise natural enamel surface with and without wear. The authors reported that *Sa*, *Sq*, and *Ssk* roughness values were insufficient at distinguishing between worn and unworn natural enamel, whereas the *Sku* parameter was lower for the worn enamel. Similarly, Mullan, Bartlett, et al., (2017) reported statistically significant differences in *Sa* values for polished human enamel at 15, 30, 45 mins of erosive wear compared to baseline whilst for natural enamel only wear after 45 mins was significantly different. Furthermore, Mann et al., (2014) investigated the effect of two different hydrochloric acid challenges (pH 1.5) and (pH 3.0) over 2 min on polished enamel samples by measuring the *Sa* roughness. They identified significant increases in roughness after only 30 s for both pH values; however, a plateau was observed thereafter once initial demineralisation occurred. This supports suggestions that roughness measurements are better at identifying early surface change as opposed to bulk extensive loss.

1.3.5 Surface form measurement and analysis

Changes in surface form of tooth tissues between the wear lesion and the reference unworn region is one of the most common methods utilised to measure tissue or material loss due to wear (Austin et al., 2015; Wulfman et al., 2018; Young and Tenuta, 2011). Currently, different protocols and

techniques have been proposed for quantitative wear analysis which will be defined below by the number of scans required as well as the type of metrological calculation.

1.3.5.1 Single-scan technique

The use of a single scan of a sample surface following wear simulation is the most commonly described measurement technique in dental erosion studies *in vitro* (Young and Tenuta, 2011). The majority of ETW studies have been conducted on flat polished enamel and dentine samples (Almohefer et al., 2021; Mistry, 2016; Mylonas et al., 2018; Poggio et al., 2009; Young and Tenuta, 2011; Zheng et al., 2010, 2009) for two main reasons. Firstly, polishing eliminates natural variations and ensures standardised sample preparation resulting in a more repeatable and reproducible technique which facilitates lesion characterisation (Poggio et al., 2009; Young and Tenuta, 2011). Secondly, most experimental techniques require planar polished surfaces for precise measurements of the early wear defects and for creating reference regions with protective barriers surfaces (Attin and Wegehaupt, 2014). However, polishing removes the aprismatic outer enamel layer, which is often fluoridated and can resist acid dissolution better (Ganss et al., 2000); a concern that does not apply for this thesis as the investigation of the histopathological mechanism of wear was not within its scope.

The two most common protective barrier materials used in erosion studies when simulating wear are nail varnish and acid resistant adhesive tape. Nail varnish is painted on the tooth sample leaving a window of exposed tooth tissue and following experimentation is removed with acetone (Alexandria et al., 2017; Ionta et al., 2019). However, the application and removal of the varnish may affect the surface topography of the underlying tissue. Adhesive tape has been placed on the polished tooth samples in a similar manner to nail varnish (Almohefer et al., 2021; Gracia et al., 2010; Mylonas et al., 2018). Tape is easier to remove, and any adhesive residue left on the tissue

once removed can be cleaned with ethanol. Using tape as a barrier has demonstrated no effects on tissue topography (Gracia et al., 2010), nonetheless, as alcohol is present in many mouthwashes and drinks, any effects on the tissue topography would be consistent with *in vivo* conditions.

Step height calculations for determining the amount of tooth tissue of material lost from wear is considered the gold standard which is described in Section 1.3.5.1.1 below. As this method is optimised for flat surfaces, it cannot be applied in the same way for freeform surfaces, such as seen in natural enamel, simply because conventional form removal techniques and the use of curved reference regions present several challenges (Mylonas et al., 2019). Previous studies have reported that wear quantification on natural enamel requires the comparison of two sequential scans, i.e., a pre- and a post-wear scan, either via surface subtraction (Holme et al., 2005; Stenhagen et al., 2011) or via scan superimposition (Mylonas et al., 2019; J M Rodriguez et al., 2012; Rodriguez and Bartlett, 2010). Interestingly, (Ganss et al., 2000) demonstrated measurement of erosive wear on natural human enamel samples utilising a regression line method to determine the vertical distance between the reference unworn enamel and the lesion. However, their technique was not based on ISO standards and the lesions created on natural enamel were relatively deep (≳50 µm) and distinct for measurement; therefore, its reproducibility and accuracy remain uncertain.

1.3.5.1.1 Step height measurement (ISO 5436-1)

Step height is a measurement technique that has been extensively used in dental research and more specifically for measuring tooth tissue loss. In the field of surface metrology, step height artefacts (of known dimensions within a measurement uncertainty) are used to calibrate a measuring instrument as well as demonstrate traceability i.e., to demonstrate its high accuracy. According to the ISO 5436-1 standard, a step height is calculated as the difference in height between the mid-third region of a valley (step) and two reference regions on either side on a measured profile (de

Groot and Fitzgerald, 2017; Leach, 2015), as shown in Figure 1-10~~Figure 1-10~~. As mentioned above, this type of measurement is optimised for use on flat surfaces such as polished enamel and dentine. When the form is a line or a plane (planar profile or surface) any slope/tilt can be corrected by levelling. This is a function offered in metrology software and is based on the calculation of the least-squares line/plane associated with the profile/surface. This is the same line that is used as a reference for the calculation of surface texture parameters (discussed in Section 1.3.4 above). When the form is non-planar, the equivalent of levelling is form removal using an estimated polynomial shape, and optionally excluding a portion of the surface that is intended to be measured. Removing the form, makes it possible to define a flat reference around the region of interest for vertical or volumetric measurements of features such as wear lesions and surface changes (DigitalSurf, 2022a). Step height calculations can also be conducted on the residual output following subtraction of freeform surfaces (Mylonas et al., 2019), a method that is described in more detail in Section 1.3.5.2.1 below on page 55.

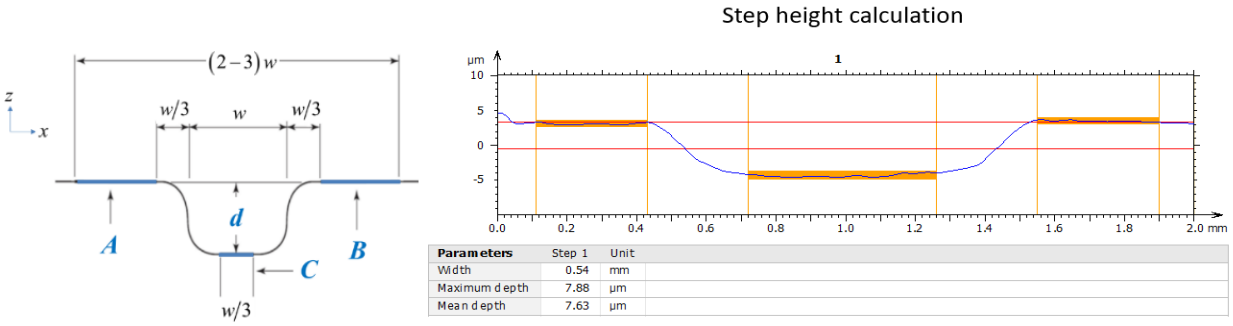

Figure 1-10 – Step height calculation (ISO 5436-1).
Left, change in height d is calculated as the difference in height between the reference regions (A and B) and the central mid-third region of the valley (C) (de Groot and Fitzgerald, 2017). Right, example of an automated step height calculation to measure enamel loss following erosion (Mountains8, DigitalSurf, France)

In the case of ETW studies, a step height measurement would be carried out after the central zone of enamel or dentine is exposed to wear simulation producing a lesion whilst reference areas on

either side are covered by a protective barrier, leaving them unaffected from erosion. Figure 1-10~~Figure 1-10~~ above (right side) shows an example of using an automated step height calculation to measure enamel loss following erosion (Mountains8, DigitalSurf, France)

There are several metrology software packages which offer different ways of calculating step heights. Previously, step heights have been calculated using a single profile across the middle of the sample, known as mid-point step height (O'Toole et al., 2015) or by measuring the average from multiple profile lines; this has been previously calculated using five (Mistry et al., 2015) or ten profiles (Mutahar et al., 2017). The use of single or a few line profiles may not necessarily be representative of the erosion lesion as both the lesion and the reference enamel may not be uniformly the same.

3D step height measurement methods have been developed based on the entire surface of the lesion to overcome this issue; however, each type is defined differently according to different studies. A type of 3D step height commonly reported in the literature and utilising the ISO 5436-1, is calculated based on the average profile formulated from all-series of profiles that compose the entire selected surface (Mylonas et al., 2018; Sar Sancakli et al., 2015). Using the ISO 5436-1 function of the software, this type of 3D step height does not require the operator to select the location of a single or a few profiles across the lesion nor where the reference and the lesion mid-third is; instead, this is an automatic calculation made by the software based on all extracted profiles and therefore is a more objective technique of measuring surface loss (DigitalSurf, 2022a). Sar Sancakli et al., (2015) validated this type of 3D step height to an accuracy of 0.042 µm; however, the technique the authors used was not made clear in their publication.

1.3.5.1.2 Non-ISO wear measurement

Some studies have measured wear on polished enamel using only one reference area (Conceição et al., 2015; Ganss et al., 2000) and therefore did not comply with ISO standards. Having one reference area may introduce errors during levelling and may be difficult to judge if the measured value is a true reflection of the wear or an anomaly/artefact of the sample or the analysis process. Ganss et al., (2000) measured erosive wear on both polished and natural enamel samples. For polished samples wear was measured as the average vertical distance between the highest and lower point of six profiles. For natural enamel, the profile tracing was adjusted to the X axis using a 0.3 mm regression line constructed as close as possible to the eroded lesion trace; erosive wear was then calculated as the vertical distance between the highest point of the reference region and the lower point of the eroded region within the first 0.3 mm of the regression line. The problem with this approach is in the variation that exists within natural enamel and the fact that the highest/lowest points need to be defined by the operator introducing bias and inconsistency across samples. A different type of 3D step height described in the literature was defined by dividing the volume of the lesion (μm^3) by its surface area (μm^2) (Paepegaey et al., 2013; Rodriguez and Bartlett, 2010). This method, however, does not conform to the ISO 5436-1 standard and is technique sensitive as it relies on the operator defining the edges of the erosion lesion.

1.3.5.2 Bi-scan techniques

Measuring wear on freeform surfaces such as seen in teeth presents significant measurement challenges for which are not yet fully elucidated (Savio et al., 2007). The main challenges are found within the surface complexity making form removal difficult as well as creating reference surfaces required for metrological measurements. As described above, to overcome these challenges, most of ETW studies were conducted on polished tooth tissue samples. Previous studies have quantified

wear on freeform surfaces via surface subtraction or scan superimposition which are described below.

1.3.5.2.1 Surface subtraction

Surface or profile subtraction refers to the software computation of the difference in a single dimension (usually in the Z axis), between corresponding surface points of two sequential datasets; the subtraction of a pre- and post-wear dataset produces a relatively flat residual or 'difference' dataset which can be used for measurements of surface change (Holme et al., 2005; Mylonas et al., 2019; Stenhagen et al., 2011). This technique is particularly useful in industries assessing topographic change such as surface wear, corrosion, or the degree of similarity between two manufactured parts, in a relatively small area in relation to the entire sample (Mansouri, 2014). If no surface changes occur and assuming no scanning errors, the subtraction of two perfectly identical datasets would result in form removal and a flat residual dataset, regardless of the original freeform shape of the surface. On the other hand, if localised wear occurs on a surface, the residual dataset would reveal change with data of negative Z heights in relation to a surrounding flat surface where no change has occurred (Holme et al., 2005; Stenhagen et al., 2011).

The first ETW study to utilise this technique was described by Holme et al., (2005). Prior to scanning each sample, a specially designed holder was used which allowed reproducible repositioning by a few microns. Therefore, the pre- and post-wear datasets of these samples made by a white light interferometer were pre-aligned using a jig during scanning prior to the subtraction analysis which resulted in a 'difference' image from which enamel loss was calculated. Using a software programme, loss in polished enamel was determined by calculating the depth distribution of the pixels in the worn enamel region relative to uneroded amalgam used as the reference (Holme et al., 2005); The subtraction of the two datasets allowed for the calculation of step height on local

changes in the topography. Stenhagen et al., (2011) measured wear in polished human enamel samples in the same manner. They reported that using surface subtraction of scans from a white light interferometer allowed for calculation of step heights as low as 5.1 (1.1) µm. However, it is not clear how dataset alignment was carried out in this study. A more recent study investigated ETW on natural enamel by subtracting pre- and post-wear datasets from NCLP scans. They also utilised a bespoke repositioning jig on the stage of the NCLP to facilitate alignment of before and after erosion datasets prior to subtraction which allowed for step height measurement of the wear scar (Mylonas et al., 2019). Although the use of a physical repositioning jig can be useful in *in vitro* studies, this would not be practical for direct *in vivo* scanning of oral surfaces due to the movement of both the patient and intraoral scanners which are described in Section 1.3.5.3 below.

The surface subtraction technique is subject to errors inherent to the way the two datasets are aligned (Figure 1-11~~Figure 1-11~~). Where there is a difference in slope between the two datasets; it is crucial that they are perfectly aligned in the X and Y axes before subtraction occurs: otherwise, this will introduce errors in the step height measurements. These errors can be minimised using functions available in surface metrology software to improve alignment. Holme et al., (2005) using metrology software carried out a two-step shift in the X and Y axes of each dataset relative to the original prior to subtraction. Similarly, Mylonas et al. (2019) using similar software corrected the offset and rotational differences between the two datasets prior to subtraction. Although these additional steps reduce errors, the alignment described in both studies was manually controlled by the operator and therefore introduces operator errors. No study reported the use of surface subtraction without the use of a physical repositioning jig or software correction of dataset alignment and therefore further research is required for automating the process.

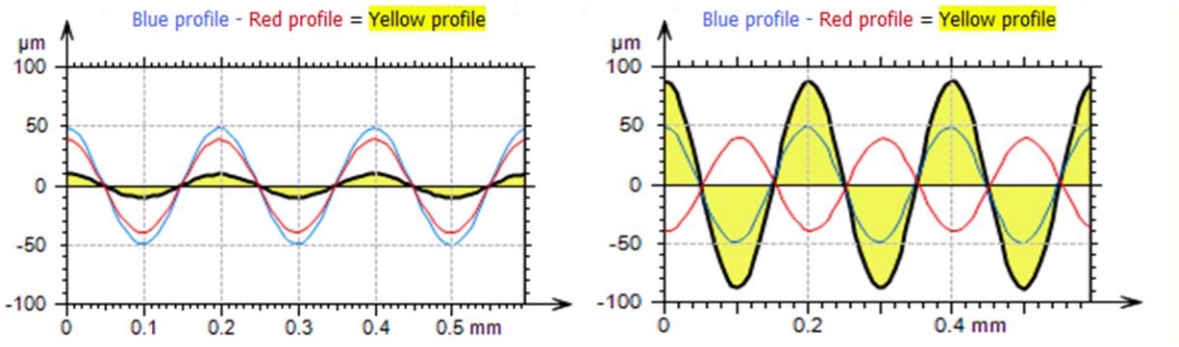

Figure 1-11 – Surface subtraction of two datasets and the importance of correct alignment between datasets prior to subtraction (DigitalSurf, 2022a).
The subtraction of perfectly aligned peaks and valleys of the blue and red profile result in a residual profile (yellow). If peaks and valleys are erroneously aligned and not located at the same place, the amplitude values of the residual profile can be bigger than the source profile.

1.3.5.2.2 Surface registration (superimposition)

Surface registration refers to the superimposition or alignment of 3D point cloud datasets produced by optical scanners, such as profilometers and intraoral scanners, for comparison and analysis of surface change. Reverse-engineering superimposition software use point clouds and apply surface matching algorithms, to find registration parameters and compute a transformation which aligns a moving dataset to a fixed reference dataset. Sourced from engineering, surface-registration techniques has been adopted in dental research to quantify surface change in several fields such as orthodontics (Becker et al., 2018a; Camardella et al., 2017b) and periodontics (Clozza et al., 2012); and has shown great promise as a method to quantify wear of teeth and dental materials (Kühne et al., 2021; J.M. Rodriguez et al., 2012). Figure 1-12~~Figure 1-12~~ shows two datasets of a tooth, before and after a crater was created on one of its cusps using a dental bur, and their surface registration for surface change quantification. The baseline surface (1) and post-wear surfaces (2) of a tooth are aligned based on a surface matching algorithm excluding the areas of surface change from alignment (3) to produce a colour-coded 3D comparison (4) in which negative deviations (surface loss) is represented in blue and no change is seen as green (5).

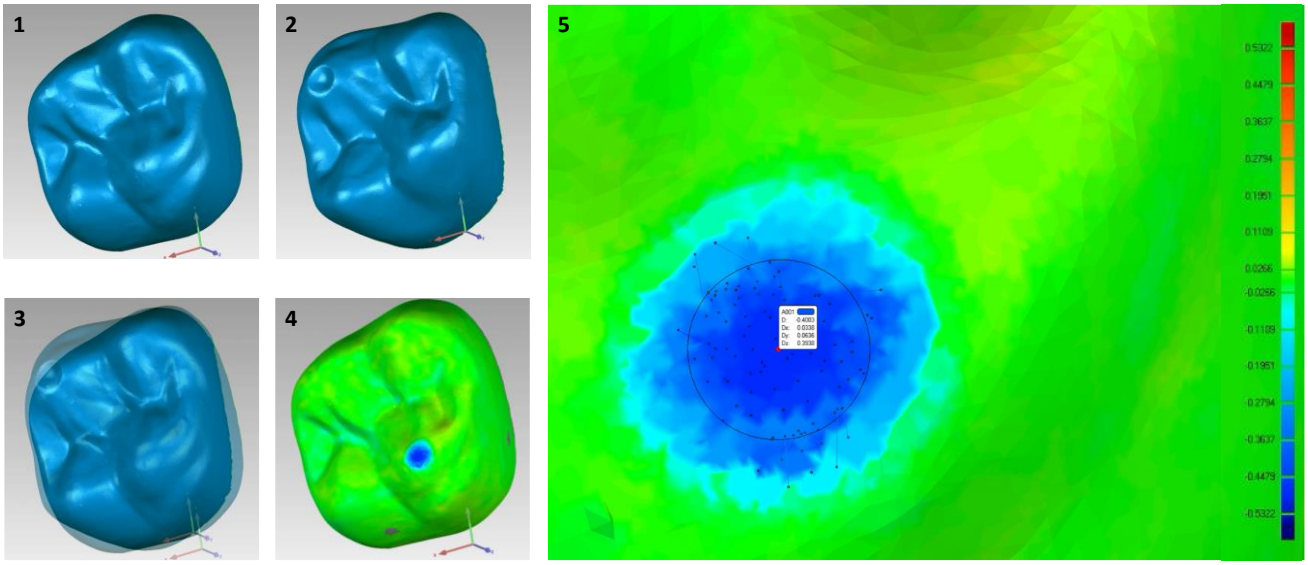

Figure 1-12 – Surface registration of two datasets for ETW quantification.
The baseline surface (1) and post-wear surfaces (2) of a tooth are aligned based on the computation of a surface-matching algorithm (3) to produce a colour-coded 3D comparison as a function of deviations in Z between datasets (4) in which negative deviations, representing surface loss, are seen in blue colour shades and surface regions with no significant wear are seen as green colour shades (5) (Images used from GeomagicControl 2014, 3DSystems).

The alignment of two datasets can be conducted utilising one of three different methods: landmark-based alignment, best-fit alignment, and reference best-fit alignment; however, the exact mathematical complexities of the algorithms used in software are often hidden to the operator for ease of software use (O'Toole et al., 2019a).

Landmark-based alignment is performed manually by the user who selects a series of common landmarks or points on each dataset for alignment by the software. This method is highly subjective and dependent on the operator's skill and understanding of alignment (O'Toole et al., 2019a).

Best-fit alignment is an automated method which aligns consecutive scan datasets based on iterative-closest-point (ICP) algorithms which can somewhat differ according to the software used; and does not involve user-based decision-making. ICP was originally introduced by (Besl and McKay, 1992) and is one of the most widely utilised algorithms for structural engineering applications. It works based on an iterative search of 3D correspondences between point pairs from two sets of

point clouds to determine the rigid transformation (translation and rotation matrices) to the moving dataset (i.e., the subsequent scan) whose application can lead to the least-squares best fit on the fixed reference dataset (i.e., the baseline scan) in terms of minimising the root-mean-square distance. The process of estimating the closest points and application of the rigid transformation is repeated until convergence (Becker et al., 2018a; Marani et al., 2016; O'Toole et al., 2019a). One of the biggest disadvantages of ICP is that surfaces are forced to be aligned in a way that is not biologically informed which can lead to local distortions and inaccurate measurements. Due to the nature of the iterative algorithms' termination criteria, the alignment process will minimise the mesh distance error and spread errors evenly over both positive and negative deviations between the aligning datasets. In the case of wear measurements, the large deviations between the two datasets in the wear region would be underestimated due to the algorithm forcing the two datasets together whilst, unworn regions may appear to have "gained" in surface which is impossible and unconvincing (O'Toole et al., 2019a, 2019b).

A reference best-fit alignment also aligns two datasets by means of the ICP algorithm. However, it aligns the datasets by employing reference regions, defined by the operator, which are least likely to have undergone change. This avoids the error of underestimating the defect of interest but introduces operator bias when selecting the reference regions on the datasets.

Rodriguez & Bartlett, (2010) conducted *in vitro* study quantifying dietary erosion-abrasion wear on polished enamel samples by superimposing TL NCLP scans. Although, the authors reported a strong positive correlation (p=0.76) between 2D and 3D step height measurements; only 3D step height measurements demonstrated significant differences between different fruit drinks tested, whilst 2D measurements did not apart versus water control. This suggested that compared to 2D, 3D measurements are a more sensitive to surface changes and a more accurate representation of the

activity of the wear as it account for the overall lesion (Rodriguez and Bartlett, 2010). Rodriguez et al., (2012b) showed that the superimposition procedure using NCLP scans for volumetric ETW measurements was accurate with a mean (SD) error 2.7 (0.7) µm (repeated superimpositions of same cast) and 14.8 (2.8) µm (repeated superimpositions of five identical casts).

As direct scanning of teeth using high accuracy scanners is not possible, replica techniques have been proposed as an important step towards *in vivo* measurements of ETW. Hjortsjö et al., (2012) used NCLP scans of enamel samples and their associated positive replicas made in acrylic resin to measure tissue loss. Results revealed a strong correlation between enamel and replica scans for tissue loss measurements. This technique did not use superimposition of two datasets but is considered important as the concept of replicating the dentition using impression or casting materials at different points of time can be adopted for *in vivo* ETW progression monitoring superimposition of subsequent impressions/casts. 3D virtual models have previously been made *ex vivo* with profilometry (Chadwick et al., 2005; Pintado et al., 1997; J.M. Rodriguez et al., 2012) or dental laboratory scanners (Ahmed et al., 2016; Gkantidis et al., 2020; Zou et al., 2009), indirectly via gypsum study casts (Ahmed et al., 2016; J.M. Rodriguez et al., 2012), electro-conductive coated gypsum (Chadwick et al., 2005), or epoxy-resin (Pintado et al., 1997).

Rodriguez et al., (2012a) conducted an *in vivo* study to investigate progression of tissue loss on patients with diagnosed ETW. Using NCLP scans and ICP superimposition software, they quantified surface changes on the patients' dental stone casts over a period of 12 months. The average wear of all subjects detected was less than the measurement error (15 µm) of the technique used; however, they suggested that focussing upon the most severely affected teeth in future studies would make wear monitoring measurement easier. Ahmed et al., (2016) assessed the accuracy of a 3D contact scanning system and superimposition of dental stone casts in measuring ETW

progression in a patient over a 12-month period. At first, the accuracy of the scanner, 2.8 ± 0.8 µm, and of different types of impression materials being tested (alginate, −35 ± 64 µm, polyether -25 ± 29- µm, and polyvinyl siloxane, 12 ± 34 µm) in measuring a stainless steel model consisting of seven ball bearings (Ø10 mm) was ascertained, the authors demonstrated that the overall accuracy of the workflow *in vitro* was 33 µm for each cast production; therefore 66 µm for the scanning of two successive casts and superimposition. The use of this workflow was clinically translated on a patient; it demonstrated localised areas of noticeable wear extended to a depth of 500 µm and therefore more research is required for detection of less severe wear progression rates.

The concept of indirect digitisation of plaster casts can be applied to measure wear of clinical materials. A recent clinical study investigated the *in vivo* wear of composite and lithium disilicate ceramic restorations on molars and premolars of 12 patients over a period of 3 years (Burian et al., 2021). The data was obtained by scanning casts using a laboratory scanner and superimposed with the baseline using ICP to measure mean vertical loss. Results for composite restorations revealed that the mean wear rate per month over the first year was 15.5 ± 8.9 µm and 28.5 ± 20.2 µm, for the premolar and molar restorations, respectively; whilst for the lithium disilicate ceramic restorations, it was 7.5 ± 3.4 µm and 7.8 ± 2.0 µm.

1.3.5.3 Surface feature detection methods

Software dedicated to surface metrology may offer functionalities to detect and quantify surface features with boundaries such as particles, pores, and grains. Such surface feature analysis is used in research and industry across many fields such as quality control and characterization of structured and nano-structured materials and assemblies. There are several feature detection methods such as threshold segmentation, watershed segmentation (ISO 25178-2), edge detection, and circle detection which are described in more detail below. Depending on the method or the field of

application, surface features can be described using different names, some examples of which can be seen in Table 1-1. Generally speaking, there are two types of features, those above the background topography (protruding feature) and those below (receding feature) (DigitalSurf, 2022a). The terms “groove” or “crater” were selected to be used throughout this thesis to describe round or elongated recessive surface features created on enamel surfaces or other experimental surface substrates representing surface loss / wear (Gao et al., 2019; Leach, 2013). Regardless of the detection method, once a feature is detected by the software, different parameters can be calculated associated with the feature such as height, area, and volumetric measurements.

Table 1-1 – Common vocabulary used to describe surface features in metrology.

Surface feature vocabulary	**Description**
Particle/Pore	Object above/below a reference height (or intensity). Obtained using a threshold, or by segmentation with a gradient.
Island	Hill above a plane used as a threshold.
Crater	Valley below a plane used as a threshold.
Groove	Elongated valley below a plane used as a threshold
Hill and its peak / Dale and its pit	Portion of a surface (‘motif’) obtained by watershed segmentation as defined in ISO 25178-2.
Hole	Dark object on an image, or a group of non-measured points on a surface. Its content cannot be analysed, only its horizontal characteristics (lateral size or area).
Grain	Used in metallography for crystal grains on a sample slice.
Structure	Geometric shape above or below the surface, for example on a microelectronic structure such as a micro-electromechanical systems.

1.3.5.3.1 Threshold detection

Threshold detection, or also known as threshold segmentation, is a fast method to detect surface features on a surface with a flat and horizontal background topography such as seen in polished enamel or in residual 'difference' surfaces following subtraction of two scans of the same surface. The roughness of the surface must be smaller than the height of the feature. Using the analogy of water flooding a landscape, particles are the islands left when the landscape is flooded up to the chosen threshold, whilst craters/pores are holes below the water surface. Figure 1-13 below illustrates the threshold detection method to distinguish surface loss on a flat polished enamel surface. The scanned dataset of an eroded polished enamel surface is displayed as a colour-coded surface. Colours act as a function of Z heights where the eroded enamel is displayed as a dark blue valley and non-eroded flat enamel as a grey flat background topography. The valley of eroded enamel is detected using the threshold settings to distinguish surface heights below the mean plane based on the histogram of the surface heights distribution (light blue colour) and the Abbot-Firestone curve (red). The vertical axis represents the depth of the surface heights while the horizontal axis represents the bearing ratio which is the cumulative sum of all the surface depths (DigitalSurf, 2022a).

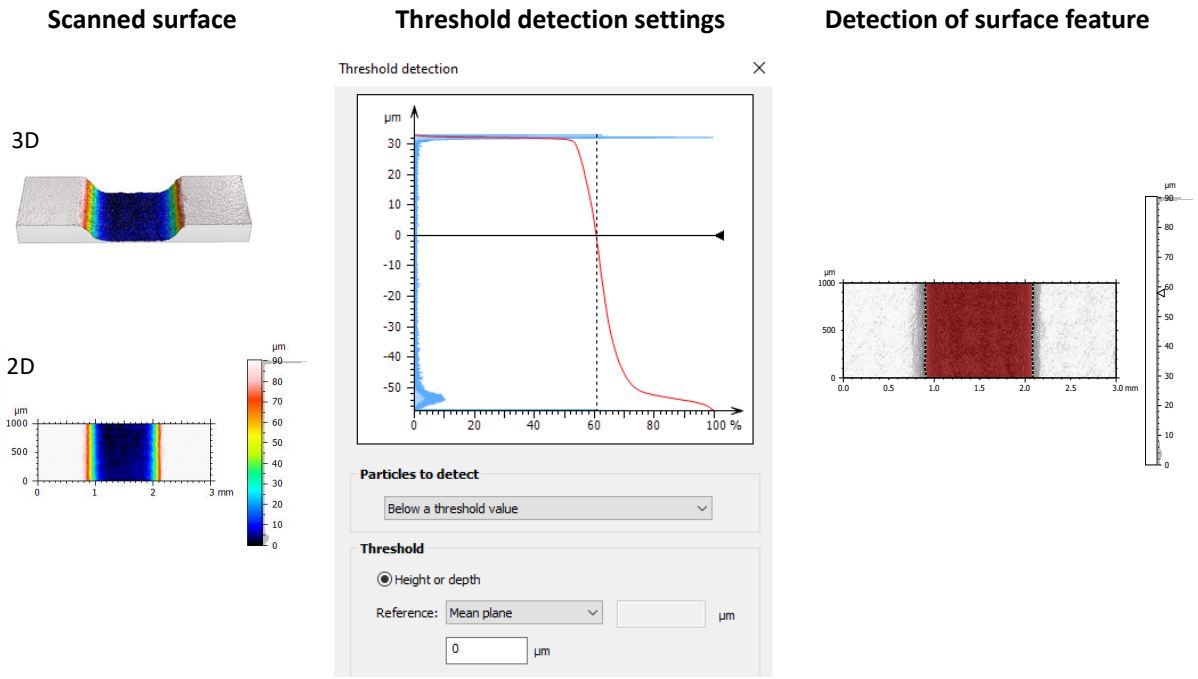

Figure 1-13 – Threshold detection method to distinguish surface loss on a flat polished enamel surface.

1.3.5.3.2 Watershed segmentation

The term “motif” in surface metrology originated in the 1980s in the French automotive industry when a new method for characterising mechanical components was developed based on a graphical segmentation of the profile with respect to motif shapes that were divided as shapes of hills and dales (Leach, 2013) such as seen in Figure 1-14. A surface point higher than its surrounding area is called a peak (P) and its neighbourhood is called a hill (H). All points belonging to a hill are enclosed by a course line. Similarly, a surface point that is lower than its surrounding area is called a pit (N) and its neighbouring area is called a dale (D). All points belonging to a dale are enclosed by a ridge line (R). The method of utilizing a segmentation algorithm to divide (segment) a surface into dale or hill motifs has been adopted as an international standard under the reference ISO 25178-2 (DigitalSurf, 2022a).

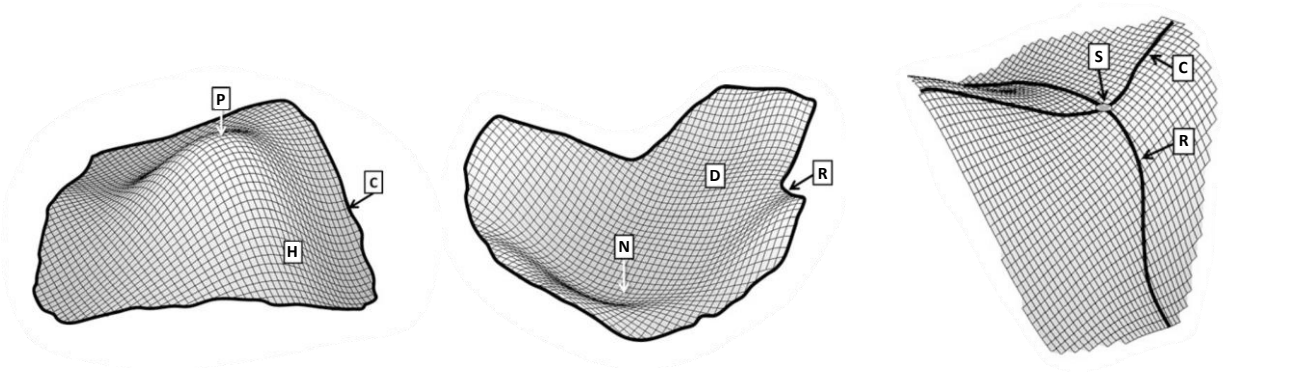

A hill (H), its highest point, the peak (P) and its surrounding course line (C)

A dale (D), its lowest point, the pit (N) and its surrounding ridge line (R)

A saddle point (S) which is at the intersection of a ridge line (R) and a course line (C).

Figure 1-14 – Illustration of hill and dale motifs on a surface defined by ISO25178-2.
Figure adapted from R. Leach, (2013)

The process of watershed segmentation starts from the lowest point of the surface. Using the analogy of water flooding, virtual water is poured over the whole surface from above, so that the dales are flooded progressively. At any time point, the water pouring process occupies an area surrounded by a contour line. As the water level increases, the contour lines move higher. When two adjacent dales are flooded to a level at which their contour lines come into contact, a virtual wall is recorded at the contact points which are the ridge lines surrounding dales. When the water level reaches the highest point on the surface, the watershed segmentation is complete, and all dales are segmented by ridge lines. This process of surface division can lead to over-segmentation i.e., thousands of small and insignificant dales, therefore an additional processing step in the algorithm may be required, such as user-selected filtering, thresholding or using pruning criteria to merge small dales into larger ones and only retain the significant dales of interest (DigitalSurf, 2022a; Leach, 2014, 2013).

1.3.5.3.3 Edge detection

This method can be used to detect dispersed features on a surface with a wavy or uneven background or when features have different heights. It can also be used if these features are

connected, i.e., not clearly separated. A derivative of the surface (gradient filter) is used to aggregate hills and dales that in the end is coincident to the feature of interest and calculate the outline of the detected motifs. For example, a groove can be imagined as a large elongated dale and therefore further processing can lead to the merging of smaller individual dales (originated from the irregularities in the internal regions of the groove) into a large one. The challenge is the identification of appropriate combination techniques and threshold values, which currently requires trial and error (DigitalSurf, 2022a; Leach, 2013).

1.3.5.3.4 Circle detection

This method is used for detecting round or spherical features which are difficult to detect or separate using the other methods described above, either because these features are adjacent or overlapping, or have a weak imaging contrast. This method works best when the features have similar sizes as the calculation time increases with the range of circle diameters (DigitalSurf, 2022a).

1.3.6 The use of metrology software

There are several commercial and open-source software designed for surface alignment and metrology applications. Each of these come with unique functionalities and purposes, so operators must choose carefully a software depending on their intentions of use. Although primarily used in engineering, scholars have adopted such software for dental research. The software allows them to use virtual reconstructions of dental surfaces produced by optical devices at each evaluation timepoint and perform surface loss quantification through subtraction and superimposition technique, statistical analysis, and produce coloured-scaled 3D images (Wulfman et al., 2018). The use of subtraction and superimposition techniques for wear quantification are described in Sections 1.3.5.2.1 and 1.3.5.2.2, respectively. It must be noted that not all software or their different versions are capable of superimposition of virtual surface reconstruction. Mountains® (DigitalSurf, Besançon,

France) (previously named as MountainsMap®) is a software dedicated for surface imaging such as 2D & 3D profilometry with a focus on surface texture, topography, and form analysis and is extensively used throughout this thesis. However, only after the release of version 8, was it able to perform 3D manipulation and analysis on freeform surfaces from files such as Standard Tessellation Language (STL), Wavefront (OBJ), and Polygon File Format (PLY) files (DigitalSurf, 2022b). On the other hand, surface matching software capable of superimposing virtual surfaces, such as Geomagic Control (v2014, 3D Systems, Morrisville, NC, USA), are designed to achieve accurate digital 3D models and CAD assemblies of physical objects for design engineering and manufacturing and have been primarily adopted in dental research for surface form wear quantification (3D systems, 2022). Furthermore, although most surface-matching software are capable of 2D analysis once two surfaces are aligned, 3D analysis is only possible with some (Wulfman et al., 2018).

There is a wealth of physical artefact standards that are used to calibrate surface measuring instruments through ISO 10360-2:2009, but such artefacts do not offer validation or demonstrate the accuracy of the software aspect of the measuring workflow (Leach et al., 2006). Indeed, there is lack of information in dental research determining the degree of accuracy of different software and algorithms used for measuring surface change. Instead, most studies have focussed on determining a global workflow accuracy, i.e., accuracy accredited to the use of both the hardware scanner and software analysis technique, which is reported to be approximately ±15 µm by digitising and superimposing replica casts of dentitions using high accuracy laser scanners (Wulfman et al., 2018).

International standards ISO 5436-2: 2012 introduced the concept of software measurement standards or softgauges for testing the numerical correctness of the software and therefore their validation. Using reference softgauges (data) describes a Type F1 measurement standard whilst using reference software (traceable computer) describes Type F2 measurement standard (Chiboub

et al., 2021). Softgauges are in fact restricted to surface texture measuring software, but according to Arezki et al., (2018), the principle of softgauge use can be extended to any measurement software. The method of using a softgauge is shown in Figure 1-15. A softgauge would consist of reference data with known measurand parameter values. This is loaded to the software under test and the resulting value is compared to the reference measurand value. The software would be validated if the error is within the maximum permissible margins (Arezki et al., 2018).

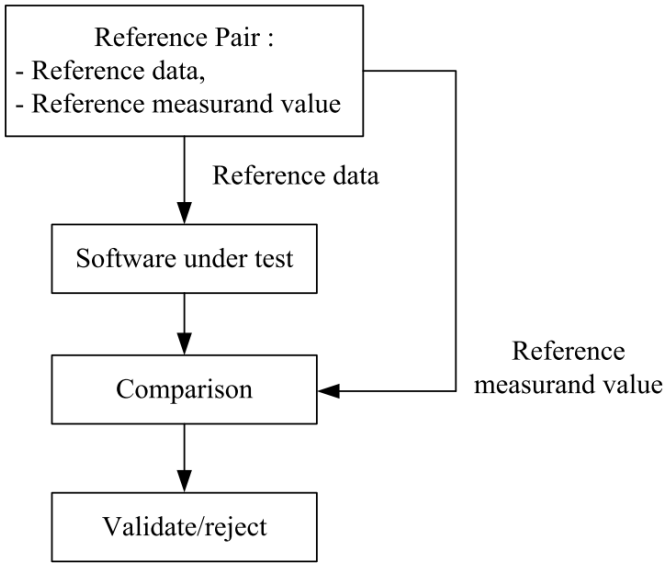

Figure 1-15 – Software validation using reference softgauge (type F1) (Arezki et al., 2018).

Several National Metrology Institutes, such as, National Physics Laboratory (NPL, UK), Physikalisch-Technische Bundesanstal (PTB, Germany) and National Institute of Standards and Technology (NIST, USA) have set up a number of platforms that provide generated softgauges with known surface texture parameters. NIST is the only one that provides type F1 and Type F2 standards for both 2D (profiles) and 3D surfaces; whilst the other two only work for 2D profiles. An example of the concept of softgauges is a study by O'Toole et al., (2019a) in which the authors used datasets of lower molars obtained by a dental model scanner and mathematically created a virtual defect of

300 µm on the occlusal surface to investigate the accuracy of commonly used superimposition techniques described in more detail in Section 1.3.5.2.2, on page 57.

1.4 Intraoral scanners

Intraoral scanners (IOSs) are unquestionably a significant chapter of the digital revolution that has radically transformed dentistry in the last decades. These devices are able to capture direct optical impressions of oral surfaces which in turn can be displayed and converted to files for virtual restoration design and subsequent construction of the respective restoration. The first intraoral scanning system, CEREC® (Sirona Dental Systems LLC, Charlotte, NC, USA) was introduced in 1987 (Brandestini and Moermann, 1989), and since then IOSs have become increasingly more common within clinical practice (Logozzo et al., 2014). There are several IOSs in the current market, each utilizing different imaging technologies and optical phenomena to capture the 3D geometry of oral surfaces. In 2021, 13 latest-generation IOSs were featured at the International Dental Show, whilst their older versions or other older scanners from different manufacturers are still available on the market (Al-Hassiny, 2022).

IOSs consist of a wand (camera), a computer, and a proprietary software. The wand is designed to be as small, light, and ergonomic as possible for ease of access to the oral cavity, as well as having the space for their proprietary hardware technology. The computer and software process the captured images to register the 3D geometry of oral surfaces (Mangano et al., 2017; Richert et al., 2017).

1.4.1 From conventional to digital workflows

An accurate impression technique is key for the successful replication of the dentition and fabrication of dental prostheses. The well-established conventional workflow involves an analogue

impression of the prepared dentition using elastomeric impression material, its transfer to a dental laboratory for fabricating a stone model, waxing-up, investing and producing the restoration through the lost-wax technique (Heshmati et al., 2002; Sim et al., 2019). The development of computer-aided design and manufacturing (CAD/CAM) technology and the use of IOSs have allowed an alternative, fully digital workflow for the fabrication of casts and dental prosthesis (Keul and Güth, 2020). Using IOSs, the dentition can be directly scanned, and its topography captured, eliminating the need for impression materials and model fabrication (Sim et al., 2019). The digital files produced by IOSs are then sent to either a chairside unit or a dental laboratory for the fabrication of the planned prosthesis using additive (3D printing) or subtractive (milling) manufacturing techniques (Haddadi et al., 2021). In cases where a physical model would be required, as with certain types of restorations or when the restoration–antagonist occlusal relationship needs to be established, this can be created in the same fashion, based on the dataset produced by the IOS. IOSs have brought many advantages to dentistry which are discussed in detail below.

1.4.2 Patient experience

Optical impressions and their ability for immediate chairside assessment are powerful tools for patient communication and marketing as patients can feel involved in their treatment planning and a more effective communication can be established (Mangano et al., 2017). The ability to directly capture optically all 3D information of the patient's dentition using IOSs, without the physical contact of analogue physical impression materials is a major advantage. Physical impressions can cause momentary discomfort. Children, or patients with strong gag reflex, often appear not to tolerate the traditional procedure. Therefore, replacing the use of these materials with minimally-contacting optical techniques would make the procedure more appealing (Ahlholm et al., 2018).

Several studies have indicated that optical impressions using IOSs were faster and more comfortable than conventional impression techniques (Burhardt et al., 2016; Gjelvold et al., 2016). A more recent study showed that intraoral digital impressions performed better in terms of comfort and gag reflex compared to traditional impression techniques whilst also having shorter chairside and processing times (Sfondrini et al., 2018). Similarly, patients preferred the use of intraoral digital impressions instead of conventional irreversible hydrocolloid (alginate) impressions in terms of comfort, vomiting reflex, and breathing during impression taking; however, the conventional impressions required slightly less time (Mangano et al., 2018). A different study demonstrated that two different types of IOSs required longer impression times than the conventional method, but the overall patient satisfaction was high regardless (Burzynski et al., 2018).

1.4.3 Clinical efficiency

Optical impressions have been shown to result in reduced working times when compared to conventional impressions and therefore are generally considered more time-efficient (Burhardt et al., 2016; Goracci et al., 2016). The major differences observed in time efficiency for optical impressions do not appear to arise from the impression procedure itself (relatively small chair-time differences between optical and conventional impressions may not necessarily be clinically significant), but rather from the time saved during all subsequent steps (Mangano et al., 2017). The 3D models from IOSs can be sent via email or cloud-based systems directly to the dental laboratory which is much faster than delivery via courier/mail. Additionally, there is no need to pour stone casts to obtain plaster models, a vital step for the conventional impression workflow. This not only translates to lower consumable costs but also reduces the need for storage (Zimmermann et al., 2015). Furthermore, the clinician would be able to get real-time advice from the technician and if there are any concerns with the quality of the impression, this can be repeated immediately

preventing a second appointment and loss of clinical time (Mangano et al., 2017). Eliminating these steps result in saving considerable amount of time and costs during the working year. Dental clinics equipped with integrated CAD-CAM units can offer same-day fabrication of restorations (Aragón et al., 2016; Imburgia et al., 2017). In complex cases, where multiple implants or severe undercuts render a conventional impression problematic, IOSs may offer a simplified means of recording these geometries (Abduo and Elseyoufi, 2018). Moreover, if part of the impression is not deemed satisfactory, that area can be deleted and recaptured without having to repeat the entire procedure (Mangano et al., 2017).

As each scanner utilises a specific technology, different ergonomics and software, the learning curve can be initially slow. Indeed, a study investigating experience curves of two IOSs (TRIOS and iTero) using confocal technology showed that scanning time decreased with training, though the use of TRIOS always resulted in shorter average scanning time than iTero (Kim et al., 2016).

Depending on the model, the purchasing cost of an IOS can range between 15,000 to 35,000 € (Mangano et al., 2017). This high cost may be a major drawback that currently limits the use of IOSs in clinical practice.

1.4.4 3D Surface Reconstruction

For the 3D reconstruction of the object, distances between different pictures can be estimated using an accelerometer integrated on the camera, but more often a similarity calculation of the images is performed. The latter uses algorithms to detect coincident points of measurement on different images, most notably on transition areas such as strong curvatures, physical limits and edges, or differences of grey intensity (silhouette shadowing) (Aubreton et al., 2013; Cheung et al., 2005; Richert et al., 2017). After the similarity between the images is evaluated via methods such as rotation and homothety, a transformation matrix is calculated that stitches the images together

producing a point cloud file with each point having cartesian coordinates (X, Y, Z) (Richert et al., 2017). A polygonal mesh can be interpolated from this cloud of points, representing the scanned object (Imburgia et al., 2017). An optical impression of the maxillary and mandibular dento-gingival tissues as well as their occlusal registration would result in a pair of 3D surface models which can be used as the 'virtual' alternative to traditional plaster casts (Mangano et al., 2017).

1.4.5 Mesh quality

Generated 3D datasets amongst different IOSs, may consist of different point cloud densities and subsequently, different mesh polygon densities (Nedelcu et al., 2018), such as seen in Figure 1-16~~Figure 1-16~~A. On relatively flat surfaces, a routine mesh may be created whilst a denser mesh may be constructed for surfaces with complex morphology such as incisal edges, fissures, or gingival sulci (Richert et al., 2017). IOSs producing high density point clouds can be converted more easily into an accurate virtual model of the real surface (as long as the accuracy of each point is high), while those with low density may produce 'chord errors' due to the lack of digital information between them which can cause smoother topographies, dimensional defects, non-existent curvatures, or discontinuity in the digital image (Figure 1-16~~Figure 1-16~~B) (Medina-Sotomayor et al., 2018; Tapie et al., 2015). The resolution of different clouds has been reported to range between 34.20 to 79.82 points/mm^2 (Medina-Sotomayor et al., 2018).

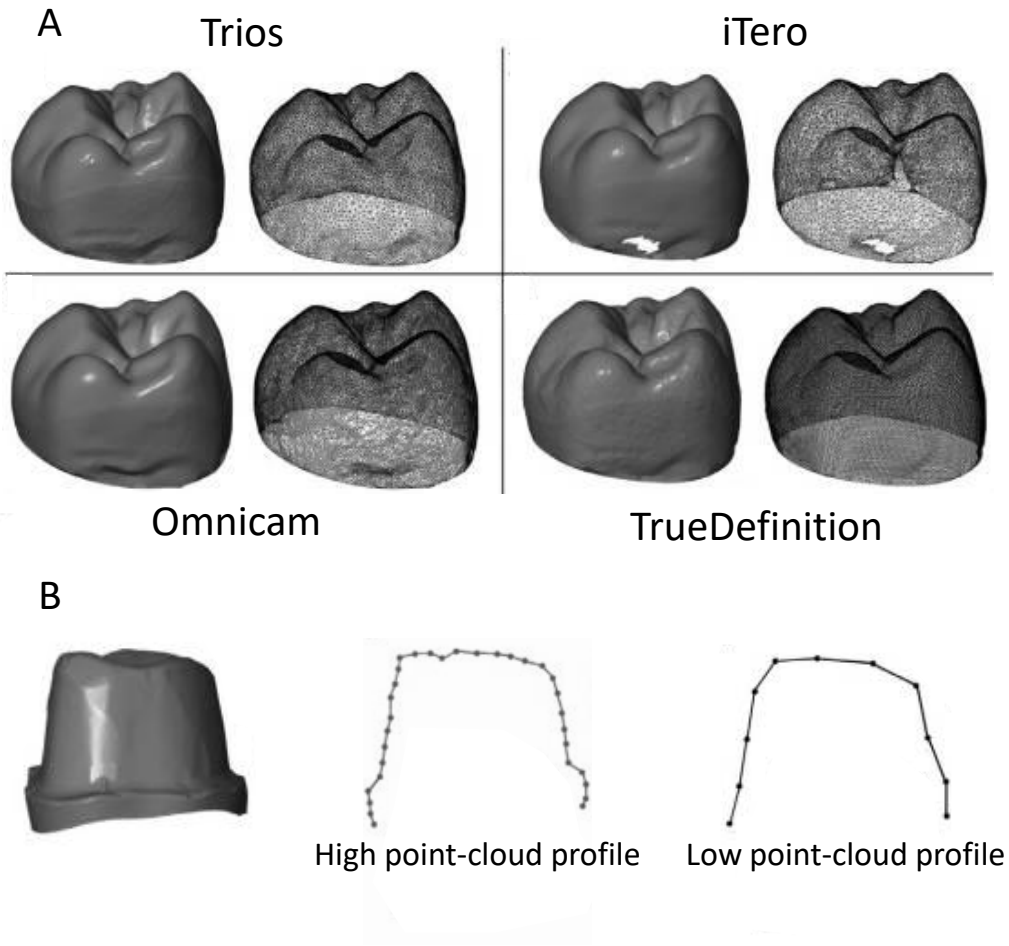

Figure 1-16 – Interpolation of point clouds into meshes.
Different IOSs produce point clouds of different densities (A). A high-density point cloud is interpolated into a more accurate profile than a low density point cloud (B) (Adapted from Jeong et al., 2016); Medina-Sotomayor et al., 2018).

1.4.6 Optical principles of IOSs

Irrespective of the type of imaging technologies used to record the 3D geometry of oral surfaces, all IOS cameras require the projection of light, which is then captured as separate images or video, and stitched together by the software by recognising overlapping points of measurements (Richert et al., 2017).

There are two ways light is projected and captured: passive or active. Passive techniques use available ambient light that illuminates the oral tissues and rely to some extent on surface texture,

while active techniques project structured lights onto the object and are less reliant on surface texture for reconstruction (Logozzo et al., 2014). Each point recorded would have three coordinates: X and Y are determined by the captured image, while Z is calculated based on the object-to-camera distance, by the proprietary technology of the device. The working principles of some of the most popular IOSs include confocal microscopy (TRIOS 3Shape, iTero Align Technology, and ZFX IntraScan), active wavefront sampling (TrueDefinition 3M), and active triangulation (Cerec Omnicam Dentsply Sirona, and CS3600 Carestream Dental, DWIO Dental Wings) (Kim et al., 2021; Zhang et al., 2021).

1.4.6.1 Optical Triangulation

Triangulation technique is described in detail in Section 1.3.3.2.1, above. It is based on the principle that the position of a point on an object can be calculated based on the known positions and angles of two points of view. These two points of view may be captured by two separate detectors, a single detector using a prism, or captured at two different times (Richert et al., 2017). In the case of IOSs, where space for the optics (seen in Figure 1-4~~Figure 1-4~~ above) is restricted, mirrors are used to deflect the light beam on to the target surface. Both passive and active triangulation methods may be used with IOSs. In active triangulation, the device projects light onto the surface and its reflection is captured to calculate the position of the target object whilst in passive triangulation there is no emission of light and the capturing of the surface is based on the detection of reflected ambient light (Logozzo et al., 2014). Furthermore, unlike profilometers that use a single point sensor to scan the entire area of a large surface, which can be time consuming; active triangulation IOSs can be more practical as they use laser strips (2D), or a projected light image with a known structure or pattern (3D) which speeds up the acquisition process (Leach, 2014; Logozzo et al., 2014). Commercial scanners that utilise this optical principle include CS3600 (Carestream Dental,

Stevenage, UK), DWIO (Dental Wings, Straumann, Basel, Switzerland), CEREC BlueCam and Omnicam (Sirona Dental Systems, Bensheim, Germany) (Kim et al., 2021; Logozzo et al., 2014).

1.4.6.2 Stereophotogrammetry

This technique is a form of passive triangulation. X, Y, Z coordinates are calculated using photogrammetric algorithms processing numerous images taken by different cameras, whose respective positions and angulations are known, based on their configuration within the optical system. A line of sight can be constructed from each camera location to the point on the object. This forms a triangulation that determines the 3D location of the point (Gangapurwala, 2021). Points with corresponding features on the different images, captured by these cameras, are identified to apply triangulation calculations, with respect to the same corresponding points on the epipolar line (Logozzo et al., 2014). The epipolar line of one camera is the straight line in its image plane that interacts with the epipolar plane. As this technique relies on passive projection of ambient light rather than having a light source, the IOS camera is relatively small and cheaper (Richert et al., 2017). However, only high contrast targets and well defined edges can be measured with high accuracy whilst featureless surfaces may not be measured at all (Logozzo et al., 2014).

1.4.6.3 Parallel Confocal Imaging

This technique is based on similar principles as confocal profilometry described in Section 1.3.3.2.2 above. It uses successive focused and defocused images from selected depths and different angles and aperture levels to infer the distance to the object which is determined by the focal length of the lens. It is sensitive to motion blur; hence the wand needs to be held steadily by the operator (Mangano et al., 2017).

A light beam passes through a pinhole on a focal filter and penetrates the target tissue. The position of the receptor sensor unit lies confocal to the target. A minute aperture is positioned in front of

the focal filter to prevent any light astray. As the focused light (good data) reflects back on the target tissue, through the wand lens, it re-enters the pinhole, to reach the sensor, whilst all out-of-focussed light (bad data) is eliminated. A 3D scan of the target is obtained by stitching tomographic slices (Figure 1-17~~Figure 1-17~~) (Sehrawat et al., 2022). Some commercial scanners that utilise this optical technique are CEREC Omnicam and Primescan (Sirona Dental Systems, Bensheim, Germany), Trios (3Shape, Copenhagen, Denmark), Planscan (Planmeca, Richardson, Texas, United States) and iTero Element® (Align Technologies, San Jose, California, USA) (Abduo and Elseyoufi, 2018; Braian and Wennerberg, 2019a).

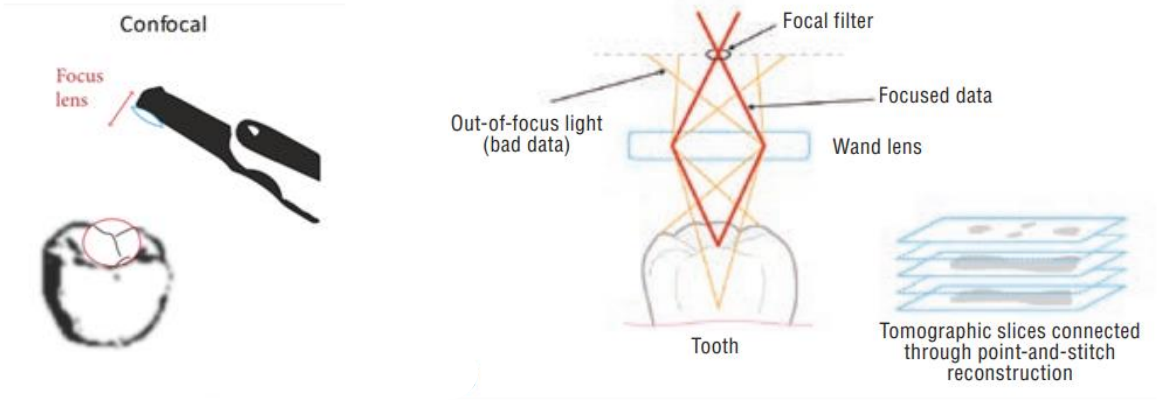

Figure 1-17 – Parallel Confocal Imaging.
This technique uses the focal length of the lens and focused and defocused images to determine distance to the object (adapted from Richert et al., 2017; Sehrawat et al., 2022).

1.4.6.4 Accordion Fringe Interferometry

Accordion Fringe Interferometry (AFI) is an imaging technology that uses two different light sources to project light through channels to produce different patterns of parallel bands, namely fringe patterns (Figure 1-18). When this pattern falls on the target object, it splits and reframes to take up a new pattern due to the unique topography of the scanned surface. A camera is used to record the curvature of the fringes i.e., the distortion in the original pattern on the object subjected to AFI. The degree of the apparent fringe curvature, coupled with the known geometries between the camera and laser source, enable the AFI algorithms to digitise the surface of the target object (Bloss, 2008;

Logozzo et al., 2014; Sehrawat et al., 2022). Dimensional Photonics International, Inc (DPI) has been developing an intraoral scanner based in these optical principles; however, it is still not available on the market (Logozzo et al., 2014).

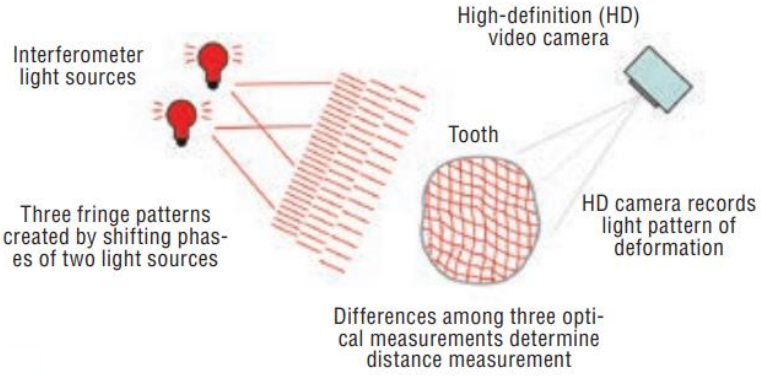

Figure 1-18 – Accordion Fringe Interferometry (Sehrawat et al., 2022).

1.4.6.5 Optical Coherence Tomography

Optical Coherence Tomography (OCT) is a high-resolution technique, based on the principle of light interferometry using broadband light, that produces cross-sectional sub-surface images. OCT works in a similar way to ultrasound but uses high frequency light instead of high frequency sound. The optical system focuses a near-infrared laser beam (820 nm) onto the target surface and detects backscattered light back to the interferometer, analysing its magnitude and echo time delay (Attin and Wegehaupt, 2014; Joshi et al., 2016; Sehrawat et al., 2022). Due to its high frequency, projected light can penetrate significantly deeper into the subsurface of tissues of up to 100 µm thick (Logozzo et al., 2014). Hence, OCT images can show light scattering intensity from different layers of hard and soft tissues. This technique is commonly used in specialised branches of medicine such as cardiology and ophthalmology. However, its use has also been reported in dental research to characterise the surface and subsurface of enamel and dentine to provide information such as enamel thickness, morphology, porosity, reflectivity and absorbance, which can be associated with the degree of

mineral loss (Attin and Wegehaupt, 2014; Joshi et al., 2016). In the case of IOSs, the spectral range of blue and ultraviolet light wavelengths would be used, as the mean scattering length of photos in tissue at these spectral regions is very short which makes it ideal to analyse the surface of the target tissue (Logozzo et al., 2014). Example of commercial scanners that utilise this optical principle is E4D (E4D, Technologies, USA) and Planscan (Planmeca Oy, Helsinki, Finland) (Logozzo et al., 2014; Wulfman et al., 2020).

1.4.6.6 Active Wavefront Sampling

This surface imaging technique refers to reconstructing 3D information from a single camera imaging system and an Active Wavefront Sampling (AWS) module by measuring depth based on the defocus of the primary optical system (Figure 1-19~~Figure 1-19~~). In its simplest form, an AWS module requires an off-axis aperture which rotates on a circular path around the optical axis. This movement produces the rotation of quasi-focused target points on a circle on the image plane (assuming the realisation of ideal non-aberrated conditions). The target point's depth information (camera-to-object distance) can be encoded from the diameter of the rotating point pattern produced by each point. A target point located on the in-focus plane will have a rotating pattern with zero diameter and thus will remain constant, whereas target points located at increasing distances from the in-focus plane will rotate along circles with increasing defocused blur-spot diameters (Heber, 2010). In principle, the AWS imaging technique allows any system with a digital camera to acquire 3D geometries, requiring only one optical path and thus eliminating the need for multiple cameras.

Aside from a rotating off-axis aperture, there are other possible paths that can be used with AWS, such as simple translations along horizontal, vertical, or diagonal lines, or in more general any path following any arbitrary closed loop. In theory, the depth can be calculated as long as the aperture

path is known. However, a simple circular aperture path is advantageous due to its relatively simple mathematical implementations.

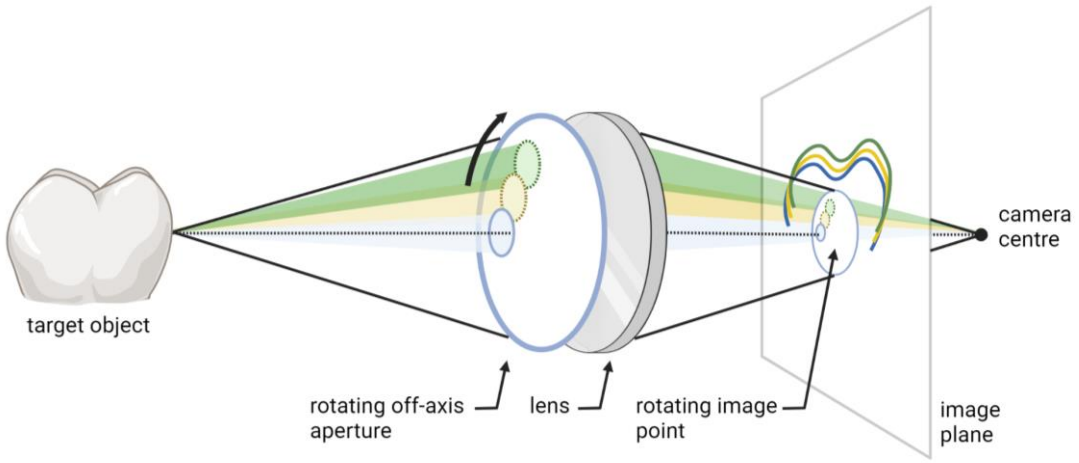

Figure 1-19 – Active Wavefront Sampling (AWS).
AWS produces rotation of points of measurement through an off-axis aperture moving on a circular path around the optical axis of the camera (Figure created with BioRender.com).

A big advantage of the AWS technique is the possibility to adjust the system with respect to accuracy and processing speed. For high-speed imaging applications where some measurement accuracy can be sacrificed, the sampling positions can be reduced to a minimum of two, whilst for high-accuracy applications, where speed can be sacrificed, a higher number of target points can be sampled for the calculation.

Two intraoral scanners utilising the active wavefront sampling principle are Lava COS (3M ESPE, St.Paul, Minnessota, USA) and its successor True Definition® scanner (Midmark Corp., Ohio, USA); the latter has been widely used throughout this thesis and is described in more detail in Chapter 2 on page 102 below.

1.4.7 Powdering

Certain IOSs require the use of a ~20 - 40 µm light powder coating, prior to the digitising process, applied with proprietary spraying devices (Richert et al., 2017). The coating serves two purposes. Firstly, it acts as an opacifier reducing the high reflectivity often seen on oral surfaces such as polished enamel and saliva-covered teeth and mucosa, which can affect the accuracy of IOSs. Secondly, the applied powder particles act as a stochastic pattern on the target surface during image stitching and 3D acquisition process (Güth et al., 2017a). Theoretically, the reproducibility of powder thickness could vary between procedures and operators which could reduce the overall quality of the scan, however, software of IOSs are capable of taking an average thickness into account (Richert et al., 2017). Furthermore, powdering can be less comfortable for patients and an inconvenience for the clinician, adding extra scanning time to the procedure, especially when contaminated with saliva as this requires cleaning and reapplication of the powder (Richert et al., 2017). Ideally, a scanner that would allow a clinician to work without the use of powder should be preferred and latest-generation devices typically use other techniques such as polarizing filters integrated to minimise light exposure from reflective surfaces (Mangano et al., 2017; Richert et al., 2017).

Several studies have previously shown that powder-based impressions are accurate for partial impressions (Güth et al., 2017a; Hack and Patzelt, 2015). An *in vitro* study using powder-based IOSs to scan a single-unit reference model suggested that excessive coating did not negatively affect the accuracy of scans (Nedelcu and Persson, 2014a). A different study reported that titanium trioxide powder application resulted in an improved vertical fit and volumetric 3D internal fit values of the luting space of crowns using a non-powder based IOS (Prudente et al., 2018). Greater homogeneity and thinner coatings 43.10 ± 14.09 µm were reported with experienced clinicians when compared to an inexperienced group (Dehurtevent et al., 2015).

1.4.8 Scanning strategy

Scanning strategy refers to a specific movement pattern in which an IOS must be used according to its manufacturer's instructions to increase the accuracy of the virtual model when a hemi or full-arch needs to be scanned. One such strategy is the occlusal-palatal-lingual path where the arch is scanned in a linear movement on all occlusal-palatal surfaces around the arch followed by the buccal surfaces. Another strategy is the zig-zag technique which involves making an 'S' sweep on buccal, occlusal, and palatal of each tooth successively. Two other scanning paths include the circular and the merging halves (Zhang et al., 2021).

Several studies have shown the influence of the scanning strategy on the accuracy of the IOS. An *in vitro* study using a TRIOS (3Shape, Copenhagen, Denmark) confocal IOS showed no statistically significant differences in trueness or precision between three different scan strategies (Müller et al., 2016). Mandelli et al., (2018) suggested that scanning separate halves and stitching them together showed better accuracy (44 µm) than continuously scanning from side to side (56 µm). A more recent study investigated four different scanning patterns using four different IOSs. They demonstrated that the stitching halves technique showed the highest overall trueness (60 µm) and precision (18 µm); however, not all scanners performed best with this technique (Latham et al., 2020). On the other hand, an *in vitro* study showed significant differences between three different scanning techniques using TRIOS IOS; however, the scanned models were completely edentulous (Zarone et al., 2020).

Depending on the scanners and their technologies, the camera should be held within a range of 5 – 30 mm of the scanned surface (Richert et al., 2017; Zimmermann et al., 2015). During the scanning process, tracking could be lost if the distance to the object or movement is too fast or too jerky. Some manufacturers include real-time guides that help the operator stay within the device range of

focus. The movement during scanning must be fluid at a steady distance and the target surface in the centre of the field of view (Richert et al., 2017). When tracking is lost, software algorithms have been developed that allow operators to continue scanning. This is done mainly by rematching saved topography, given that, prior to the loss of tracking, the scanner was able to save a meaningful area with enough information (Richert et al., 2017; Yuan et al., 2010). Gómez-Polo et al., (2021) concluded that presence of mesh holes requiring rescanning to complete the digital model decreased the accuracy of the IOS; furthermore, the number and dimensions of these negatively influenced accuracy (Gómez-Polo et al., 2021).

1.4.9 Dataset formats

The most widely used format of datasets produced by the IOSs after scanning is open-source Standard Tessellation Language (STL) or a locked proprietary STL-like file, with the latter being compatible only with 'closed' systems of the device's manufacturer (Richert et al., 2017). There are two main types of STL files: binary and ASCII. Binary STL files use binary encoding and are generally smaller and better for 3D printing than ASCII files. ASCII STL files use ASCII encoding and are generally larger than binary files, but easier to manually inspect and debug (Autodesk, 2022). Other file formats have been developed, such as Wavefront OBJ. and Polygon File Format (PLY) which aside from surface geometry, they contain additional information such as colour, transparency and texture of the oral tissues (Corbett, 2021; Mangano et al., 2017; Richert et al., 2017).

1.4.10 *In vivo* conditions

In vivo conditions may compromise the accuracy of IOSs. Patient and soft tissue mobility, limited space, presence of saliva and oral humidity, gingival-crevicular fluid, and blood make the scanning process more challenging and can lead to an increase of acquisition errors (Camardella et al., 2017a; Renne et al., 2017; Richert et al., 2017). Furthermore, in comparison to other scanning techniques,

neither the patient, nor the IOS are stationary during scanning (Richert et al., 2017). Flügge et al., (2013) showed that *in vivo* intraoral scanning of a patient was less precise (mean deviations of 50 µm) compared to *ex vivo* scanning of the patient's plaster model (mean deviations of 25 µm) using the same protocol and IOS (iTero). The more-recently introduced IOSs can capture colour and texture which can increase perception of clinical situations such as the capturing of preparation margins (Daly et al., 2021).

1.4.11 Accuracy of IOSs

Accuracy is the combination of trueness and precision. This is explained in more detail in Section 1.3.1 above. In respect to digital scanning, trueness refers to the measurement deviation of the virtual geometry from the true geometry, whereas precision describes the deviation between measurements from repeated scans (Ender et al., 2016a).

Clinical studies investigating the accuracy of IOSs are limited. This is primarily because, unlike *in vitro* studies that can utilize highly accurate desktop scanners, the 'true' geometry of the oral tissues cannot be measured directly *in vivo* and therefore no comparison can be conducted against the tested IOSs. *In vitro*, the use of plaster models, scanned by extraoral scanning technologies such as profilometers (Hartkamp et al., 2017b) or desktop laboratory scanners (Jeong et al., 2016), are currently considered the gold standard to provide reference models for comparison. However, it is difficult to compare these results with IOS data that was acquired *in vivo*, as the construction of the reference model would rely on the indirect physicochemical impression that is likely to contain inaccuracies (Jeong et al., 2016).

The accuracy of IOSs has been evaluated using different methodologies. This increases heterogeneity between studies and makes it more difficult to compare results. Overall, these methodologies consist of, but are not limited to:

a) Dimensional measurement – measuring the distance or angular deviations between two landmarks on an IOS digital model, generated either *in vivo* or *in vitro*, and comparing it to the distance between these landmarks on a physical model using high-resolution scanners or hand-held devices such as callipers as the reference (Abduo and Elseyoufi, 2018; Rajshekar et al., 2017; Rasaie et al., 2021; Zhang et al., 2021).

b) Accuracy via superimposition – quantifying the distance deviations between two virtual models after superimposing (aligning) them using surface registration software. Trueness is measured by superimposing and comparing the digital model generated by the IOS with the reference digital model, i.e., the trueness measures the deviation between the IOS and the reference models. Precision is measured by superimposing and comparing digital models generated by the same IOS, and therefore reflects the repeatability of the procedure (Abduo and Elseyoufi, 2018). The iterative closest point algorithm utilised by software to align the two datasets is described in Section 1.3.5.2.2 above.

   A similar approach described in several implant-focused studies involves superimposing reference and IOS datasets of a master model by matching standard cylinders and planes to them in order to obtain linear and angular deviations defining reference points and central axes of scan bodies (Kim et al., 2021).

c) Qualitative evaluation – following superimposition of two digital models using surface registration software, a colour map is generated with the colours representing a pattern of positive and negative differences as a function of Z between the two models (Rasaie et al., 2021). This type of evaluation is only semi-quantitative and is used to visualise differences between the digital models corroborating quantitative data.

1.4.11.1 Dimensional measurement accuracy

Camardella, Breuning, & de Vasconcellos Vilella (2017) showed that linear measurements on digital models made intraorally by TRIOS Colour IOS showed statistically significant differences compared to calliper measurements on casts made by alginate impressions. Kuhr et al., (2016) using reference measurements with a coordinate measurement machine (CMM), observed that polyether conventional impressions demonstrated the smallest deviations (min: 17 ± 12 µm, max: 43 ± 30 µm) in measuring linear distances compared to three tested IOSs. Amongst the IOSs, TrueDefinition® performed best (min: 23 ± 13 mm, max: 86 ± 73 mm) which also showed the lowest angle deviations (0.06° ± 0.07°) without statistically significant differences to the conventional impression. As the actual differences were minimal, the authors concluded that the overall performances of the IOSs were clinically acceptable.

On the other hand, J.-F. Güth et al., (2016) showed that mean (SD) trueness of TrueDefinition IOS, 89 (48) µm, measuring a metal bar fixed across a model arch was not statistically significantly different to that of a reference CMM, 77 (36) µm. A study reported that measurements of arch dimensions and tooth positions using IOS virtual models were similar to alginate impressions (Grünheid et al., 2014). Wesemann et al., (2017) reported a mean (SD) trueness of 27 (19), 50 (39), and 37 (22) µm for measuring inter-canine widths, inter-molar widths, and arch lengths, respectively, after scanning a master model with TRIOS Color IOS. These results were comparable to R700 and R900 (3Shape) desktop scanners tested in the same study.

1.4.11.2 Accuracy via superimposition

Several studies showed that IOSs had a suitable accuracy, for single-tooth scanning. Rudolph et al., (2016) showed that the use of four different IOSs (Cerec Bluecam, Cadent iTero, Lava C.O.S, and TRIOS) *in vitro* resulted in trueness ranging from 6.4 µm to 14.4 µm, after superimposing their virtual

models with those made by a high-precision optical white light fringe projection system as the reference. Another study evaluating the accuracy of four IOSs (TRIOS, D700, MHT, inEos) for single-tooth scanning reported a mean precision range of 3.35 – 12.49 µm using ten repeated scans and a mean (SD) trueness range of 61.89 ± 3.45 µm to 71.19 ± 1.70 µm, via superimposition using a micro-CT as the reference device; however, the accuracy of the micro-CT and its traceability to a reference device was not mentioned in the study (Yang et al., 2015). Similarly, Lee et al., (2017) and Rudolph et al., (2016) showed trueness and precision of 17.5 µm and 12.7 µm, respectively, for Cerec Bluecam IOS, and 13.8 and 12.5 µm for Cerec Omnicam IOS. R. G. Nedelcu & Persson, (2014b) showed that the accuracy differed between four IOSs for crown preparation scanning; a similar mean (SD) accuracy was found for Lava COS 12-17 (12-14) µm, Cerec Bluecam 8-14 (12-13) µm, and iTero 7-16 (10-19) µm, which was greater than E4D IOS, 29-40 (31-46) µm. Furthermore, the accuracy was shown to be influenced by the type of scanned surface substrate, where zirconia scanning tended to be more accurate, followed by titanium and polymethyl methacrylate (PMMA). A study investigating the marginal fit of crowns comparing two IOSs, a laboratory scanner, and conventional impressions, demonstrated comparable and clinically acceptable results with TrueDefinition and TRIOS scans, producing marginal gaps of 88 (95% C.I. 68-136) µm and 112 (95% C.I. 94-149) µm (Boeddinghaus et al., 2015).

Regarding short-span scanning, it has been suggested that IOS systems are satisfactorily accurate and comparable to indirect scanning of conventional impressions by laboratory scanners (Abduo and Elseyoufi, 2018). For scanning of three-unit prostheses, it was reported that following superimposition, the mean (SD) trueness of iTero and Lava COS IOSs showed trueness of 23 (3) µm and 36 (19) µm, respectively, that was not statistically significant with laboratory scanning of conventional impressions, 44 (18) µm. However, other IOSs, Cerec Bluecam, 68 (12) µm and E4D, 84 (4) µm showed inferior trueness (Ali, 2015). Another study showed that models produced by IOSs

had greater trueness than digitised casts produced by conventional impressions for four-unit bridge scanning (J.-F. F. Güth et al., 2013). More recently, the same research group evaluated the accuracy of five IOSs and showed that TrueDefinition and CS3500 IOSs exhibited the highest overall trueness and precision, both performing better than indirect digitisation of an impression using a D-810 laboratory scanner (Güth et al., 2017a). The other three IOSs (Cerec Bluecam, Zfx Intrascan, and Cerec Omnicam) had worse trueness than the control group. In a different study, it was shown that although generally IOSs showed lower trueness and precision than a D800 laboratory scanner for sextant scanning, the differences were marginal and therefore clinically acceptable. In fact, Planscan IOS showed better trueness, 51.2 µm, and very similar precision, 79.8 µm, than D800 which showed trueness and precision of 53.0 µm and 79.0 µm, respectively (Renne et al., 2017). An *in vivo* clinical study reported that quadrant scanning by seven IOSs had a superior mean (SD) precision to extraoral scanning of casts produced by partial-tray polyvinyl siloxane (PVS) impressions, 58.5 (22.8) µm; however, all were inferior to full-tray impressions, 18.8 (7.1) µm. True Definition IOS showed the highest mean (SD) precision of 21.8 (7.4) µm (Ender et al., 2016b).

Based on whole arch studies, it is generally accepted that there is a reduction in accuracy of IOSs as the scanning span increases due to the propagation of errors arising during the stitching of multiple images (Abduo and Elseyoufi, 2018; Renne et al., 2017). Renne et al., (2017) suggested that scanning a whole arch resulted in less trueness and precision than sextant scanning. A clinical study reported that polyether impressions of four defined spheres fixed across patients' dental arches and scanned by a high-precision CMM showed trueness of 15 ± 4 µm via a superimposition procedure and were more accurate than the tested IOSs. However, TrueDefinition and Cara Trios showed comparable trueness of 23 ± 9 µm and 37 ± 14 µm, respectively, whereas Cerec Omnicam showed an inferior trueness of 214 ± 38 µm (Kuhr et al., 2016). Ender & Mehl, (2013) showed that digital impressions of a reference steel model were less accurate than conventional impressions with a mean trueness

of 58.6 (15.8) µm and precision 32.4 (9.6) µm. Another clinical study showed that intraoral scanning with iTero IOS resulted in the lowest precision, 50 µm, followed by scanning a cast made from a conventional impression with the same IOS, 25 µm, whilst laboratory scanning of the cast was the most precise, 10 µm (Flügge et al., 2013). Jeong et al., (2016) showed that PVS impression scanned by a laboratory scanner was more precise, 78 µm, than Cerec Bluecam, 116 µm, but less than Cerec Omnicam IOS, 58 µm. Cerec Omnicam IOS and the scanned conventional impression showed similar trueness of 197 µm and 170 µm, respectively, compared to Cerec Bluecam IOS, 378 µm. Gan et al., 2016 investigated the accuracy of Trios IOS for the maxillary dentition as well as the palatal soft tissues using a laboratory scanner as the gold standard. For scanning the whole maxillary dentition, the trueness and precision were 80.01 ± 17.78 µm and 59.52 ± 11.29 µm, respectively, whilst for the palatal soft tissues, were 130.54 ± 33.95 µm and 55.26 ± 11.21 µm. An *in vitro* study found that four of the five tested IOSs showed comparable levels of trueness and precision in full-arch scans than an industrial lab-scanner (Patzelt et al., 2014).

For the provision of dental implants, previous studies have suggested that IOS impressions of single implants showed a satisfactory accuracy (Delize et al., 2019; Zhang et al., 2019). However, a recent systematic review concluded that its appraised studies investigating full-arch intraoral scanning revealed errors that were too large (trueness ranged from 7.6 to 731.7 µm and precision ranged from 15.2 to 204.2 µm) for clinical application (Zhang et al., 2021). Another systematic review and meta-analysis suggested that the reported distance and angulation errors were too great for multi-unit prostheses (Flügge et al., 2018). In contrast, as systematic review by Wulfman et al., (2020) concluded that digital scanning of multiple implants in edentulous patients were similarly accurate as conventional impressions *in vitro.* In another study, TrueDefinition and CEREC Omnicam IOSs were significantly more accurate with less 3D-deviations than conventional impressions of five internal connection-implant analogues (Amin et al., 2017a).

1.4.12 Measuring surface wear using IOSs

Whilst IOSs primarily designed for digital production of CAD/CAM restorations, their advancing technologies may provide a more suitable means of directly quantifying ETW progression in both clinical practice and laboratory experimentation. In recent years there has been an increase in the number of studies utilising IOSs for investigating wear. Table 1-2 below shows a summary of all the *in vivo* and *in vitro* studies investigating surface loss/wear using IOS systems after a literature search was conducted. The details of the search strategy can be seen in the Appendix , page 279. Twenty-two studies were identified of which ten were clinical *in vivo* studies (Aladağ et al., 2019; Alaraudanjoki et al., 2017; Bronkhorst et al., 2022; Esquivel-Upshaw et al., 2020; V. D.-F. García et al., 2022a; Hartkamp et al., 2017a; Marro et al., 2022; O'Toole et al., 2020; Schlenz et al., 2022; Travassos da Rosa Moreira Bastos et al., 2021a) and twelve were *in vitro* (Alwadai et al., 2020; Charalambous et al., 2022, 2021; Hartkamp et al., 2017b; Kühne et al., 2021; Kumar et al., 2019; Marro et al., 2020, 2018a; Meireles et al., 2016a; Michou et al., 2020; Mitrirattanakul et al., 2022a; Witecy et al., 2021).

Of the *in vivo* studies, none utilised a reference device for comparison with the use of IOSs intraorally. However, three studies used qualitative tooth wear indices during clinical examinations (Alaraudanjoki et al., 2017; V. D.-F. García et al., 2022a; Travassos da Rosa Moreira Bastos et al., 2021a). Victor et al., (2022) showed that, compared to the Smith and Knight wear index, digital impressions taken by TrueDefinition IOS *in vivo* resulted in an overall 100% sensitivity and 84.95% specificity for measuring dental wear. Similarly, a study reported no statistically significant differences between qualitative wear index assessment of clinical examinations, photographic examinations, and virtual models of Trios Pod IOS (Travassos da Rosa Moreira Bastos et al., 2021a). On the other hand, Alaraudanjoki et al., (2017) suggested that ETW was recorded as more severe in

virtual models of iTero IOS than clinical examination. The rest of the *in vivo* studies demonstrated a progression of tooth tissue loss with time suggesting that intraoral scanners would be useful as diagnostic tools in monitoring wear (Aladağ et al., 2019; Hartkamp et al., 2017a; O'Toole et al., 2020; Schlenz et al., 2022). O'Toole et al., (2020) described that wear analysis of bimaxillary digital intraoral scans of 30 patients over three years using TrueDefinition IOS demonstrated volumetric wear progression using incisors and molars as index teeth. Another clinical study investigated ETW of mandibular molars in young adults utilising Trios3 IOS. They suggested that following 3D superimposition analysis of the IOS datasets the maximum vertical tissue loss over 12 months ranged between 34 (95%CI 27,36) µm and 43 (38,47) µm (Schlenz et al., 2022).

The majority of the studies that investigated surface loss using IOSs were carried out within a laboratory setting. Marro et al., (2018) showed that ETW changes could be detected better with 3D virtual models by Trios IOS than casts using the BEWE index. Another study investigated the accuracy of two IOSs, Trios3 and CS3600, at measuring simulated enamel wear at different levels compared to an optical profilometer as the gold standard. They reported that, both IOSs were able to measure the progression of wear from ∼15 to ∼110 µm, having good agreement with the profilometer regardless of the order of the tissue loss (Witecy et al., 2021). Kühne et al., (2021) investigated the suitability of Cerec Omnicam, Trios3, and TrueDefinition IOSs for wear measurements (221 – 417 µm) on a zirconia cast of teeth 24-28 (FDI). Compared to profilometry, they reported differences from 0% up to +19% for Cerec Omnicam, -3% up to +13% for TrueDefinition, and ±2% up to +16% with Trios3 for the different levels of simulated wear. Furthermore, good quantitative agreement was observed when comparing depth and volume measurements obtained from micro-CT and TrueDefinition IOS scanning of a typodont model (Esquivel-Upshaw et al., 2020). Furthermore, Hartkamp, Peters, et al., (2017) showed that for simulated wear depths from 73 to 96 µm the maximum difference between the data obtained from profilometry and Lava C.O.S IOS was 12.6%,

which was equal to a metrical value of 15 µm. Two studies which are part of this thesis and are described in more detail in Chapter 3 and Chapter 5 below showed that the depth discrimination threshold of TrueDefinition IOS in measuring surface change on polished enamel was 44 µm (Charalambous et al., 2021) and 73 µm on natural unpolished enamel samples (Charalambous et al., 2022).

The methodologies among the studies investigating surface loss using IOS systems varied considerably. The surface substrate used for scanning included polished enamel (Charalambous et al., 2021; Witecy et al., 2021), natural enamel (Charalambous et al., 2022; Meireles et al., 2016a), extracted teeth (Alwadai et al., 2020; Meireles et al., 2016a; Michou et al., 2020), phantom teeth (Hartkamp et al., 2017b), zirconia casts (Kühne et al., 2021), and plaster casts (Marro et al., 2020, 2018a). The majority of studies used 3D superimposition analysis between two datasets to determine depth of volumetric analysis; whilst one relied on step height analysis on single scans (Charalambous et al., 2021). Furthermore, the majority of the studies have utilised external engineering or metrology software for the analysis of the IOS's datasets; however, certain IOSs offer internal software functions or apps made by the same manufacturer that allow quantification of surface loss such as the Trios patient monitoring app (Witecy et al., 2021), and OraCheck (Dentsply Sirona, North Carolina, United States) (Hartkamp et al., 2017b).

Table 1-2 – *In vivo* (grey-shaded) and *in vitro* (white-shaded) studies investigating surface loss/wear using IOS systems.

Study	Study type	Intraoral scanner	Reference device	Surface scanned/analysed	Study methodology	Result
Schlenz et al., (2022)	*In vivo*	3Shape Trios3	n/a	Occlusal surface of patients' mandibular teeth #36 or #46	Baseline (T0) and second intraoral scan (T1) after 373 days were superimposed with 3D analysis software (GOM Inspect). The occlusal surface of the study tooth was divided into 7 areas (5 cusps, 2 ridges) and maximum vertical substance loss was measured between T0 and T1.	The mesiobuccal cusps showed the greatest amount of wear (43, 38/47 µm; median, 95%CI) followed by distobuccal (36, 33/39 µm), mesiolingual (35, 26/40 µm), distolingual (34, 27/36 µm) and distal (31, 25/34 µm).
García et al., (2022)	*In vivo*	3M True Definition	n/a Smith and Knight tooth wear index	Patients' dental arches. Sextants were used for superimposition.	The scans were conducted at baseline, 6 months, and 12 months. The baseline and subsequent scans were superimposed, and 3D compared using Geomagic software. Sensitivity and specificity were calculated using the Smith and Knight index as the reference method of evaluating wear.	The overall sensitivity and predictive values were 100%, while the specificity and positive predictive values decreased to 84.9% and 71.0%, respectively.
Bronkhorst et al., (2022)	*In vivo*	3M True Definition 3M ESPE Lava	n/a	Scanning patients' full arches but comparing surface changes on single teeth	Scans of 55 patients' dentitions by an IOS were made at baseline, year 1, year 3, and year 5. The precision of a 3D wear protocol for measuring wear though maximum height loss (mm) and volume change (mm^3) was investigated prospectively at 1, 3, 5 year intervals to determine rates of wear. Measurements of the two individual scanners used were combined together and not presented separately.	For protocol precision, the mean difference was 0.015 mm (-0.002; 0.032, p = 0.076) for height and -0.111 mm^3 (-0.250; 0.023, p = 0.101) for volume. The duplicate measurement error was 0.062 mm for height and 0.268 mm^3 for volume. The height measurements were precise for wear measurements after year-3 and year-5 intervals; however, volume measurements were susceptible to procedural error and operator sensitivity. The 3D wear assessment protocol was precise enough to adequately measure tooth height loss after intervals of a minimum of 3 years or in patients with severe wear progression, but it is not suited to measuring volumetric changes.
Marro et al., (2022)	*In vitro*	3Shape Trios3	n/a	Scanning patients' full arches but comparing surface changes on first permanent molars and central upper incisors chosen as index teeth after	IOS scans of 70 patients' dentitions were made at baseline and after 1 year. WearCompare 3D comparison was performed to measure wear progression (volume loss per mm^2).	The mean volume loss per mm^2 of dental surfaces was -0.013 mm^3 (SD: 0.009). Greater volume loss was observed amongst adolescents with higher baseline BEWE scores and those whose parents had lower education as well as on molar than incisor surfaces.

				sectioning the scans to single teeth		
Travassos da Rosa Moreira Bastos et al., (2021)	*In vivo*	3Shape TRIOS Pod	n/a Mockers et al modified tooth wear index	Both arches of patients	Tooth wear was qualitatively evaluated utilising a modified classification tooth wear index (Mockers et al) after conducting a clinical examination, and obtaining intraoral photographs, and coloured scans from the IOS. The digital scans were assessed using OrthoAnalyzer™ 3D software (OrthoAnalyzer Orthodontics, 3Shape Medical A/S, Copenhagen, DK).	There was no significant difference among clinical, photographic exams and IOS analysis for each evaluator ($p = 0.7343$ for examiner 1 and $p = 0.8007$ for examiner 2)
O'Toole et al., (2020)	*In vivo*	3M True Definition	n/a	The occlusal/incisal surface of each tooth excluding 3rd molars, was analysed. The occlusal surfaces of the first molars and the incisal surface of the upper central incisors were chosen as index teeth and wear on these surfaces was compared to the mean wear on all surfaces.	Bimaxillary digital intraoral scans of 30 patients were taken at baseline and at 3 years (±10 months). The scans from the IOS were analysed using purpose-built freeware, WearCompare. An initial feature-based global alignment on the full arch was performed. A selective surface alignment protocol was then adopted using buccal and lingual surfaces as the reference areas to perform a refined iterative closest point (ICP) alignment. Following alignment, the volume change in mm^3 over the occlusal surface, as determined by the software, was recorded in addition to the volume loss per mm^2 of surface area. The alignment quality was noted by quantifying the percentage of data points within 25 microns of each other	Per patient, mean volume loss (95%CI) was -0.91mm^3 (-1.28,-0.53) on all surfaces, -1.85mm^3(-2.83,-0.86) on index surfaces, -2.53mm^3(-3.91,-1.15) on molar surfaces and -0.83 mm^3(-1.34,-0.31) on upper central incisal surfaces. Statistical differences were observed between analysing all surfaces and index teeth ($p = 0.002$) in addition to molar surfaces ($p<0.0001$). Mean volume loss per mm^2 of surface analysed was -0.024 mm^3 (-0.031,-0.017), -0.028mm^3 (-0.041,-0.014), -0.030mm^3 (-0.046,-0.013) and -0.025mm^3 (-0.041,-0.010) for all surfaces, index surfaces, first molar surfaces and central incisor surfaces, respectively, with no statistical differences between groups.
Esquivel-Upshaw et al., (2020)	*In vivo* (only IOS) and *In vitro* (IOS and micro-CT)	3M True Definition	X-ray computed microtomography (micro-CT) measurements	Quadrants of patients' teeth with a metal-ceramic and monolithic zirconia crowns as well as enamel surfaces of antagonists. A maxillary left first molar Dentoform® (Columbia Dentoform®) tooth was scanned in vitro	Thirty prepared teeth of patients were randomized to receive a monolithic zirconia or metal-ceramic crown. After cementation, quadrants were scanned using an IOS. Patients were recalled at 6-months and 1-year for re-scanning. Scanned images were compared using a software (Geomagic Control 2014) to determine maximum vertical wear and volume loss (mm3) of teeth. Separately, the scanning accuracy of the IOS was compared with X-ray computed microtomography (micro-CT) measurements for scanning a maxillary first molar dentoform. Maximum depth and volume wear were analyzed based on the surface determination for	There was no significant difference between the wear of enamel against polished monolithic zirconia crowns and enamel against enamel. Validity measurement with micro-CT - Regression analysis showed that dental wear values estimated by intraoral scanning employing the metrology software as a tool agree with the depth and volume wear quantification based on micro-CT analysis using surface determinations and wall thickness analysis procedures in VGStudio Max 3.0. Good quantitative agreement was observed when comparing depth (R^2=0.9980) and

				for the validation accuracy of IOS and micro-CT	Dentoform® tooth baseline and wear tooth samples using VGStudio Max 3.0 (Volume Graphics, Heidelberg, Germany). Wear levels used from approximately 40 -300 µm	volume measurements (R^2=0.9984) obtained from micro-CT and intraoral scanning approaches.
Aladağ et al., (2019)	*In vivo*	Cerec Bluecam	n/a	Patients' sextant containing a cemented molar crown, from the distal surface of second molar to the mesial surface of second premolar tooth. The same procedure was applied to the antagonistic jaw with natural first molar in occlusion.	Crowns of 4 different materials: [lithium disilicate (IPS E-max CAD), lithium silicate and zirconia based (Vita Suprinity CAD), resin matrix ceramic material (Cerasmart, GC), and dual matrix (Vita Enamic CAD) blocks.] and the enamel surface of the antagonist were scanned with the IOS at baseline (24hr after cementation), 3 months, and 6 months. Digital impressions were superimposed on software (David-Laserscanner, V3.10.4, Berlin, Germany). These superimposed images were then converted into digital solid models by using software (Siemens Unigraphics NX 10, Siemens PLM Software, Plano, TX, USA). Volume loss due to wear was calculated from baseline to follow-up periods.	All materials including enamel showed increased volume loss due to wear from baseline to 6months.
Alaraudanjoki et al., (2017)	*In vivo*	Cadent iTero	n/a BEWE index	Natural dentition full arches	3D models were obtained using an iTero 3D scanner. The 3D models were assessed on a PC screen using 3Shape Ortho Analyzer™ software. Erosive tooth wear was assessed using the BEWE index and the same scoring criteria as in the clinical examination	Erosive tooth wear was recorded as more severe in 3D models than in the clinical examination, and inter-method agreement was 0.41 for severe erosive wear (BEWE sum > 8). The biggest inter-method differences were found in upper posterior sextants
Hartkamp, Lohbauer and Reich, (2017)	*In vivo*	3M Lava C.O.S.	n/a	13 zirconia crowns cemented on patients' teeth together with their respective neighbouring teeth and corresponding antagonists	The zirconia crowns and corresponding neighbouring and antagonist teeth were scanned using the IOS at baseline, 12 and 24 months after crown placement. Geomagic Qualify software was used to superimpose the follow-up data sets onto the corresponding baseline data set, identify wear sites, and measure maximum vertical height loss in each individual wear site.	The maximum mean (SD) wear in the overall sample with a total of nine patients, 13 antagonist units, and 98 evaluable wear sites was 86 ± 23 µm at 12 months, and 103 ± 39 µm at 24 months. The maximum mean wear in the enamel antagonist sub-group was 87 ± 41 µm at 12 months, and 115 ± 71 µm at 24 months; and in the ceramic antagonist subgroup 107 ± 22 µm at 12 months, and 120 ± 27 µm at 24 months
Mitrirattanakul et al., (2022)	*In vitro*	Cadent iTero Element 2	Micro computed tomography (micro-CT)	20 human premolars	Baseline and post wear scans by the IOS and the micro-CT were conducted to measure tooth surface loss in the ranges 50-200 µm, 200-400 µm, and 400-750 µm	The specificity, PPV, and accuracy of the IOS in measuring experimental tooth surface loss were 98%, 98%, and 97%, respectively.
Charalambous et al., (2022)	*In vitro*	3M True Definition	optical profilometry	Natural enamel slabs	Baseline and post-wear scans were aligned using ICP alignment (Geomagic software) and subtracted from each	The depth discrimination threshold of the IOS was approx. 70 microns.

					other (Mountains8 software). Surface loss was measured using the IOS and compared to profilometry.	
Kühne et al., (2021)	*In vitro*	Cerec Omnicam 3Shape Trios3 3M True Definition	optical profilometry	Zirconia cast presenting the teeth 24-28 (FDI). One wear-facet on FDI 26 and FDI 27	The scans of the zirconia cast were conducted at baseline (t0) and at three different stages of simulated wear (t1–t3), each at one wear-facet on FDI 26 and FDI 27. Profilometry was used as a reference method. Within each acquisition system, the maximum vertical wear at each facet was analysed by superimposing the STL data of t0 with t1–t3. During superimposition, ICP surface registration using reference areas (reference-based superimposition)	At wear-facet FDI 27, differences from +4% t1 TD up to +19% t2 OC, corresponding to a metric value of 8 µm and 45 µm, were measured. At FDI 26 deviations between −2% t1 Tr3, and +10% OC and Tr3, were observed.
Witecy et al., (2021)	*In vitro*	3Shape Trios3 Carestream CS3600	optical profilometry (only on polished enamel)	Polished enamel Natural enamel (no profilometric data)	The polished enamel samples were scanned using the two IOSs and profilometry at increasing depths (µm) (approx. 18-110 µm). The natural enamel samples were scanned using the two IOSs without a profilometer. IOS datasets (T0 to T8) were analyzed with an external 3-D measurement software (TRIe and CARe) as well as with the internal software using measuring tools of the IOS (TRIi and CARi). Best-fit ICP alignment was used to measure vertical tissue loss.	Profilometry revealed a mean (±SD) tissue loss of 17.1 ± 4.7 µm after 30-s etching steps and 10.1 ± 5.1 µm after the 15-s etching steps. IOSs and software types were able to detect the progression of tissue loss after each etching step ($p \leq 0.001$ each); Bland- Altmann plots revealed good agreement with PRO regardless of the order of tissue loss, and no systematic difference was found. Increasing cupped lesion depths were detected by all IOSs, with no significant differences between IOSs and analysis methods. IOSs were able to detect small amounts of tissue loss under simulated clinical conditions and seem to be a promising tool for monitoring even initial erosive tooth wear.
Charalambous et al., (2021)	*In vitro*	3M True Definition	optical profilometry	Polished enamel slabs	The enamel samples were scanned using the IOS and profilometer at increasing enamel loss step height depths (µm) (1.87-86.46 µm) and quantified according to ISO:5436-1. Mountains8 surface metrology software was used. Step-height analysis was corroborated by Gaussian skewness (Ssk) and kurtosis (Sku) analysis, to assess the minimum step height measured on each enamel sample.	On polished enamel, the automated minimum detectable step height measurable on each sample was 44 µm. No statistically significantly different step-height enamel lesion measurements were observed between NCLP and IOS above this threshold ($p>0.05$).
Alwadai et al., (2020)	*In vitro*	3M True Definition	cross-polarization optical coherence tomography (CP-OCT) and micro-	Occlusal surfaces of premolars	Ten sound extracted human premolars were selected and submitted to four occlusal tooth wear simulation levels in 0.5-mm steps (0/0.5/1.0/1.5 mm). The occlusal surface of each premolar was scanned at each step using an IOS, followed by morphological characterization using standard topography attributes (Slope, Relief, RFI, OPCr). Differences were assessed in	Using the IOS, topography parameters were shown to reflect surface changes between the progressive wear stages of each cast Slope decreased consistently from 0.5 to 1.5 mm, as did Relief and RFI. OPCr demonstrated a positive association with wear levels, since more worn casts had higher patch counts and respective OPCr values

			computed tomography (μ-CT) were also used to measure enamel thickness		simulated wear levels for the μ-CT and CP-OCT data as well as the topography values. Correlations were also calculated between the μ-CT/CP-OCT and topography data. Meshlab and Geomagic Wrap were used for analysis. These edited scans were then imported into RStudio software (RStudio, Inc., Boston, MA, USA) to produce the four topography parameters of interest	
Michou et al., (2020)	*In vitro*	3Shape Trios	n/a	Two shortened dental arches of assembled extracted permanent teeth. Twelve (N=12) sound human teeth (anterior and posterior) were used.	The two shortened artificial dental arches and scanned at different intervals with an IOS before and after an erosion/abrasion protocol to obtain 3D models at different time points. Median profile difference (IQR) [mm] as tooth surface loss was measured	The overall median surface profile difference between the baseline models and those obtained following erosive-abrasive challenge gradually increased from 0.01mm (IQR=0.02) to 0.18mm (IQR=0.03) after 6 h and, for the first dental semi-arch, up to 0.32mm (IQR=0.04) after 24 h. The first significant surface profile difference considering the median from both models was 0.11mm (IQR = 0.02, p=0.038). Mean surface profile difference when assessing the alignment of identical 3D models was 0.00mm (SD=0.00); this value after alignment of non-identical 3D models of the same dental semi-arch was 0.00mm (SD = 0.01 mm).
Marro et al., (2020)	*In vitro*	3Shape Trios	n/a	Pre- and post-orthodontic casts (29.5 months apart) Occlusal surfaces of first molars were analysed.	3D models were superimposed using an initial global ICP alignment with a more refined ICP alignment on non-worn areas. WearCompare software was used for the analysis. The measured outputs were volume change (mm3), volume change/ mm^2 (mm^3), maximum point loss (μm) and mean profile loss (μm).	42 teeth showed no wear progression whilst 54 teeth showed progression The progression group was -2.19 mm^3 (IQR -3.65, -0.91) and non-progression was -0.37 mm^3 (IQR-1.02, 0.16), ($p < 0.001$). Overall, the volume loss (in mm^3) differed significantly between groups, whereas the maximum point loss and mean profile loss did not.
Kumar et al., (2018)	*In vitro*	3M True Definition	n/a	Buccal surfaces of natural enamel (n=8)	Baseline and post-wear scans were superimposed with ICP-alignment using Geomagic Control. Maximum profile loss, average profile loss, and volume change were measured.	Wear correlated with increasing acid exposure for both maximum profile loss wear ($r=0.877$ $p < 0.001$) and average profile loss ($r=0.663$ $p=0.019$) respectively. Volume measurements were inconsistent at this level of wear. After the first 10-minute immersion volume change (mm^3) was -0.45 mm^3 (±2.59) which increased to -1.31 (±3.78) mm^3. Large standard deviations were noted and a poor correlation (r=0.074) with
Marro et al., (2018)	*In vitro*	3Shape Trios	n/a	Orthodontic casts (n=240)	A total of 480 pre-treatment and 2-year post-treatment orthodontic models (n=240 cast models and n=240 3D image	A strong significant correlation (τb: 0.74; $p < 0.001$) was shown between both methods However, 3D image-

			BEWE index on models		replicas) from 120 adolescents treated. 3D image replicas from the cast models at baseline and follow-up were obtained from the IOS and were transferred to the software Preview 8.1 which allowed the zooming in, rotation and inclination of the images during examination of the models. Qualitative assessment was carried out using BEWE index on casts and 3D models.	BEWE index combination showed a higher probability for detecting initial surface changes and scored significantly higher than casts ($p < 0.001$).
Hartkamp et al., (2017)	*In vitro*	3M Lava C.O.S	optical profilometry	Cobalt chromium alloy phantom tooth sandblasted with 50 µm alumina oxide	The phantom tooth was scanned 6 times at 4 different wear points [baseline, wear 1, wear 2, wear 3]. The 3D models were superimposed (best-fit algorithm) against the baseline with and without excluding the lesion area using Geomagic Qualify. Aside from Geomagic Qualify, Oracheck wear analysis application was used to measure mean maximum vertical height loss.	Apart from one outlier of 16% difference between the data obtained from profilometry and IOS, the maximum difference was 12.6%, which was equal to a metrical value of 15 µm. For the corresponding values, which were calculated with Geomagic Qualify and Oracheck at identical wear facets, maximum differences between +7% and -6.7% were obtained.
Meireles et al., (2016)	*In vitro*	3M Lava C.O.S	n/a	Extracted teeth	Scanning with IOS at 4 different levels of wear [baseline, 1 min, 5 mins, 10 mins of phosphoric acid erosion. Superimposition (ICP algorithm) was applied with baseline datasets to measure volume loss in mm^3	Volume loss median for the three exposure times: 0.88 (1 min), 4.12 (5 min), and 9.19 mm^3 (10 min). p-values of 0.000 show a significant difference for the exposure times.

1.5 Overall aims and objectives

1.5.1 Methodology outline

A series of distinct experiments were systematically conducted to investigate factors related to intraoral scanning, measuring surface roughness and form changes, and developing dedicated software analysis workflows for flat and freeform surfaces. Chapter 2 investigated IOS-TD's accuracy using two different handling techniques (handheld Vs jig-guided scanning) as well as different surface-to-camera distances. Furthermore, its titanium dioxide (TiO2) scanning powder required for scanning was characterised. Chapter 3 investigated the IOS-TD accuracy to measure roughness on flat textured surfaces as well as its threshold for measuring grooves of different depths on polished human enamel. Chapter 4 focused solely on profilometric data to compare two bi-scan analyses namely, surface-subtraction and surface-registration analyses. Both were also compared the gold standard single-scan analysis technique. Chapter 5 investigated further the measurement errors of four different bi-scan analyses using mathematically-created craters of known depths on freeform softgauges. These consisted of two analyses involving surface-registration alone, with best-fit or reference-based alignment, and two combining surface-registration and surface-subtraction, with best-fit or reference-based alignment. Consequently, using the combination of referenced-based surface-registration and surface-subtraction, the IOS-TD threshold to measure craters of different depths on natural human enamel was determined by comparing its measurements to profilometry. Finally, Chapter 6 investigated the effect of different scan sizes (cusp/tooth/sextant/quadrant/full-arch) on the accuracy of the IOS-TD for measuring different crater depths.

1.5.2 Aims

The overall aim of this thesis were to:

1. Determine the depth measurement threshold and accuracy of a clinical IOS to detect and quantify surface loss.

1.5.3 Objectives

1. To investigate the factors of scanner handling technique and surface-to-camera distance on the accuracy of the IOS and characterise the powdering layer required for scanning.
2. To determine the depth measurement threshold of the IOS for measuring grooves on polished human enamel surfaces, using NCLP as the gold standard to compare step height and area data, as well as compare surface roughness data on textured surfaces.
3. To compare surface loss measurements of polished enamel grooves using a single scan analysis, a bi-scan surface-subtraction analysis, and a bi-scan surface-registration analysis.
4. To develop and validate a surface analysis technique using metrology software and sequential scans from the IOS and NCLP to quantify surface loss on freeform surfaces such as seen in natural enamel.
5. To determine the depth measurement threshold of IOS on natural human enamel surfaces, using the gold standard NCLP for comparison of step height measurements of enamel craters.
6. To investigate the effect of crater diameter on the accuracy of IOS for measuring surface change

1.6 To investigate the effect of different scan sizes, ranging from a cusp to a full-arch scan, on the accuracy of the IOS in measuring surface change of different depths.Overall null hypotheses

1. The scanner handling technique would not affect the accuracy of the IOS for measuring surface loss.

2. The IOS measurements of surface roughness on different textured surfaces would be the same as the NCLP.
3. The IOS step height measurements would be the same as the NCLP for measuring grooves of different depths on polished enamel using a single scan technique.
4. There would be no differences between single-scan, bi-scan surface-subtraction, and bi-scan surface-registration analyses for measuring crater depths on polished enamel surfaces using profilometry.
5. There would be no differences in the accuracy of four different bi-scan analysis techniques for measuring mathematically-simulated crater depths on freeform softgauges.
6. The accuracy of the IOS (compared to the NCLP measurements), would be the same for measuring surface loss (craters of different depths) on natural enamel surfaces.
7. The accuracy of the IOS (compared to the NCLP measurements) would be the same for measuring surface loss (craters) of different diameters on natural enamel surfaces.
8. The accuracy of IOS for measuring surface loss (craters) would be the same using scans of increasing size, from cusp to full-arch.

Chapter 2 Investigating the effect of handling technique and surface-to-camera distance on IOS accuracy

2.1 Introduction

IOSs are designed to be held by hand during the scanning of patients' dentition; however, little is known whether this leads to more measurement errors. Furthermore, depending on the optical technology utilised by an IOS, the camera on the wand should be held within its focus range, which is usually between 5 – 30 mm (Richert et al., 2017; Zimmermann et al., 2015) and the movement of the wand should be fluid at a steady distance from the target surface (Richert et al., 2017). Very few studies have compared whether the distance of the wand from the surface scanned (surface-to-camera distance) has an effect on the accuracy of IOSs (Kim et al., 2019). Additionally, certain IOSs require the use of light powder coating (~20 – 40 µm) on the target surface for capturing surface topography (Richert et al., 2017), which is commonly known as 'scanning spray'. This scanning spray applies an optically active coating which acts as an opacifier reducing surface reflectivity as well as providing randomly distributed landmarks assisting in the image stitching process for the creation of a 3D model (Güth et al., 2017a). Until now, there is scarcity in the literature of studies reporting particle size distributions of these powders and their effect on roughness and form measurements after surface application.

With the aim of better understanding and determining the capabilities of intraoral scanning for measuring surface change, *in vitro* experimental investigations were designed and conducted pertaining to the handling technique and the surface-to-camera distance during scanning as well as characterising the required scanning spray powder.

This Chapter also describes general methods and materials used for these investigations, some of which are used throughout this thesis such as enamel sample and acidic solution preparation, and the methodology utilised for software analysis.

2.1.1 Aims

The aims of this Chapter were to:

1. Investigate the influence of the scanner handling technique (handheld Vs. jig-guided scanning) on the accuracy of an IOS for measuring surface loss in the form of 3D step heights (µm).
2. Investigate the influence of surface-to-camera distance on the accuracy of the IOS for measuring surface loss in the form of 3D step heights (µm).
3. Determine the effect of scanning spray powdering on flat surfaces by measuring surface roughness (µm) and step heights (µm) using profilometry.

2.1.2 Objectives

The objectives of this Chapter were to:

1. Create a groove of an adequate depth on a polished human enamel sample and measure it in the form of step height measurements using an IOS (tested device) and gold standard profilometry as the reference for comparison.
2. Determine the accuracy of the IOS in measuring the depth of the enamel groove in the form of step height (µm) by holding the IOS's wand by hand (handheld technique) or mounted on a jig (jig-guided technique) during scanning.
3. Investigate the accuracy of the IOS in measuring the depth of the enamel groove as step heights at different surface-to-camera distances.

4. Characterise the powdering layer applied on a flat surface by measuring the difference in *Sq* roughness and height between powdered and non-powdered surfaces on a glass slide using profilometry.

2.1.3 Null hypotheses:

1. The accuracy of the IOS for measuring the depth of a surface groove on polished enamel would be the same between handheld and jig-guided scanning.
2. The accuracy of the IOS in measuring the depth of a surface groove on polished enamel would be the same between different surface-to-camera distances.
3. The measurements of surface roughness and heights between powdered and non-powdered sites on a flat surface would be the same.

2.2 Materials and methods

2.2.1 Enamel sample preparation

Extracted caries-free human molars were sourced from the oral surgery department of Guy's Hospital after obtaining informed consent from patients (REC ref:18/WM/0351). The teeth were disinfected in domestic bleach (Sodium hypochlorite, <5%, 1:10 with deionised water) for three days, and kept in deionised water thereafter. The molars were sectioned along the cemento-enamel junction, mesio-distally, and bucco-lingually, using a water-cooled diamond blade (XL 12205, Benetec Ltd., London, UK) on a cutting machine (Labcut 1010, Agar Scientific Limited), to produce enamel slabs (Figure 2-1~~Figure 2-1~~).

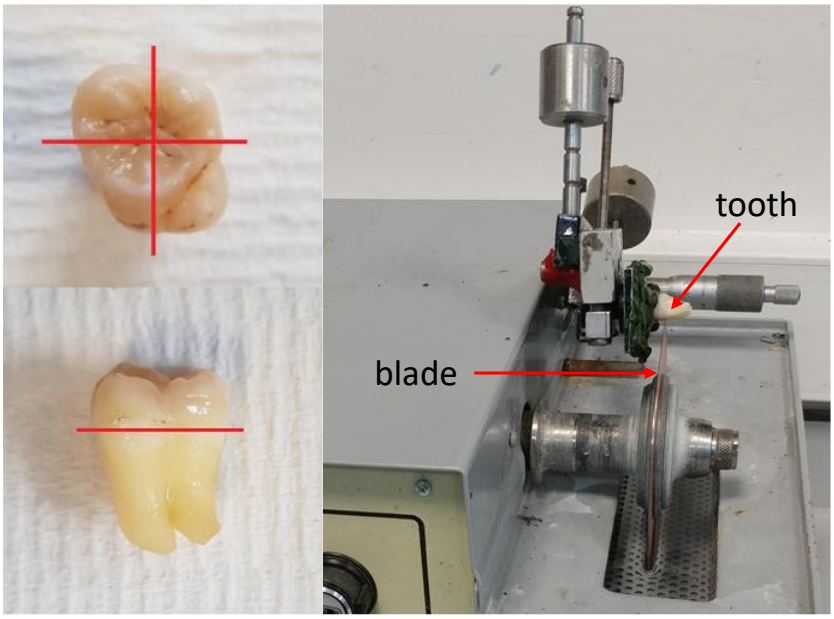

Figure 2-1 – Sectioning of teeth across the cemento-enamel junction, mesiodistally and buccolingually to create enamel specimens using a cutting machine (Labcut1010, Agar Scientific Limited).

A single slab of enamel was embedded in self-cured bis-acryl material (Protemp™4, 3M ESPE, Seefeld, Germany) of dimensions 5.0 x 25 x 20 mm, using a custom-made silicone mould. The sample was polished using a water-cooled polishing machine (LaboPol-30, Struers ApS, Ballerup, Denmark) with silica-carbide discs (Versocit, Struers A/S, Copenhagen, Denmark) of successively finer grits (500, 1200, 2000, 4000 grit), for 5s, 25s, 30s, and 60s, respectively, at 150 rpm, achieving flatness tolerance ±0.4 µm (Austin, 2011). Fiducial markers were geometrically placed in a 'cross' shape on the bis-acrylic surrounding the enamel slab, using round diamond burs Hi-Di 520 and 522 (Dentsply Sirona, USA) of diameters 1.3mm and 0.5mm, respectively. The fiducial markers were designed to facilitate the localisation of the groove during analysis. The polished sample was ultrasonicated (GP-70, Nusonics, Lakewood, USA) in 100 ml deionised water for 15 mins and air-dried for 24 hours at room temperature (Mistry et al., 2015). A 1 mm wide precision masking tape (Model Craft Collection, Shesto Ltd, Watford, UK) was firstly placed over the centre of the enamel sample (i.e. where the groove was to be created) and prior its removal, polyvinyl chloride (PVC) tape was used on either side of the masking tape to create two protected reference zones and a 1 mm window of

exposed enamel (Figure 2-2~~Figure 2-2~~), based on a previously published protocol (Mistry et al., 2015).

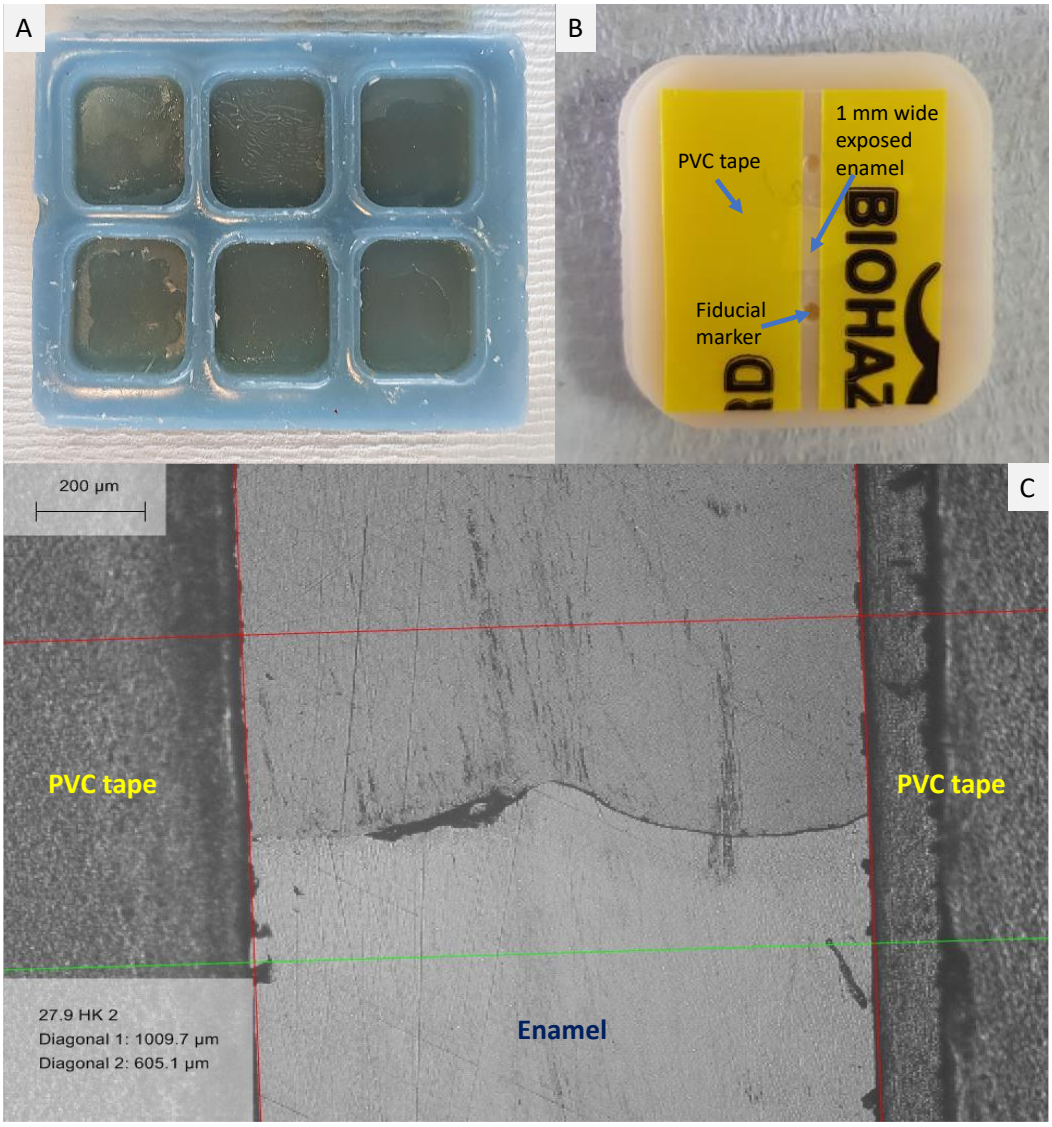

Figure 2-2 – Enamel sample creation and taping.
A custom-made silicone mould (A) used to embed the enamel slab into bis-acryl material prior to polishing. The sample were taped using a 1 mm wide precision masking tape to create a window of exposed enamel and two reference zones (B). A microscope image (5x/0.15) showing a 1.0 mm wide window of exposed enamel between the PVC tapes (C).

2.2.2 Creating a groove on enamel

A 0.3% citric acid solution with a pH 2.7 was prepared using 3 g anhydrous citric acid powder (Thermo Fisher Scientific, Geel, Belgium) dissolved in 1 L deionised water. Its titratable acidity was 10.2 ml, defined as the amount of 0.1 M sodium hydroxide required to neutralise 20 mL of the

solution to pH 7.0. An erosive groove of 44.8 µm depth was created on the enamel sample after it was exposed to 5-minute immersion cycles, in 100 ml of the citric acid solution (pH 2.7) and agitated using an orbital shaker (62.5 rpm) for a total of 75 mins. The depth of the groove was measured by a gold standard profilometer which is described in more detail in Section 2.2.3 below. Between each 5-min immersion cycle, the enamel sample was washed in deionised water for 2 minutes and after the final cycle, it was washed and left to air-dry for 24 hours before the tape was carefully removed.

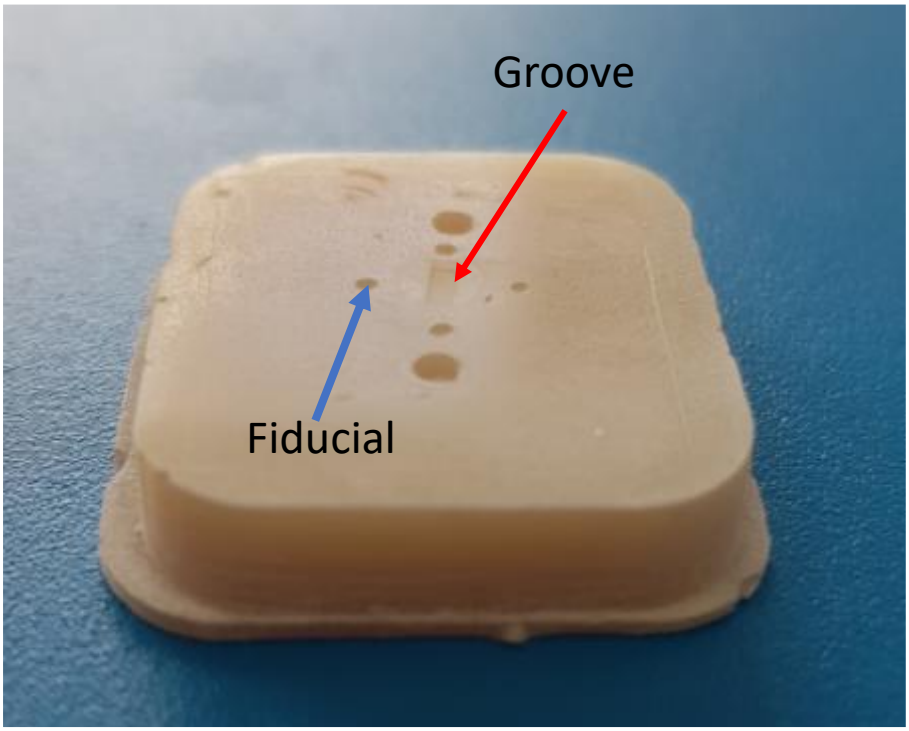

Figure 2-3 – Groove on the polished enamel sample following citric acid erosion.

2.2.3 Profilometry

Profilometric scanning was conducted using a non-contacting laser profilometer (NCLP) (TaiCaan Technologies™, XYRIS 2000CL, UK) with a laser confocal displacement scanner sensor (LT-9010 M, Keyence Corporation, Japan), employing a red 655 nm-wavelength laser with spot diameter Ø2 µm, 600 µm vertical gauge and 10 nm vertical resolution (Figure 2-4). The NCLP sensor and motion control system were connected to a personal computer running Microsoft® WindowsXP® and an

Intel Pentium® 3GHz processor. The personal computer controlled the NCLP measurement process using the proprietary measurement software, STAGES™ (TaiCaan Technologies Ltd., Southampton, England).

The surface of the sample was brought into the gauge range and an areal measurement was carried out by moving the XY stage over a specified measurement area. The sample was moved line by line in a raster pattern from left to right along the X axis, whilst individual data points were allocated a z co-ordinate (according to the sensor output) and XY co-ordinates (according to the motion controller output) in rectilinear grid spacing of 10 µm X, Y intervals, resulting in a 'point cloud' of individual data points, each 10 µm apart from each other, according to previously published protocols for surface form and roughness measurements (Mistry et al., 2015; F. Mullan et al., 2018). An area of 4 × 4 mm was chosen for scanning the enamel surface containing the groove. The datasets collected from the profilometer were saved in the ASCII format (.tai extension) which were then converted to a text file (.txt extension) for compatibility with the analysis software.

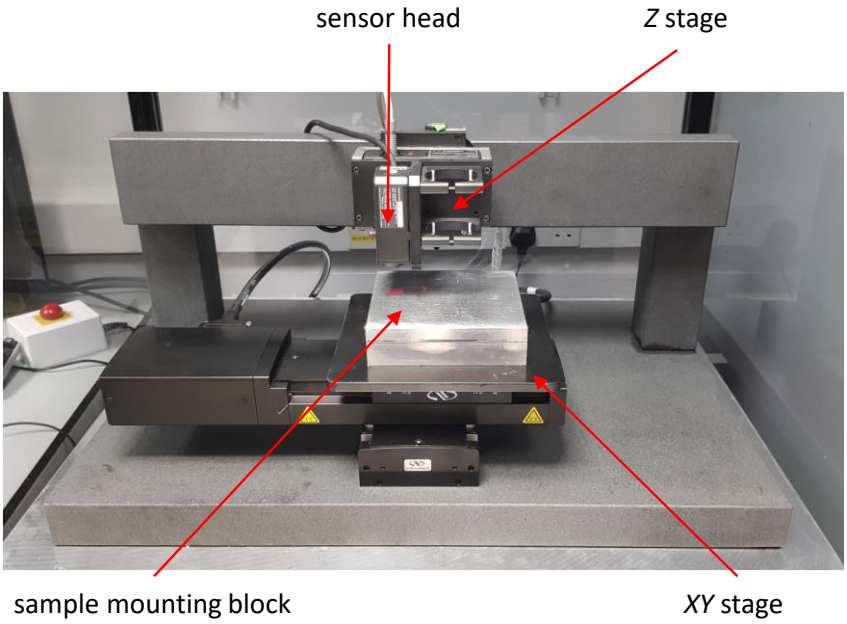

Figure 2-4 – Non-contacting confocal laser profilometer

Prior to using the NCLP as the reference device for *in vitro* enamel surface form measurements, a pilot investigation was conducted to determine its accuracy in measuring a Taylor-Hobson 2.64 µm step height reference standard (Figure 2-5) for validation. After scanning the 2.64 µm step height standard ten times using a 10 x 10 µm XY measurement spacing, the NCLP produced a mean (SD) step height measurement of 2.63 (0.01) µm, i.e., the NCLP showed a trueness (precision) of 10 (10) nm.

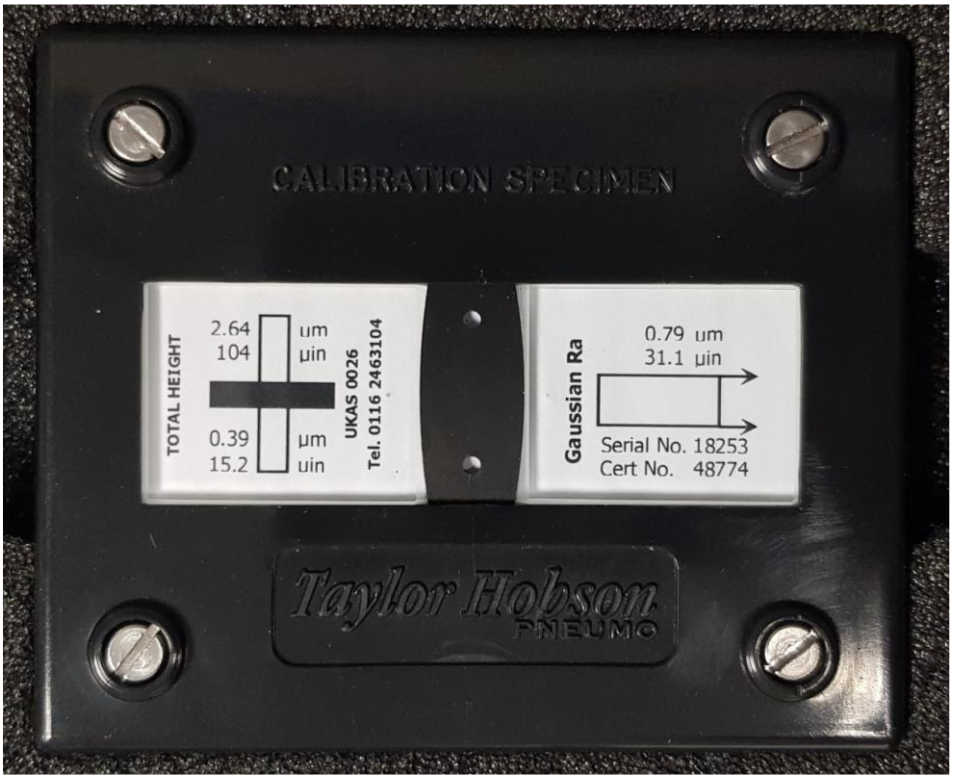

Figure 2-5 – Taylor Hobson calibration standard used to assess the accuracy of the NCLP in measuring a 2.64 µm step height reference standard.

2.2.4 IOS scanning

The intraoral scanning system investigated in this study and used throughout the thesis was the True Definition® intraoral scanner (IOS-TD) (Midmark Corp., Ohio, USA). It was originally manufactured and introduced to the market by 3M™ ESPE (St. Paul, USA) in 2012. In 2019, 3M announced the sale of assets related to 3M™ True Definition IOS platform to Midmark Corporation,

a manufacturer and supplier of equipment in the dental market (3M ESPE, 2019). The scanner can be currently purchased in two different options: the cart or the mobile system; however, both utilise the same wand and software to capture digital impressions and offer the same scanning experience. The original option, the cart system, consists of a mobile cart housing a computer and a 21.5-inch touch-screen monitor. The mobile system was introduced in the market in 2016 which can be operated solely on a tablet in a more compact design that allows more freedom of movement between dental surgeries (3M, 2016). The wand connects to the computer/tablet via a heavy-duty universal serial bus (USB) cable.

IOS-TD uses a pulsating structured visible blue light and utilizes active-wavefront-sampling (AWS) video technology which is described in detail in 1.4.6.6, on page 79 above. Its wand has a pen-grasp design, weighing 233 g, with sensor dimensions of 254 mm length, 16.2 mm width at the tip, 14.4 mm height, and 24.3 mm maximum diameter. The sensor has a field of view 10 mm x 13 mm, working depth up to 17 mm, and captures 60 frames per second during scanning (V. D.-F. García et al., 2022a; Wong et al., 2018).

Unlike other IOSs, it requires application of a light coating of titanium dioxide (TiO_2) powder on the target surface to be scanned. The TiO_2 particles act as randomly distributed landmarks, dispersing the light uniformly to enhance the accuracy of the scan (Imburgia et al., 2017). During scanning, monochrome images are captured via a video sequence acquisition method and displayed on the computer screen. On completion of the scan a digital 3D model is produced that can be manipulated by the operator and then finally exported as an STL data file which can be downloaded from a cloud-based platform (Midmark Connection Centre).

Prior to using IOS-TD in this study, the eroded enamel sample was sprayed with a light coating of titanium dioxide (TiO_2) (3M® High-resolution scanning spray, St. Paul, USA) using a powdering

sprayer (3M® High-resolution Sprayer, St. Paul, USA) in a circular motion with its tip held approximately 2.5 cm from the sample to ensure an even light coating of spray, as per manufacturer's instructions (Figure 2-6~~Figure 2-6~~).

Figure 2-6 – Powdering of the enamel sample

Table 2-1 below shows the composition of the scanning spray consisting of three main ingredients whilst its Material Safety Data sheet can be found in the Appendix, page277~~279~~ below. The spraying was conducted in a cabinet with constant airflow to simulate the presence of a high-volume dental suction and avoid inhalation of the powder. The requirement of scanning spray for IOS-TD scanning meant that profilometric scanning was always conducted prior to the application of the spray.

Table 2-1 – Ingredients of 3M® High-resolution scanning spray

Ingredients	**Percentage (%) by Weight**
Titanium dioxide	50-60
Zirconium oxide	30-40
Zinc stearate	5 -10

Scanning of the enamel groove using IOS-TD was carried out using two different techniques defined by the way the IOS wand was handled during scanning: handheld or jig-guided. For handheld scanning, the sample was positioned on a flat surface and scanned by a single operator holding the wand in their hands at an optimal distance (~3 – 7 mm), guided by the depth and rotation indicators on the computer screen (Figure 2-7).

Figure 2-7 – Handheld scanning of the enamel sample and 3D data produced on the computer screen of IOS-TD.

For jig-guided scanning, the wand of IOS-TD was mounted on a geometry-stabilising unit which comprised of a mounting platform for securing the wand in place, a sample holder ensuring the sample remained static during scanning, and a lever system which allowed the movement of the wand's camera in the X and Y axes in a controlled manner, following a previously published protocol (Austin et al., 2017). The platform of the sample holder could be adjusted in the Z axis using two knobs on either side controlling the surface-to-camera distance (Figure 2-8~~Figure 2-8~~).

Repeated measurements (n=10) of the eroded enamel sample were undertaken using the handheld technique, as well as the jig-guided technique at different surface-to-camera distances of 3, 4, 5, and 7 mm. The number of repetitions was chosen based on a previously published study (Kim et al., 2019). Each time the surface-to-camera distance was adjusted on the geometry-stabilising jig, a

small spirit level was used to ensure the platform was horizontal to the ground. To optimise the scan quality of all IOS scans (handheld or jig-mounted), the datasets were exported using the option of maximal resolution (i.e., ~60 µm point-spacing) and downloaded as STL files from the scanner's cloud-based platform.

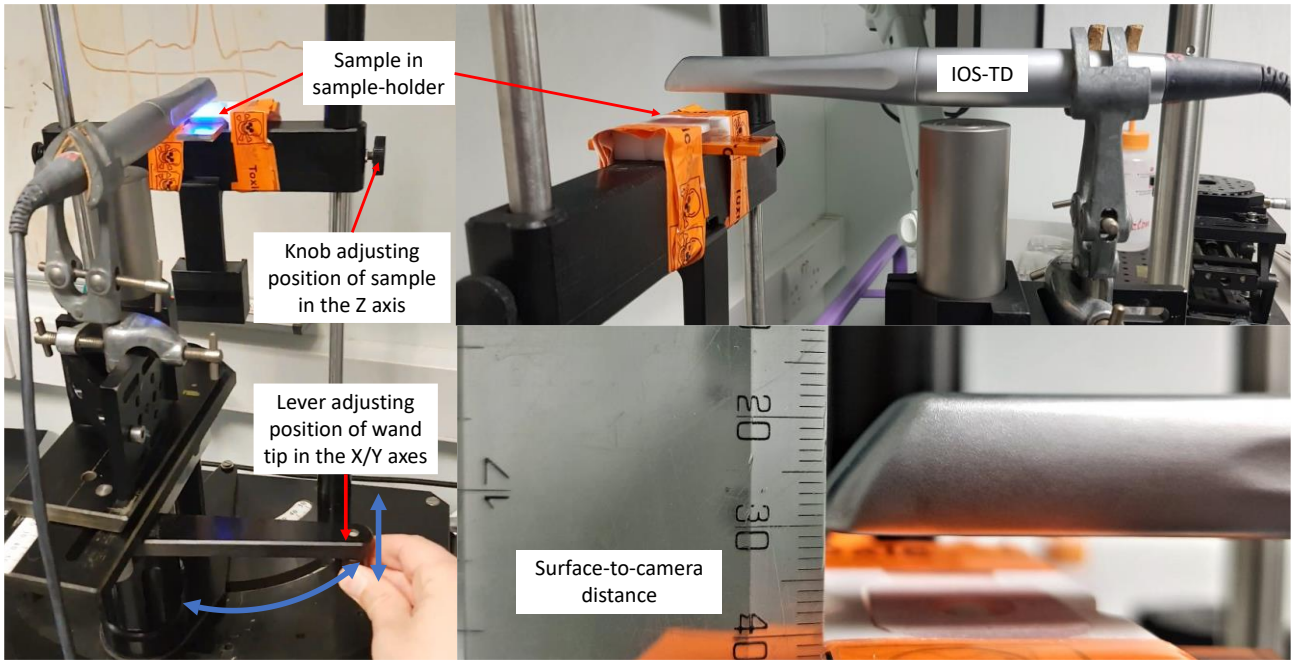

Figure 2-8 – Geometry-stabilising jig comprising of a wand holder, a height-adjustable sample holder, and a lever system which allowed the movement of the wand's camera in the X and Y axes in a controlled manner.

2.2.5 Characterising the TiO_2 powder coating

Glass slides (Academy™ Science, UK) (n=10) were covered on one side using PVC tape and a light TiO_2 coating applied on their un-taped sides in the same manner as described above. The tapes were then removed, resulting in ten glass slides with a powdered half on one side and a clean non-powdered half on the other (Figure 2-9 below).

The powdered and non-powdered sides of each glass slide, as well as the intersection area in the middle, were scanned once by the NCLP, using scanning areas of 4 × 4 mm to represent each site. This resulted in 10 scans for each of the powdered, non-powdered, and intersection areas. Within

the scanned areas from the powdered and non-powdered sites, five smaller areas of 1 × 1 mm were conveniently selected which were used for roughness analysis according to a previously published protocol (F. Mullan et al., 2018); whilst the entirety of the scanned areas at the intersection were used for step height analysis (Figure 2-9). This resulted in 50 roughness measurements for the powdered and 50 for the non-powdered sites, and ten step height measurements at the intersection.

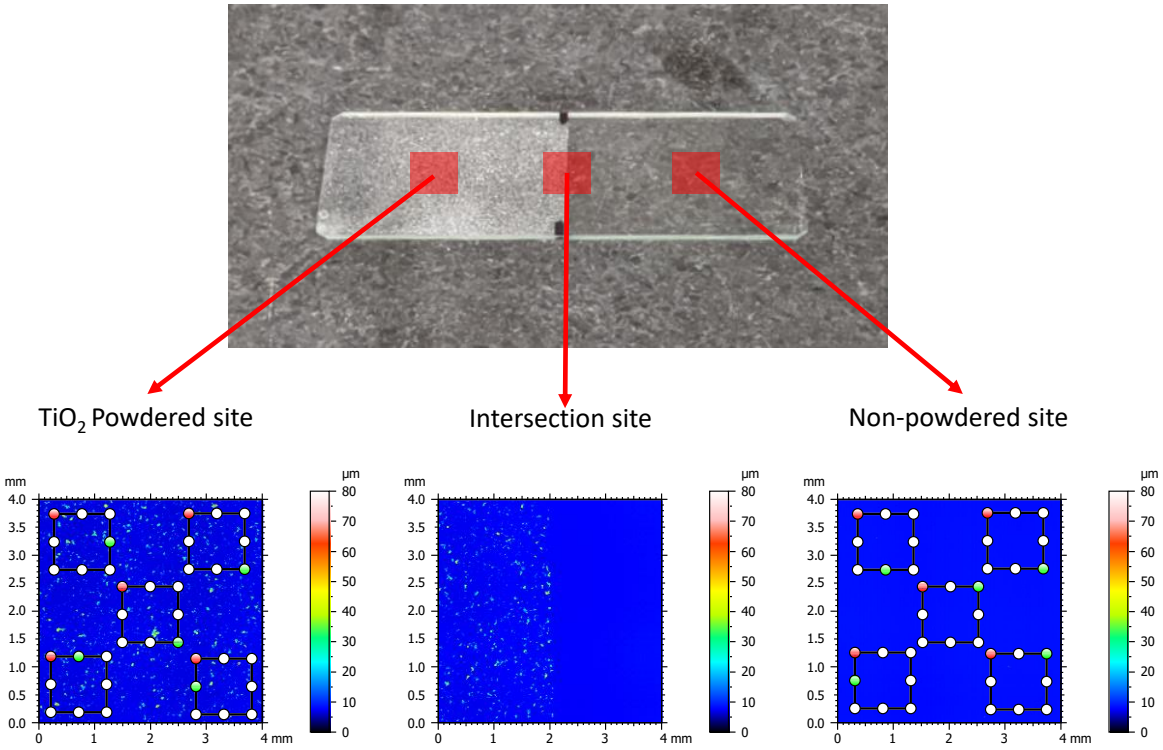

Figure 2-9 – Example of sites scanned on each glass slide using the NCLP at the powdered, intersection, and non-powdered sites.

2.2.6 Analysis

2.2.6.1 Depth measurement of enamel groove

The analysis of the datasets from the NCLP and IOS-TD was conducted using a surface metrology software (MountainsMap7®, Digitalsurf, Besançon, France). Each dataset consisting of a Cartesian point-cloud, were loaded into the software. Outliers were removed and a surface levelling operator

utilising a linear least-squares plane best fit was applied, excluding the area of the groove on the enamel surface. The groove depth was determined as a 3D step height (µm), defined by ISO 5436-1 standard, according to previous published protocols (Mylonas et al., 2018). This was calculated by converting a 3 x 1 mm region of interest containing the groove in the middle, into a series of profiles along the X axis of the scan and using the calculated average profile to provide an automatic software calculation of the 3D step height (µm) (Figure 2-10). The absolute errors of the IOS-TD measurements against the NCLP (44.8 µm) were used for statistical analysis defined by the equation: $Absolute\ error = |IOS - NCLP|$.

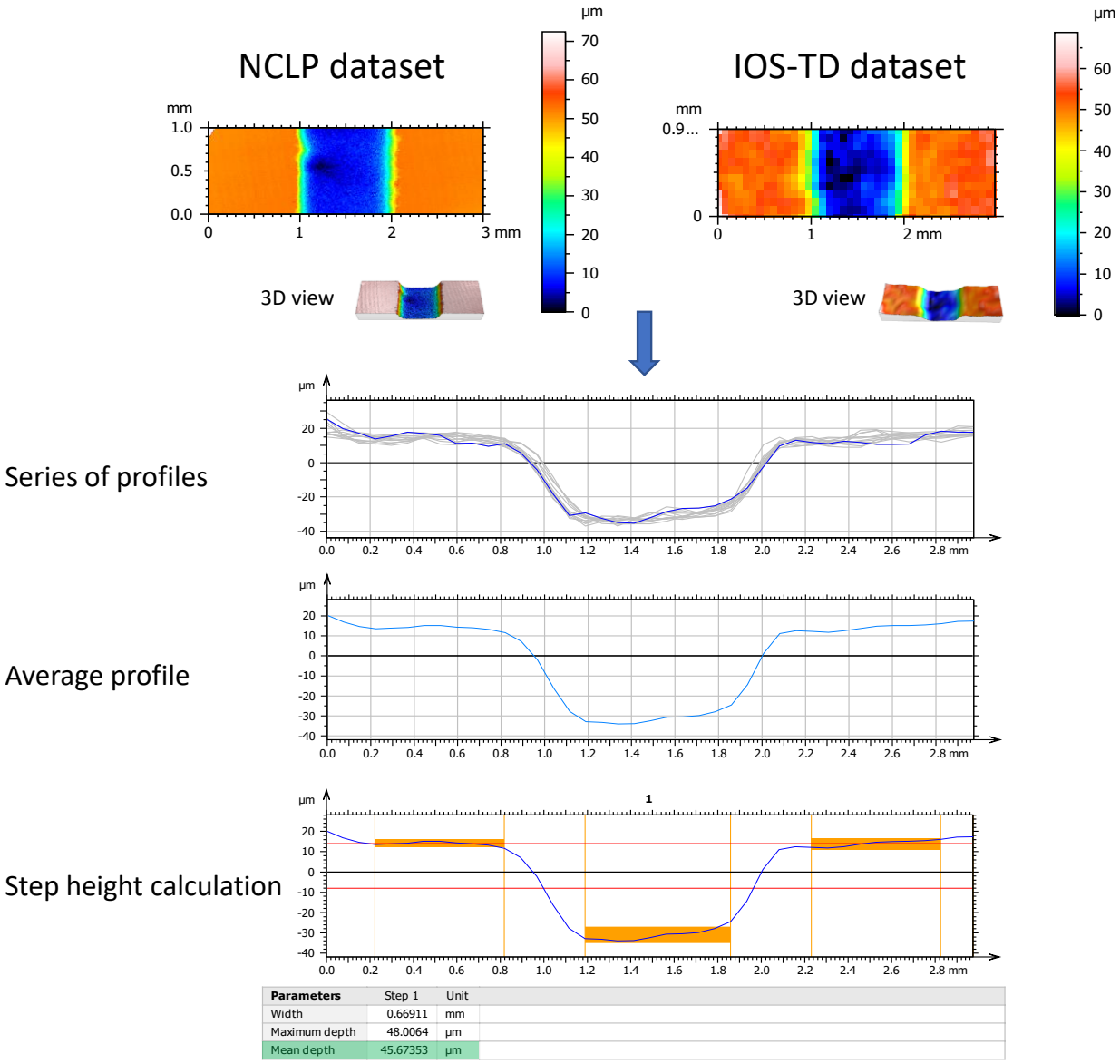

Figure 2-10 – NCLP and IOS-TD datasets and the analysis workflow for step height calculation using MountainsMap7® metrology software.
The colour-coded datasets show different colours as a function of Z measurements. The profile analysis shown for the step height calculation is a representative example from the IOS-TD generated dataset.

2.2.6.2 TiO_2 powder measurement

The difference in surface heights between the powdered and non-powdered sites at their intersection was determined as a 3D step height, in the same manner as described above. Additionally, a 25 µm Gaussian filter was applied on the datasets of the powdered and non-powdered scanned areas, to isolate roughness data, outliers were removed, and the surface levelled

using a linear least-squares best-fit plane according to a previous published protocol (F. Mullan et al., 2017; Francesca Mullan et al., 2017). The mean (SD) *Sq* surface roughness (root-mean-square 3D surface roughness) of the powdered and unpowdered sites was calculated.

In addition, images were taken using a digital microscope (Keyence VHX-7000, Japan) VHX-7000 with ×700 magnification and a mix co-axial light with full ring lighting for quantitative analysis of the TiO_2 particles. The 'grain particle analysis' function of the digital microscope was used to measure the mean (SD) maximum and the mean (SD) minimum diameter (µm) of the TiO_2 particles identified on the glass slide.

2.2.7 Statistical analysis

Statistical analysis was conducted using GraphPad Prism 9 (GraphPad Software Inc, California, USA). Data were assessed for normal distribution using four normality tests: D'Agostino & Pearson, Anderson-Darling, Kolmogorov-Smirnov and Shapiro-Wilk tests, and visually assessed using QQ plots. All the data were found to be normally distributed, and therefore mean and standard deviation was reported. Inter-group analysis between the different IOS measurement techniques was conducted using one-way ANOVA with post-hoc Tukey test for multiple comparisons. An unpaired t-test was used to compare *Sq* roughness measurements between powdered and non-powdered sites on the glass slides.

2.3 Results

2.3.1 Handheld Vs. Jig-guided IOS scanning

The NCLP depth measurement of the erosive groove was 44.8 µm which was used as the accepted reference value. The mean (SD) IOS-TD depth measurements were 42.9 (1.8) µm for the handheld

technique, and 42.5 (2.0), 42.5 (1.8), 43.2 (1.5) and 43. (1.9) µm for the jig-guided technique at 3-, 4-, 5- and 7-mm surface-to-camera distances, respectively.

Figure 2-11 shows the – Mean (SD) absolute error (µm) of IOS-TD measurements (against the NCLP measurement of 44.8 µm) using the handheld and the jig-mounted scanning techniques at different surface-to-camera distances (3, 4, 5, 7 mm). ~~– Mean (SD) absolute error (µm) of IOS-TD measurements (against the NCLP measurement of 44.8 µm) using the handheld and the jig-mounted scanning techniques at different surface-to-camera distances (3, 4, 5, 7 mm).~~ The mean (SD) absolute error for handheld scanning was 2.0 (1.6) µm and 2.6 (1.5), 2.4 (1.6), 1.8 (1.3), and 2.0 (1.7) µm for jig-guided scanning at 3-, 4-, 5-, and 7-mm surface-to-camera distances, respectively.

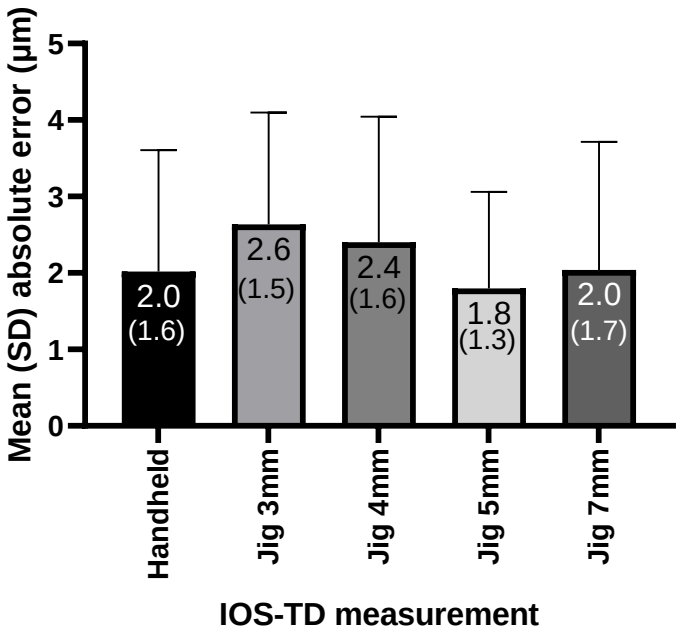

Figure 2-11 – Mean (SD) absolute error (µm) of IOS-TD measurements (against the NCLP measurement of 44.8 µm) using the handheld and the jig-mounted scanning techniques at different surface-to-camera distances (3, 4, 5, 7 mm).

No statistically significant differences were observed among means of the different scanning groups (p=0.7354). No statistically significant differences were observed between the handheld and any of the jig-mounted measurements (p=0.8946-0.9999). Additionally, no statistically significant

differences were observed between the jig-guided measurements at different surface-to-camera distances (p=0.7379-0.9969). The smallest absolute error was observed by jig-guided scanning 5 mm surface-to-camera distance, followed closely by handheld scanning and jig-guided scanning at 7mm.

2.3.2 TiO_2 powder measurement

The mean (SD) *Sq* roughness for the non-powdered sites was 0.17 (0.02) µm, whilst there was a statistically significant increase to 3.96 (0.59) µm ($p<0.0001$) for the TiO_2 powdered sites. The mean (SD) step height at the intersection between the powdered and non-powdered surfaces of the glass slides was 0.88 (0.09) µm. The grain particle analysis on the digital microscope based on automatic threshold segmentation by its internal software revealed a mean (SD) maximum diameter of 30 (16) µm and minimum diameter of 22 (12) µm for the TiO_2 particles on the surface (Figure 2-12). An increased particle density was observed at the intersection where the tape used to be on the microscopy slide which is believed to be as a result of residual adhesive on the surface.

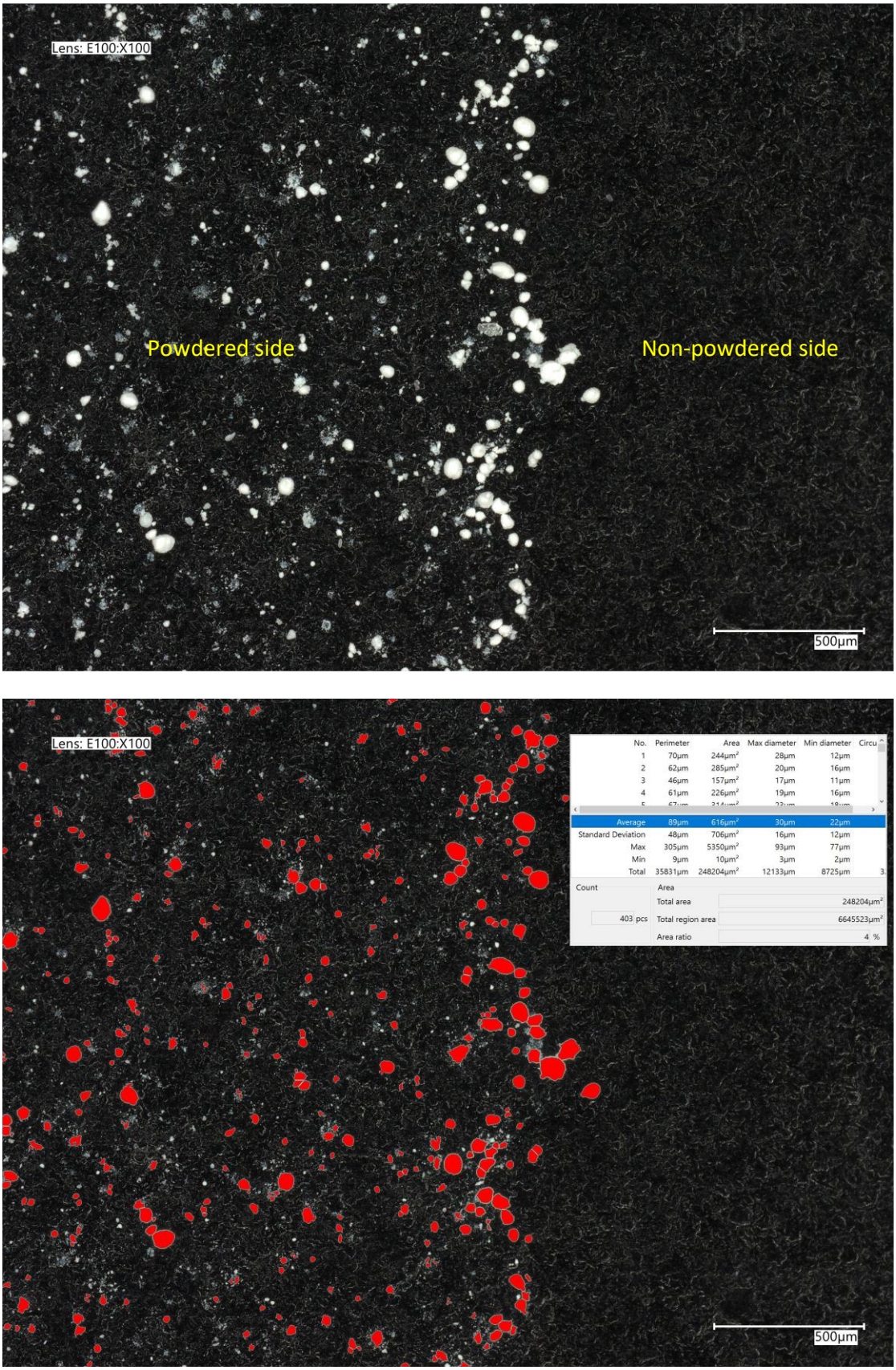

Figure 2-12 – Digital microscopy image (lens 100x100) at the intersection between powdered and non-powdered sides of the glass slide (above) and grain particle analysis measuring the diameter of the TiO_2 particles (below).

2.4 Discussion

This study assessed the influence of factors on the accuracy of an intraoral scanner in measuring a standard depth of a 44.8 µm polished enamel groove, (as measured by the gold standard NCLP), according to the scanner handling technique (i.e., handheld Vs. jig-guided IOS scanning) and surface-to-camera distance. Four different surface-to-camera distances were investigated ranging from 3 – 7 mm based on the depth indicators on the computer screen within which IOS-TD would start automatically capturing the surface of the sample.

The results of this study demonstrated that the accuracy of the IOS-TD in measuring the depth of the enamel groove, evaluated as the absolute difference between the NCLP and IOS-TD measurements, did not statistically significantly differ between handheld and jig-guided scanning. Therefore, the first hypothesis stating that the accuracy of the IOS-TD for measuring the depth of a surface groove on polished enamel would be the same between handheld and jig-guided scanning, could not be rejected . This reinforced the intent of carrying out handheld scanning using the IOS-TD throughout the rest of the thesis, as originally intended by its manufacturers. In addition, no statistically significant differences were observed between the different surface-to-camera distances, which suggests that the accuracy of the IOS-TD remained the same no matter the distance of the wand camera from the sample, as long as it was within the tested scanning range (3–7 mm) indicated by the depth guides on the computer screen. Therefore, the second hypothesis stating that, the accuracy of the IOS in measuring the depth of a surface groove on polished enamel would be the same between different surface-to-camera distances, could not be rejected based on these findings.

The accuracy of surface profilometry has already been established and validated in the literature, with a combined uncertainty in measurement of ±0.28 µm and maximum vertical linearity errors of

40 nm (F. Mullan et al., 2017) and precision of 5 nm measuring wear on polished enamel and 23 nm on natural enamel (F. Mullan et al., 2018). Prior to using the NCLP for this study, its accuracy was tested against a calibration 2.64 µm step height standard which demonstrated a high trueness (precision) of 10 (10) nm; therefore, a single NCLP measurement of the enamel groove was thought to suffice as the accepted 'true' value for comparison against the different IOS-TD scanning techniques investigated in this present study.

The accuracy of IOS-TD measuring the 44.8 µm groove using the handheld method was 1.6 (1.0) µm, whilst its accuracy when mounted on the jig ranged between 1.5 (1.1) µm and 2.1 (1.1) µm which could be considered acceptable for both clinical monitoring and erosive tooth wear experimental measurements. Although non-statistically significant, these results implied that the optimal surface-to-camera distance for IOS-TD is at ~5 mm. The accuracy was the lowest at 3- and 4-mm surface-to-camera distance which might be attributed to insufficient depth of field for the IOS-TD to obtain an accurate image. Since IOS-TD operates on the AWS principle by measuring depth based on the defocus of the primary optical system, challenging its depth of field (which controls the in-focus area within an image) can affect the accuracy of the scan due to increased noise and image blur (Kim et al., 2019).

To the authors' knowledge, this is the first study that investigated whether surface-to-camera distance affects the accuracy of an intraoral scanner for measuring the depth of an erosive groove on enamel and the first to compare handheld to jig-guided scanning. A recent study that also investigated the effect of surface-to-camera distances of 0 mm, 2.5 mm, 5.0 mm, 7.5 mm in the scanning accuracy of three intraoral scanners (TRIOS, CS 3500, and PlanScan), compared 2D measurement parameters of linear distances across a digitised stone model as well as 3D root-mean-square differences between a reference dataset made by a high-accuracy laboratory

scanner and the IOS datasets after superimposition (Kim et al., 2019). Due to several methodological differences between the two studies such as the type of IOS and measurement outputs used, any comparisons should be done with caution. The authors reported mixed findings, with no significant differences observed in some 2D linear distances whilst statistically differences were observed in others, depending on the intraoral scanner used. The accuracy was the highest for both 2D and 3D measurements at 2.5- and 5.0-mm surface-to-camera distances (Kim et al., 2019).

Characterisation of the TiO_2 powder layer, which is an essential requirement prior to the use of the IOS-TD, revealed that its application on a flat glass slide surface resulted in a significantly rougher surface compared to an equivalent non-powdered surface; therefore, the third null hypothesis was rejected. This should be taken into consideration if future experimental studies intend to use IOSs for surface roughness measurements, and perhaps scanners that do not require surface powder application should be selected for such purposes. Indeed, it would be interesting to investigate whether the intraoral scanner itself can measure differences in surface roughness which is something investigated in the next Chapter of this Thesis. Grain particle analysis using microscopic images demonstrated that the mean diameter of TiO_2 particles ranged in the order of ~20 - 30 μm, which is comparable to what is reported in the literature (Ochsmann et al., 2020; Richert et al., 2017). Interestingly, a recent study has identified presence of ultrafine particles in the nanometre scale in dental spray-powders which could lead to inhalation exposures and work-related health problems; therefore, the use of high-volume suction must always be used near the tip of the sprayer gun when applying the powder. Nevertheless, the deposited fraction of hazardous particles in the lung of employees in dental practices seems to be small (15%) during this dental procedure (Ochsmann et al., 2020).

Following step height profile analysis between the powdered and non-powdered glass slide surface, the powder layer resulted in an overall increase in surface heights of less than one micron. This may be attributed to the fact that although the powder particles can have a diameter of a few microns, especially after coalescing, they only cover a very small proportion of the wider scanned surface. This suggests that the use of IOSs requiring the application of powder on the target surface would be unlikely to influence surface form measurements in the order of tens of microns. Indeed, the powder might be advantageous as it provides landmarks which could lead to a better image-stitching procedure of the single point clouds during the scanning process. Ender et al., (2016) suggested that the powder provided a more consistent reflection of the scanners' projected light which is helpful as different oral surfaces such as enamel, dentine and gingiva have different light reflecting properties. In addition, Prudente et al., (2018) reported that powder application prior to IOS scanning improved the vertical fit of crowns and reduced their volumetric 3D internal fit compared to scanning without powder application using the same scanner. Furthermore, the very low standard deviation of step height measurements between the powdered and non-powdered surfaces also suggests a high reproducibility of powder layer thickness.

A depth of 44.8 µm for the erosive groove was considered adequate for the purposes of this study. This was based on a previous published study which also used the IOS-TD for measuring erosive tooth wear ranging between 33 to 72.8 µm (Kumar et al., 2018). Unlike Kumar et al., (2018), a flat polished enamel was used in this study, which as discussed in Section 1.3.5.1.1 above, its planar surface allows surface loss measurements in the form of step heights using a single post-wear scan. Kumar et al., (2018) used natural enamel which presents a freeform surface of higher complexity requiring the need of superimposition between the pre- and post-wear scans which may have led to further measurement errors as seen with higher standard deviations in their study compared to this. A strength of this present study is that a reference NCLP measurement of the enamel groove

was taken which allowed the evaluation of the accuracy of IOS-TD whereas Kumar et al., (2018) did not utilise a reference device and therefore could only assess precision. Another study compared IOS surface loss measurements on a cobalt chromium alloy phantom tooth to profilometry. They reported a comparable accuracy to this present study, ranging between 0 – 15 μm difference for measuring wear depths ranging between 66 to 174 μm, even though they used what is considered the predecessor intraoral scanner (Lava C.O.S) to IOS-TD (Hartkamp et al., 2017b).

For the purposes of the study only one groove depth was used to compare the different scanning techniques in order to know how the scanning should be conducted in the studies of the thesis thereafter. Following these experiments an obvious question was raised as to what is the minimum groove depth that IOS-TD can detect and measure accurately and this is investigated and reported in the subsequent Chapters.

During pilot experimentation, scans were attempted at 0- and 10-mm surface-to-scanning distances with IOS-TD; however, at such distances the device was not initiating the capturing of the surface and therefore these options were excluded from the study. The manufacturers of IOS-TD claim a scanning depth of up to 17 mm, and although a live image presents on the screen of the computer within this range, the capturing starts only when the surface-to-camera distance was below 10 mm depth. Interestingly, other scanners in the market, such as Trios3, have been tested and reported to be able to scan at a distance of >10 mm (Kim et al., 2019).

Addressing the limitations of the present study, this was conducted in *in vitro* conditions which can be considerably different than the actual oral environment. Presence of saliva, blood, and body movement can all decrease scan accuracy (Richert et al., 2017).

2.5 Conclusions

This chapter evaluated the effects of handling technique and surface-to-camera distance on the scan accuracy of a clinical intraoral scanner (IOS-TD) for measuring a groove depth on polished enamel. No significant differences were observed between the handheld and jig-guided scanning techniques. Furthermore, no significant differences were observed between the different surface-to-camera distances tested in this study using the jig. The presence of a scanning powder coating on a flat surface resulted in increased roughness measurements but caused only a sub-micron increase of surface heights that should be considered acceptable for surface form measurements. Further research is required to determine the lowest threshold of IOS-TD for measuring surface change and investigations in the subsequent chapters are focused on answering this question.

Chapter 3 The depth measurement threshold of the IOS-TD in measuring surface loss on polished human enamel

3.1 Introduction

Profilometry has been extensively utilised and validated for distinguishing and measuring short wavelength (high frequency) surface components, such as seen in the analysis of surface texture and roughness (Hara et al., 2016; F. Mullan et al., 2018, 2017); however, it is not clear whether IOSs are capable of such a task.

Additionally, in Chapter 2, the accuracy of the IOS-TD for measuring a groove with a 44.8 µm depth on a polished enamel surface was demonstrated to be within 2.0 - 2.6 µm of gold standard profilometry; this may be considered satisfactory for clinical monitoring of oral surface changes such as seen in tooth wear *in vivo*, and *in vitro* (Michou et al., 2020; Mitrirattanakul et al., 2022b). Yet, the depth threshold of IOSs for measuring surface change has not been determined, i.e., what is the smallest depth that IOSs can detect, localise, and reliably measure. Whether the IOSs can measure surface phenomena with a sensitivity relevant to pathologies such as erosive tooth wear in the sub-50 µm range (Lambrechts et al., 1989) has yet to be elucidated.

This chapter explores the limits of the IOS-TD for measuring changes in surface roughness and form and is split into two interconnected investigations. Firstly, it investigates the scanning performance of the IOS-TD in distinguishing changes in roughness on flat textured surfaces. Secondly, it develops a new *in vitro* workflow for automated detection and measurement of surface loss and focuses on determining the depth measurement threshold of the IOS-TD on polished human enamel samples.

3.2 Aims, Objectives, and Hypotheses

3.2.1 Aims

The aims of this study were to:

1. Determine the ability of the IOS-TD to discriminate surface roughness change on bespoke flat textured surfaces of different roughness.
2. Determine the depth measurement threshold of the IOS-TD in measuring the depth of grooves made on human polished enamel *in vitro*.

3.2.2 Objectives

The objectives were to:

1. Scan and measure *Sq* surface roughness on bespoke flat textured surfaces of different roughness using the IOS-TD and compare the measurements to a gold standard NCLP.
2. Scan and analyse grooves of different depths created on polished enamel using the IOS-TD and compare measurements to the gold standard NCLP to determine its depth measurement threshold and noise floor.
3. Develop an automated detection and analysis workflow of grooves on polished human enamel for measuring their depth in the form of 3D step heights, their XY area, as well as the surface skewness and kurtosis.

3.2.3 Null Hypotheses

1. The IOS-TD will not be able to distinguish changes on bespoke flat textured surfaces with increasing surface roughness.
2. There will be no differences in depth and XY area measurements between the IOS-TD and the NCLP for grooves of increasing depths on polished human enamel.

3.3 Materials and Methods

3.3.1 Study design

Bespoke flat textured surfaces (n=7) consisting of different surface roughness were created and each scanned five times by the NCLP and IOS-TD to calculate and compare surface roughness measurements between the two scanners. Additionally, grooves of different depths were created on polished human enamel samples (n=80, one groove per sample). Each sample was scanned once by the gold standard NCLP as the reference device and the IOS-TD as the investigated device, and their measurements compared.

3.3.2 Creation of flat textured surfaces

Flat surfaces (n=7) with controlled texture characteristics and optical properties were created. Firstly, a smooth flat surface, used as the control, was prepared by applying a coating of gloss-black cellulose spray paint (Holts® Minimix, Manchester, UK) to a microscopy glass slide, to create a smooth surface, optimised for optical scanning. Additionally, silicon carbide grinding papers (Versocit, Struers A/S, Copenhagen, Denmark) with increasing roughness consisting of grit grades P800, P500, P320, P220, P120, and P60 and hence increasing average silicon carbide particle size of 21.8, 30.2, 46.2, 68.0, 125.0, and 269.0 µm, respectively, as determined by ISO:6344-2/3, were bonded with cyanoacrylate resin (UHU super glue, GmbH & Co., Bühl, Germany) to microscopy slides (Figure 3-1 below). The painted microscopy slide, and the grinding papers were scanned five times each, by the NCLP and IOS-TD. The number of scan repetitions was based on a power calculation by means of GPower 3.1.9 using an unpaired t-test of triplicate pilot measurements by the NCLP between the painted microscopy slide surface (smoothest), 1.5 (0.9) µm, and the P60 grinding paper surface (roughest), 48.1 (3.6) µm, indicating 4 repetitions per textured surface, yielding 95% power.

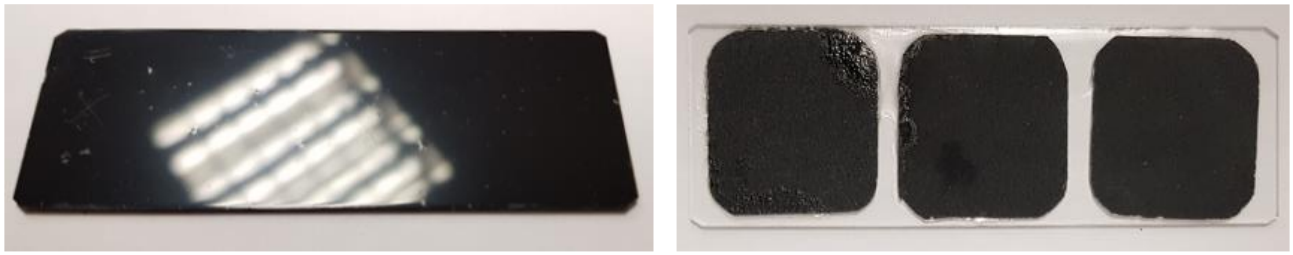

Figure 3-1 – Microscopy glass slide painted with gloss-black cellulose spray paint (left) and examples of grinding papers consisting of different surface roughness glued on a microscopy slide (right).

3.3.3 Enamel sample creation

Extracted sound permanent human molars were obtained after gaining informed consent from patients (REC ref:12/LO/1836) in the Oral Surgery department of Guy's Hospital. The molars were sectioned and prepared to produce polished enamel samples (n=80) following the method described in detail in Section 2.2.1 above achieving flatness tolerance of ±0.6 μm, following a previously published protocol (Mylonas et al., 2018).

3.3.4 Creating grooves on polished enamel

Following enamel sample preparation, a 1 mm-wide window of exposed enamel was created using modelling tape (Model Craft, Shesto Ltd, UK) to provide reference zones surrounding the created groove following the method described in Section 2.2.2 above. The samples were randomised into eight groups (n=10/group). The number of samples per group was determined based on previous pilot data of a single polished sample scanned three times by the NCLP and IOS-TD and using GPower 3.1.9 using paired t-test between two means (SD) of 11.0 (1.3) μm for the NCLP and 7.9 (2.1) μm for the IOS-TD, indicating a total sample size of 8 per group, yielding 95% power. Erosive grooves were created by immersing each group to 5-min cycles of 100 ml citric acid solution (0.3%, pH 2.7, titratable acidity 10.2 mL) at eight different total immersion times (0, 5, 10, 15, 20, 25, 75, and 150 min), under 62.5 rpm orbital agitation (Stuart mini-Orbital Shaker SST1, Bibby Scientific, England). The total immersion times selected for this study were based on previous pilot data that

estimated the depth of enamel grooves after repeated 5 min citric acid exposures between 0 – 150 min. The samples were washed and left to air-dry for 24 hours before tape removal, and then scanned and analysed, in randomised order so that the operator was blinded to the depth.

3.3.5 Scanning

Profilometric scans of the enamel samples as well as the textured surfaces created on the microscopy slides were conducted using the NCLP following the method described in Chapter 2 Section 2.2.3 above2.2.4, and previously published protocols (Mylonas et al., 2018).

IOS-TD scanning (True Definition™, Midmark Corp., USA) was conducted following the manufacturer's instructions and the handheld scanning method described in Chapter 2 Section 2.2.4 above. The datasets were exported with maximal resolution to optimise scan quality and downloaded as STL files from the scanner's cloud-based platform.

Prior to IOS-TD scanning, the samples were lightly coated with titanium dioxide scanning spray (True Definition™ High-resolution scanning spray, Midmark Corp., USA), via a powder gun (True Definition™ powder gun, Midmark Corp., USA), following manufacturer's instructions. As powdering was an essential step prior to IOS-TD scanning, profilometric scans of the enamel samples as well as of the flat textured surfaces were conducted beforehand.

3.3.5.1 Baseline scanning of polished enamel samples

Prior to acid exposure, baseline scanning of each polished enamel sample was conducted using the NCLP and IOS-TD producing 80 datasets. These datasets were used to determine the measurement noise floor of the IOS-TD and NCLP when scanning flat polished enamel before surface loss has occurred.

3.3.6 Analysis

Analysis of the datasets, generated from the NCLP and IOS-TD scanning of the enamel samples as well as the textured surfaces, was carried out using the MountainsMap7® surface metrology software.

3.3.6.1 Analysis of roughness on the flat textured surfaces

Using the datasets from the NCLP and IOS-TD, the mean (SD) *Sq* surface roughness was calculated for each of the flat textured surfaces on the microscopy slides (Figure 3-2). The calculation was conducted over a 4 × 4 mm area within each dataset, after applying a 25 μm Gaussian filter to isolate the roughness data, removing outliers (*i.e.,* erroneous spikes on flat surfaces), and levelling the surface using a linear least-squares best-fit plane, according to a previous published protocol (F. Mullan et al., 2017). This was repeated five times for each textured surface based on previous surface roughness studies (F. Mullan et al., 2017). As the gloss-black painted microscope slide constituted the smoothest out of all the textured surfaces, and therefore, as the control, its *Sq* surface roughness was compared to the grinding papers of increasing silicon carbide particle size and hence increasing roughness.

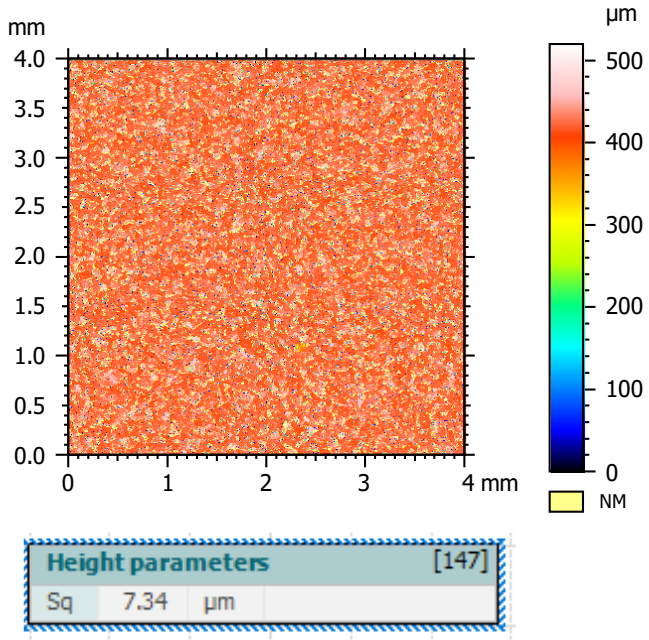

Figure 3-2 – *Sq* surface roughness calculation of a grinding paper (P500, 30.2 µm silica carbide grain size) on microscopy slides.

3.3.6.2 Noise floor measurement on polished enamel samples

Baseline NCLP and IOS-TD datasets were loaded into the surface-metrology software and a 3 × 1 mm area of scanned polished enamel was extracted. Using these 3 × 1 mm areas, the mean (SD) *Sq* surface roughness was calculated as described in Section 3.3.6.1 above. To quantify the noise floor measurement of the IOS-TD and NCLP the following formula was used: $mean + (3 \times SD)$, according to bioanalytical analysis guidelines (Attin et al., 2009; Mylonas et al., 2019).

3.3.6.3 Depth, area, skewness and kurtosis measurements of grooves on polished enamel

A bespoke analysis workflow was developed for polished enamel to 1. measure groove depths as 3D surface step-heights, 2. automatically localise and measure the XY groove area (mm^2) and 3. analyse the surface skewness and kurtosis of each dataset. This workflow was applied to 3 × 1 mm areas of polished enamel from each dataset, with the 1 mm-wide groove in the centre, following removal of outliers and levelling, excluding the central 1/3rd of the area corresponding to the groove from the levelling process (Figure 3-3~~Figure 3-3~~A, below).

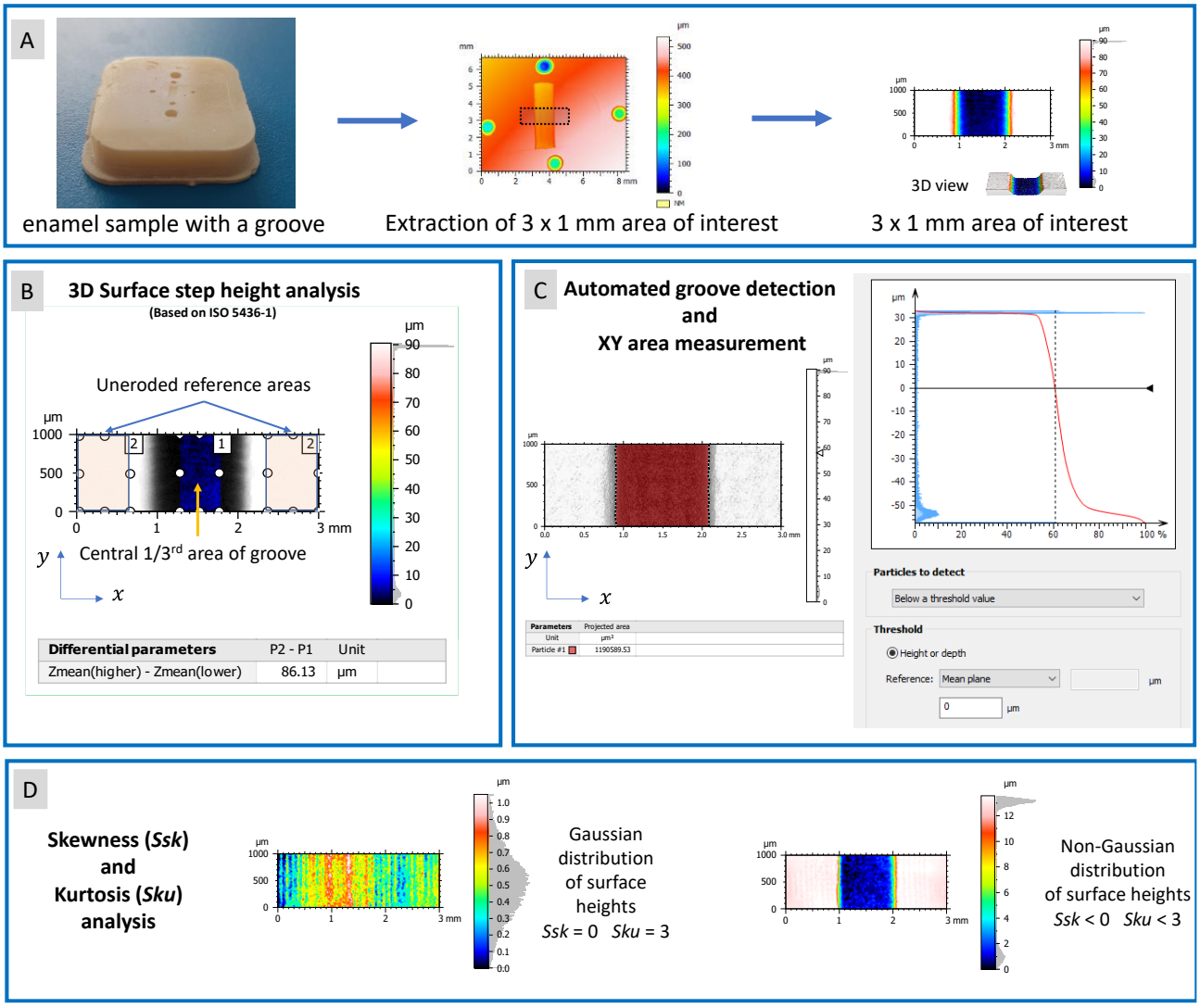

Figure 3-3 – Analysis workflow on 3 x 1 mm areas of interest with the enamel groove in the middle (A) to calculate the depth of the groove in the form of a 3D surface step height (B), detect and measure its XY area (C), and determine the skewness and kurtosis (D).

Firstly, the 3D step-height (µm) of the 1 mm-wide central groove was calculated using predefined selection of the central 1/3rd of the groove compared to the uneroded reference areas of polished enamel, as shown in Figure 3-3~~Figure 3-3~~B above. The average height difference between these areas were then used to calculate the 3D step-height, based on ISO:5436-1. These predefined areas were programmed to automatically have the same size and location within each 3 × 1 mm dataset from the NCLP and IOS-TD, eliminating operator bias.

Secondly, an automated detection algorithm was used to determine the measurement threshold of the IOS-TD by localising and measuring the XY groove area (mm^2), as seen in Figure 3-3~~Figure 3-3~~C. This consisted of utilising a 'particle analysis' software function based on the threshold segmentation algorithm that is described in detail in Chapter 1 Section 1.3.5.3.1 on page 63. The algorithm was set to distinguish surface points of measurement (POMs) with Z heights below the mean plane of all the surface heights within the 3 x 1 mm dataset, according to the histogram of the surface heights distribution and the Abbot-Firestone curve. The Z heights of a recessive surface feature, such as the enamel grooves in this study, would have a lower value than the mean plane of surface heights in an otherwise planar surface, resulting in the detection of the feature.

The surface area (mm^2) of the groove consisting of these surface points was calculated for each IOS-TD scan and was compared to the gold standard NCLP. Based on the standard deviation (0.09 mm^2) of the groove area (mm^2) measurements by the NCLP for all samples, a <0.18 mm^2 area difference cut-off (i.e., 2 × SD) between the IOS-TD and NCLP area measurements was selected as an acceptable margin of error, following metrology good practice guidelines (JCGM, 2012). Therefore, grooves with an area measured on an IOS-TD scan > 0.18 mm^2 Vs. the NCLP would be considered as a cut off determining failure to correctly detect the groove shape. The detection threshold of the IOS-TD was thus defined as the minimum groove depth that the IOS-TD did not statistically significantly differ from the NCLP and could achieve ≥ 90% groove area detection based on the <0.18 mm^2 margin of error described above (i.e., the IOS-TD would correctly measure the XY surface area of nine out of ten samples of a specific depth compared to the NCLP measurements).

Finally, surface height distribution on each 3 × 1 mm dataset was analysed by calculating the surface skewness (*Ssk)* and kurtosis (*Sku)* parameters (Figure 3-3~~Figure 3-3~~D) in order to determine whether the surface height distribution was Gaussian/non-Gaussian. As described in Chapter 1 Section 1.3.4

above, the surface distribution curve of a nominally flat surface superimposed with a random roughness has a Gaussian distribution symmetrical about the height of the nominal plane which is quantified by *Ssk* equal to zero and *Sku* equal to three i.e., no groove is present. In contrast, a surface with a detectable central recessive feature such as the grooves on the enamel samples, consisting of surface heights below the mean plane, will display a non-gaussian distribution of surface heights with negative skewness (i.e., below zero) and kurtosis of less than three (Meireles et al., 2015).

3.3.7 Statistical analysis

Statistical analysis was conducted using Prism9 (GraphPad Software Inc, California, USA). All data were assessed for normal distribution using four normality tests: D'Agostino & Pearson, Anderson-Darling, Kolmogorov-Smirnov and Shapiro-Wilk tests, and visually assessed using QQ plots. A paired t-test was conducted to compare the noise floor measurements between NCLP and IOS-TD. Paired two-way ANOVAs with post-hoc Sidak's tests were conducted for enamel groove depth (µm), area (mm^2), skewness and kurtosis data to compare measurements between the NCLP and IOS-TD. Furthermore, a paired two-way ANOVA was conducted for roughness measurements (µm) between the NCLP and IOS-TD for the flat textured surfaces on the microscopy slides. Statistical significance was set as $p < 0.05$ in all tests.

3.4 Results

3.4.1 Roughness measurement of textured surfaces

Table 3-1 shows the mean (SD) *Sq* surface roughness (μm) for the textured surfaces measured by the NLCP and IOS-TD. The NCLP demonstrated a 1.2 (0.2) μm *Sq* surface roughness for the gloss-painted slide (control), whilst for the grinding papers with silicon carbide particle sizes of 21.8, 30.2, 46.2, 68.0, 125.0, 269 μm, it measured 5.9 (0.1), 8.1 (0.1), 11.0 (0.3), 13.9 (0.1), 30.8 (0.5) and 49.1 (2.1) μm, respectively. The IOS-TD demonstrated a 4.1 (0.5) μm *Sq* surface roughness for the gloss-painted slide (control), whilst for the grinding papers with silicon carbide particle sizes of 21.8, 30.2, 46.2, 68.0, 125.0, 269 μm, it measured 3.3 (0.3), 3.0 (0.3), 3.7 (0.9), 5.4 (0.6), 7.9 (0.3) and 14.4 (0.8) μm, respectively.

Statistically significant differences were observed between the NCLP and IOS-TD for each textured surface ($p<0.0001$). The NCLP showed consistently statistically significant differences in mean (SD) surface roughness for all grit sizes compared to the control painted slide ($p<0.0001$). In contrast, the IOS-TD scans showed statistical differences between the control slide and the sandpaper above 68.0 μm particle size ($p\leq0.02$). This highlighted the inferior resolution and limitation of IOS in distinguishing short-wavelength (i.e., below ≈70 μm) surface features such as roughness.

Table 3-1 – Mean (SD) Sq surface roughness (µm) for the gloss-black painted microscopy glass slide (control) and silicon carbide grinding surfaces of increasing particle size (21.8–269.0 µm), scanned with NCLP and IOS-TD.
Within each column, statistical significance (* = $p < 0.05$ and ** $p < 0.001$) is demonstrated compared to the control.

Flat textured surfaces		**Mean (SD) *Sq* Roughness (µm)**	
		NCLP	**IOS-TD**
Gloss-black painted glass slide (control)		1.2 (0.2)	4.1 (0.5)
Silicon carbide grinding paper particle size (µm)	21.8	5.9 (0.1) **	3.3 (0.3)
	30.2	8.1 (0.1) **	3.0 (0.3)
	46.2	11.0 (0.3) **	3.7 (0.9)
	68.0	13.9 (0.1) **	5.4 (0.6)
	125.0	30.8 (0.5) **	7.9 (0.3) **
	269.0	49.1 (2.1) **	14.4 (0.8) **

3.4.2 Noise floor measurement of polished enamel

Profilometric NCLP baseline scans of polished enamel demonstrated a mean (SD) *Sq* roughness of 0.1 (0.1) µm, whereas the IOS-TD data was significantly greater at 1.5 (0.8) µm ($p<0.0001$). Therefore, the noise floor measurement of the IOS-TD, when measuring a highly polished flat enamel surface, was 3.8 µm, in comparison to 0.5 µm for the NCLP.

3.4.3 Enamel groove measurements

Figure 3-4 shows representative datasets of polished enamel for groups of increasing groove depths of 7.2, 16.0, 44.0, and 86.5 µm, together with the automated groove detection analysis and the corresponding POMs/mm^2 produced by each device. The NCLP was able to localise and define all the grooves with sharp margins. In contrast, the IOS-TD scans displayed grooves with irregular and unclear margins and regions of positive or negative outliers, within and outside the groove boundaries. At increased groove depths, as seen in the examples of 44.0 µm and 86.5 µm, grooves were displayed more clearly; however, the transition between the groove margin and reference surface was less distinct than the NCLP scans. The IOS-TD datasets consisted of far fewer POMs/mm^2 ranging between 114 – 164 POMs/mm^2 compared to the NCLP which consistently produced 10,201 POMs/mm^2. Therefore, IOS-TD had approximately ×70 lower spatial resolution than the NCLP.

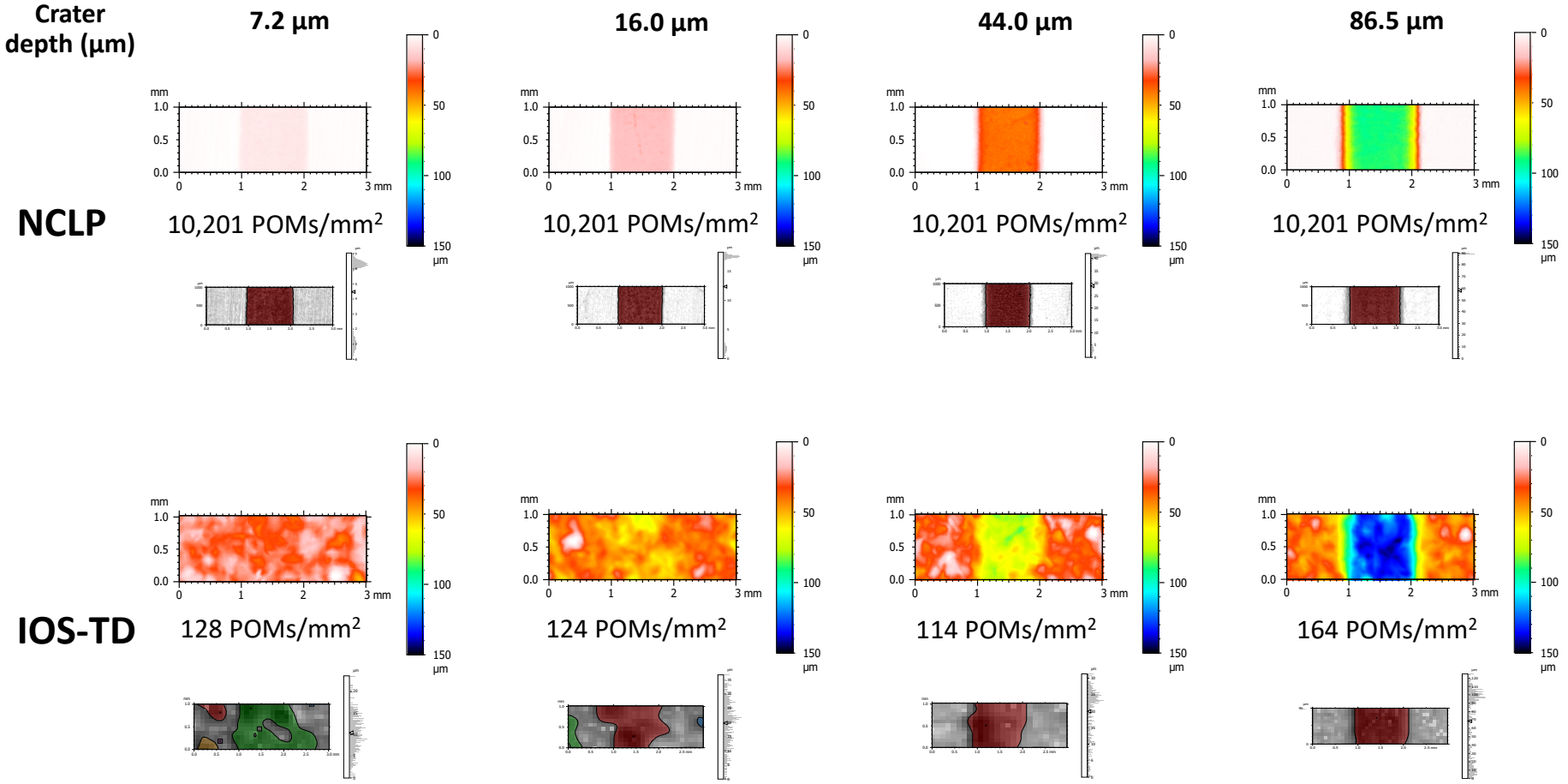

Figure 3-4 – Representative pseudo-colour NCLP and IOS-TD scans of enamel grooves of increasing depth (7.2-86.5 µm) with the number of points-of-measurement per mm^2 (POMs/mm^2) for each corresponding surface (3×1 mm) using surface-metrology software MountainsMap7®.
The digital scans show different colours as a function of Z-measurements. The NCLP produced more defined grooves with straight margins. In contrast, the IOS-TD often produced grooves with atypical shapes and unclear boundaries. The IOS-TD produced less POMs/mm^2 than the NCLP.

Table 3-2 shows the mean (SD) step-height measurements (µm) at increasing groove depth measured by the NCLP and IOS-TD, along with the XY area measurements (mm^2) and automated detection (%). The mean groove depth at baseline (0 mins of erosion) for the NCLP was 0.0 µm, and this increased from 1.9 µm to 86.5 µm. Based on the automated detection, the IOS-TD could not automatically identify the location and correctly measure surface area of any grooves shallower than 16.0 µm, while it could detect 20% of the grooves in the 18.8 µm group, 90% of grooves in the 44.0 µm group and 100% of grooves in the 86.5 µm group. Therefore, the measurement threshold of IOS-TD was determined to be 44.0 µm as at that depth level there were no statistically significant differences in depth or area measurements and a 90% of groove detection was achieved.

Table 3-2 – Mean (SD) groove depth (µm) and XY area (mm^2) measured by the NCLP and IOS-TD, with the percent of successful automated detection (%).
Statistically significant differences in depth and area measurements between NCLP (reference) and IOS-TD are shown (* = p < 0.05, ** p < 0.01, *** = p ≤ 0.001 and **** p ≤ 0.0001). Groove depth measurements are correct to one decimal place.

Mean (SD) enamel groove depth (µm)		**Mean (SD) enamel xy groove area (mm^2)**		**Automated detection of IOS (%)**
NCLP	**IOS**	**NCLP**	**IOS**	
0.0 (0.1)	1.3 (2.0)	0.02 (0.03)	0.34 (0.15) ***	0
1.9 (1.0)	-0.3 (3.4)	0.93 (0.06)	0.36 (0.34) ****	0
7.2 (1.2)	5.6 (2.7)	1.07 (0.04)	1.20 (0.46)	0
11.0 (1.1)	7.3 (2.9)	1.09 (0.07)	1.35 (0.26) *	0
16.0 (1.5)	16.0 (3.9)	1.11 (0.06)	1.29 (0.13)	0
18.8 (1.8)	18.0 (5.8)	1.10 (0.08)	1.33 (0.17) *	20
44.0 (4.8)	42.2 (6.2)	1.01 (0.08)	1.13 (0.09)	90
86.5 (5.0)	88.0 (7.2)	1.07 (0.09)	1.13 (0.08)	100

Figure 3-5 shows the mean (SD) skewness (*Ssk*) and kurtosis (*Sku*) of the NCLP and IOS-TD scans for the increasing groove-depth groups. At baseline (0.0 µm group, 0 mins of erosion), both the NCLP and IOS-TD scans produced surface amplitudes which conformed to a Gaussian distribution, representing flat and featureless surfaces, only the NCLP displayed statistically significant reductions in skewness and kurtosis vs. baseline, from the 1.9 µm depth group onwards ($p<0.0001$). On the contrary, the IOS-TD did not show any statistically significant reductions vs. baseline until the 11.0 µm groove-depth group for skewness ($p=0.0005$) and the 16.0 µm groove-depth group for kurtosis ($p=0.0014$).

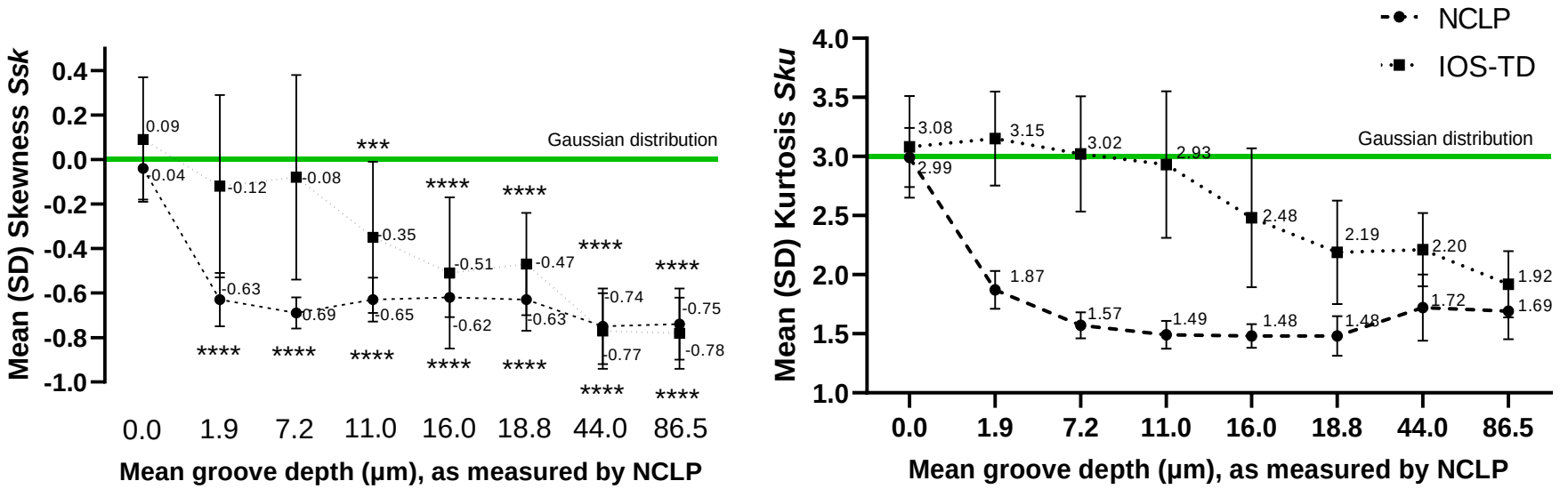

Figure 3-5 – Mean (SD) Skewness (*Ssk*) and Kurtosis (*Sku*) of the NCLP and IOS-TD scans for increasing groove depth groups.
Horizontal green lines of skewness (*Ssk*) equal to zero and kurtosis (*Sku*) equal to three equate to a Gaussian distribution of the surface heights.
Statistically significant differences are shown compared to the 0.0 µm mean grove depth (* = $p < 0.05$, ** $p < 0.01$, *** = $p \leq 0.001$ and **** $p \leq 0.0001$).

3.5 Discussion

This Chapter explored the limits of the IOS-TD for measuring changes in surface roughness on bespoke textured surfaces as well as changes in surface form on polished enamel. Measuring the roughness of textured surfaces using the IOS-TD demonstrated that the scanner was not able to discriminate changes in roughness until the 125.0 µm-particle grinding paper was measured; whilst the NCLP could discriminate all increases in roughness. Therefore, the first null hypothesis was rejected.

This is the first study to quantify the measurement threshold of a commonly reported IOS for measurement of surface loss on polished human enamel surfaces, based on a standardised protocol. It revealed that 90% of groove depths at 44.0 µm could be measured using automated detection and by implication depths greater than this could be confidently detected by the IOS-TD. Significant differences in XY area measurements and lower automated detection was observed below 44.0 µm; therefore, the second hypothesis was rejected.

An NCLP with a previously reported ±40 nm accuracy (F. Mullan et al., 2017) and ∼5 nm precision (F. Mullan et al., 2018) was used in this study as a gold standard, and its measurements were used as the accepted 'true' measurements of the enamel grooves. This instrument has nanometre-level accuracy and represents instruments of the highest resolution; similar NCLPs have reported comparable accuracies in the order of ∼30 nm, measuring V-shaped groove artefacts with 0.24, 0.75, 2.4, 7.5, 24 and 75 µm depths while using the same surface metrology software as this study (Nouira et al., 2014).

For the purposes of the investigation a single IOS was sampled. This might be considered a limitation as the resolution of different IOSs varies. However, the choice of IOS-TD (True Definition™, Midmark Corp., USA) was deemed suitable as it has been extensively investigated previously and is considered

amongst the best performing intraoral scanners in terms of resolution and accuracy (Boeddinghaus et al., 2015; Medina-Sotomayor et al., 2019a, 2018).

The spatial resolution of IOS-TD was scrutinised by measuring surface roughness on flat textured surfaces (gloss-paint and grinding papers on microscopy slides). IOS-TD demonstrated significant differences in *Sq* roughness measurements compared to the NCLP and could detect change in surface roughness only when the grinding paper with a silicon carbide particle size of 68 µm and *Sq* roughness of 30.8 µm was measured. This suggests that the IOS-TD may not be suitable for measuring short wavelength surface components, such as seen in texture and roughness analyses; instead, it would be more optimised for surface form measurements. Additionally, the IOS-TD scans of polished enamel consisted of approximately 114 – 164 POMs/mm^2 in contrast to 10,201 POMs/mm^2 for the NCLP scans. IOS-TD had approximately ×70 lower spatial resolution than the NCLP which resulted in an overall smoother topography of the enamel grooves.

The noise floor measurement of the IOS-TD, when measuring highly polished enamel, was 3.8 µm, in comparison to 0.5 µm for the NCLP. This suggests that readings and differences of the IOS-TD below 3.8 µm would not be distinguishable from “zero” and therefore would be below its detection limit (Attin et al., 2009).

Utilising the ISO:5436-1 step-height measurement technique, no significant differences were observed between the two devices for mean groove depths of 1.9- 86.5 µm. This is probably reflective of the larger standard deviations demonstrated from the IOS-TD, something that was also reported by (Kumar et al., 2019). Groove measurements were carried out based on a *priori* knowledge of their location on the sample and therefore potentially lead to the false assumption that IOSs can measure surface change of ≥1.9 µm. For IOSs to be useful in measuring features such

as depth, area and volume of enamel loss, the surface data needs to be amenable to automated surface loss localisation prior to measurement.

In addition to the low automated detection and significant differences in XY area measurements compared to the NCLP, the IOS-TD also demonstrated skewness and kurtosis measurements conforming to normal distribution below 11.0 µm groove depth for skewness and 16.0 µm groove depth for kurtosis and therefore it did not begin detecting a groove until these depths were reached, indicating limitations in detecting features of such depths on a flat surface. On the contrary, the NCLP datasets indicated consistent detection of the enamel grooves at all depths. These limitations can be explained by IOS-TD's lower point-cloud density compared to NCLP. The scanner's data-point interpolation between XY lateral measurements during surface formation, results in a polygon-mesh, which has a smoothing effect and results in larger triangles and smoother topography, which further limits its resolution. This smoothing effect may not have an impact on the scanner accuracy for grooves with larger surfaces but can be apparent when evaluating groove boundary distinctness, leading to poor depiction of the undulating transition area of the 'step' in a step-height or discrete ETW and hence false groove topography.

Nonetheless, the use of IOSs should be balanced against its speed of acquisition, higher automation, clinical application, and cost-effectiveness. This study suggests that using intraoral scanners could be a valid technique which may have advantages over profilometry for studies measuring wear ≥44.0 µm, including direct intra-oral measurement. This threshold is comparable to the reported mean annual vertical wear on molars, 38 µm (Lambrechts et al., 1989), showing promise for IOSs as diagnostic and monitoring tools of erosive tooth wear *in vivo*.

Previous studies have used wear modelling protocols involving 37% phosphoric acid (Meireles et al., 2016a) or drilling on a metal tooth (Hartkamp et al., 2017b), while only a few utilised a reference

device such as profilometry, in which the simulated wear depths were in the order of ≥17 µm (Witecy et al., 2021), ≥ 68 µm (Hartkamp et al., 2017b), or ≥ 221 µm (Kühne et al., 2021). Indeed, the study by Witecy et al., (2021) was the only other study that measured surface loss on polished enamel using IOSs. They demonstrated a lower agreement (approximately 10-20 µm IOS depth underestimation) in polished enamel loss measurements between the IOSs and profilometry than this present study. This may be because their study, together with all the other studies that used profilometry for comparison against the tested IOSs, measured surface loss by comparing sequential scans using iterative-contact-point (ICP) superimposition; a method which is described in Chapter 1 Section 1.3.5.2.2 above and is investigated in the subsequent chapters of this thesis. Although, this workflow might be more clinically relevant and commonly reported (Becker et al., 2018a; O'Toole et al., 2019a), as it allows wear measurements on natural enamel, its analysis performance is more prone to errors as each time-point scan and dataset alignment process introduce an individual set of errors (Ahmed et al., 2016). The quality of ICP-alignment for an optimal fit of two datasets, which is itself dependant on the scanner's accuracy and resolution, affects the accuracy of the measurement (DeLong, 2006). The analysis workflow in this Chapter was highly controlled and standardised. Polished enamel samples were used which consisted of flat planar surfaces optimised for step height measurements using a single scan, only after surface loss has occurred, therefore avoiding introduction of alignment errors. This 'single-scan analysis' is a commonly reported method and is considered to be the gold standard for *in vitro* erosion studies (Young and Tenuta, 2011). Nevertheless, since teeth consist of freeform surfaces, further research is necessary to develop and optimise methods for measuring change on such surfaces.

A key strength of this study was the use of automated algorithms on the 3 × 1 mm datasets, thus minimising operator bias regarding *a priori* knowledge of where the groove is located, which is crucial when discriminating topography changes in the order of microns. The analysis was not

restricted to only measuring vertical tissue loss; instead, additional surface metrology parameters were investigated as the depth increased, namely, automated measurement of the groove area as well as changes in skewness and kurtosis. Indeed, if a measurement process cannot automatically localise the groove, the groove would be unmeasurable. Therefore, studies purely relying on 3D step-height data measured based on predefined locations using reference or fiducial markers, must be interpreted with caution. To the author's knowledge, this is the first study that the threshold detection (also known as threshold segmentation) method was used to automatically localise and analyse the area of the grooves which is a recognised surface-feature detection method in metrology optimised when the background topography is flat and horizontal such as seen in polished enamel.

The dimensions of the artificial grooves on enamel were 1 mm wide and long whereas only a few microns deep, in an otherwise highly polished surface. These dimensions were designed to overcome the significant handicap of IOS-TD inferior spatial resolution; however, they represent a limitation of this present study. It is possible that smaller lateral dimensions on naturally complex native tooth surfaces may display a depth detection threshold even greater than 44 µm. Established protocols using relatively small flat surfaces are optimised for NCLP step-height measurement. This represents a specific measurement challenge for IOSs, as they operate using optical principles which are optimised for freeform shapes. Newer protocols, using complex more biologically appropriate samples, may reduce the disparity in measurements observed between the NCLP and IOS.

In summary, the combination of IOS-TD scanning and bespoke automated algorithms for surface loss detection and measurement on polished human enamel resulted in a depth measurement threshold of 44.0 µm. Above this, there were no significant differences between the NCLP and IOS-TD step-heights nor area measurements, suggesting that surface loss can be consistently quantified

using IOSs to a level of accuracy that maybe acceptable for clinical monitoring of material or tooth wear. However, caution needs to be applied as the study highlighted fundamental limitations of IOSs, necessitating further research.

3.6 Conclusions

This study reports on the limitations of the IOS-TD for measuring changes in surface roughness and form. Using novel optimised imaging algorithms, it was demonstrated for the first time that grooves on polished enamel can be reliably quantified using automated detection in the order of sub-50 µm depth, showing promise as a suitable tool for experimental laboratory-based studies investigating surface change or wear. Additionally, it revealed that IOS scanning is not suitable for surface roughness measurements and is more optimised for measuring surface form. The limitations of IOS-TD resolution revealed a pressing requirement for further research and technological advancements to optimise the performance of IOSs systems for measuring tooth surfaces, especially if below the sub-50 µm detection threshold.

Chapter 4 Comparison between two bi-scan analyses for measuring surface change

4.1 Introduction

Step heights can be calculated in different ways. A single profile across the middle of the sample, known as mid-point step height (O'Toole et al., 2015) is the simplest, followed by measuring the average from multiple profile lines, for example five (Mistry et al., 2015) or ten profiles (Mutahar et al., 2017). However, for more complex surface features, such as seen in erosive tooth wear, the use of a single profile or the average from a number of profiles may not necessarily be representative of the 3D complexity of the lesion topography. Whether there are differences in measurements between step heights calculated based on different number of profiles remains to be elucidated.

In contrast to polished enamel, measuring change on natural enamel surfaces requires more advanced surface metrology. This is because such surfaces consist of non-uniform geometrical features and freeform curved topographies (Savio et al., 2007) which are therefore not optimised for step height calculations using a single scan of a surface after change has occurred (single-scan analysis). To overcome this, quantitative bi-scan techniques have been proposed which allow for alignment and comparison of two sequential scans taken at different epochs (before and after surface change), to measure relative surface loss/gain over the intervening time between the two scans. Previous studies have quantified oral surface change via surface registration (superimposition) techniques using iterative-closest-point (ICP) algorithms (Kühne et al., 2021; J.M. Rodriguez et al., 2012) or via surface subtraction techniques (Holme et al., 2005; Mylonas et al., 2019; Stenhagen et al., 2011); though, each method suffers from inherent limitations which are described in detail in Chapter 1 Section 1.3.5.2 above. There is sparsity in the literature of studies

which compare the surface registration and the surface subtraction techniques for measuring topographical change of sequential scans of surfaces undergoing change.

Therefore, this current Chapter describes an investigation into polished enamel analysis, which firstly compares three different step height techniques, based on the number of profiles used during their calculation and secondly investigates two bi-scan analysis techniques, namely, surface-subtraction and surface-registration vs. the single-scan analysis described in the previous Chapter. As explained below, for the purpose of these investigations, the single-scan analysis is considered as the 'gold standard' reference method in comparison to the more complex bi-scan analyses techniques. Sequential scans of surfaces undergoing change will be referred to in the remainder of this thesis as bi-scans.

4.2 Aims and Null Hypotheses

4.2.1 Aims

The aims of this study were to:

1. Investigate differences in step height measurements on polished enamel using single-midline step height (Single-SH), ten-line step height (Ten-SH), and total 3D step height (Total-SH).
2. Investigate and determine the agreement between two bi-scan techniques: surface-registration and the surface-subtraction analyses; and compare them to a single-scan analysis for measuring groove depths on polished enamel.

4.2.2 Null Hypotheses

1. There will be no differences in step height measurements between the single-SH, the ten-SH, and the total-SH for measuring the depths of enamel grooves.

2. There will be no differences in groove depth measurements between the single-scan analysis, the bi-scan surface-registration, and the bi-scan surface-subtraction analyses.

4.3 Materials and methods

4.3.1 Enamel samples

Following previous sample size calculations, five groups of eroded polished enamel samples (n=50, 10 samples per group), were selected from the previous study in Chapter 3; each exhibiting a 1 mm-wide groove surrounded by fiducial markers on the acrylic embedding the enamel. The five enamel groups consisted of those that had undergone citric acid immersion (0.3%, pH 2.7, titratable acidity 10.2 mL) for a total of 5, 10, 15, 20, and 25 mins, respectively, to generate mean (SD) depths of 1.87 (0.50), 7.21 (1.19), 10.99 (1.06), 15.99 (1.49), 18.79 (1.80) µm, measured by the NCLP following a single-scan 3D step height analysis, described in Section 3.3.6.3 above, on page 133. For convenience, these five groups were labelled by their respective average depth to the nearest micron, i.e., 2 µm, 7 µm, 11 µm, 16 µm, and 19 µm. These depths were used in each analysis protocol.

4.3.2 Scanning

Profilometric scans of the eroded enamel samples (n=50) were carried out using the NCLP in rectilinear grid spacing of 10 µm X, Y intervals, resulting in 'point clouds' of individual data points, each 10 µm apart from each other, following the method described in Section 2.2.3 above on page 107, and according to previously published protocols (Mistry et al., 2015; F. Mullan et al., 2018; Mylonas et al., 2018). The datasets were saved in ASCII format as .tai filename which were then converted to a .txt file extension for compatibility with the analysis software. Baseline scanning

datasets (prior to eroding the samples) were already available from the study described in Chapter 3.

4.3.3 Depth analysis of enamel grooves

Two bi-scan analyses: surface-registration and surface-subtraction, were used to quantify depths of enamel grooves by a single blinded operator, by comparing respective baseline and post-exposure datasets of each sample.

4.3.3.1 Bi-scan surface-subtraction analysis

Figure 4-1~~Figure 4-1~~ shows the workflow of the bi-scan surface-subtraction technique. Baseline and post-exposure (following acid immersion) datasets for each sample, consisting of cartesian point clouds, were loaded into MountainsMap7® surface-metrology software. Using the function 'series of surfaces', a pair of baseline and respective post-exposure datasets were selected for alignment. The two datasets were manually aligned by pin-pointing the same two fiducial markers placed on the acrylic material surrounding the enamel (Figure 4-1~~Figure 4-1~~A), (Mylonas et al., 2019).

Following manual alignment, the post-exposure dataset was subtracted from its respective baseline, to yield a residual or 'difference' dataset (Figure 4-1~~Figure 4-1~~B). The accuracy of the XY correspondence between the two subtracted surfaces was quantitatively inspected by looking at the root-mean-square (RMS) error value (µm) between the two datasets calculated by the software (i.e., the smaller the RMS value of the residual surface, the better the surfaces were aligned), as well as qualitatively by the colour-coded display of the residual surface with colours acting as a function of Z heights. Within the residual dataset, a 3 x 1 mm area of interest was extracted containing the groove in the middle third (Figure 4-1~~Figure 4-1~~C). Outliers, such as erroneous spikes, were manually removed from the 3 x 1 mm residual dataset and the surface levelled, using a linear least-squares place of best fit method, excluding the 1 mm-wide central lesion.

The depth of the enamel grooves was determined using three different types of step height calculations (µm), based on the ISO 5436-1 standard, which measures the height difference between the mid-third region of a groove (step) and two reference regions on either side (de Groot and Fitzgerald, 2017; Leach, 2015). The three techniques measuring the 2 µm, 7 µm, 11 µm, 16 µm, and 19 µm step heights consisted of the following (Figure 4-1~~Figure 4-1~~D):

1. Single-midline step height (single-SH) – calculated from a single profile across the groove (O'Toole et al., 2015)
2. Ten-line step height (ten-SH) – calculated as a mean from 10 profiles of the step height taken at manually selected regions across the groove (Mutahar et al., 2017)
3. Total 3D step height (Total-SH) – calculated as a mean profile automatically created by the software from all the profiles across the groove within the analysed area (Mylonas, 2017; Rodriguez and Bartlett, 2010); i.e., 101 horizontal profiles from the 3 x 1 mm area.

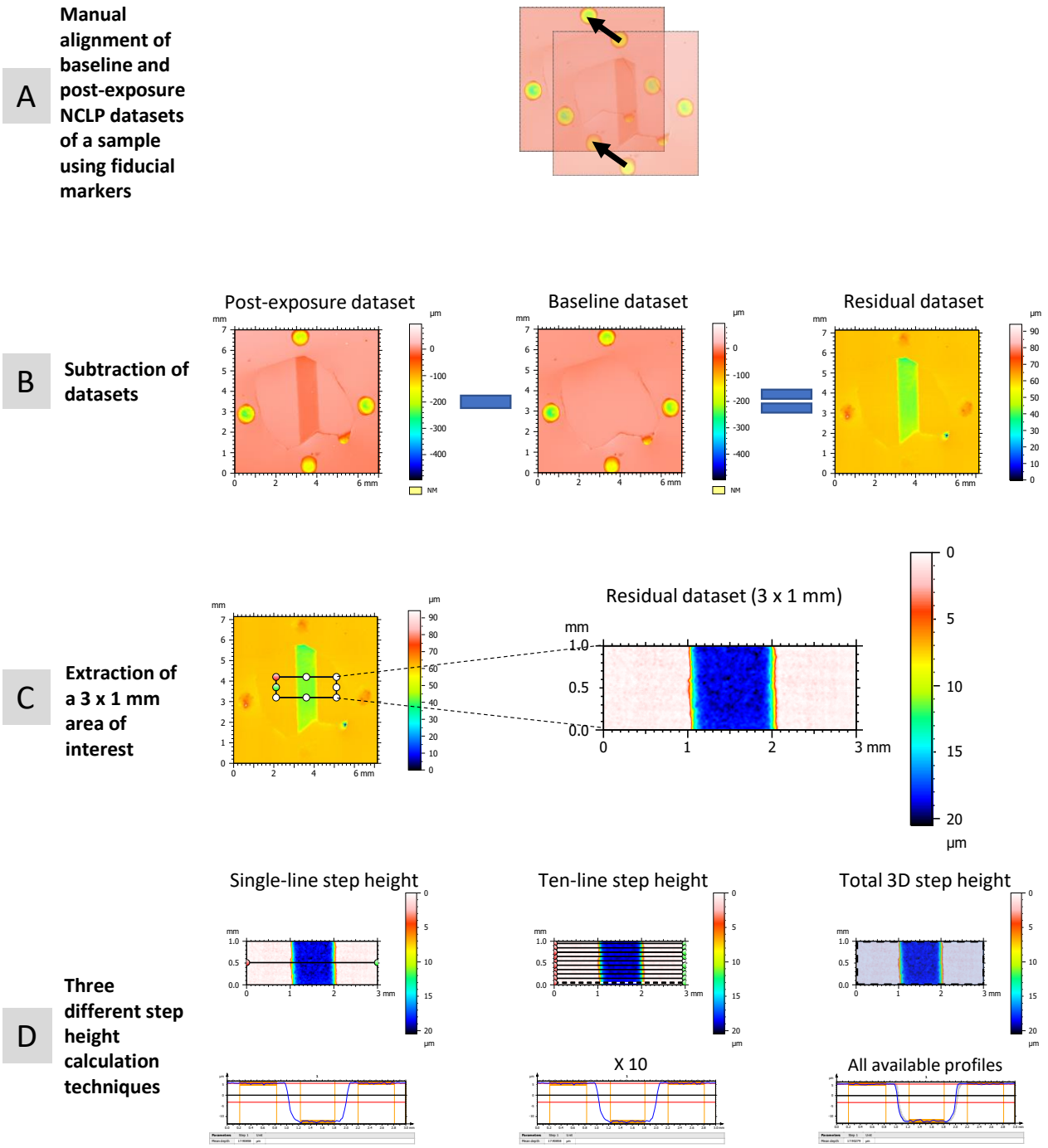

Figure 4-1 – Workflow of bi-scan surface-subtraction analysis.
The baseline and post-exposure datasets were manually aligned (A) before subtracted from each other to produce a residual/difference dataset (B). A 3 x 1 mm area was extracted from within the residual surface containing the groove in the middle third (C), prior to calculating the depth of the groove using three different step height techniques (D).

4.3.3.2 Bi-scan surface-registration analysis

Figure 4-2 shows the workflow of the bi-scan surface-registration technique for the same groove depths (2 µm, 7 µm, 11 µm, 16 µm, and 19 µm). The baseline and post-exposure NCLP datasets from

each sample, were loaded into a different software, a reverse-engineering software package (Geomagic Control 2014, Geomagic Inc, North Carolina, USA). The point clouds of each dataset were transformed into 3D polygon meshes.

After setting the baseline dataset as the 'reference' and the post-exposure dataset as the 'test', the fiducial markers on each dataset were highlighted and used as reference regions to facilitate the superimposition (registration) process (Figure 4-2A). An initial best-fit alignment based on an ICP algorithm was conducted using 300 iterative pairs of points, before a more precise fine-superimposition was performed using 1500 pairs of points (Figure 4-2B). The registration between the 3D meshes was inspected by the operator prior to conducting a 3D comparison which displayed a colour-coded heatmap to represent the distance deviations between the pair of datasets (Figure 4-2C). Surface change between the aligned datasets was measured by calculating the mean deviations in Z (μm) of five areas of 0.4 mm radius, conveniently spaced vertically apart inside the groove.

4.3.3.3 Reproducibility

The workflows for each bi-scan analysis, the surface-subtraction (using the Total-SH output) and the surface-registration, were repeated three times (Repeat 1, Repeat 2, and Repeat 3) on different days for all 50 samples, to investigate their reproducibility.

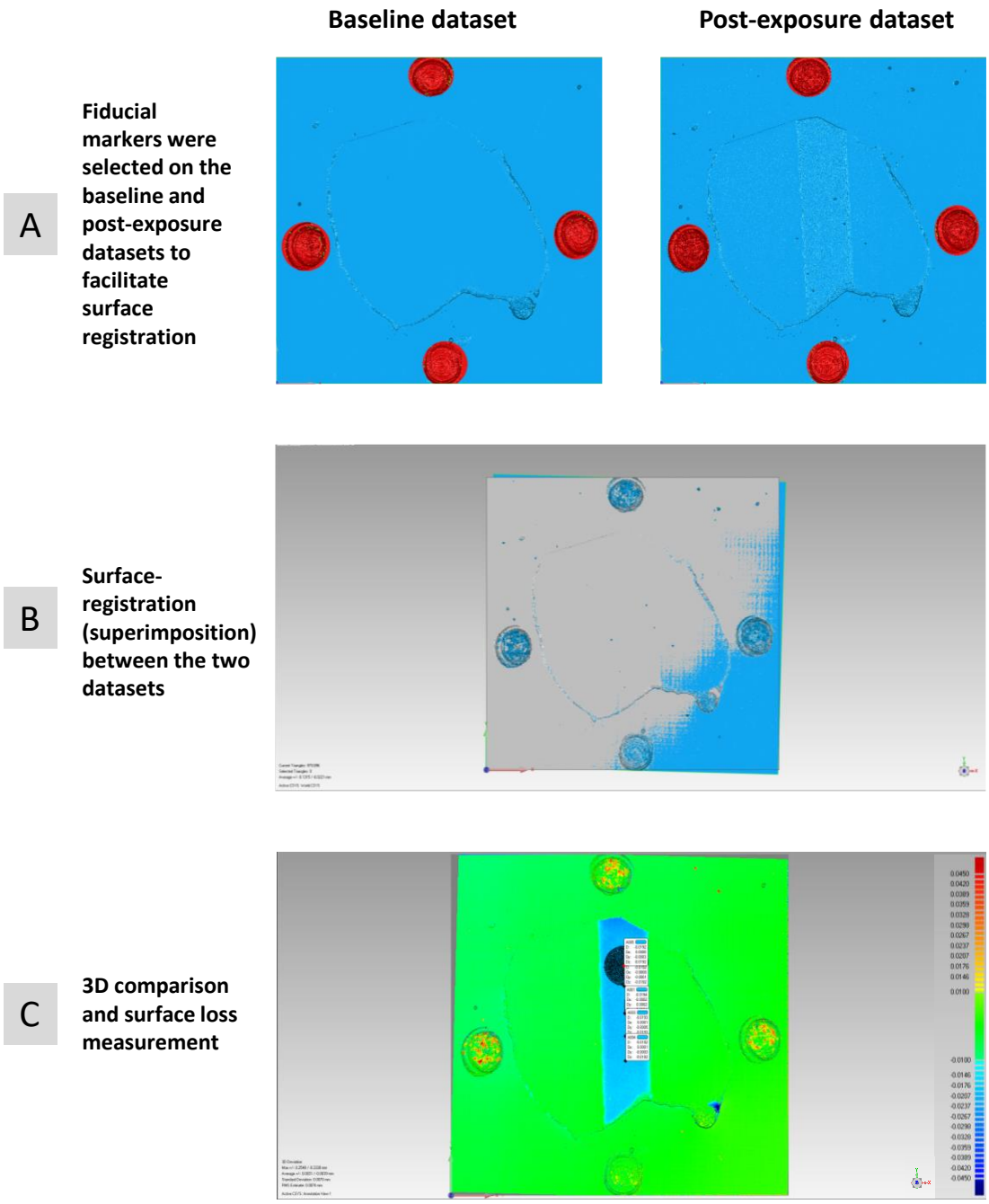

Figure 4-2 – Workflow of bi-scan surface-registration technique.
Baseline and post-exposure datasets were transformed into 3D polygon meshes and fiducial markers were selected (A) prior to conducting ICP surface-registration (superimposition) (B). A 3D comparison was then carried out displaying a colour-coded heatmap to represent distance deviations between the pair of datasets (C). Surface change between aligned datasets was measured as the mean deviation in Z (µm) of five areas of 0.4 mm radius inside the groove.

4.3.4 Statistical analysis

Statistical analyses were conducted using Prism9 (GraphPad Software Inc, California, USA). All data were assessed for normality using the Kolmogorov-Smirnov test and visually assessed using QQ

plots. A paired two-way ANOVA with post-hoc Sidak's tests were conducted to compare depth measurements between each step height technique following bi-scan surface-subtraction analysis. A paired two-way ANOVA with post-hoc Sidak's tests were also conducted to compare groove depth measurements between the reference single-scan analysis (acquired in Chapter 3), the bi-scan surface-subtraction (using the Total-SH output) and the bi-scan surface-registration analyses. Additionally, a Bland-Altman analysis was conducted to calculate the bias and 95% limits of agreement (LOA) between the surface-subtraction and surface-registration analyses. Pearson's correlations and Bland-Altman analyses were conducted to assess the reproducibility between repeated measurements (Repeats 1, 2, and 3). Statistical significance was set as $p \leq 0.05$ in all tests.

4.4 Result

Table 4-1 shows the mean (SD) NCLP groove depth measurements of the enamel groups using the reference single-scan analysis, the bi-scan surface-subtraction analysis using three different step height techniques (Single-SH, the Ten-SH, and the Total-SH), and finally the bi-scan surface-registration analysis. The mean (SD) groove depth measurements of the five enamel groups using the reference single-scan analysis were acquired from Chapter 3 and were 1.87 (0.50), 7.21 (1.19), 10.99 (1.06), 15.99 (1.49), 18.79 (1.80) μm, respectively.

4.4.1 Comparison between three types of step height techniques

Following bi-scan surface-subtraction analysis, the mean (SD) groove depths of the five enamel groups using the single-SH technique were 2.34 (0.47), 7.24 (1.30), 11.46 (1.11), 16.06 (2.39), and 19.05 (1.93) μm, respectively. For the ten-SH technique, the mean (SD) groove depths of the five different groups were 2.35 (0.62), 7.17 (1.17), 11.50 (1.13), 16.07 (2.28), and 19.04 (1.87) μm; and for the Total-SH technique, these were 2.31 (0.53), 7.16 (1.16), 11.46 (1.15), 16.12 (2.32), and 19.07 (1.87) μm. No statistically significant differences were observed between any of the three investigated step height techniques of the bi-scan surface-subtraction analysis, at any of the five enamel groups ($p>0.05$), nor when compared to the reference single-scan analysis ($p=0.3627$).

Table 4-1 – Measurements of the polished enamel groove depths from NCLP datasets using the reference Single-scan analysis, the Bi-scan surface-subtraction analysis with the three different step height techniques: Single-SH, Ten-SH, and Total-SH, and finally the Bi-scan surface-registration analysis with its deviation in Z output.

Name of enamel group (based on average depth)	**Number of samples per group**	**Acid immersion time (min)**	**Single-scan analysis (Reference method)**	**Bi-scan surface-subtraction analysis**			**Bi-scan surface-registration analysis**
			Mean (SD) Total-SH (µm)	Mean (SD) Single-SH (µm)	Mean (SD) Ten-SH (µm)	Mean (SD) Total-SH (µm)	Mean (SD) Deviation in z (µm)
2 µm	10	5	1.87 (0.50)	2.34 (0.56)	2.35 (0.62)	2.31 (0.53)	1.99 (1.24)
7 µm	10	10	7.21 (1.19)	7.24 (1.30)	7.17 (1.17)	7.16 (1.16)	11.34 (4.80)
11 µm	10	15	10.99 (1.06)	11.46 (1.11)	11.50 (1.13)	11.46 (1.15)	15.06 (2.60)
16 µm	10	20	15.99 (1.49)	16.06 (2.39)	16.07 (2.28)	16.12 (2.32)	19.17 (4.48)
19 µm	10	25	18.79 (1.80)	19.05 (1.93)	19.04 (1.87)	19.07 (1.87)	24.22 (4.85)

4.4.2 Comparison between the single-scan, bi-scan surface-subtraction, and bi-scan surface-registration techniques

Figure 4-3 shows the mean (SD) groove depth (μm) measurements using the single-scan, the bi-scan surface-subtraction and the bi-scan surface-registration analyses for the five different enamel group depths. The mean (SD) groove depths of the five enamel groups using the single-scan analysis and bi-scan surface-subtraction technique (with the Total-SH output) were described above. The mean (SD) groove depths of different enamel groups using the surface-registration technique were 1.99 (1.24), 11.34 (4.80), 15.06 (2.60), 19.17 (4.48), and 24.22 (4.85) μm. No statistically significant differences were observed between the single-scan analysis and the bi-scan surface-subtraction analysis for any of the enamel groups. Statistically significant differences were observed between the single-scan analysis and the bi-scan surface-registration analysis for the 7 μm ($p= 0.0002$), 11 μm ($p=0.0002$), 16 μm ($p=0.0050$) and 19 μm ($p<0.0001$) enamel groups (Figure 4-3). The measurements of the bi-scan surface registration analysis were statistically significantly higher than those of the bi-scan surface-subtraction analysis at the 7 μm ($p=0.0002$), 11 μm ($p=0.0024$), 16 μm ($p=0.0119$), and 19 μm ($p<0.0001$) enamel groups.

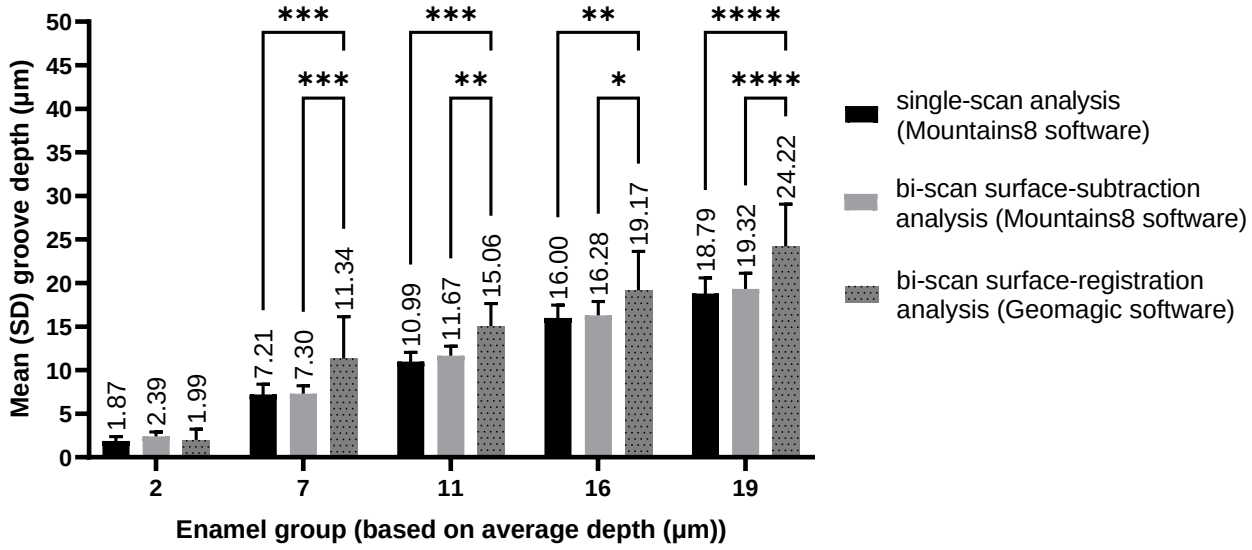

Figure 4-3 – Mean (SD) groove depth (µm) measurements using the single-scan, the bi-scan surface-subtraction and the bi-scan surface-registration techniques for the five different enamel group depths.
Statistical significance is denoted by * ($p<0.05$), ** ($p<0.01$), *** ($p<0.005$), and ****($p<0.0001$).

Bland-Altman plot analysis shown in Figure 4-4 revealed a bias of 3.05 µm between the surface-subtraction technique and the surface-registration with 95% LOA of - 4.91, 11.01 µm. The differences between the two techniques were smallest at the 2 µm reference group groove depth (µm), whilst no particular trend was observed for any of the other groups.

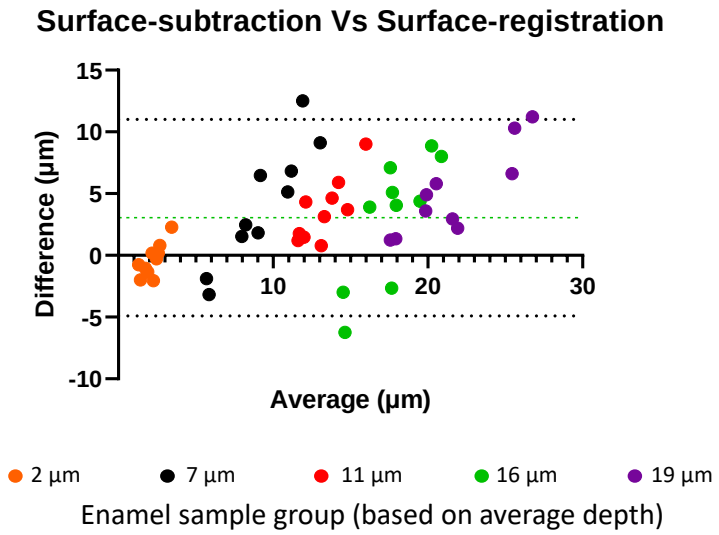

Figure 4-4 – Bland-Altman plot of differences between Bi-scan surface-subtraction and surface-registration techniques for measuring groove depths. The overall bias (green line) was 3.05 µm with 95% Limits of Agreement (LOA) (black lines) of - 4.91, 11.01 µm.

4.4.3 Reproducibility

4.4.3.1 Bi-scan surface-subtraction analysis

Bland-Altman analyses between repeated total-SH measurements of the bi-scan surface-subtraction analysis revealed biases (95% LOA) close to zero [Repeat 1 Vs 2: -0.42 (+2.39/-3.22) µm; Repeat 1 Vs 3: -0.09 (+1.79/-1.97) µm; Repeat 2 Vs 3: -0.32 (+2.34/-1.70) µm] (Figure 4-5). Pearson's correlation analysis showed strong positive correlations between repeats 1, 2, and 3 of Total-SH measurements of the bi-scan surface-subtraction analysis (Repeat 1 Vs 2: $R^2 = 0.9500$, n = 50, $p<0.0001$; Repeat 1 Vs 3: $R^2 = 0.9766$, n = 50, $p<0.0001$; Repeat 2 Vs 3: $R^2 = 0.9743$, n = 50, $p<0.0001$) (Figure 4-5).

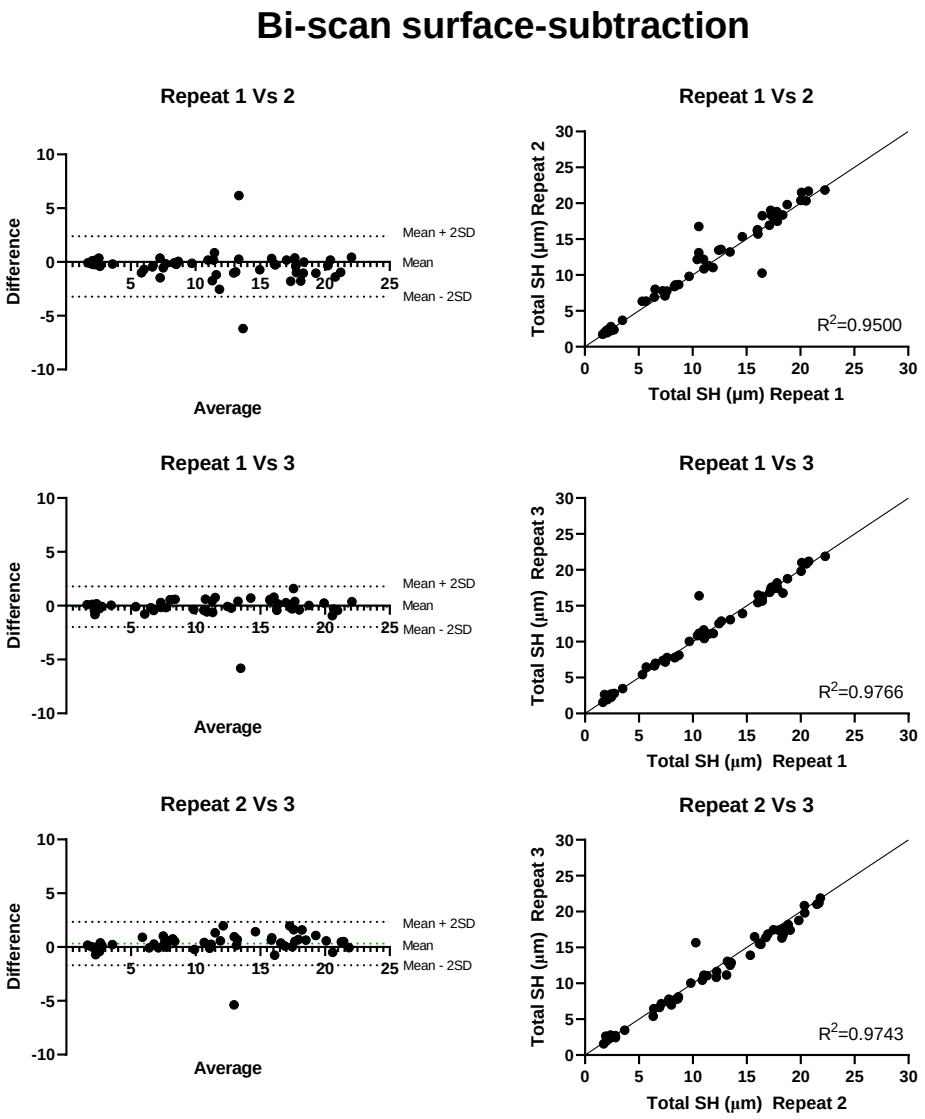

Figure 4-5 – Bland-Altman and Pearson's correlations of repeated measurements (Repeat 1, 2, and 3) of Bi-scan surface-subtraction analysis.

4.4.3.2 Bi-scan surface-registration analysis

Bland-Altman analyses between repeated deviation in *Z* (µm) measurements of the bi-scan surface-registration analysis also revealed biases (95% LOA) nearing zero [Repeat 1 Vs 2: 2.79 (+9.88/-4.30) µm; Repeat 1 Vs 3: 2.23 (+9.19/-4.72) µm; Repeat 2 Vs 3: -0.55 (+2.84/-3.94) µm]. Pearson's correlation analysis showed strong positive correlations between repeated measurements of the bi-scan surface-subtraction analysis (Repeat 1 Vs 2: R^2=0.8420, n=50, p<0.0001; Repeat 1 Vs 3: R^2=0.8330, n=50, p < 0.0001; Repeat 2 Vs 3: R^2=0.9390, n = 50, p < 0.0001).

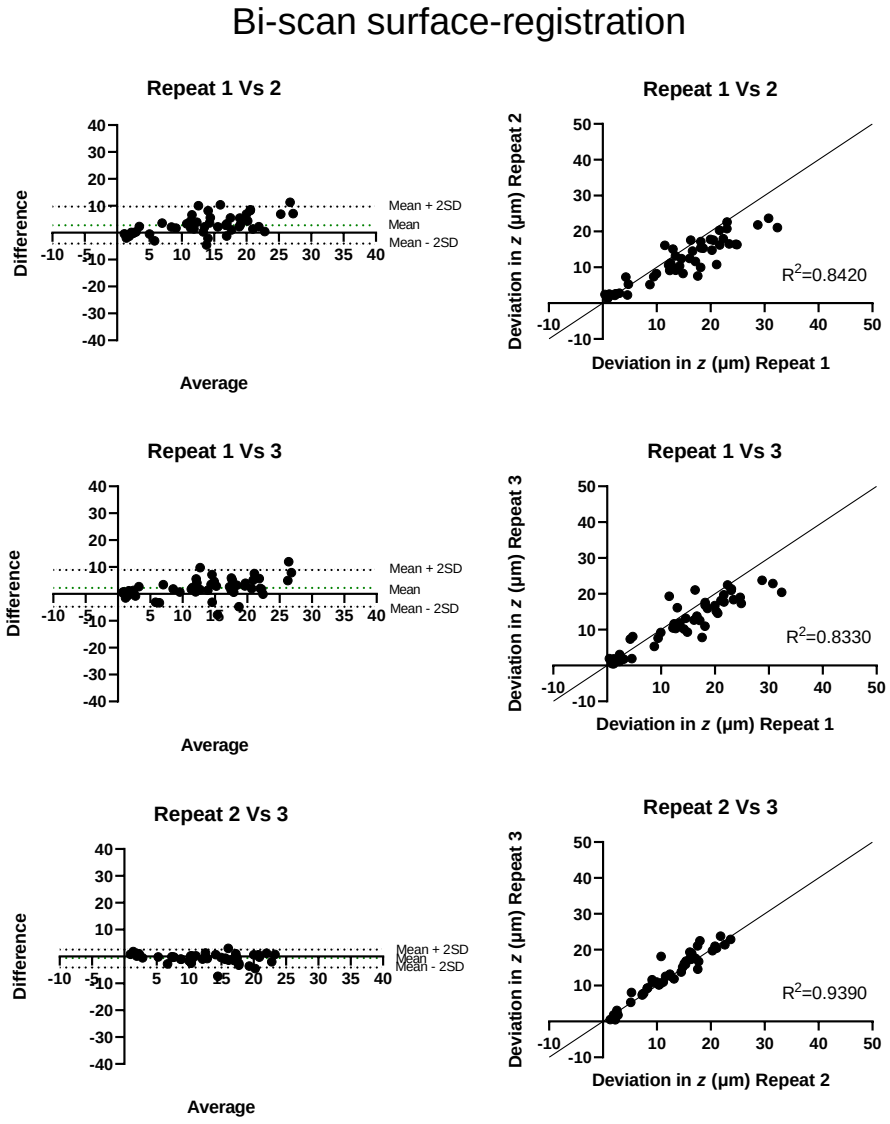

Figure 4-6 – Bland-Altman and Pearson's correlations of repeated measurements (Repeat 1, 2, and 3) of Bi-scan Surface-registration analysis.

4.5 Discussion

Measuring surface change on teeth using bi-scan techniques such as the surface-subtraction or the surface-registration analyses has been previously reported in the literature (Mylonas et al., 2019); however, there is lack of studies comparing the two together. In this chapter, measurements of enamel groove depths using the surface-registration in the form of three different step height outputs namely, single-SH, ten-SH, and total-SH revealed no significant differences between them and therefore the first null hypothesis, stating that the different step height techniques would result in similar measurements, could not be rejected. When the surface-subtraction technique (using the total-SH measurement output) was compared against the surface-registration technique (using the deviation in Z output) for measuring enamel groove depths revealed statistically significant differences between the two at most depth groups; therefore, the second null hypothesis was rejected.

To the author's knowledge the number of studies comparing different types of step heights based on the number of profiles used during the calculation is sparse. In this present study, no differences were observed between the three different step height techniques, single-SH, ten-SH, and total-SH using NCLP datasets; therefore, a uniform enamel loss within the created grooves was assumed. For the single-SH and ten-SH techniques, the operator manually selects the profiles across the groove to record the step height and hence may be prone to bias. However, a groove with less homogenous tomography (i.e., without a uniform floor) may not necessarily be truly represented by a single or a small number of profiles; therefore, a 3D analysis which includes all datapoints/profiles should be utilised if the metrology software used offers this option. Nevertheless, the high level of agreement between all three step height calculations demonstrated that they are all regarded as viable methods of step height measurement. Similar to this study, a thesis by Almohefer (2021), also

demonstrated no statistically significant differences between a mid-point profile and a means of five profiles for measuring step height on polished dentine samples at multiple immersion times using citric acid solutions of pH 2.6 and 3.2.

Scanning datasets were generated using a NCLP which is characterised by a high level of accuracy that had already been established in the literature, exhibiting a combined measurement uncertainty of ±0.28 µm (F. Mullan et al., 2017) and precision of 5 nm (polished enamel) and 23 nm (natural enamel) (F. Mullan et al., 2018). The fact that the NCLP is so accurate may also explain why step height analysis using a single profile resulted in similar measurements than when ten profiles or all available profiles were used. Perhaps using datasets from scanners of lower accuracy and resolution, such as IOSs, may result in significant differences between the different types of step height analyses.

Polished enamel was the surface substrate of choice for scanning, both for convenience and simplicity. The use of an effective acid-resistant barrier protocol on natural enamel to produce an exposed area of enamel with corresponding areas of protected/uneroded enamel to serve as reference for comparison after exposure would have presented a significant challenge. This was relatively easy to achieve for polished enamel samples and is one reason why *in vitro* research studying dental wear has primarily used polished enamel surfaces (Attin and Wegehaupt, 2014; Young and Tenuta, 2011).

The measurements using the single-scan analysis described in Chapter 3, on the same samples used in this present study, were adopted as the 'gold standard' reference analytical method as it represented the simplest and most standardised analysis workflow requiring a single post-exposure scan only, to quantify the depth of groove on enamel. Although both surface-subtraction and surface-registration analyses were developed for freeform surface metrology, the use of polished

enamel which is a non-freeform surface allowed comparison against the gold standard single-scan analysis, that is commonly utilised in *in vitro* erosive tooth wear studies (Young and Tenuta, 2011).

However, oral surfaces, such as teeth, consist of complex non-planar freeform geometries, and unlike planar flat surfaces such as polished enamel, are not ideal for single-scan step height analysis. Both the bi-scan surface-subtraction and the surface-registration analyses enable comparison of sequential datasets taken at different points of time and surface change quantification; therefore, are more relevant for clinical monitoring in the surgery. On the other hand, their relative analysis performance compared to the single-scan analysis is more prone to errors as each scan as well as their alignment process introduce an individual set of errors (Ahmed et al., 2016).

The bi-scan surface-subtraction analysis demonstrated similar measurements as those of the reference single-scan analysis. This may be because no software algorithms were involved during the alignment of the pair of datasets; instead, a manual alignment was conducted by the operator by the use of fiducials which was scrutinised quantitatively and qualitatively by the RMS error between the two datasets and by the pseudo-colour residual surface displayed by the software, respectively. A key limitation of this technique is that it is subject to errors inherent to the way the two datasets are aligned, especially when freeform surfaces are being subtracted. Where there is a difference in slope between the two datasets; it is crucial that they are perfectly aligned in the X and Y axes before subtraction occurs to produce a difference measurement in the Z axis; otherwise, this will introduce errors in the step height measurements (DigitalSurf, 2022a). Additionally, having to manually align the two datasets is a less automatic and intuitive process and requires high operator experience. Nevertheless, this limitation was not obvious in this study. This is believed to be because the surfaces used were flat and therefore any errors from manual alignment would be of little consequence to the residual surface produced after subtraction.

Variations of the surface-subtraction analysis were described in several previous studies (Holme et al., 2005; Mylonas et al., 2019; Stenhagen et al., 2011). For the accurate subtraction between the baseline and post-exposure datasets, these studies used a specially designed holder or jig which allowed reproducible repositioning of the samples prior to scanning; therefore, the baseline and post-exposure datasets appeared in the same Cartesian location when loaded on to their software. In this present study, such jigs were not used. Instead, fiducial markers were created on the acrylic surrounding the enamel surface on the samples as reference pin-points for manually aligning each pair of datasets using software functionalities. Although, this introduces operator error in the analysis workflow, it better simulated *in vivo* conditions as the use of a physical repositioning jigs would not be practical for translation to direct *in vivo* scanning of oral surfaces due to the movement of the patient and oral surfaces/teeth.

The bi-scan surface-registration analysis demonstrated significantly higher measurements compared to the reference single-scan analysis as well as the bi-scan surface-subtraction analysis with a bias (95% LOA) between the two investigated bi-scan analyses of 3.05 (- 4.91, 11.01) µm. It also demonstrated higher standard deviations and slightly lower reproducibility than the bi-scan surface-registration analysis based on the Bland-Altman and Pearson's correlation tests between repeated measurements. This may be explained by the fact that, although the surface-registration analysis required two sets of scans (similar to the surface-subtraction analysis), it utilised software automated ICP algorithms for alignment whose mathematical complexities are often hidden from the operator. An automated workflow combining the two techniques together i.e., an initial surface-registration followed by surface-subtraction may offer improvements for freeform metrology of more complex surfaces, such as those seen intra-orally.

Although offering a more automated alignment process, the quality of the ICP-based registration for an optimal fit of two datasets affects the accuracy of the measurement output (Becker et al., 2018a; DeLong, 2006). ICP algorithms have been reported to introduce errors due to their nature to minimise the distance and spread the error across the entire area of the two surfaces (O'Toole et al., 2020, 2019a). If the algorithm 'decides' that the absolute error between two surfaces is optimally minimised by causing a positive deviation in one area to counteract a large negative deviation (such as seen with surface loss) in another, it will align the two scans in this way, regardless of the clinical outcome.

Surface registration procedures are yet to be standardised. O'Toole et al., (2019a) investigated the accuracy of different types of ICP-based surface registrations (alignments), suggesting that *reference-based alignment* resulted in a significantly more accurate alignment (22 µm translation-error), followed by *best-fit alignment* (130 µm), and landmark-based alignment (139 µm). Therefore, in this present study the ICP algorithm during the surface-registration technique was restricted to the fiducial markers as reference landmarks. Similar to this present study, Mylonas et al., (2019) demonstrated increased groove depth measurements using the surface-registration analysis than their respective subtractive technique. O'Toole et al., (2019) argued that indiscriminate use of ICP-based surface alignments result in underestimations of surface change. Conducting a best-fit alignment (including the area of surface change during alignment) pulls the 'worn' dataset excessively towards the 'unworn' baseline dataset to minimise the inter-surface distances across the entire surface giving an erroneous underestimate of the amount of surface loss and in some cases when surface change is minimal, reporting surface gain. However, when the same authors conducted alignment that was restricted to landmarks (landmark-based registration) this resulted in an overestimation of surface loss (O'Toole et al., 2019a), which is comparable to this present study.

The increased depth measurements shown by the surface-registration analysis in this present study may be because the alignment process was restricted to four fiducial markers only which represent a relatively small area compared to the total area of the scanned surfaces. By manually highlighting these fiducials, the alignment algorithms were restricted on areas that remained uneroded; however, this may have introduced bias to a certain degree. Additionally, the concave shape of the fiducials may have challenged the angular tolerance of the NCLP resulting in measurement spikes in those regions affecting the overall alignment and subsequently overestimating surface changes. Another possible explanation is that the concave nature of the fiducials made it difficult to keep them free of any dust particles which if present during scanning may have interfered with the alignment process more than the manual pin-point alignment used for the surface subtraction analysis. Nevertheless, the use of larger reference areas if available that are less likely to have occurred changes would have perhaps resulted in similar findings to (O'Toole et al., 2019a). The use of softgauges (software measurement standards) as digital surfaces with mathematically created features would allow to test the numerical correctness of these bi-scan analyses without the errors introduced from scanning.

Alignment of digital impressions of oral surfaces is challenging requiring stable anatomical landmarks. O'Toole et al., (2019) suggested using the smooth buccal and palatal surfaces of molars as they are least likely to undergo changes. On the other hand, Becker et al., (2018) suggested using palatal rugae and concluded that reliable superimposition of dental models is possible if ten carefully selected areas with deviations below 0.5 mm are used for landmark-based registration. Due to the lack of reference features on the polished enamel samples, four fiducial-markers were used in this study, which is a methodological compromise to the clinical situation. Finding such reference areas, which have not undergone any wear, within a clinical setting continues to remain

an unresolved challenge and requires further *in vivo* research which is out with the scope of this present investigation.

4.6 Conclusions

This study demonstrated no significant differences in groove depth measurements using three different types of step height calculations (Single-SH, Ten-SH, and Total-SH) via the bi-scan surface subtraction analysis. Additionally, it demonstrated that the bi-scan surface-registration analysis, although more automated, resulted in significantly increased groove depths than the reference single-scan analysis and the bi-scan surface-subtraction analysis using fiducial markers as reference areas to aid in the alignment. This is believed to be primarily because of the use of ICP-based algorithms restricted to relatively small areas (fiducials) as reference regions for alignment. Both bi-scan techniques investigated in this study have limitations inherent to the way their alignment process works therefore further research is required to minimise errors and make the workflows more automated.

Chapter 5 The threshold of the IOS-TD for measuring crater depths on natural enamel combining the surface-registration and surface-subtraction techniques

5.1 Introduction

Traditionally, quantification of change on dental surfaces using 3D digital scans has been made possible by extra-oral digitisation of replicas (silicone impression or resulting dental stone casts) using high-resolution profilometers (S. O'Toole et al., 2018; J M Rodriguez et al., 2012) or laboratory scanners, which are lower resolution than profilometers, but have the advantage of being able to capture undercut areas (Ahmed et al., 2016; Gkantidis et al., 2020). More recently the use of IOSs has been proposed as a means of directly capturing the 3D geometry of teeth (Kühne et al., 2021; Zimmermann et al., 2015), thus removing the need for intermediate steps such as impressions or cast production. Chapter 3 demonstrated a depth measurement threshold of 44 µm for a clinical intraoral scanner (IOS-TD) on polished enamel (Charalambous et al., 2021). However, to date, no study has described an analogous threshold of intraoral scanning systems for measuring change on unpolished natural surfaces which consist of a more complex freeform topography.

This Chapter focuses primarily on the quantification of surface change on natural unpolished enamel. It is split into three interconnected investigations. These investigations explore the validation of a novel workflow which combines the techniques of surface-registration and surface-subtraction described in the previous chapter (Chapter 4), before proceeding to explore the measurement threshold and limitations of the IOS-TD for discriminating surface loss on natural unpolished enamel.

5.2 Aims, Objectives and Null Hypotheses

5.2.1 Aims

The aims of this study were to:

1. Determine the accuracy of the combination of surface-registration and surface-subtraction compared to surface-registration alone; with or without using reference areas during the alignment process.
2. Determine the threshold of the IOS-TD for measuring crater depths on natural unpolished enamel.
3. Determine the effect of increasing crater diameter on the sensitivity of the IOS-TD to measure depth.

5.2.2 Objectives

The objectives were to:

1. Mathematically create softgauges of known depths to investigate the accuracy of four bi-scan analysis workflows:
    a. Best-fit surface-registration (BF-Reg),
    b. Reference-based surface-registration (Ref-Reg),
    c. Best-fit surface-registration and surface-subtraction (BF-Sub), and
    d. Reference-based surface-registration and surface-subtraction (Ref-Sub).
2. Determine the depth measurement threshold of the IOS-TD on freeform enamel surfaces using the optimal analysis technique by creating, scanning, and analysing different crater depths on natural enamel vs. gold standard NCLP.

3. Determine the effect of diameter on the sensitivity of the IOS-TD by creating, scanning, and analysing different crater diameters vs. NCLP.

5.2.3 Null hypotheses

1. There would be no differences in the accuracy of the four bi-scan analysis workflows investigated in this study for measuring simulated crater depths on softgauges.
2. The accuracy of the IOS-TD compared to the NCLP measurements, would be the same for measuring craters of different depths on natural enamel surfaces.
3. The accuracy of the IOS-TD compared to the NCLP measurements would be the same for measuring craters of different diameters on natural enamel surfaces.

5.3 Materials and Methods

5.3.1 Study design

This study was split into three investigations. The first investigation assessed the accuracy of four bi-scan analysis techniques for measuring digitally simulated craters of known depths on softgauges:

a) Best-fit surface-registration (BF-Reg),
b) Reference-based surface-registration (Ref-Reg),
c) Best-fit surface-registration and surface-subtraction (BF-Sub), and
d) Reference-based surface-registration and surface-subtraction (Ref-Sub).

For the second investigation, after having established the optimal bi-scan technique, craters with increasing depths were created on natural unpolished human enamel samples and scanned by the IOS-TD and the gold standard NCLP to determine the depth measurement threshold of IOS-TD.

The third and final investigation assessed the effect of increasing diameter on the accuracy of IOS-TD in measuring crater depths on natural enamel.

5.3.2 Investigation 1 – Validation of combined surface-registration and surface-subtraction using softgauges

5.3.2.1 Creation of softgauges

As described in Chapter 1, Section 1.3.6, page 66, a softgauge is a digital measurement standard for testing the numerical correctness of surface metrology software (Chiboub et al., 2021), which can be either mathematically generated *de novo* or generated in a scan which has previously been measured by an instrument (DigitalSurf, 2022c). For the purposes of this present study, a sound natural enamel sample from the buccal surface of a human molar was conveniently selected and scanned using the NCLP in order to obtain a point-cloud dataset comprising of X, Y, Z cartesian coordinates, into which profiles were mathematically-created as described below.

Firstly, the baseline dataset were converted into a text file (.txt extension) and loaded into Mountains®8 surface metrology software where a surface of 3 mm diameter encompassing the zenith of the enamel surface was extracted and saved again as a text file. Figure 5-1 illustrates how the data appeared as a text file, consisting of the scan settings in the first 15 lines and further below, of the first 18 lines of the X, Y, Z coordinates of the digital surface.

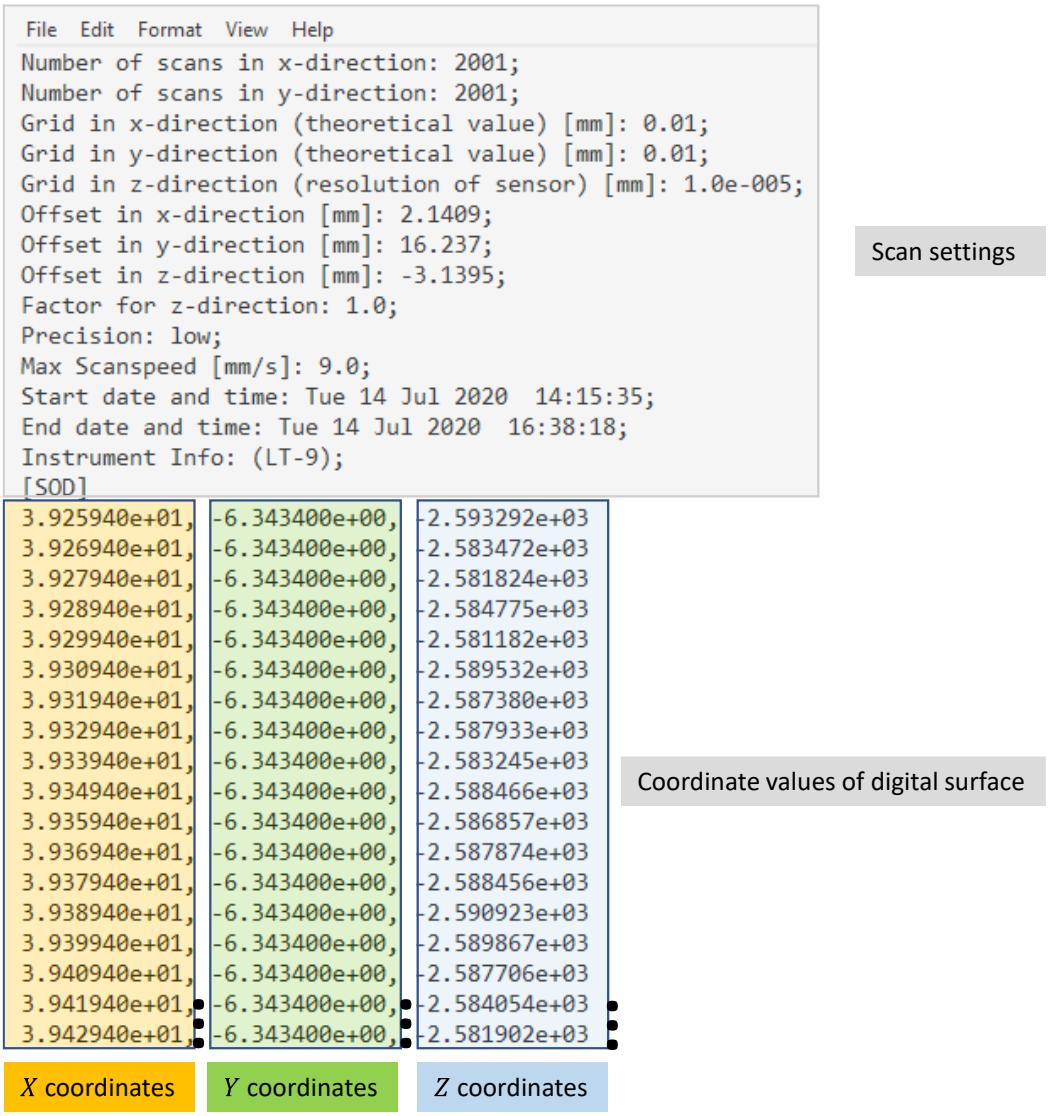

Figure 5-1 – Appearance of a dataset in the text file format, consisting of the scanning settings (first 15 lines) and the XYZ coordinates per measurement point (first 18 lines).

As shown in Figure 5-1 above, the X, Y, Z coordinate values of the 3 mm dataset appeared as three separate columns. These were copied into a spreadsheet software (Excel® Microsoft®, version 2008) and the Z column was manipulated to digitally create softgauges with known depths of 20, 40, 60, 80, and 160 µm and a consistent diameter of 1.5 mm at its centre (Figure 5-2).

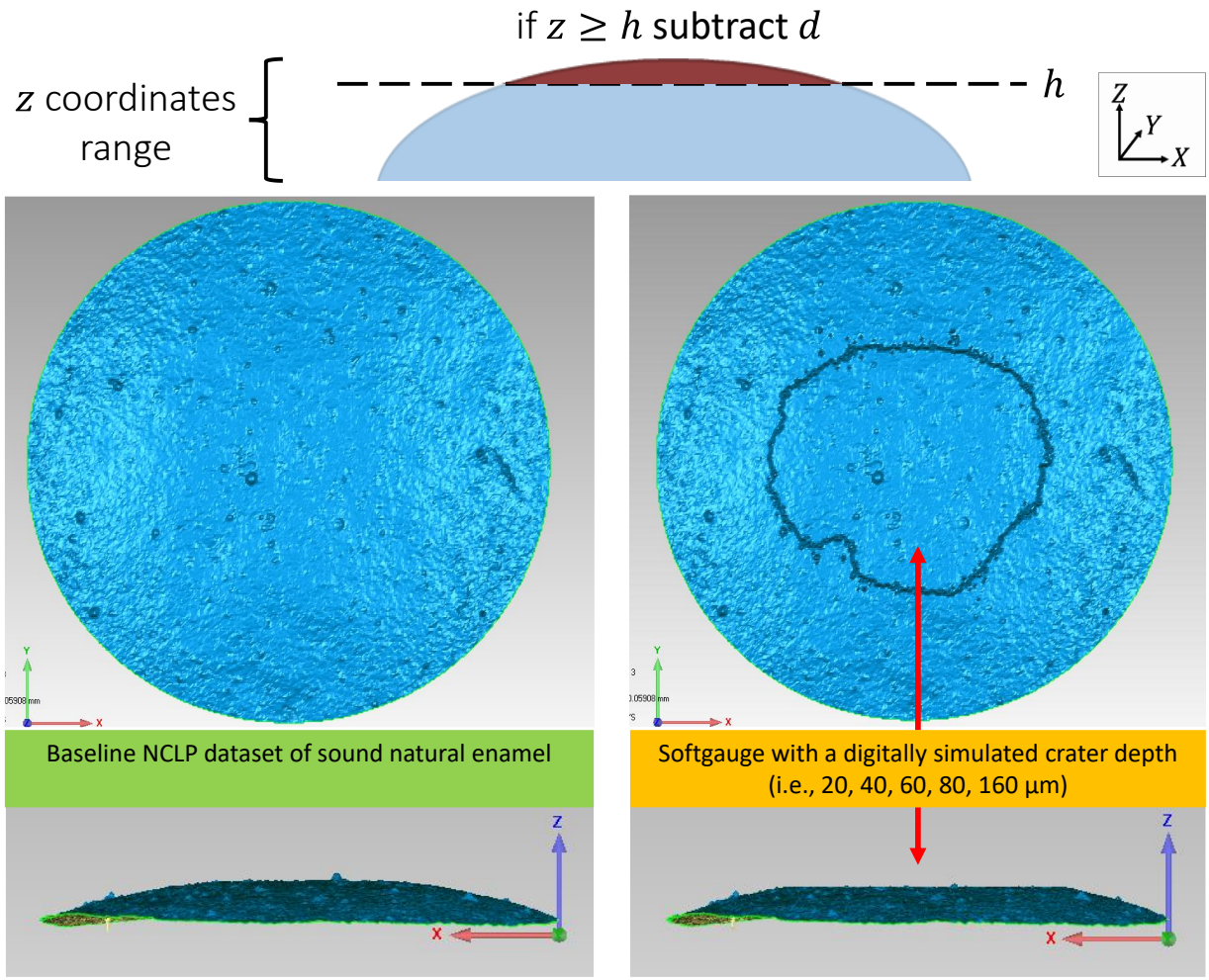

Figure 5-2 – Schematic diagram depicting the methodology of digitally simulated craters of known depth on a natural enamel surface (top), together with representative images of the baseline NCLP dataset of a sound natural enamel (left) and an example of a softgauge with a central crater (right).
z – coordinate value, h – a selected value within the top inter-quartile range of *Z* coordinates representing an imaginary plane that intersects the curved surface horizontally and dictating the sought diameter of the crater, d – the depth of the sought crater (µm).

In order to create this soft gauge with profiles of the correct dimensions, this manipulation involved calculating the range of the z coordinates of the point-cloud and using the following excel function: $IF\ (z\ \geq h,\ z-d,\ z)$, where z is the z coordinate value, h is a selected value within the top inter-quartile range of the z coordinates representing an imaginary plane that intersects the curved surface horizontally and dictating the diameter, and d is the crater depth. This function was translated as follows: 'if z is above h, subtract d from z, otherwise keep z value the same'.

Therefore, to create a softgauge with a 20 µm crater depth, the value of 20 was subtracted from all the z values above or equal to the chosen base-height (h) of the crater.

The datasets of the baseline surface and the softgauges featuring the different known depths of 20, 40, 60, 80, and 160 µm were saved as STL files using Mountains®8 software and then loaded into Geomagic Control 2014 reverse-engineering software for analysis.

5.3.2.2 Comparison of bi-scan analysis techniques

Each individual bi-scan technique can be used separately or in combination, however when used in combination, surface-registration must be performed before surface-subtraction and not *vice versa*. This is because the result of surface-subtraction is to end up with a residual dataset which is a single surface, which cannot be registered to another scan, whereas in contrast the result of surface-registration is two scans which still exist independently but have been aligned.

Therefore, in the present study, best-fit surface-registration (BF-Reg) and reference-based surface-registration (Ref-Reg) were first individually tested, following which best-fit surface-registration combined with surface-subtraction (BF-Sub) was tested and finally, reference-based surface-registration combined with surface-subtraction (Ref-Sub) was tested. Each technique was repeated ten times for simulated crater depths of 20, 40, 60, 80, and 160 µm, based on *a priori* sample size calculation from previous pilot data measuring the 80 µm simulated depth, using GPower freeware, version 3.1.9 (Heinrich Heine, Dusseldorf, Germany), and based on paired t-tests between two means (SD) of 76.80 (2.40) µm for the BF-Reg and 79.90 (0.03) µm for the Ref-Sub (α error = 0.05, power = 0.80, effect size 1.30), indicating a total sample size of ≥ 9 per group.

Figure 5-3 shows the outline of the workflows of the four bi-scan analysis techniques (BF-Reg, Ref-Reg, BF-Sub, Ref-Sub) to calculate the percentage error (%) in measuring the different crater depths from 20 to 160 µm on the softgauges. For the BF-Reg technique, an initial best-fit alignment using

300 randomly software-selected data points were conducted before a 'fine' alignment using 1500 data points to align the two meshes. For the Ref-Reg technique, after an initial alignment using 300 followed by 1500 randomly software-selected data points, the surface-registration was repeated, restricted to selected unchanged reference regions. For the BF-Sub and Ref-Sub techniques, the now registered (aligned) surfaces (following the BF-Reg and Ref-Reg techniques, respectively) were loaded into a different software package, Mountains®8, and subtracted to produce a residual surface representing the difference between the two surfaces. Then a levelling process, utilising a best-fit-linear-least-squares plane, excluding the central crater area was applied. The accuracy of the XY correspondence between the two subtracted surfaces was quantitatively inspected by looking at the root-mean-square (RMS) error value (µm) between the two datasets calculated by the software (i.e., the smaller the RMS value between the two surfaces to be subtracted, the better the surfaces were aligned), as well as qualitatively by the colour-coded display of the residual surface with colours acting as a function of Z heights.

For the BF-Reg and Ref-Reg techniques, the depth of the craters were reported as the mean mesh-distance (deviation in Z) (µm) inside the crater area between the baseline and the softgauge surfaces. For the BF-SS and Ref-SS techniques, crater depths were reported as step-heights (µm) based on ISO:5436-1.

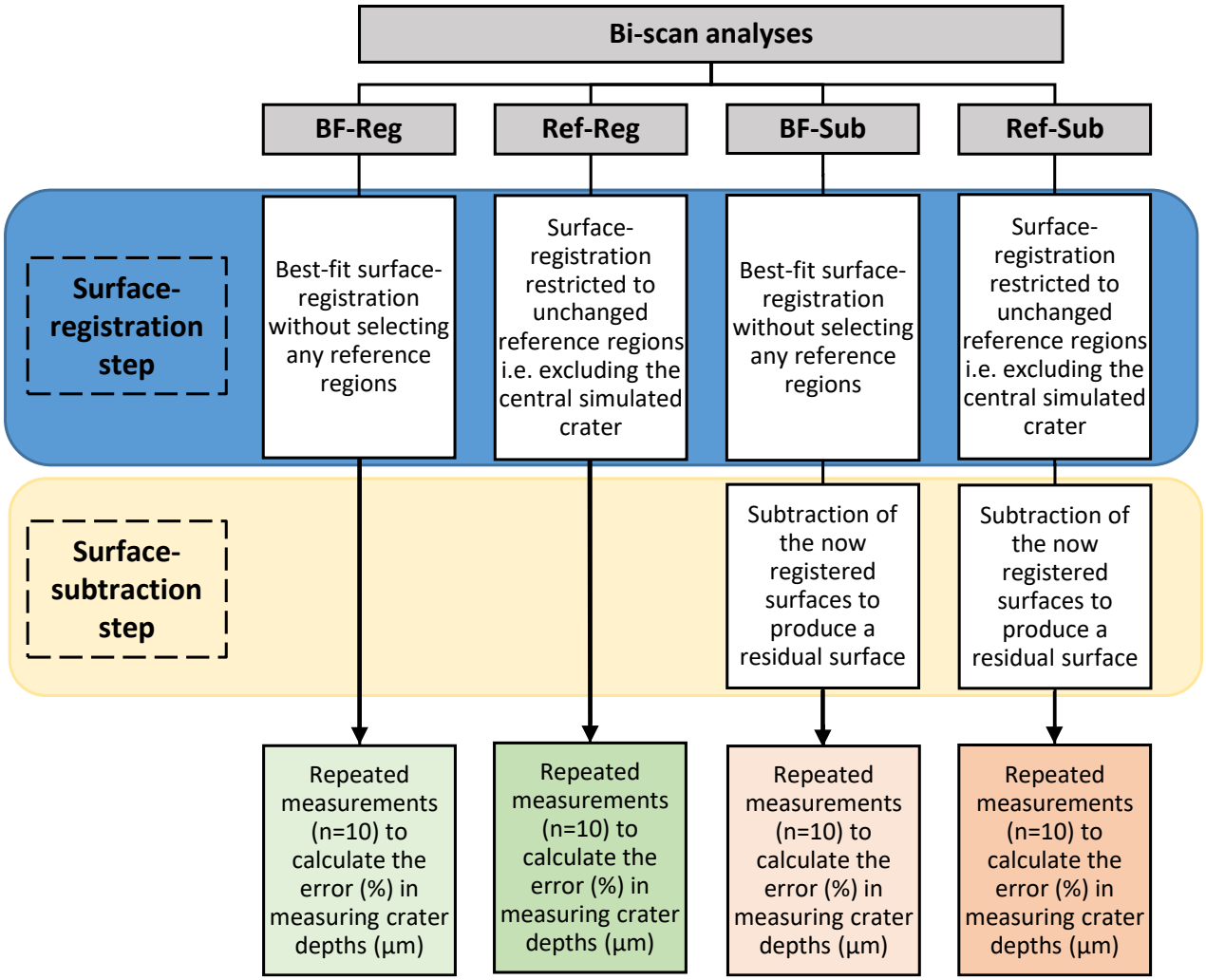

Figure 5-3 – Workflow outline of the four bi-scan analyses (BF-Reg, Ref-Reg, BF-SS, Ref-SS) investigated to calculate the percentage error (%) in measuring the crater depths (i.e., 20 - 160 µm) that were digitally created on the softgauges. BF-Reg - Best-fit surface registration, Ref-Reg - Reference-based surface-registration, BF-SS - Best-fit surface-registration and surface-subtraction, Ref-SS - Reference-based surface-registration and surface-subtraction.

5.3.3 Investigation 2 – The threshold of the IOS-TD measuring crater depths on natural enamel

5.3.3.1 Natural enamel sample preparation

Figure 5-4 demonstrates the methodology used for setting up natural enamel samples.

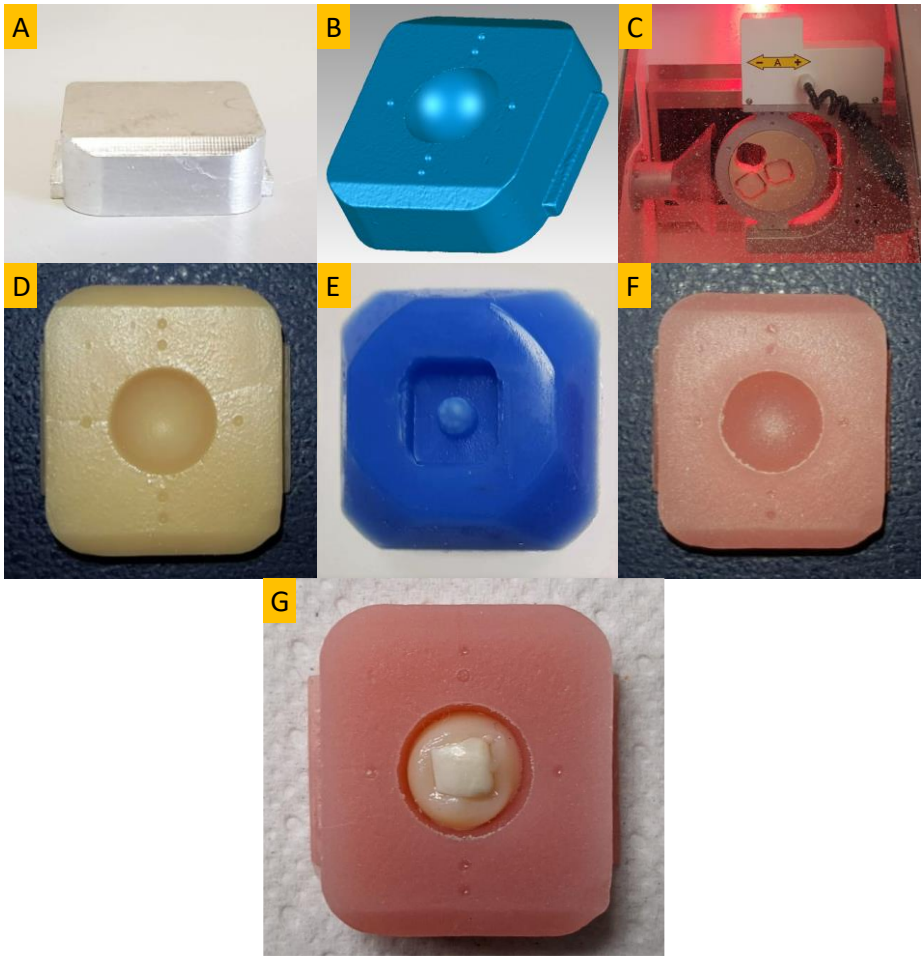

Figure 5-4 - Natural enamel sample preparation

Firstly, acrylic blocks were designed to act as sample holders. To achieve this a hard-ionised aluminium and brass object (A) with dimensions of 25 × 22 × 8 mm (Syndicad Ingenieurbüro, München, Germany) was handheld-scanned using the IOS-TD to capture its geometry as an STL file. The dataset was loaded into Geomagic Control 2014 software and edited by adding a central concave hemisphere of 8 mm diameter on its flat surface to act as a well to embed the enamel sample (B). The final design was then 3D-milled from a polymethyl methacrylate (PMMA) disc (part number 10036895, shade A2, 20 mm thickness, Planmeca, Helsinki-Uisuimaa, Finland) using PlanMill 50, a 5-axis milling unit (Planmeca, Helsinki-Uisuimaa, Finland) (C) which had been calibrated using a 500 µm thickness calibration object to a tolerance of ± 30µm (Planmeca, 2022). Using the sample holder prototype (D), hand-mixed PMMA (Oracryl self-cured acrylic, Bracon

Limited, Heathfield, UK) was poured into custom made silicon moulds (E) (Gemini Two Part Silicone Model Duplicating Material, Bracon Limited, Heathfield, UK) to create multiple sample holder replicas (F). Extracted sound permanent human molars were collected following ethical approval (REC ref:18/WM/0351). Following disinfection, the teeth were sectioned to produce buccal/lingual samples (n=14) of approximate dimensions 5 × 5 mm and each embedded inside the acrylic sample holders. The samples were then ultrasonicated to remove contaminants and left to air-dry for 24 h prior to baseline scanning by a single experienced operator.

5.3.3.2 Creation of craters of different depth on natural enamel

An electrical polyvinylchloride adhesive tape/barrier with a 1.5 mm diameter circular hole, made using a punch-biopsy (BP-15F 1.5 mm KAI Medical, Seki, Japan) was placed over the zenith of the enamel surface to provide reference regions surrounding the central exposed enamel. The tape also covered the flat surface of the sample holder to prevent any acid going into the well that the enamel was embedded in. Each taped sample was visually assessed for air-voids/gaps at the tooth-tape interface using an optical coherence tomography device (OCT) which displayed live cross-sectional scanning images of the sample.

Crater depths, each 1.5 mm in diameter, at 11, 18, 23, 24, 34, 40, 56, 58, 62, 70, 73, 75, 79, and 81 µm, as measured by the NCLP as the reference device, were created on the enamel samples (one crater per sample) using 1% citric acid (pH 2.2, titratable acidity 31.3 mL) at different immersion times, ranging from 90 to 270 mins, under 62.5 rpm orbital agitation (Stuart mini-Orbital Shaker SST1, Bibby Scientific, England). The samples were washed and air-dried for 24 h before tape removal. Figure 5-5 illustrates the barrier method using PVC adhesive tape (A) to create a 1.5 mm diameter crater depth (B) and examples of OCT B-scans before and after erosive challenge indicating the direct contact between the tape and enamel surface with no evidence of an air gap present (C).

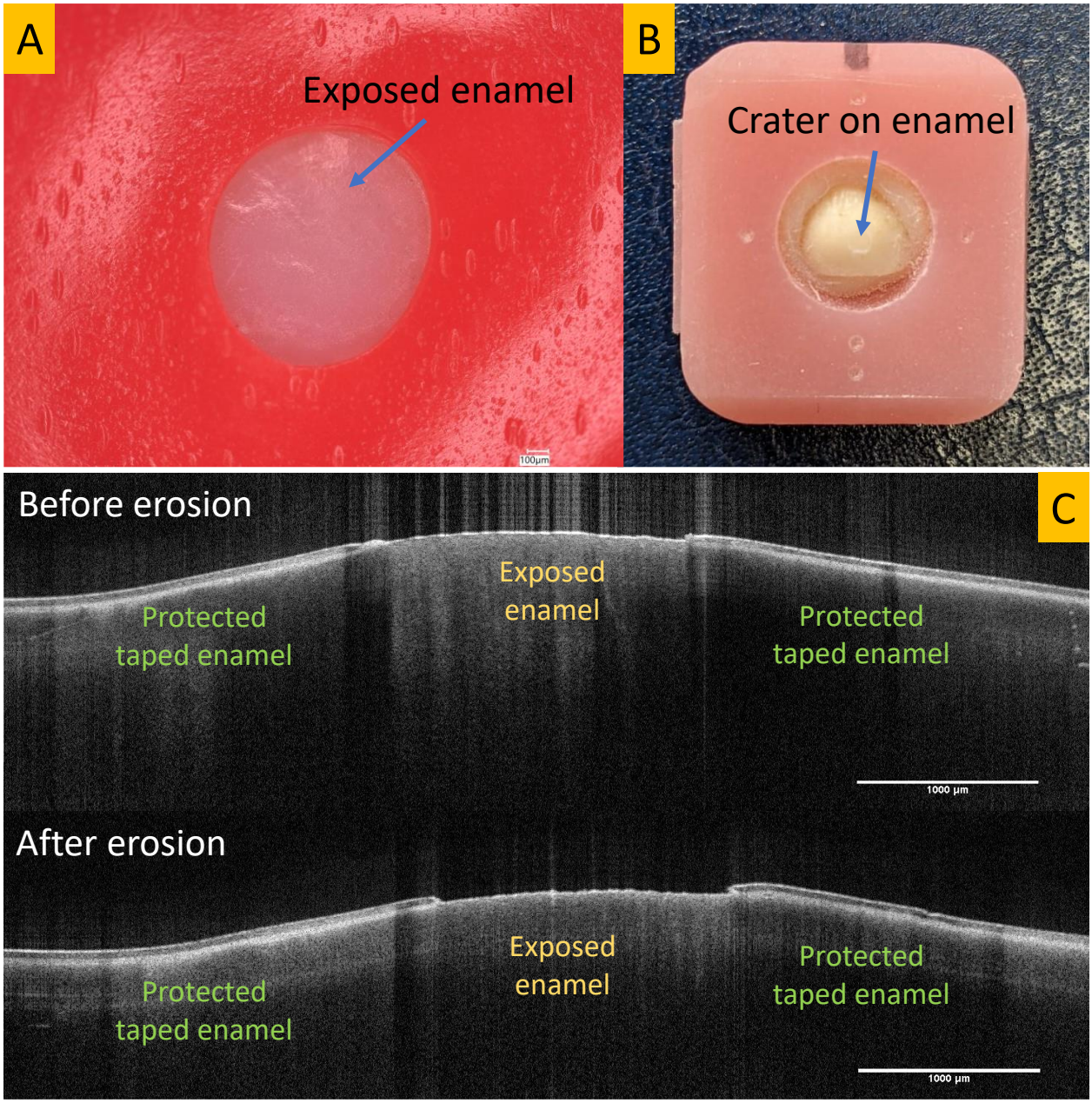

Figure 5-5 – Barrier method using PVC adhesive tape.
Close up of a natural enamel sample with PVC adhesive tape and 1.5 mm hole placed on the zenith of natural enamel surface (A). A natural enamel sample after erosion featuring a 1.5 mm circular crater (B). Cross sectional OCT B-scans of a taped sample before and after erosion indicating no air gaps between the tape and tooth (C).

5.3.3.3 Scanning

NCLP scans of the natural enamel samples were carried out with a rectilinear grid spacing of 10 µm X, Y intervals, resulting in point clouds, each point being 10 µm apart from each other, following

the method described in Chapter 2 Section 2.2.32.2.3 above, on page 107. Scanning using the IOS-TD was conducted following manufacturer's instructions and the handheld scanning method (Chapter 2 Section 2.2.4 above, page 109). The IOS-TD datasets were exported with maximal resolution to optimise scan quality and downloaded as STL files from the scanner's cloud-based platform.

Each natural enamel sample (n=14) was scanned five times at baseline (T0) and five times post acid-exposure (T1) by both the NCLP and the IOS-TD to create pairs (T0 + T1). The number of repeated scans per sample was determined based on a priori sample size calculation using GPower freeware, version 3.1.9, based on a paired t-test with mean (SD) depth measurements of 143 (1) μm for NCLP and 149 (3) μm for IOS-TD indicating five (T0 + T1) scan pairs per depth level (80% power, α=0.05, effect size 2.28 μm for NCLP vs. IOS-TD).

5.3.3.4 Quantification of crater depths

Following determination of the optimal software technique in investigation 1, randomised pairs of baseline and post-exposure scans (T0 + T1) for each enamel sample, from the NCLP and IOS-TD, were analysed using the Ref-Sub technique (Figure 5-6) to calculate the discrimination threshold of the IOS-TD by comparing the data from the gold standard NCLP.

Following surface-registration on reference enamel regions surrounding the enamel craters in the Geomagic software, extraneous areas of scanned acrylic from the aligned scans were trimmed, leaving behind data of natural enamel only, after which, the alignment was repeated to facilitate a greater fit. The two datasets were then subtracted from each other as described above to produce a residual dataset, from which surface change was measured.

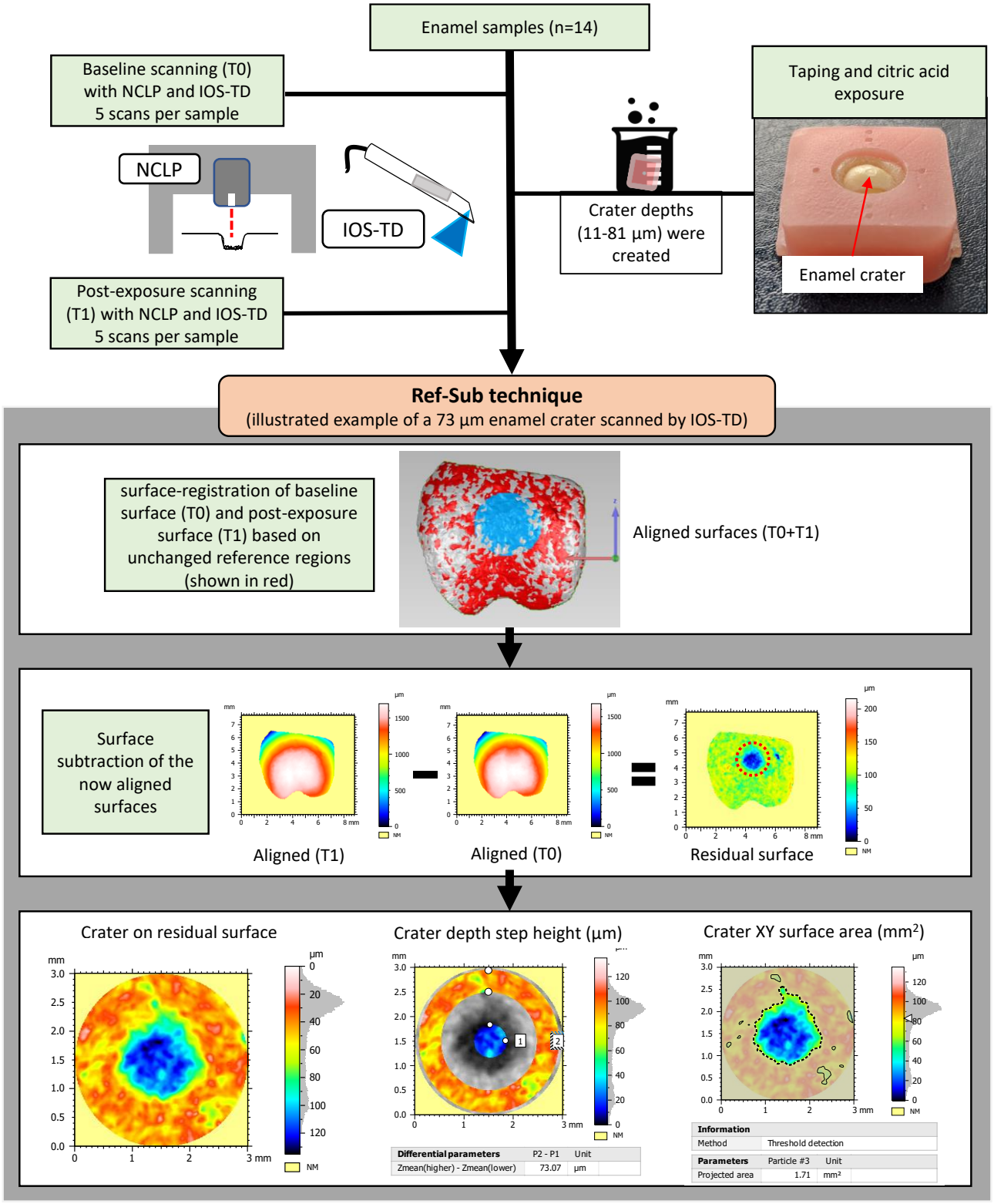

Figure 5-6 – Outline of the quantification of natural enamel crater depths using the Ref-Sub analysis technique.

An automated 3D surface step-height (µm) algorithm was run on all residual datasets that resulted from the subtraction process to measure depths (µm), which also auto-located and measured the

XY crater surface area (mm^2) for comparison between the NCLP and IOS-TD, following a previously published protocol (Charalambous et al., 2021) and described in Chapter 3, Section 3.3.6.3 above, on page 133, based on the 'threshold detection' particle analysis method available by the software that detects surface features on a flat or horizontal background. The depth discrimination threshold of the IOS-TD was determined as the smallest depth (µm) showing no statistically significant difference to the NCLP, as well as achieving 100% automated detection (i.e., 5 out of 5 XY surface area, mm^2, measurements using the IOS-TD scans were equivalent to the NCLP). A 10% difference between the IOS-TD and NCLP XY crater area measurements was selected as an acceptable margin.

5.3.4 Investigation 3 – Assessing the effect of crater diameter on the accuracy of the IOS-TD

Once the depth measurement threshold of the IOS-TD was determined in Investigation 2, three additional enamel samples were prepared and eroded to create a single crater on each with a ~83 ± 1 µm depth. These three craters differed in diameter, measuring Ø 1.0, 1.5 and 2.0 mm, using punch-biopsies of appropriate size (BP-10F, BP-15F, and BP-20F, KAI Medical, Seki, Japan), to investigate the effect of increasing XY crater area on the IOS-TD accuracy for measuring depth. The scanning and analyses were repeated as described in Investigation 2, Section 5.3.3 above, on page 181.

5.3.5 Statistical analysis

Statistical analyses were conducted using Prism 9 statistical software package. All data were checked for normality using Shapiro-Wilk test. A two-way repeated-measures ANOVA with post-hoc Bonferroni tests was undertaken for Investigation 1 to compare measurements between the software bi-scan analysis techniques, and for Investigation 2 to compare data between IOS-TD and NCLP measurements of the enamel crater depths. Bland-Altman analysis was also used to calculate

the bias and 95% limits of agreement (95% LOA) between the IOS-TD and NCLP. A two-way ANOVA with post-hoc Bonferroni's tests was also conducted for Investigation 3 to compare the IOS-TD and NCLP data of the three different crater diameters. Statistical significance was set as $p \leq 0.05$.

5.4 Results

5.4.1 Investigation 1

Table 5-1 shows the mean (SD) depth measurement percentage error (%), using softgauges with 20, 40, 60, 80 and 160 µm nominal crater depths, using the four bi-scan analysis techniques. These data showed that the largest errors of -29.7 to -32.5 %, were observed in BF-Reg which were reduced to -2.4 to -3.6 % in Ref-Reg ($p < 0.0001$). The combination of surface-registration and subtraction using BF-Sub further reduced these errors to -0.1 to -0.3 % ($p < 0.0001$) and finally 0.0% error with Ref-Sub ($p < 0.0001$).

Table 5-1 – mean (SD) depth measurement percentage error (%), using softgauges with 20, 40, 60, 80 and 160 µm nominal depths, using the four bi-scan analysis techniques.
Within each row, lowercase letters denote statistically significant differences ($p < 0.05$) between the four techniques.
BF-Reg – Best fit surface-registration. Ref-Reg – Reference-based surface-registration. BF-Sub – Best-fit surface-registration and surface-subtraction. Ref-Sub – Reference-based surface-registration and surface-subtraction

	Mean (SD) depth measurement percentage error			
Softgauge depth of crater (µm)	**BF-Reg (%)**	**Ref-Reg (%)**	**BF-Sub (%)**	**Ref-Sub (%)**
20	-30.6 (4.8) a, b, c	-3.4 (0.7) a, d, e	-0.3 (0.0) b, d	0.0 (0.0) c, e
40	-30.1 (3.6) f, g, h	-3.3 (1.5) f, i, j	-0.1 (0.0) g, i	0.0 (0.0) h, j
60	-30.4 (1.7) k, l, m	-2.4 (0.2) k	-0.2 (0.0) l	0.0 (0.0) m
80	-29.7 (0.9) n, o, p	-2.7 (0.6) n, q, r	-0.1 (0.0) o, q	0.0 (0.0) p, r
160	-32.5 (0.9) s, t, u	-3.6 (1.5) s, v, w	-0.1 (0.0) t, v	0.0 (0.0) u, w

5.4.2 Investigation 2

Figure 5-7 shows representative pseudo-colour images of natural enamel with depths of 11, 23, 40, 58, 81 µm. The NCLP was able to discriminate all depths better than the IOS-TD demonstrating a higher spatial resolution. In contrast, the IOS-TD scans displayed areas of smoother topography, with irregular and unclear margins. At increased depths (seen in the examples of 58, 73 and 81 µm crater depth), craters were displayed more clearly; however, the transition between the crater and reference enamel was less distinct than the NCLP scans.

Table 5-2~~Table 5-2~~ shows crater depths from each of the fourteen samples, as measured by the reference NCLP, and the mean (SD) step height and area percentage error (%) for IOS-TD, along with the automated detection (%) of IOS-TD. The step heights ranged from 11 to 81 µm measured by the NCLP. The IOS-TD recorded the same depths and revealed mean (SD) percentage errors in depth measurements from -57 (14) % at the shallower depths improving to -2 (2) % in deeper craters. Statistically significant differences were observed between the NCLP and IOS-TD data at depths from 18 µm (-57 (14) %, $p = 0.0002$) to 40 µm (-35 (9) %, $p<0.0001$), and 56 µm (-17 (7) %, $p = 0.0005$). The percentage errors of IOS-TD for both depth and XY area measurements dropped below 10% at depths ≥ 62 µm. The automated detection algorithm revealed confidence in the depth measurement from 73 µm. No statistically significant differences were observed between the NCLP and the IOS-TD depth measurements above 73 µm ($p>0.05$).

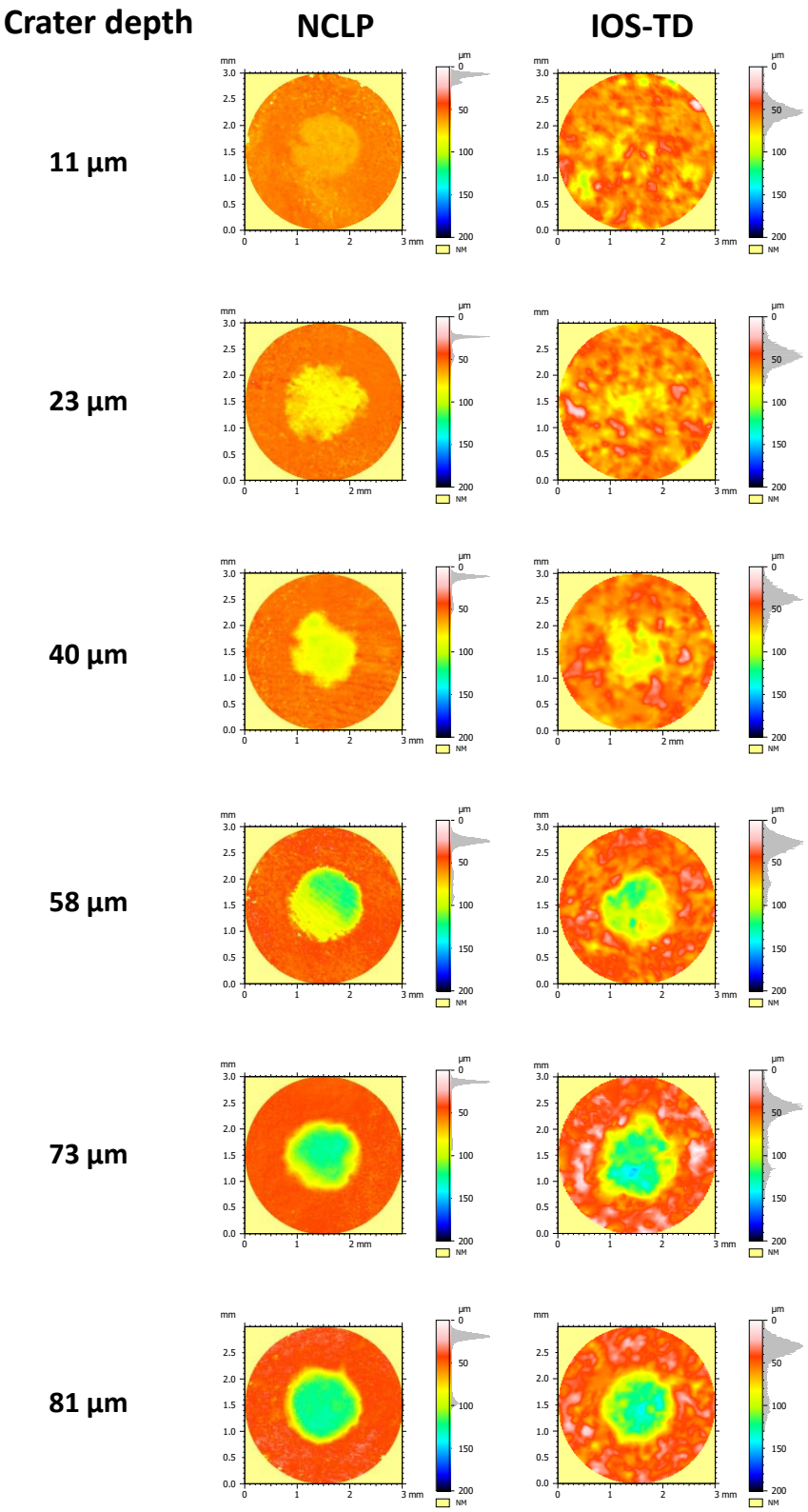

Figure 5-7 – Representative pseudo-colour NCLP and IOS-TD images of enamel craters of increasing depths (11 -81 µm) after using the Ref-SS analysis. The images are colour-coded as a function of *z*-measurements.

Table 5-2 – Crater depths of each of the fourteen samples, as measured by the reference NCLP, and the mean (SD) step height and area percentage error (%) for IOS-TD, along with the automated detection (%) of IOS-TD.
Statistically significant differences between the NCLP and IOS-TD step height measurements are shown (* = $p < 0.05$, ** $p < 0.01$, *** = $p \leq 0.001$ and **** $p \leq 0.0001$).

Sample number #	Number of scans with NCLP and IOS-TD	NCLP crater depth (µm) (reference)	Mean (SD) percentage step height error (%) of IOS-TD	Mean (SD) percentage area error (%) of IOS-TD	Automated detection (%) of IOS-TD
1	5	11	-43 (41)	9 (51)	0
2	5	18	-57 (14) ***	-8 (28)	0
3	5	23	-41 (33) ***	71 (35)	0
4	5	24	-44 (22) ****	25 (11)	0
5	5	34	-12 (11)	-3 (26)	0
6	5	40	-35 (9) ****	3 (15)	0
7	5	56	-17 (7) **	8 (4)	60
8	5	58	6 (6)	10 (6)	60
9	5	62	-6 (5)	-9 (8)	60
10	5	69	4 (5)	5 (5)	80
11	5	73	-5 (4)	2 (5)	100
12	5	75	-6 (3)	-5 (3)	100
13	5	78	-2 (2)	1 (5)	100
14	5	81	-4 (1)	-4 (2)	100

Crater depth measurements (µm) are correct to the nearest micron.

Figure 5-8 shows a Bland-Altman plot of differences between the NCLP and IOS-TD depth (step height) measurements, expressed as percentage (100 x (IOS-TD – NCLP) / average). Due to the high percentage difference between the IOS-TD and NCLP at shallower depths, the overall bias was -27% with wide 95% Limits of Agreement (LOA), 56 to -109%. However, as the magnitude of the crater depth increased the agreement between the two scanners increased, nearing zero percent above 70 µm depths.

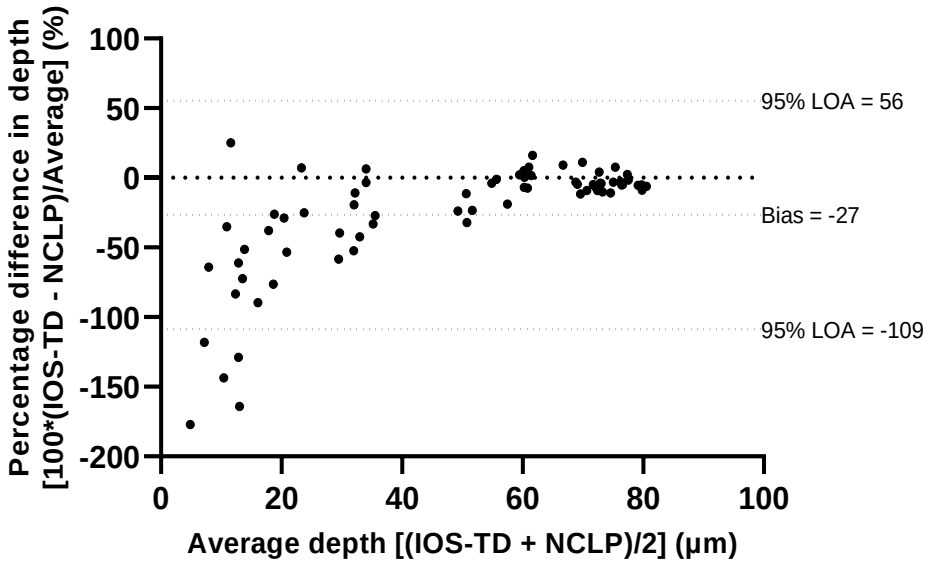

Figure 5-8 – Bland-Altman plot of differences between NCLP and IOS depth (step height) measurements, expressed as percentage (%) [100 x (IOS – NCLP)/Average)].

5.4.3 Investigation 3

Table 5-3 shows the depths of the three craters with different diameters, as measured by the reference NCLP, and the mean (SD) step height and area percentage errors (%) for IOS-TD, along with the automated detection (%) of the IOS-TD. As the diameter of the crater increased, the mean (SD) percentage error of IOS-TD depth measurements, compared to NCLP, decreased from -10 (4) % for the Ø1.0 mm, to -7 (1) % for the Ø1.5 mm, and to 3 (2) % for the Ø2.0 mm crater diameter. The diameter as a factor had a statistically significant effect (p=0.0063). The IOS-TD depth measurement

of the Ø1.0 mm crater was statistically significantly lower than that of the NCLP (p=0.0053). As the diameter of the crater increased the mean (SD) percentage error of the IOS-TD area measurements decreased from -2 (13) % for the Ø1.0 mm, to 2 (2) % for the Ø1.5 mm, and to -1 (2) % for the Ø2.0 mm crater. Only two out of five area measurements by the IOS-TD of the Ø1.0 mm crater were ≤10% different than the NCLP and therefore the crater automated detection was 40%; whilst that of the Ø1.5 mm and Ø2.0 mm craters was 100%, achieving five out of five measurements within a 10% difference from the equivalent NCLP area measurement.

Table 5-3 – Depths of the three diameter craters, as measured by the reference NCLP, and the mean (SD) step height and area percentage errors (%) for IOS-TD, along with the automated detection (%) of IOS-TD
Statistically significant differences between NCLP and IOS-TD step height measurements are shown (* = $p < 0.05$, ** $p < 0.01$, *** = $p \leq 0.001$ and **** $p \leq 0.0001$). Crater depth measurements (µm) are correct to the nearest micron.

Sample number #	Ø Diameter of crater (mm)	Number of scans with NCLP and IOS-TD	NCLP crater depth (µm) (reference)	Mean (SD) percentage step height error (%) of IOS-TD	Mean (SD) percentage area error (%) of IOS-TD	Automated detection (%) of IOS-TD
1	1.0	5	83	-10 (4) **	2 (13)	40
2	1.5	5	82	-7 (1)	2 (2)	100
3	2.0	5	83	3 (2)	-1 (2)	100

5.5 Discussion

Freeform surface metrology refers to quantifying specific features on a point-cloud mesh produced from optical scans of complex geometrical surfaces, such as seen on teeth. Change on non-flat, freeform surfaces presents challenges for measurement of Z heights using optical scanners (Chen et al., 2020). However, over the last few years, there have been significant advances in software and hardware of surface metrology which allow a pair of 3D digital scans, each taken at different epochs, to be aligned and compared to quantify vertical or volumetric surface changes over time (Becker et al., 2018b; Kuralt and Fidler, 2021; S. O'Toole et al., 2018; Vasilakos et al., 2017). However, there remain errors that impact on reliable quantification of change at the micron scale.

This study demonstrated that the combination of surface-registration and surface-subtraction, with or without using reference areas during alignment (i.e., the BF-Sub and Ref-Sub techniques) significantly reduced errors for measurement of change on freeform surfaces using softgauges compared to the techniques involving surface-registration alone (i.e., the BF-Reg and Ref-Reg techniques). Therefore, the first null hypothesis was rejected.

Additionally, significant differences were observed between the NCLP and IOS-TD measurements of crater depths on natural enamel utilising the Ref-SS technique, therefore the second null hypothesis was rejected. The discrimination threshold for the IOS-TD was 73 µm, above which there was confidence that any measurement was an accurate reflection of depth.

Lastly, scanning and measuring craters of different diameters (but of similar depth), resulted in different measurement accuracies by the IOS-TD and therefore the third null hypothesis was also rejected.

These findings, although specific to this intraoral scanner, have broader impact for assessing the confidence and accuracy of any scanner used to record the surface of complex oral structures. As

most intraoral scanners utilise similar physics to record the surface of teeth it is reasonable to propose that the limits around 73 µm are probable. Further work would be needed to establish criteria for each scanner, but a broad interpretation would be there are limits on their ability to distinguish varying crater depths on teeth.

The value of using mathematically created softguages was to establish which bi-scan analysis workflow produced the optimum and most accurate results, without introducing sources of error from hardware and scanning. No significant differences were observed between the BF-Sub and Ref-Sub techniques suggesting that relying on reference regions during the initial step of alignment to reduce errors may not be necessary when a combination technique is used. This may be because the subtraction of two sequential surfaces, that are well-aligned in the XY plane generates a 'difference' 3D profile of the same shape no matter the matching error in Z, hence any step height measurement to quantify change on this residual surface thereafter would be the same. This concept is illustrated further in Figure 5-9 below.

Figure 5-9 – Concept of measuring surface change using surface-subtraction following good alignment (top) or incorrect alignment (bottom) between two surfaces during surface-registration.

Once this concept is clarified, it is relatively straightforward to visualise registration errors in scans in the XY dimension, which is further elucidated when the root-mean-square (RMS) error is quantified once the surface-registered scans are imported into the surface-subtraction software as shown in Figure 5-10 below.

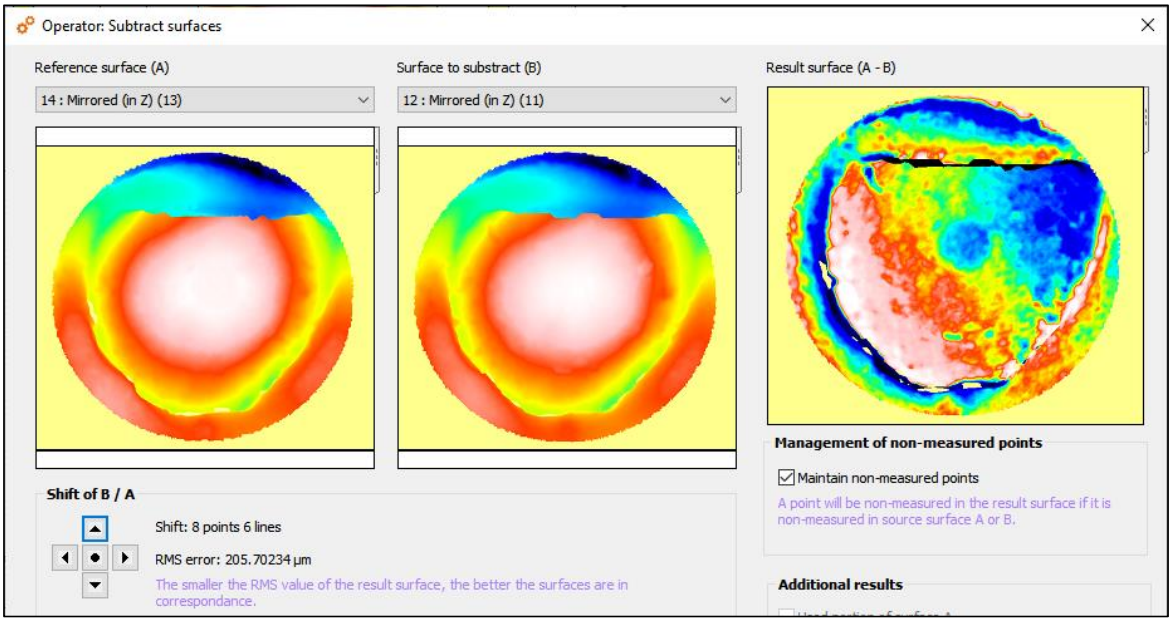

High RMS error between the two surfaces to be subtracted, suggests poor alignment, resulting in a less accurate residual surface.
The RMS error can be improved by shifting the surfaces in the XY direction.

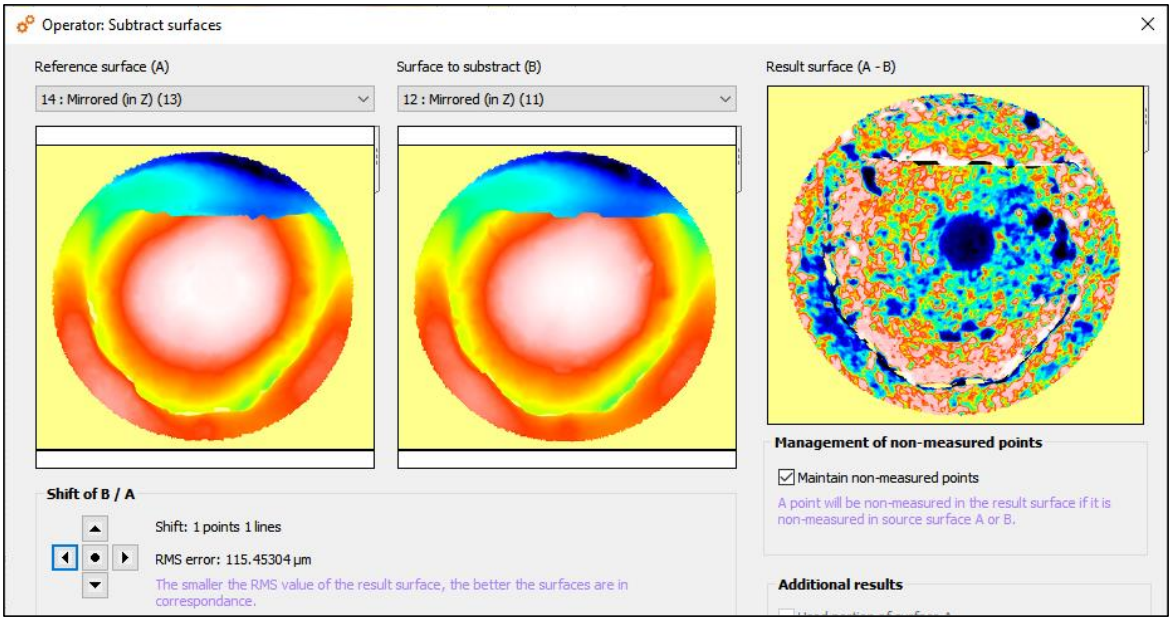

Lower RMS error between the two surfaces to be subtracted, suggests good alignment resulting in a more accurate residual surface.

Figure 5-10 – High (above) and low (below) root-mean-square (RMS) error between the two surfaces to be subtracted.

The additional step of surface subtraction eliminated errors in the Z direction, which are harder to visualise, particularly across a large 3D scan (Stenhagen et al., 2011). Finding reference surfaces for

alignment which have not undergone changes in the oral cavity remains a significant barrier for measuring erosion (O'Toole et al., 2019a) and therefore the additional improvement with the surface-subtraction overcomes them. Caution should be applied though as the combination of surface-registration and subtraction was tested using softgauges (Paricio et al., 2015). This only represents differences from the software analysis aspect and does not exclude errors from the sources of hardware or the operator, which can be significant.

Although best-fit surface-registration is relatively more straightforward and automated, it has been previously demonstrated by O'Toole et al. (2019) that restricting the alignment of two 3D surfaces to unchanged reference regions minimises measurement errors and improves the accuracy of surface change (O'Toole et al., 2019a). However, these previous investigations were limited to techniques involving surface-registration alone, without the additional step of surface subtraction. The authors reported reduced depth measurement errors using reference-based registration compared to best-fit registration or manual alignment of sequential surfaces (O'Toole et al., 2019a). This is because standardised best-fit algorithms are forced to draw 3D datasets into the closest mathematical proximity possible, in a way that is not biologically informed of the crater location, often resulting in inaccurate quantification that limits diagnostic potential. Restricting these algorithms to surfaces that are least likely to have undergone change means they are less susceptible to outliers and results in a more accurate analysis (O'Toole et al., 2019a; Ren et al., 2012). On the other hand, Mylonas et al., (2019) investigated the use of surface-subtraction alone in characterising early erosion on natural enamel, however, the authors used a physical positioning jig to ensure repeatable placement of each enamel sample prior to scanning and analysis, which is less automated and cannot be easily translated in a clinical situation.

Once the combination of surface registration and subtraction was validated, it was applied to sequential scans to show the threshold of the IOS-TD for measuring craters on unpolished enamel. In contrast to the intraoral scanner, the high-resolution NCLP detected all simulated crater depths. Craters with shallow depths were particularly challenging for the IOS-TD to measure accurately. This was highlighted by the wide standard deviations in depth and area measurements, poor automated crater detection in shallow craters, as well as the Bland-Altman plot which showed wide limits of agreement and a clear trend of improved percentage differences between the two devices as the depth increased.

The data showed that as the depth increased, the IOS-TD percentage difference to the NCLP and the standard deviations reduced. The resolution of the intraoral scanner at the lower values of depth was insufficient to discriminate an accurate value and both the step height and the area measurement had variation. This was also confirmed by the automated detection which is a previously published method to identify the point at which the crater image seen on the scans taken by the intraoral scanner became clear (Charalambous et al., 2021). As the depth increased the crater detection improved. At 73 µm, the step height and area percentage errors had reduced to minimal levels and the automated detection was 100%. This showed there was high confidence that the intraoral scanner was able to discriminate and so measure depth. Measuring such depth on natural enamel by an intraoral scanner has not been previously demonstrated with accuracy as high as this present study. Though, the underlying constraints associated with the physics of sampling remained and limit the threshold.

Unlike point-measuring high-resolution scanners, such as profilometers, which can sharply focus an optical beam onto a surface, intraoral scanners capture surface features and their optical interactions over an area simultaneously. They achieve this by oversampling and averaging multiple

points of measurement representing the same area (Sehrawat et al., 2022). Although intraoral scanners capture surface topography significantly faster than profilometers, their drawback is lower spatial resolution (i.e., lower point cloud density) and point measuring accuracy (DeLong, 2006). The impact of lower spatial resolution results in surfaces with smoother topography and poorer depiction of the margins of the crater (Charalambous et al., 2021). This may explain the observation of investigation 3 that the accuracy of the IOS-TD improved as the crater diameter increased from 1.0 mm to 1.5 mm and finally to 2.0 mm. A feature on a surface with a bigger area would be depicted on the point-cloud dataset with more points of measurement than a similar feature with a smaller area and therefore it would be easier to be converted truthfully on the digital model to its real geometry (Medina-Sotomayor et al., 2018; Tapie et al., 2015).

Several *in vitro* and *in vivo* studies utilising intraoral scanners for wear quantification have been published, most of which do not compare data to a gold standard (Alwadai et al., 2020; Hartkamp et al., 2017b; Kumar et al., 2018; Marro et al., 2020; Michou et al., 2020; O'Toole et al., 2020). Recently, good quantitative agreement was demonstrated between an intraoral scanner and micro-CT volumetric and depth wear measurements (Esquivel-Upshaw et al., 2020). Hartkamp *et al*. (2017) were the first to use a profilometer compared to an intraoral scanner to measure vertical wear which suggested an agreement within approximately 20 µm; however, the depths were over 70 µm while lateral measurements of the craters were not specified (Hartkamp et al., 2017b). A different intraoral scanner was utilised in this present study to assess surface change as small as 11 µm depth. Furthermore, IOS surface change analysis was not restricted to measuring vertical tissue loss (µm); instead, the XY area measurements (mm^2) were compared against profilometry to further scrutinize IOS's performance. Similarly, Witecy et al., (2021) demonstrated good agreement between four different intraoral scanners and profilometry in measuring natural enamel cusp loss; however, the depths investigated were above 150 µm.

The threshold of the IOS-TD for measuring crater depths on polished enamel was previously demonstrated in Chapter 3 to be 44 µm (Charalambous et al., 2021). This is lower than the observed measurement threshold, 73 µm, in this study. This probably reflects on the fact that polished enamel has a simpler and flatter morphology, but more importantly, it allows single-scan analysis, utilising reference areas around the crater to measure tissue loss. Furthermore, simulated depths on polished enamel have more distinct boundaries which would favour an automated system. The relative performance of the multi-step process required for measuring change on complex freeform surfaces is more prone to measurement uncertainty as each sequential scan introduces an individual set of errors (Ahmed et al., 2016) while the alignment process, which is itself dependant on the scanner's accuracy and resolution, is a major contributor of measurement error (O'Toole et al., 2019a).

Addressing the limitations of the study, scans and measurements were conducted by an operator with over three years of experience in the scanners and software packages used in this study and therefore the author acknowledges that such skilled techniques would require extensive operator training. The impact of operators with different levels of experience on these systems needs further investigation. Furthermore, software algorithms and mathematical complexities are often purposely hidden from the operator and different software from the ones used in this study may have shown decreased or increased errors.

One key limitation to valid quantification of surface features using the optimised surface-registration and subtraction technique developed in this thesis, is that the user has to define the angle at which the surface is extracted and measured (Leach et al., 2018). The surface data presented in this Chapter, was extracted from slightly curved 3D scans, therefore the selection of the angle of the measurement plane was chosen at convenience to be perpendicular (a bird's eye

view) over the surface, which did not impact the measurement of the craters. However, when more complex freeform surfaces are to be considered, this angle of extraction will be a key variable to the validity of the final measurement, especially if the feature to be measured presents in an undercut area. This is a recognised limitation of extracting surface data from a 'shell' or '3D object' (Scott and Jiang, 2014). Therefore, when considering measurement of complex freeform measurement tasks, that are out of scope of this thesis, further work is needed to understand how best to measure any surface gain/loss on multiple sides of an object cannot be measured with a single application. This is an unresolved issue that commercially available software, such as OraCheck (Dentsply Sirona, North Carolina, USA) have compensated for by allowing users to select the direction of the measurement; however, this limits the ability of the measurement to known areas of change.

Therefore, a key unresolved issue is defining the nature of the subtraction process to create a residual surface that was calculated at the correct angle between the two aligned surfaces. To measure changes on different sides/regions of an object, individual subtraction analyses would be required on the different sides of the measured object as shown in Figure 5-11 below.

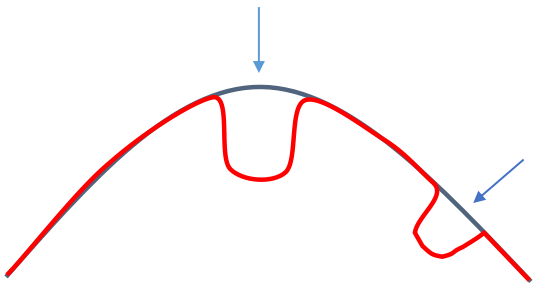

Figure 5-11 – Surface loss on different sides of an object require individual subtraction and measurement perpendicular to the horizonal plane of each surface feature.

Another limitation is that the combination of surface-registration and surface subtraction can be a time-consuming and cumbersome process, having to use two different software, requiring roughly double the analysis time than a stand-alone surface-registration technique without the subtraction step. Therefore, further work is needed on resolving these known challenges with simultaneous measurement of multiple features on complex structured and freeform surfaces.

5.6 Conclusion

In conclusion, the combination of surface-subtraction after surface-registration improved the accuracy of measuring surface change on freeform surfaces. This has potential to improve diagnostics in many fields of dentistry. Using this technique, the IOS-TD was able to predictably determine loss of 73 μm on natural enamel, a level of accuracy that may be acceptable for future studies and clinical monitoring of surface changes over time such as tooth or dental material wear.

Chapter 6 The effect of scan size on the accuracy of the IOS-TD for measuring surface loss

6.1 Introduction

Intra-oral scanners have the capacity to create digital maps of a whole dental arch. To date, most studies have reported data on quantifying surface loss/wear from single teeth or sextants (Alwadai et al., 2020; Bronkhorst et al., 2022; Esquivel-Upshaw et al., 2020; V. D.-F. García et al., 2022a; Kühne et al., 2021; Kumar et al., 2019; Witecy et al., 2021). There is no data on how precise and accurate full-arch scans would be for measuring change from tooth wear (Ender et al., 2016a; Ender and Mehl, 2013; Flügge et al., 2013). The accuracy and precision from scans of single teeth or a few teeth is higher as these systems are generally designed to manufacture single restorations using CAD/CAM (Ender et al., 2019a, 2016a; Güth et al., 2017a; Jeong et al., 2016). Therefore, this Chapter focused on the impact of increasing scan size, from a cusp upto a full-arch scan on the accuracy of the IOS-TD (True Definition®, Midmark Corp., Ohio, USA) to measure surface change *in vitro*.

6.2 Aim, Objective, and null hypothesis

6.2.1 Aim

The aim of this study was to investigate how the size (span) of scans affects the accuracy of the IOS-TD for quantifying surface change *in vitro*.

6.2.2 Objective

The objective was to simulate surface loss by creating craters of increasing depths, on the same location of a typodont (plastic) tooth from a complete maxillary (upper) model and record the topography using digital scans of increasing spans made by the IOS-TD for measuring surface loss.

6.2.3 Null hypothesis

The null hypothesis stated that the IOS-TD would accurately measure crater depths using scans of increasing size (span).

6.3 Materials and methods

6.3.1 Creation of different crater depths

A complete maxillary (upper) typodont model (AG-3 WU Frasaco GmbH, Tettnang, Germany), made of hard thermosetting plastic material, was used to represent a complete maxillary dental arch (Figure 6-1A). A crater with, in total, four successively increasing levels of depth (D1 - D4) were created on the mesio-buccal cusp of the plastic tooth 17 (FDI notation, upper right second molar). These depths were created using a 2 mm diameter carbide milling bur (S9042.0, DormerPramet, São Paulo, Brazil) mounted on a Computer Numerical Control (CNC) milling machine (CNC Mini-Mill/3, Minitech Machinery Corp., Norcross, Georgia, USA), which was controlled using Mach3 CNC Controller software (Newfangled Solutions., Livermore, Maine, USA).

The bur was mounted on the CNC machine and following calibration the typodont model was secured with a double-sided tape (9088 high-performance double-sided tape, 3M™, Berkshire, UK) onto the milling stage. The CNC controller was used to accurately and repeatedly position the mesio-buccal cusp of the plastic tooth 17 below the bur (Figure 6-1B). The bur was spindled at a speed of 12,000 rpm towards the surface of the tooth in steps of 10 µm until initial contact (Figure 6-1C). Following this, four different depths, were prepared. The precise measurements of the depths were validated using the NCLP at 83, 133, 195 and 297 µm.

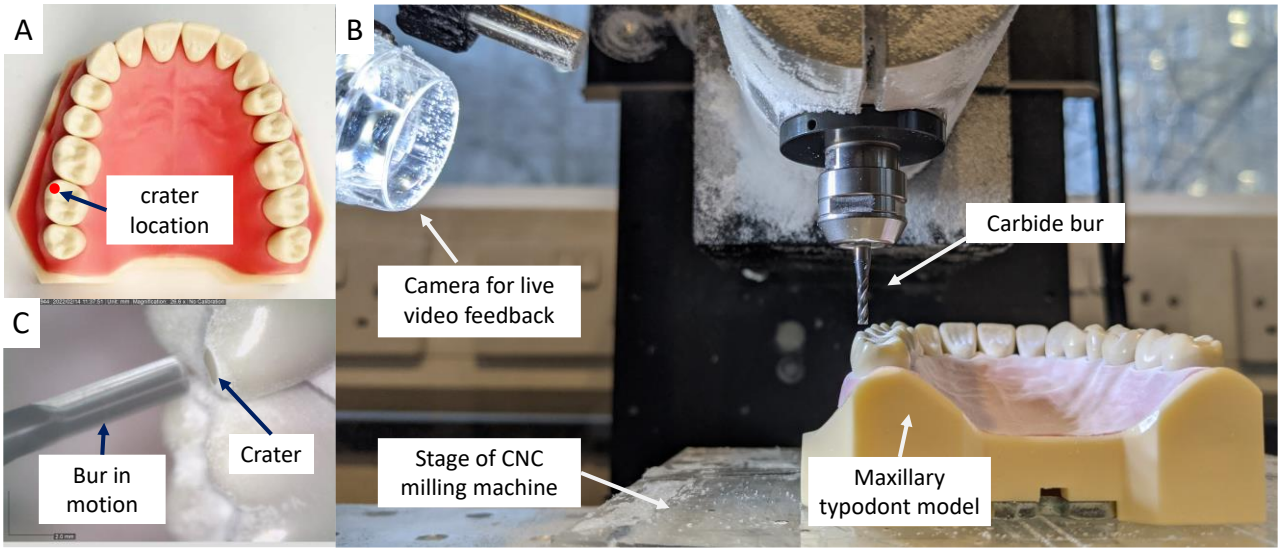

Figure 6-1 – A crater of four successively increasing levels of depth (D1 - D4) were created on the mesiobuccal cusp of plastic tooth 17 of a maxillary dental model (A), using a CNC milling machine set up (B). An image from the live video camera feedback (C) during drilling the crater.

The repeatability of the CNC milling machine to create craters of a consistent depth was investigated by drilling fifteen craters, each 50 µm depth, on the flat surface of a hybrid ceramic CAD/CAM block (Cerasmart™, GC EUROPE, Leuven, Belgium) (Figure 6-2 below).

Each crater was scanned using the NCLP and the depth measured using Mountains®8 surface metrology software using the single scan analysis described in Chapter 3 Section 3.3.6.3 above on page 133. The repeatability was expressed as the mean (SD) absolute difference between the depths measured by the NCLP and that milled by the CNC machine (50 µm). The mean (SD) repeatability was 1.60 (5.65) µm.

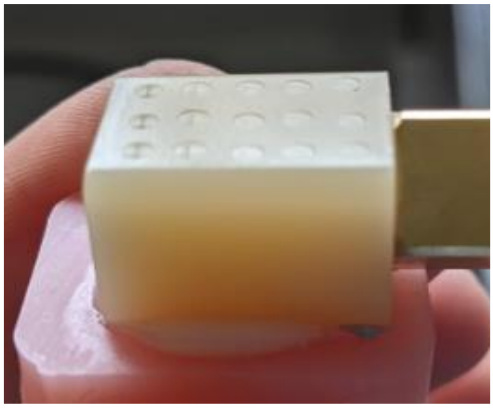

Figure 6-2 – Craters (n=15) created on the hybrid ceramic CAD/CAM block (Cerasmart™, GC EUROPE, Leuven, Belgium) to investigate the repeatability of the CNC milling machine to create holes of consistent depth.

6.3.2 Scanning

The experimental outline of the study can be seen in Figure 6-3.

Baseline (D0) and post-exposure scans at each crater depth (D1 – D4) were carried out using the IOS-TD, as the testing device, and the gold standard NCLP as the reference device. The NCLP scans (a single scan per depth) used rectilinear grid spacing of 10 µm X, Y intervals, resulting in point clouds, each point being 10 µm apart, following the method described in Chapter 2 Section 2.2.3 above. All IOS-TD scans were conducted using the handheld technique following powdering the typodont by a single experienced operator (Chapter 2 Section 2.2.4 above) following manufacturer's instructions.

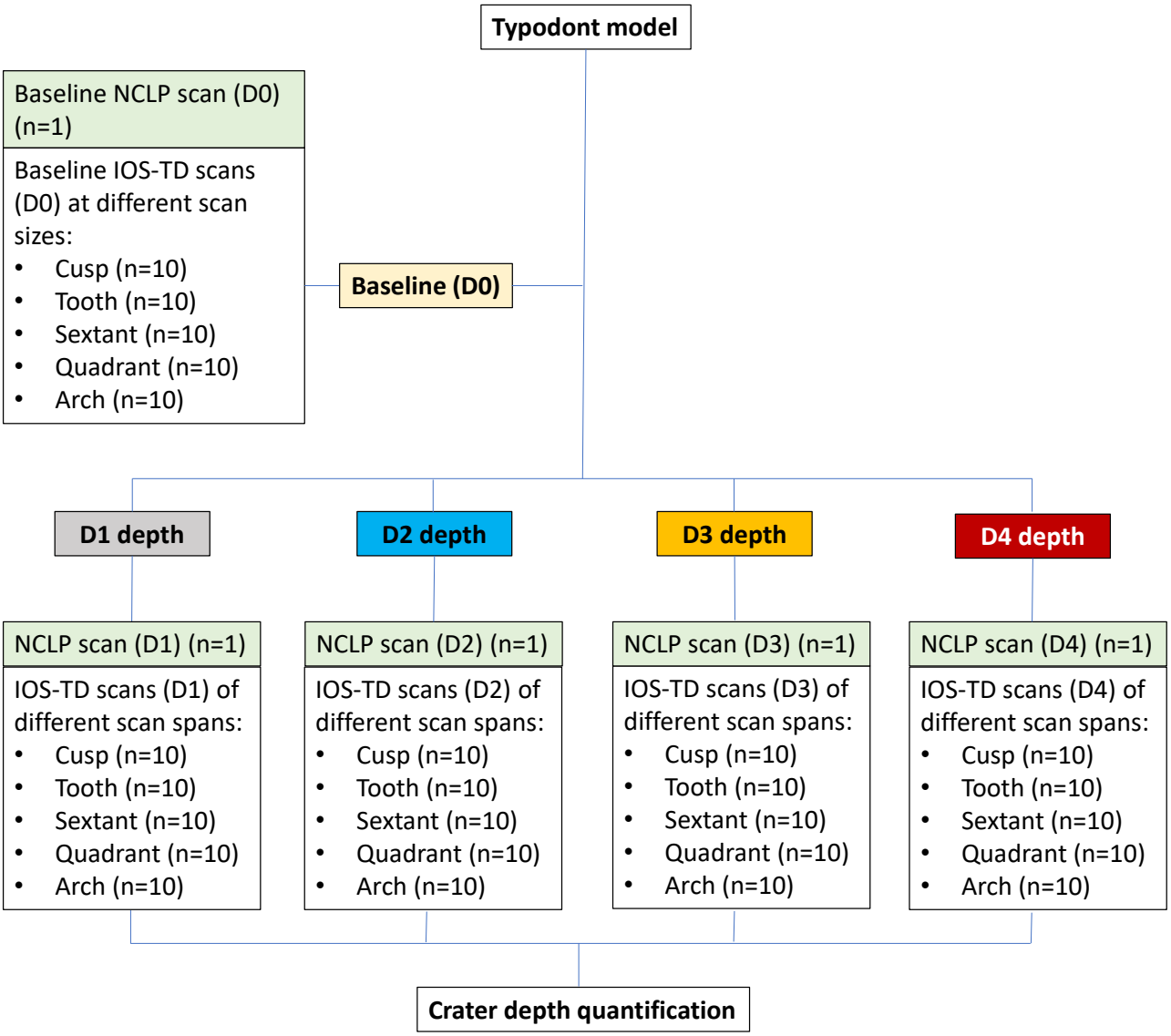

Figure 6-3 – Experimental outline of the study

IOS-TD scans (n=10) were conducted using five different scan sizes: on the cusp, tooth, across a sextant (five teeth), quadrant (eight teeth), and a full-arch at each crater depth (D1-D4) and the datasets randomised.

For the 'cusp' scan, scanning was restricted to the mesio-buccal cusp of tooth 17, and for the 'tooth' scan to all the surfaces of the same tooth, as illustrated in Figure 6-4A below. For the 'sextant' and 'quadrant' scan sizes, their scanning ranges are also illustrated in Figure 6-4A, capturing firstly the occlusal, then the palatal, and finally the buccal tooth surfaces. For the 'full-arch' scans, two

separate scans were taken, crossing the midline based on the manufacturers' scanning protocol (Figure 6-4B).

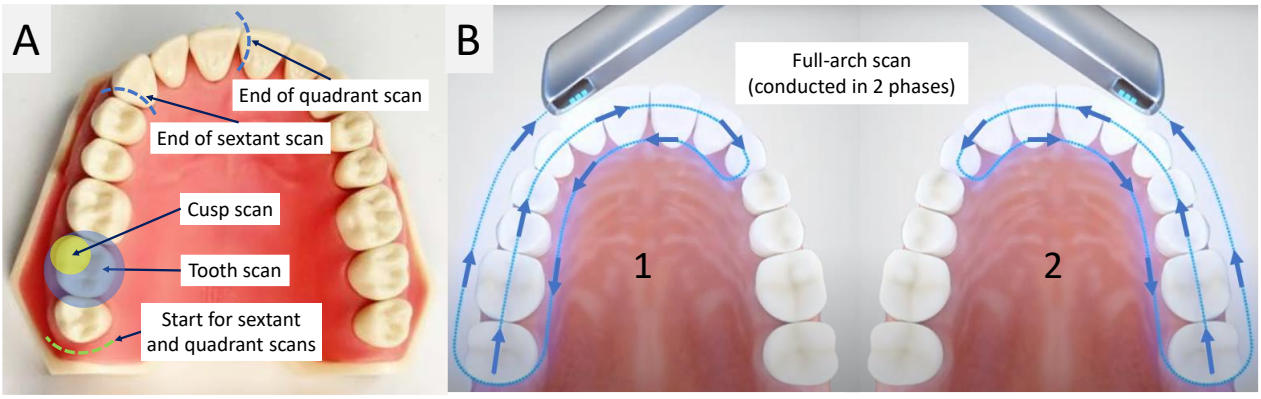

Figure 6-4 – Scanning protocols of the scan sizes investigated (cusp, tooth, sextant, and quadrant) (A) and the full-arch (B).

6.3.3 Crater depth analysis

The captured 3D data from the IOS-TD scans and the NCLP were analysed using the Ref-Sub technique described in Chapter 5 Section 5.3.3.4 above on page 185, as seen in Figure 6-5 below. Firstly, the post-exposure datasets (D1 - D4) from the NCLP and IOS-TD were aligned with their respective baseline datasets of the same scan size in Geomagic Control 2014 software. The aligned scans were loaded into Mountains®8 software and subtracted to produce a residual surface. A 4 mm circular area of the mesio-buccal cusp with the crater in the centre was extracted for measurement. Any outliers (spikes caused from scanning) were removed and then a levelling process was applied, utilizing a best-fit-linear-least-squares plan, excluding the crater. The depths of the craters were determined as 3D step heights (µm) by measuring the height difference between the central third of the crater and the surrounding reference area.

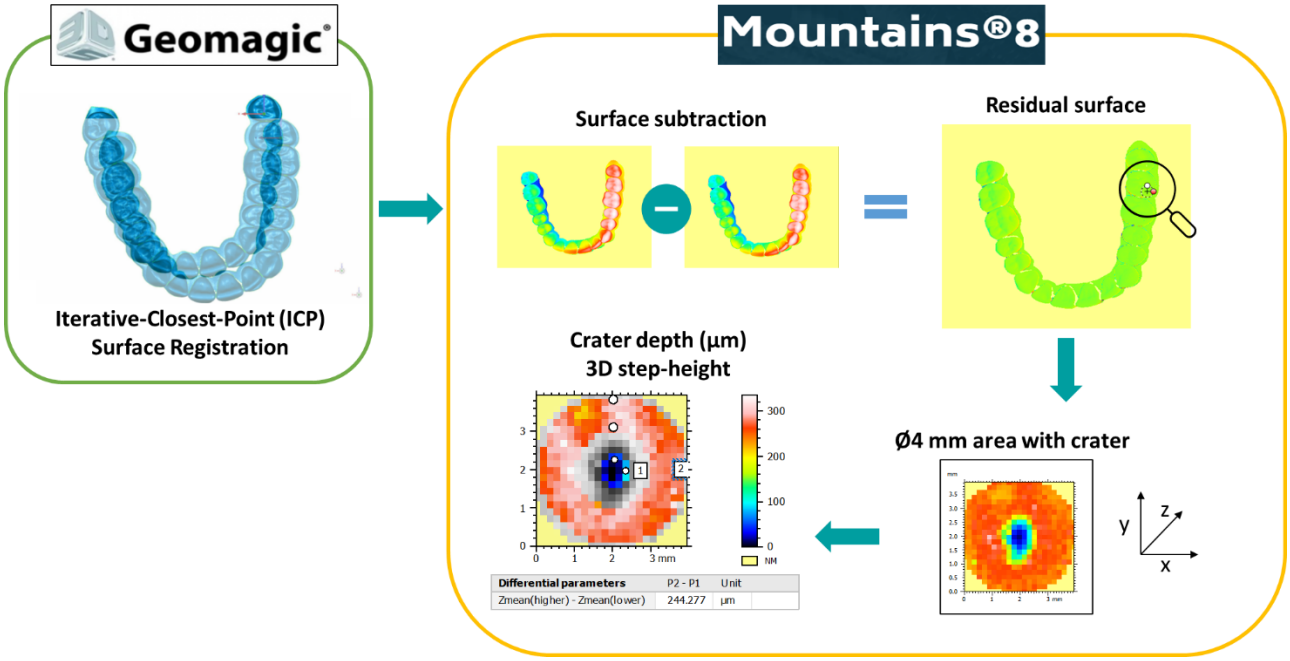

Figure 6-5 – Ref-Sub analysis workflow combining reference-based surface-registration and surface-subtraction for measuring the depth of the crater using full-arch scans as a representative example.

6.3.4 Statistical analysis

Data were collected, tabulated, and statistically analysed using Prism Version 9.3.1 (GraphPad Software Inc, California, USA). A power calculation using GPower 3.1.9 based on a one-way ANOVA comparing the scan size groups was conducted from previous pilot data. This indicated a sample size of 6 per scan size group (30 total sample size) for an effect size 0.97 yielding 95% power; however, a sample size of 10 per group was chosen to increase the power of the study even further. Data were assessed for normal distribution using Shapiro-Wilks and Kolmogorov-Smirnov tests and visually assessed with boxplots and histograms. As the data was normally distributed, means and standard deviations were reported. Inter-group analysis was conducted with a two-way repeated measures ANOVA with post-hoc Tukey's test for intra-group comparison. A p-value of < 0.05 was considered as statistically significant. To assess the accuracy (trueness and precision) of the IOS-TD step height depth, measurements of the different scan sizes were compared to those of the NCLP as a percentage error (%) using the formula $100 \times \frac{(\text{IOS–TD} - \text{NCLP})}{\text{NCLP}}$. In this instance, trueness

referred to the closeness of agreement between the IOS-TD depth measurement and the accepted reference value produced by NCLP and was expressed as a mean. Precision referred to the dispersion of percentage errors of IOS-TD repeated measurements and was expressed as a standard deviation.

6.4 Results

Figure 6-6 shows – The mean (SD) percentage (%) error of IOS-TD in measuring the crater depths (D1-D4) according to the scan size (cusp/tooth/sextant/quadrant/arch), with reference to the NCLP measurements. ~~– The mean (SD) percentage (%) error of IOS-TD in measuring the crater depths (D1-D4) according to the scan size (cusp/tooth/sextant/quadrant/arch), with reference to the NCLP measurements.~~. At D1 depth (83 µm), the mean (SD) percentage error for the cusp, tooth, sextant, quadrant, and arch were 3.5 (3.9), 1.1 (4.7), -19.1 (9.0), -25.4 (10.6), and -57.4 (13.4) %, respectively. At D2 depth (133 µm), these were -1.7 (2.4), -4.9 (3.2), -10.9 (3.1), -17.0 (3.3), and -17.9 (7.4) %, respectively. At D3 depth (195 µm), they were -1.5 (1.2), -1.9 (0.9), -12.6 (4.7), -11.8 (5.6), and -10.9 (11.1) %, respectively and at D4 depth (=297 µm), they were 0.7 (0.9), -1.6 (0.7), -12.2 (1.9), -12.3 (5.0), and -12.1 (5.5) %, respectively.

Inter-group comparisons showed that the difference in scan size had a statistically significant effect to the percentage error measuring the crater depths ($p<0.0001$). Additionally, as the depth of the craters increased there was a statistically significant reduction to the percentage error of the depths ($p<0.0001$).

Intra-group comparisons showed no statistically significant differences between the cusp and tooth scan sizes for any depth; however, statistically significant differences of various levels were observed between the cusp scans (used as reference) and the rest of the scan sizes (sextant, quadrant, and arch) for all crater depths (D1 - D4). For the D3 (195 µm) and D4 (297 µm) depths,

the percentage error for the sextant, quadrant, and arch plateaued to approximately -10 to -12% underestimation.

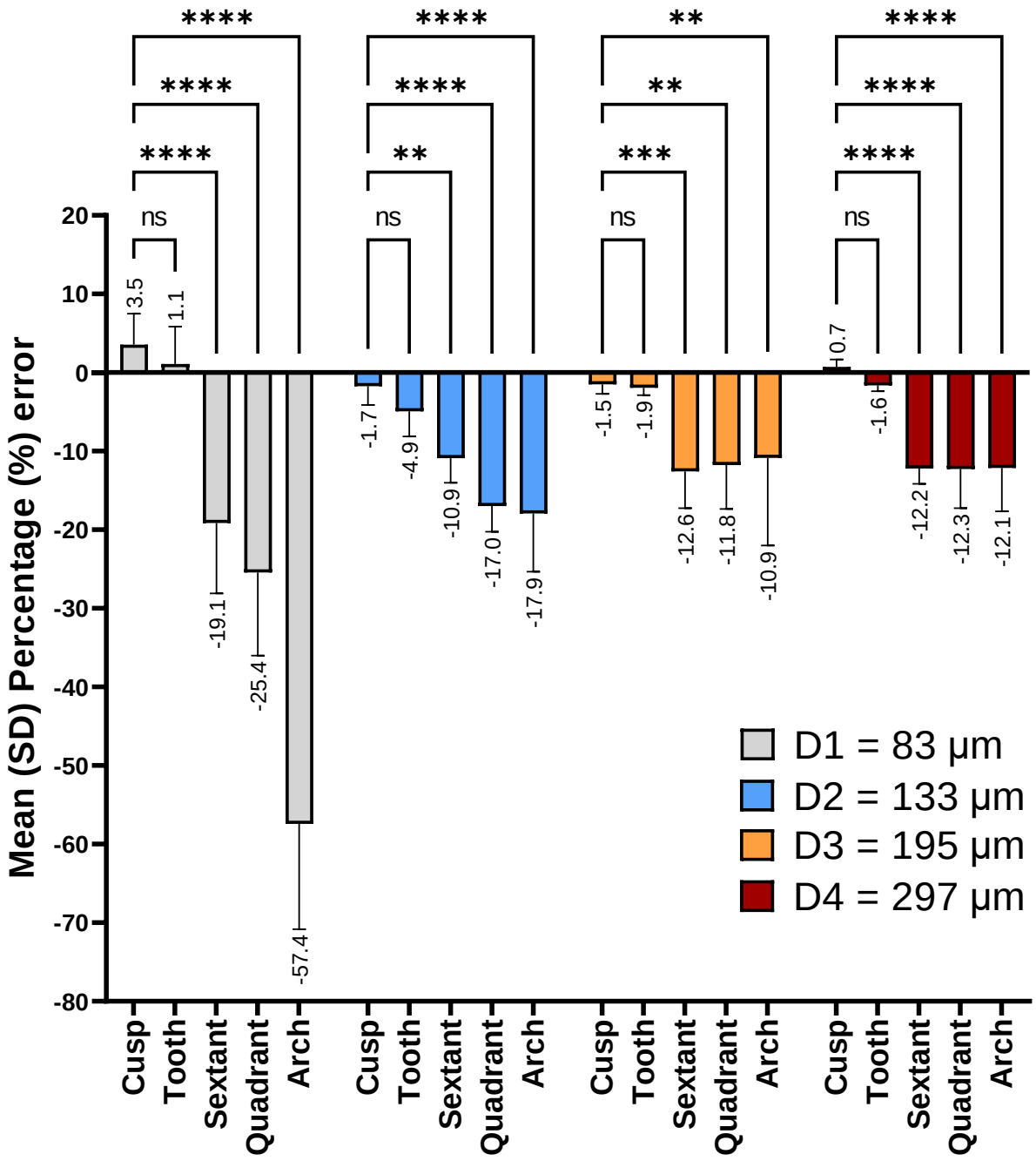

Figure 6-6 – The mean (SD) percentage (%) error of IOS-TD in measuring the crater depths (D1-D4) according to the scan size (cusp/tooth/sextant/quadrant/arch), with reference to the NCLP measurements.
For each crater depth, statistically significant differences are shown with reference to the cusp scan size (ns = no statistical significance, * = p<0.05, ** = p<0.01, *** = p<0.001, **** = p<0.0001)

Figure 6-7 shows representative polygon meshes from the IOS-TD scan sizes (Cusp/Tooth/Sextant/Quadrant/Arch) in Geomagic Control 2014 software and the respective Ø4 mm residual surfaces at D1 (83 µm) and D4 (297 µm) depths in the Mountains®8 software with their respective points of measurement per mm^2 ($POMs/mm^2$). The residual surfaces are colour-coded as a function of Z measurements.Figure 6-7 – Representative polygon meshes from IOS-TD scan sizes (Cusp/Tooth/Sextant/Quadrant/Arch) in Geomagic Control 2014 software and the respective Ø4 mm residual surfaces at D1 (83 µm) and D4 (297 µm) depths in the Mountains®8 software with their respective points of measurement per mm2 (POMs/mm2). The residual surfaces are colour-coded as a function of Z measurements.~~Figure 6-7 – Representative polygon meshes from IOS-TD scan sizes (Cusp/Tooth/Sextant/Quadrant/Arch) in Geomagic Control 2014 software and the respective Ø4 mm residual surfaces at D1 (83 µm) and D4 (297 µm) depths in the Mountains®8 software with their respective points of measurement per mm2 (POMs/mm2). The residual surfaces are colour-coded as a function of Z measurements.~~ As the scan size increased the $POMs/mm^2$ and hence the resolution of the images decreased creating a more 'pixelated' and less defined crater topography.

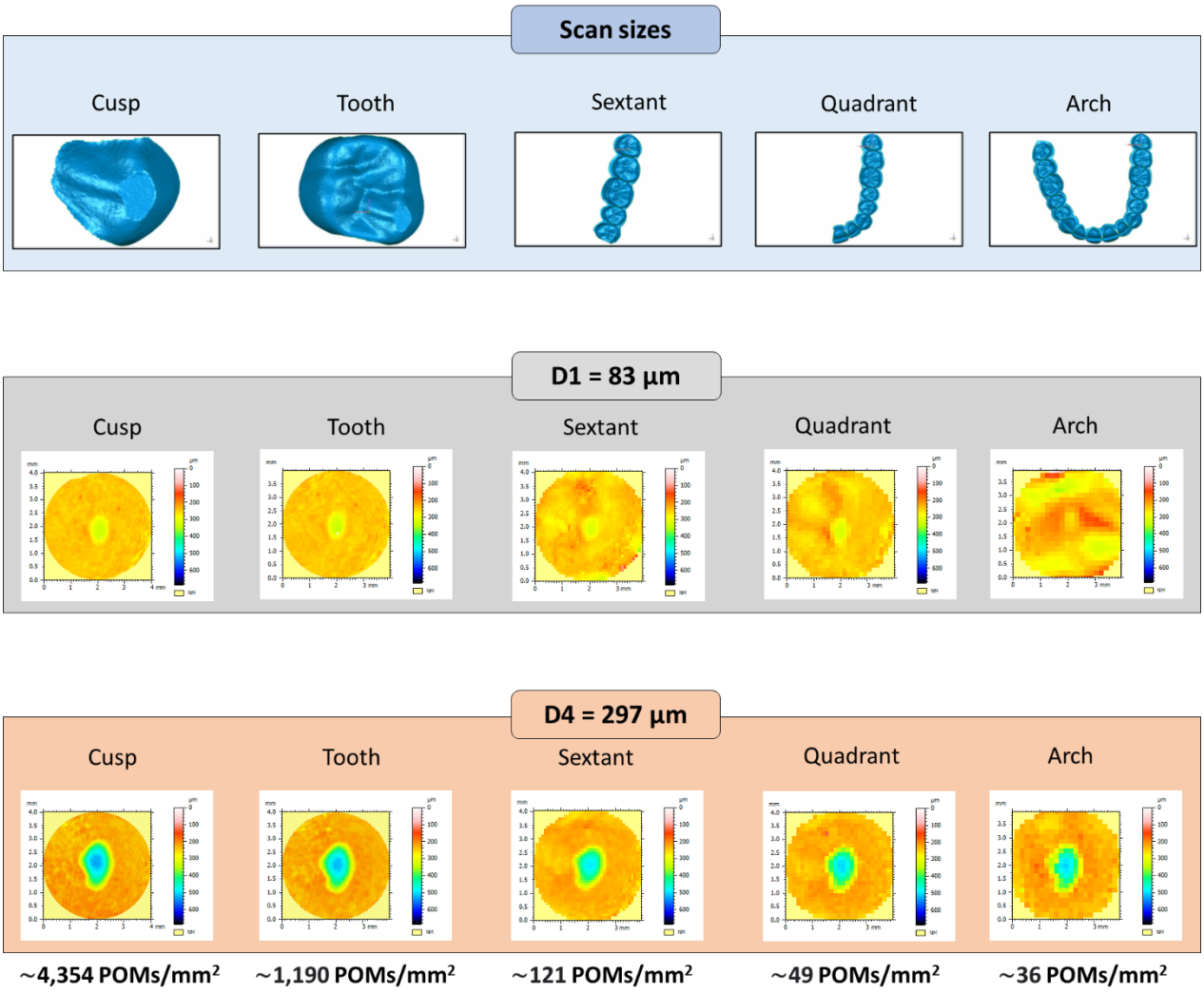

Figure 6-7 – Representative polygon meshes from IOS-TD scan sizes (Cusp/Tooth/Sextant/Quadrant/Arch) in Geomagic Control 2014 software and the respective Ø4 mm residual surfaces at D1 (83 µm) and D4 (297 µm) depths in the Mountains®8 software with their respective points of measurement per mm^2 (POMs/mm^2). The residual surfaces are colour-coded as a function of Z measurements.

6.5 Discussion

This Chapter demonstrated the effect of different scan sizes on the accuracy of an intraoral scanner for measuring crater depths. The accuracy reduced with increasing scan size and, therefore the null hypothesis was rejected.

The highest accuracy of the IOS-TD was observed using scan sizes restricted to the cusp and tooth regions which remained below ±5% error for all depths (D1 - D4). This suggests that the IOS-TD reliably measured surface loss at 83 microns depth, a similar finding to the study in Chapter 5 confirming the result from the previous chapter (Charalambous et al., 2022). Compared to this, the accuracy decreased significantly with increased scan sizes. This may be because intraoral scanners operate by capturing and sequencing multiple single images which are consequently stitched together by recognising overlapping regions using complex software algorithms to create the 3D digital model. However, the registration of overlapping images is prone to errors inherent to the iteration process, which can accumulate and propagate as the number of stitched images increases, resulting in deformation of the arch shape and an overall error in the final arch dimensions (G.-H. Park et al., 2019; Schmidt et al., 2021).

Furthermore, the point-clouds generated by the IOS-TD and the software decreased in density as the scan size increased. This might reflect the software algorithm to reduce the data size, reducing the total number of the points of measurement (Medina-Sotomayor et al., 2019b). On the other hand, different metrology software, may interpolate point clouds differently which may lead to inconsistencies in the resolution and accuracy of the 3D meshes. Datasets with high point-cloud density, can be converted more accurately into a faithful representation of a real surface, while those with low density can introduce ‘chord’ errors due to the lack of digital information between points, leading to surface defects, non-existent curvatures, or discontinuity in the surface (Medina-

Sotomayor et al., 2018; Tapie et al., 2015). The POMs/mm^2 calculated after scanning a full-arch were ~36 which is a similar density to a study reporting a range of 34.20 – 79.82 POMs/mm^2 using four different intraoral scanners (Medina-Sotomayor et al., 2018).

Previous studies demonstrated reduced accuracy for intraoral scanners with an increasing area of scanned surface (Ender et al., 2019b, 2016a, 2016c; Ender and Mehl, 2015; G.-H. Park et al., 2019). It has been suggested that intraoral scanning of single teeth, sextants and quadrants are more accurate than conventional impression techniques (Güth et al., 2017b; J. F. Güth et al., 2013; Keul et al., 2014; Nedelcu and Persson, 2014b), while differing data exist for full arch scans (Amin et al., 2017b; Jeong et al., 2016; G.-H. Park et al., 2019). One study reported that full-arch implant scans using the same intraoral scanner as the present study were more accurate than digitized conventional impressions, showing a mean (SD) RMS error of 19.32 (2.77) µm (Amin et al., 2017b). G.-H. H. Park et al. (2019) compared the 3D arch distortion of intraoral scans according to the distance from the first tooth of a dental arch, over the span of a full arch scan. They demonstrated that as the scan size increased across the arch, the inter-surface distance during alignment between the reference dataset produced by an industrial 3D scanner and those made by four intraoral scanners increased sharply. The mean (SD) inter-surface distance for all scan sizes (from single tooth to full-arch) ranged from 119 (42) µm for the Carestream CS3600® intraoral scanner, to 184 (50) µm for the 3Shape TRIOS3®, to 210 (54) µm for Carestream CS3500®, and finally to 343 (56.4) µm for the 3Shape TRIOS2® (G.-H. H. Park et al., 2019). An interesting observation was that the newer generation intraoral scanners produced more accurate digital impressions than their older versions, and in the current market there are even newer versions of these scanners which may suggest that errors may be even smaller using up-to-date technologies.

In general, the alignment of two digital models has been studied through best-fit iterative-closest-point algorithms (Lim et al., 2018; Medina-Sotomayor et al., 2019b; Saoirse O'Toole et al., 2018). The algorithm's minimizes inter-surface distances across the whole region and means that discrepancies in one part of a long scan size are autocorrected which can result in errors on the contralateral side (Persson et al., 2008). Investigating the error produced by the ICP alignment was beyond the scope of this present study; however, as alignment between a baseline and post-exposure datasets was essential prior to crater depth measurement, the results should be interpreted with caution.

Comparing the measurements of the different crater depths (D1 - D4), a significant increase in accuracy was observed as the depth increased and it seemed to reach a plateau of approximately 10 - 12% underestimation at D3 (=195 µm) and D4 (=297 µm). The improvement in accuracy may be because surface features of bigger depth are optimised by the software algorithm (Braian and Wennerberg, 2019b). This suggests that the IOS-TD may measure change on surfaces above or equal to ∼200 µm within a reasonable margin of error, even when using a full-arch scan. Nevertheless, being able to measure surface depth changes in the order of ∼200 µm using full-arch scans may not be suitable for clinical monitoring of erosive tooth wear yet where the average annual surface loss can range between 11 and 140 µm (Ahmed et al., 2017; Bartlett et al., 1997; Lambrechts et al., 1989; Pintado et al., 1997).

Recently, there have been several efforts in the literature to investigate intraoral scanners for quantifying surface loss/wear. The majority of the cases are *in vitro* studies in which scans were taken of sectioned polished (Charalambous et al., 2021; Witecy et al., 2021) and natural enamel (Charalambous et al., 2022), whole natural or phantom teeth (Alwadai et al., 2020; Hartkamp et al., 2017b; Kumar et al., 2018; Meireles et al., 2016b; Witecy et al., 2021), zirconia sextant casts (Kühne

et al., 2021), shortened dental casts made of extracted teeth (Marro et al., 2020) or full-arch dental casts (Marro et al., 2018b). Out of these, very few compared the measurements of intraoral scanners to a reference device (Charalambous et al., 2022, 2021; Hartkamp et al., 2017b; Kühne et al., 2021; Witecy et al., 2021) . Information about the effect of scanning distances on the intraoral scanner accuracy to measure surface change is sparse and to the author's knowledge, this is the first study that investigated the accuracy of an intraoral scanner using different scan sizes (spans) for quantifying surface change.

The few *in vivo* publications that investigated intraoral scanners for measuring surface change have relied on qualitative assessments, such as clinical and photographic examinations using wear indices, as the gold standard used for comparison. An exception to this is a study which presented strong quantitative agreement between X-ray computerised micro-tomography and an intraoral scanner for depth (bias = 3.7914 µm) and volume (bias = 0.0037 mm3) measurements (Esquivel-Upshaw et al., 2012). García et al. (2022) reported 100% sensitivity and 84.9% specificity between visual and intraoral scanner analysis of superimposed sequential scans (V. D.-F. García et al., 2022b), while a different study suggested no significant differences between intraoral scanner analysis, clinical or photographic wear examinations (Travassos da Rosa Moreira Bastos et al., 2021b).

The variation within the methodologies of studies in the literature makes it difficult for comparisons. Kühne et al. (2021) reported accuracy ranging from -3% to +13% for crater depths equivalent to 221 – 417 µm using the same intraoral scanner as this present study and compared to optical profilometry, using a zirconia sextant cast as the scanned surface (Kühne et al., 2021). The IOS-TD in this present study, instead, showed an underestimation of -12.6% and -12.2% measuring the D3 (=195 µm) and D4 (=297 µm) craters, respectively, however, the variations in scanned surfaces and software analysis may explain these observed differences. Studies that used scans limited to a whole

tooth area have showed similar underestimations ranging from -18.00% to -0.05% (Witecy et al., 2021).

Four different crater depths were used in this study. The order of these depths was chosen to be above 70 µm based on the conclusions of Chapter 5 that the depth measurement threshold of IOS-TD on natural enamel was 73 µm. Furthermore, it was deemed appropriate to express the IOS-TD measurement divergencies from the reference profilometric measurements as percentage errors which helped evaluate the uncertainty of the IOS-TD relative to the magnitude of the measurand. It also made it easier to compare results to other published studies which also expressed measurements as percentage errors (Kühne et al., 2021; Pottmann et al., 2006).

Like all scientific work, the present study is subject to several limitations. A typodont was used for the simulation of a maxillary arch in a laboratory setting which may not fully replicate the oral environment. Inaccuracies of intraoral scanner data may be greater when the scan is conducted *in vivo* considering factors such as the transparency of natural teeth and optical reflections, patient movement, spatial restrictions, as well as the humid nature of the oral cavity (Li et al., 2017). However, recent research suggested similar mesh distortion for both *in vivo* and *in vitro* scans (Li et al., 2017). On the other hand, using the CNC machine with a bur of 2.0 mm diameter provided a reliable and accurate method to simulate wear. The location of the crater was chosen to be near the origin of the scan path where the error generated may be less (Kontis et al., 2022). Further research is required to investigate the accuracy of intraoral scanners for surface change quantification at different locations across the arch. Perhaps the biggest limitation of the study was that a single operator, had a priori knowledge of the location of crater as well as the type of scanning spans during analysis. However, all the Ø4 mm residual surfaces consisting of the crater and reference region were extracted as separate .stl files and randomised so that the operator was

blinded to the original type of scanning span. The introduction of an independent operator to detect the crater for measurement without this prior knowledge of its location would make the study more robust and clinically relevant.

Although there are several intraoral scanners in the market, each relying on different optical principles, a single intraoral scanner was investigated in this study for convenience. The investigated intraoral scanner hardware and metrology software components are currently available in the market; however, the results of the present study should only be used as a guideline as newer-generation intraoral scanners with revised stitching algorithms and added functionalities may be able to perform better (Ender et al., 2019b; Schmidt et al., 2020). Additionally, the results may vary depending on the type of inspection metrology software because of differences in point-cloud interpolation and alignment algorithms (Minetola, 2012).

6.6 Conclusions

Within the limitations of this *in vitro* study, the following conclusions were drawn:

- The accuracy of the IOS-TD for measuring surface change (crater depth) decreased as the scan size increased from cusp to full-arch.
- Scan sizes limited to the cusp, or the tooth showed no significant differences with good IOS-TD accuracy within ± 5% for any of the four different crater depths investigated.
- Full-arch scans of the IOS-TD could measure crater depths above or equal to 200 µm only with a 10-12% underestimation accuracy, which may not be suitable for clinical or scientific purposes.

Chapter 7 General discussion, conclusions, and suggestions for future work

7.1 General discussion

The focus of this thesis was to investigate the accuracy and thresholds of a clinical intraoral scanner (IOS-TD) for measuring surface loss. This was conducted by working systematically through and investigating the influence of factors associated with IOS scanning, characterising roughness and form changes on different surfaces (including polished and natural enamel) and establishing robust software analysis workflows. One of the primary objectives was to explore the depth measurement threshold of the IOS-TD for measuring surface loss. This was explored by utilising surfaces of different complexities, ranging from flat planar to freeform topographies. Although, the experiments conducted in this thesis present knowledge with an underlying future intention of quantifying and monitoring ETW as part of standard patient care, it was beyond the scope of this thesis to investigate the histopathology of ETW. A metrological approach was followed instead; this is the reason why metrology terms such as 'groove' or 'crater' were preferred instead of 'lesions' to describe experimental surface loss.

As established by the literature review (Chapter 1), the introduction of IOSs has been one of the most transformative and increasingly popular innovations in clinical dentistry (Abduo and Elseyoufi, 2018). Whilst primarily designed for the manufacture of CAD/CAM dental restorations, advances in IOS technologies increased interest in their use for monitoring and prevention. The majority of observational ETW studies were previously conducted *in vitro* or *in situ* using laboratory-based equipment such as profilometry (Wulfman et al., 2018). Increasingly, more studies have proposed

the use of IOSs for *in vivo* scans, without the need to scan analogue impressions or dental stone casts *ex vivo,* to assess surface loss/wear (Bronkhorst et al., 2022).

Indeed, this is a fast-advancing topic of dental research. The number of publications describing the use of IOSs for measuring surface loss has increased from 1 – 3 per year between 2013 – 2019 to 5 – 6 per year in the last three years, 2020 – 2022, whilst the majority of these studies have been published during the 4-year studentship of this thesis' author.

The aim of Chapter 2 was to establish the influence of factors pertaining to the scanner handling technique and the surface-to-camera distance on the accuracy of the IOS-TD, as well as characterising the TiO_2 powder required to operate it. The idea behind this was to determine optimal scanning parameters for subsequent investigations of the thesis. The fact that no differences were observed between handheld Vs. jig-guided scanning by the IOS-TD, nor between different surface-to-camera distances reinforced the intent of carrying out handheld scanning for the rest of the thesis, as originally intended by its manufacturers. Of course, there are many more factors to consider that may affect the accuracy of IOSs, including but not limited to, ambient and scanning lights (Jivanescu et al., 2021; Koseoglu et al., 2021) or *in vivo* conditions such as the presence of saliva and oral humidity (Flügge et al., 2013) which was beyond the scope of this thesis but would merit future study.

Throughout the thesis, the NCLP was used as the reference device as it is characterised by high accuracy and considered the gold standard for *in vitro* quantification of ETW (F. Mullan et al., 2018, 2017; Wulfman et al., 2018). Its accuracy was further established in this thesis by using a Taylor-Hobson 2.64 µm step height reference standard which demonstrated trueness (precision) of 10 (10) nm. Therefore, any NCLP measurements throughout this thesis were treated as the accepted 'true' measurements for comparison against the investigated device, the IOS-TD.

The profilometric characterisation of TiO_2 powdering demonstrated that the overall height difference between powdered and unpowdered surfaces was less than 1 µm; hence its impact was not significant for measurement of surface form changes. On the other hand, powdering resulted in rougher surfaces; however, at the time it was not known whether the IOS-TD was able to discriminate surface roughness changes. This was further explored in Chapter 3 by scanning flat textured surfaces of increasing roughness using both the IOS-TD and NCLP and comparing their measurements. Overall, the IOS-TD demonstrated significantly different roughness measurements to the NCLP, and indeed, it detected change in roughness only when the 125 µm silicon-carbide particle paper was measured (NCLP *Sq* roughness = 30.8 µm) compared to the control painted glass slide (NCLP *Sq* roughness = 1.2 µm). Therefore, it was settled that the IOS-TD was not able to detect short wavelength (high-frequency) surface components such as seen in surface texture and roughness analyses and by inference, IOSs are best-suited for measuring form changes such as bulk surface loss.

The first three experimental chapters (Chapters 2, 3, and 4) involved measurement of grooves on polished human enamel which consists of a flat planar surface. The rationale behind this was mainly due to three reasons: 1. elimination of natural variation and increased homogeneity between samples 2. easier sample isolation through protective barriers (taping) and enamel exposure, and most importantly 3. facilitation of surface loss measurement using single scan analysis (Attin and Wegehaupt, 2014; Young and Tenuta, 2011). The use of polished enamel allowed the author to investigate the ability of the IOS-TD in the most simplified, controlled, and standardised experimental conditions, without incorporating other sources of error such as seen with measuring freeform surfaces. Consequently, the IOS-TD measurements on freeform surfaces were explored in Chapter 5 and 6 by utilising natural enamel samples and a typodont full-arch dentition, respectively.

In Chapter 3, the depth measurement detection threshold of the IOS-TD for measuring grooves on polished enamel was determined to be in the order of 44 μm. This study was the first to develop a robust protocol using single scan analysis for determining the minimum depth an IOS can reliably measure. This was defined not only by measuring the depth of grooves, but also by using metrological practices such as threshold detection algorithms to localise and measure the XY area of the groove as well as performing surface skewness and kurtosis analyses.

The methodology for polished enamel used in Chapter 3 involved using ten samples for each level of depth tested, whilst in Chapter 5 a single natural enamel sample was used for each depth level and scanned ten times. Using multiple samples to represent a certain depth level has the advantage of providing more representative data as an element of reproducibility is introduced; however, it has the disadvantage of introducing biological variation due to differing enamel response leading to higher standard deviations. Nevertheless, it was previously demonstrated in Chapter 2 that the accuracy of handheld IOS-TD scanning was 2.0 (1.6) μm after repeatedly measuring a groove of 45 μm-depth ten times.

Freeform surfaces create metrological challenges however it is important to have robust surface analysis workflows that can manage a wide variation of surface change. The main unresolved challenge is related to the lack of unchanged reference areas to facilitate comparison and form removal for valid surface metrology. In this thesis, step height calculations (ISO 5436-1) in polished enamel followed a method previously utilised by Mylonas et al., (2018) using single-scan analysis, which required regions of uneroded reference enamel. As these regions are not present in natural enamel samples, single-scan analysis was not possible. Therefore, this thesis explored bi-scan analysis methods which allow measurements on freeform surfaces by comparing two scans of different time-points. These methods were investigated in Chapter 4, 5, and 6.

Chapter 4 transitioned the narrative from surface measurements using single-scan analysis to the introduction of two different types of bi-scan analyses. Although, these bi-scan analyses were developed for measurements on freeform surfaces, they were tested first on polished enamel samples to compare their measurements against the gold standard single-scan analysis.

Chapter 4 considered three step heights analysis methods (Single-SH, Ten-SH, and Total-SH) to determine the optimal measurement protocol for this thesis. No differences were observed between the different step height methods therefore, it was accepted that the grooves created from acid exposure in the *in vitro* model, were uniform across the polished enamel surface. The IOS-TD was not used in this chapter as the investigations focused solely on different analysis workflows. It is therefore unknown whether there would be any differences between different types of step height analyses using datasets from intraoral scanners which are considered to have lower accuracies than profilometers.

Nonetheless, when compared to single-SH and Ten-SH, using the mean of all profile lines in the Total-SH method provided more information on the topography of the groove. This reinforced the choice to use the Total-SH method, i.e., using all datapoints available inside and outside the groove, throughout the rest of the thesis, as it would have far more bearing on the 3D topography of the surface loss being measured. It is worth noting that experimental surface loss on freeform surfaces in Chapters 5 and 6 was created in the form of round craters (rather than longitudinal grooves); as a result, a modified version of the Total-SH was used where surface loss was measured as the difference between a ring-shaped reference area around the crater and a circular area inside the crater. Additionally, although step height measurements were designed for use on flat surfaces, they were made possible in Chapters 5 and 6 (i.e., on freeform surfaces) due to the nature of the

subtraction process to remove the original surface form of the aligned scans being subtracted together and facilitate analysis of the residual surface (Mansouri, 2014).

The bi-scan surface-subtraction analysis did not show any differences to single scan analysis. This was believed to be because no software algorithms were involved during the alignment of the surfaces which were manually aligned by pin-pointing fiducial markers on each surface. Additionally, any errors caused from the manual alignment in the XY plane would be of little consequence on the residual surface following subtraction because of the flat nature of the surfaces used in this study. On the other hand, the measurements of the bi-scan surface-registration analysis were significantly different than the single-scan analysis as well as the bi-scan surface-subtraction analysis possibly because it utilised the automated ICP algorithm which is a major source of error. Additionally, the registration was conducted solely by using the fiducial markers as landmarks. These fiducials corresponded to only a small proportion of the overall scanned sample area needed aligning. On reflection, it is believed that alignment using larger reference areas would result in more accurate measurements. However, finding such reference areas in the oral cavity that do not undergo change, remains an unresolved puzzle. The suggestion of using surfaces on teeth that are least likely to undergo changes (O'Toole et al., 2019a) or using palatal rugae (Becker et al., 2018a) as references for superimposition is promising and requires further research. An additional area for future development would be the use of feature-based registration where alignment occurs on pairs of topographic landmarks automatically identified by similarity of shape descriptor values as proposed by Moretti et al., (2019).

Both bi-scan analyses investigated in Chapter 4 come with their own inherent limitations. On one hand the surface-subtraction analysis required manual alignment and on the other, relying on fiducial markers alone during the ICP-alignment led to overestimation of surface loss. Therefore, it

was felt there would be merit in automating the process by combining the two techniques in Chapter 5. As previously explained, when used in combination, surface-registration must be performed before surface-subtraction and not *vice versa*. This is because the result of surface-subtraction is to end up with a residual dataset which is a single surface, and which cannot be registered (aligned) to another; in contrast the result of surface-registration is two scans which still exist independently but have been aligned.

As such, four different bi-scan analyses were tested in Chapter 5: two involving surface-registration alone, with best-fit (BF-Reg) or reference-based alignment (Ref-Reg), and two that were a combination of surface-registration and surface-subtraction, with best-fit (BF-Sub) or reference-based alignment (Ref-Sub). The study demonstrated that the combination of surface-registration and surface-subtraction, with or without using reference areas during alignment (i.e., the BF-Sub and Ref-Sub techniques) significantly reduced errors for measurement of change on freeform surfaces using softgauges compared to the techniques involving surface-registration alone (i.e., the BF-Reg and Ref-Reg techniques). Furthermore, no significant differences were observed between the BF-Sub and Ref-Sub techniques suggesting that relying on reference regions during the alignment step may not be necessary when the combination technique is used. As explained in Chapter 5 and illustrated in Figure 5-9 above, this may be because no matter how misaligned two sequential surfaces are in the Z axis, as long as they are well-aligned in the XY plane they will generate a 'difference' 3D profile of the same shape, hence any step height measurement thereafter would yield a constant value.

In order to investigate the numerical correctness of the four bi-scan analyses, mathematically created softgauges with craters of known depths were utilised based on the international standard ISO 5436-2. This determined the measurement errors for each analysis workflow without

incorporating errors arising from hardware and scanning. Therefore, the results should be interpreted with caution as other errors should be expected when the workflow is used in conjunction with hardware, particularly with scanners of lower accuracy and resolution, such as IOSs. The concept of using softgauges for dental research was previously utilised by O'Toole et al., (2019a) who created virtual defects on molars datasets to investigate the accuracy of three different superimposition techniques, although the exact methodology differed from this thesis.

Using the Ref-Sub technique, the depth discrimination threshold of the IOS-TD for measuring surface loss on natural enamel was shown to be 73 µm. This was substantiated by the minimal step height and area percentage errors at that depth compared to the NCLP and the achieved 100% automated crater detection. The Bland-Altman plot between the NCLP and IOS-TD measurements corroborated this finding as the bias (average difference) decreased to nearly zero above ~70 µm depth. This was the first *in vitro* study to demonstrate such high agreement between an IOS and a reference device for measuring such surface loss on freeform surfaces at such depth. It is noteworthy that the majority of *in* vivo studies measuring tooth surface loss using IOSs focused on determining the precision of IOSs instead of the accuracy/agreement. This is because it is nearly impossible to use reference scanners inside the oral cavity. Of the few *in vitro* studies that utilised gold standard profilometry for comparison, they all involved measuring experimental surface loss on a variety of freeform surfaces ranging from 73 µm to approximately 550 µm (Hartkamp et al., 2017b; Kühne et al., 2021; Witecy et al., 2021) without testing any shallower depths. Similar to this thesis, depth was the primary measuring output of these studies; however, none looked at other parameters such as the area of experimental surface loss or feature detection parameters.

In previous profilometric studies analysing erosion-attrition and erosion-abrasion lesions which produced irregular wear lesions, it was suggested that the following measurement methods could

all be used to assess enamel loss: average wear depth (volume of enamel loss, mm^3 / surface area of enamel lesion mm^2) (O'Toole et al., 2020; Vieira et al., 2007), normalised enamel loss (3D step height, µm / surface area, μm^2) (Rodriguez and Bartlett, 2010), and volume loss (mm^3) (O'Toole et al., 2020; Ruben et al., 2019). Whilst these measurement methods were not utilised in this study, it would be interesting to determine whether they can be used in conjunction with IOS datasets. Interestingly, a recent *in vivo* study suggested that volumetric measurements were not suitable for 3D wear assessments using IOS datasets as they are generally more prone and sensitive to alignment errors (Bronkhorst et al., 2022).

The spatial resolution of the IOS-TD was undeniably lower than the NCLP. This was clearly observed throughout the experimental chapters by looking at the pseudo-colour dataset images of the NCLP and the IOS-TD. The datasets of the IOS-TD consisted of fewer POMs/mm^2 than the NCLP which resulted in smoother topography displaying grooves or craters less clearly. This may explain why the accuracy of the IOS-TD improved as the crater diameter increased from 1.0 mm to 1.5mm and finally to 2.0 mm in Chapter 5 Investigation 3. No matter the point cloud density, a feature on a surface with a larger area would be depicted on the point-cloud dataset with more points of measurement than one with a smaller area; as long as the accuracy of each point is high, it would be easier to convert a surface with more points of measurement to a faithful virtual model of its real geometry (Medina-Sotomayor et al., 2018; Tapie et al., 2015).

In Chapter 6, the Ref-Sub analysis technique developed in previous chapters was utilised to investigate the effect of increasing scan size, from cusp to arch, on the accuracy of the scanner for measuring different crater depths. The highest accuracy was observed using scan sizes restricted to the cusp and tooth regions (remained below ±5% error for all crater depths), whereas the accuracy decreased significantly as the scan size increased to a sextant, quadrant, or a full-arch size. The

finding is comparable with other studies which suggested that for larger spans of scanned surfaces, the IOSs are required to capture and stitch more single images which results in propagation of errors within each registration of overlapping images and therefore an increased overall error in the final arch shape (G.-H. Park et al., 2019; Schmidt et al., 2021). In addition to this, the resolution of the analysed pseudo-colour images (POMs/mm^2) decreased as the scan size increased. One explanation might be that the algorithm of the software used compresses large datasets (Medina-Sotomayor et al., 2019b); however, this is ambivalent as the mathematical complexities of software algorithms are hidden from the users. Generally speaking, datasets with lower point cloud density can introduce 'chord' errors due to the lack of digital information between points, leading to surface defects, non-existent curvatures, or discontinuity in the surface (Medina-Sotomayor et al., 2018; Tapie et al., 2015). It is worth noting that the POMs/mm^2 measured on polished enamel sample datasets using MountainsMap®7 software in Chapter 3 were 114 – 164 POMs/mm^2 only whilst those measured by the newer version of the software, Mountains®8, for the cusp scan in Chapter 6 which is a dataset of similar size was 4,354 POMs/mm^2; this indicates that different metrology software or indeed different versions of the same software can interpolate point-clouds from the same scanner differently. The impact of different versions of a software on the resolution and accuracy of measuring surface loss was not investigated in this thesis due to licencing restrictions of using both versions at the same time; however, it would merit future study.

The depth measuring accuracy of the IOS-TD improved as the crater depth increased and seemed to plateau at approximately 10 – 12% underestimation for depths ≥ 195 µm. The reason for this improvement might be due to the fact that IOSs use algorithms that are optimised to detect notable surface changes and transition areas such as strong curvatures, physical limits and edges, or differences of grey intensity (silhouette shadowing) (Aubreton et al., 2013; Braian and Wennerberg, 2019a; Cheung et al., 2005; Richert et al., 2017).

Several studies have shown relatively low progression rates in patients with physiological tooth wear, with reported annual height losses between 11 and 29 µm (Lambrechts et al., 1989; Pintado et al., 1997). In patients with advanced tooth wear or existing parafunctional habits, progression rates can be much higher between 73 and 140 µm per year (Ahmed et al., 2017; Bartlett et al., 1997). The direct quantification of surface loss using IOSs would be beneficial in clinical practice for the monitoring and management of ETW, improving awareness and patient-centred care. However, the findings of this thesis, indicating that full-arch scanning using IOS-TD discriminated crater depths of approximately 200 µm depth with underestimation errors still ranging between 10-12%, confine the use of IOSs to shorter spans and highlight the need for further research and development in both hardware and software characteristics. Perhaps a methodological compromise for now would be scanning a full arch (which lowers accuracy) but performing registration and subtraction for measuring surface loss on dataset-subdivisions of single teeth (which heightens accuracy) (Bronkhorst et al., 2022) or using index teeth such as first molars and upper central incisors (O'Toole et al., 2020). Be that as it may, IOSs and their technologies are constantly revised and updated, and improvements in their measurement accuracy are inevitable. For this thesis, a single IOS was used for convenience and to avoid product testing. This might be considered a limitation as the resolution and accuracy of different IOSs varies. However, the choice of using the IOS-TD was deemed suitable as it has been extensively investigated in previous studies and is considered amongst the best performing IOSs (Boeddinghaus et al., 2015; Medina-Sotomayor et al., 2019a, 2018).

A key limitation of surface-registration and surface-subtraction is that the user has to define the angle at which the surfaces from 3D models are extracted and subtracted. Therefore, to measure changes on different sides/regions of an object, individual subtraction analyses would be required on the different sides of the measured object. Further work is needed on resolving these known challenges with simultaneous measurement of multiple features on complex structured and

freeform surfaces. Furthermore, the technique developed remains time-consuming and the two software involved are not readily available to general practitioners which limits its use to university settings and academia for the time being. It would be vital if automation improved and the additional step of surface subtraction following registration was added in purpose-built freeware dedicated to measuring ETW such as WearCompare software (O'Toole et al., 2019b) or OraCheck software (Dentsply Sirona, Bensheim, Germany).

7.2 Overall Conclusions

Within the limitations of these *in vitro* studies, the following general conclusions were made:

- There was no significant difference in the IOS-TD accuracy between handheld and jig-guided scanning, nor between different surface-to-camera distances during scanning.
- The application of TiO_2 powder increased surface roughness but it did not change the surface form.
- Unlike the NLCP, the IOS-TD was not able to measure changes in surface roughness below Sq 30.8 µm and therefore it is best suited for surface form analysis.
- The depth measurement threshold of the IOS-TD on polished enamel using single scan analysis was determined to be 44 µm. Significant differences in XY area measurements and lower automated detection of grooves was observed below this threshold. This was corroborated by determining the presence of grooves via surface skewness and kurtosis analysis.
- Measuring the same grooves on polished enamel, no significant differences were observed between single scan analysis and the bi-scan surface-subtraction analysis. On the other hand, significant differences were observed between the bi-scan surface-registration analysis and the single-scan analysis as well as the bi-scan surface-subtraction analysis.

- Using the bi-scan surface-subtraction analysis, no significant differences were observed between different types of step height calculation techniques; however, the author recommends the use of all datapoints if offered by the metrology software in use.
- The combination of surface-registration and surface-subtraction technique improved the accuracy of measuring surface loss on freeform softgauges compared to surface-registration alone. No significant differences were observed using the former with or without using reference regions during registration.
- The depth measurement threshold of the IOS-TD using the surface-registration and surface-subtraction technique (Ref-Sub) on freeform surfaces was 73 µm, above which no significant differences were observed in depth or XY area measurements and achieving 100% automated detection and good agreement against the fold standard NCLP.
- The accuracy of the IOS-TD for measuring surface loss on freeform surfaces decreased as the scan size increased from cusp to full-arch scanning. Surface loss measurements in the order of 80 µm depth or above using IOS-TD scans of single teeth were accurate within ± 5%. Full-arch scanning achieved accuracy of 10-12% underestimation only for surface loss above or equal to 200 µm which may not be suitable for clinical monitoring purposes for the time being.
- Throughout this thesis, the IOS-TD demonstrated limitations in relation to point-cloud density and spatial and axial resolution compared to the NLCP, as well as propagation of errors from image stitching using bigger scan sizes. Errors arising from these limitations were aggravated when surface loss was measured on freeform surfaces as this involved utilising two sets of scans and performing alignment.

7.3 Future work

Whilst this thesis has provided a significant step forward in clinical dental surface metrology by providing a method to directly measure surface loss using IOSs, there are a number of further investigations that still require exploration.

- Whilst a number of different ISO and non-ISO standard methods were used throughout this thesis to evaluate surface loss in the form of depth in conjunction with IOS scanning, there would be merit in investigating volumetric methods including volume of erosion lesion (μm^3) and normalised lesion depth (µm, volume of lesion/surface area of lesion). Additionally, it would be interesting to correlate these volumetric methods to depth measurement methods described in this thesis.
- Aside from the scanner handling technique and surface-to-camera distance investigated in Chapter 2, other factors should be explored *in vitro* that may influence the accuracy of IOSs. Some of these factors include but not limited to, ambient and scanning lights (Jivanescu et al., 2021; Koseoglu et al., 2021) or scanning path strategies (Mandelli et al., 2018). Furthermore, oral cavity conditions such as the presence of saliva and oral humidity (Flügge et al., 2013) should be simulated *in vitro* to determine their impact in measurement accuracy.
- The accuracy of different latest-generation IOSs should be investigated on the measurement of surface loss. Investigations would determine whether the type of optical technology employed by each IOS impacts the accuracy. The selection of IOSs should include powdered and non-powdered based systems as well as ones that offer coloured datasets.
- Some studies that have investigated IOSs for the measurement of surface loss used software packages that were not investigated in this thesis. Examples of these include WearCompare (www.leedsdigitaldentistry.com/wearcompare Leeds, UK), GOM Inspect (GOM GmbH,

Braunschweig, Germany) (Marro et al., 2020; Witecy et al., 2021) and OraCheck (Dentsply Sirona, Bennsheim, Germany). Therefore, it would be interesting to explore these further, perhaps through collaborations with other research groups. The investigations should study the way point clouds are interpolated by different software and what impact the type of software has on the accuracy of surface loss measurements.

- Observational *in vivo* clinical studies investigating the progression of ETW of up to 5 years should be conducted using intraoral scanning against conventional methods, i.e., analogue impressions and profilometric/laboratory. This would demonstrate what clinicians would expect when looking for a method to monitor tooth wear. Aside from comparing the accuracy of IOSs for measuring ETW *in* vivo against conventional methodologies, other factors can be considered such as patient comfort and engagement and clinical efficiency.

Bibliography

3D systems, 2022. Software | 3D Systems [WWW Document]. URL https://www.3dsystems.com/software?utm_medium=search&utm_source=google&utm_campaign=&utm_term=&utm_content=&gclsrc=aw.ds&&campaign=12765103360&content=514975998425&keyword=geomagic control x&gclid=Cj0KCQjwntCVBhDdARIsAMEwAClZbvCxnzovgUgbhJH1d9eCWHVQXK4h5_v6rEA8hroDPMRgqHEn8IaAo9REALw_wcB (accessed 6.23.22).

3M, 2016. 3M ™ Mobile True Definition Scanner. Frequently Asked Questions.

3M ESPE, 2019. 3M™ True Definition Intraoral Scanner acquired by Midmark in U.S. and Canadian Markets [WWW Document]. URL https://www.3m.com/3M/en_US/dental-us/expertise/digital-dental-impressions/

Abduo, J., Elseyoufi, M., 2018. Accuracy of Intraoral Scanners: A Systematic Review of Influencing Factors. Eur J Prosthodont Restor Dent 26, 101–121. https://doi.org/10.1922/EJPRD_01752Abduo21

Ahlholm, P., Sipilä, K., Vallittu, P., Jakonen, M., Kotiranta, U., 2018. Digital Versus Conventional Impressions in Fixed Prosthodontics: A Review. Journal of Prosthodontics 27, 35–41. https://doi.org/10.1111/jopr.12527

Ahmed, K., Whitters, J., Ju, X., Pierce, S., MacLeod, C., Murray, C., 2017. Clinical Monitoring of Tooth Wear Progression in Patients over a Period of One Year Using CAD/CAM. Int J Prosthodont 30, 153–155. https://doi.org/10.11607/ijp.4990

Ahmed, K., Whitters, J., Ju, X., Pierce, S., MacLeod, C., Murray, C., 2016. A Proposed Methodology to Assess the Accuracy of 3D Scanners and Casts and Monitor Tooth Wear Progression in Patients. Int J Prosthodont 29, 514–521. https://doi.org/10.11607/ijp.4685

Aladağ, A., Oğuz, D., Çömlekoğlu, M.E., Akan, E., 2019. In vivo wear determination of novel CAD/CAM ceramic crowns by using 3D alignment. Journal of Advanced Prosthodontics 11, 120–127. https://doi.org/10.4047/jap.2019.11.2.120

Alaraudanjoki, V., Saarela, H., Pesonen, R., Laitala, M.-L.L., Kiviahde, H., Tjäderhane, L., Lussi, A., Pesonen, P., Anttonen, V., 2017. Is a Basic Erosive Wear Examination (BEWE) reliable for recording erosive tooth wear on 3D models? J Dent 59, 26–32. https://doi.org/10.1016/j.jdent.2017.02.001

Alexandria, A.K., Vieira, T.I., Pithon, M.M., da Silva Fidalgo, T.K., Fonseca-Gonçalves, A., Valença, A.M.G., Cabral, L.M., Maia, L.C., 2017. In vitro enamel erosion and abrasion-inhibiting effect of different fluoride varnishes. Arch Oral Biol 77, 39–43. https://doi.org/10.1016/j.archoralbio.2017.01.010

Al-Hassiny, A., 2022. Intraoral Scanner Reviews from IDS 2021 + Market Overview. Institute of Digital Dentistry 1–55.

Ali, A.O., 2015. Accuracy of Digital Impressions Achieved from Five Different Digital Impression Systems. Dentistry 05, 300. https://doi.org/10.4172/2161-1122.1000300

Al-Jawad, M., Steuwer, A., Kilcoyne, S.H., Shore, R.C., Cywinski, R., Wood, D.J., 2007. 2D mapping of texture and lattice parameters of dental enamel. Biomaterials 28, 2908–2914. https://doi.org/10.1016/j.biomaterials.2007.02.019

Almohefer, S., 2021. In Vitro Investigation of Erosive Changes on Dentine by Evaluating.

Almohefer, S., Moazzez, R., Bartlett, D., 2021. Comparison of metrology created by profilometry and digital microscopy on polished dentine in an erosion/abrasion model. J Dent 114, 103831. https://doi.org/10.1016/j.jdent.2021.103831

Alwadai, G.S., Roberts, G., Ungar, P.S., González-Cabezas, C., Lippert, F., Diefenderfer, K.E., Eckert, G.J., Hara, A.T., 2020. Monitoring of simulated occlusal tooth wear by objective outcome measures. J Dent 102. https://doi.org/10.1016/j.jdent.2020.103467

Amin, S., Weber, H.P., Finkelman, M., el Rafie, K., Kudara, Y., Papaspyridakos, P., 2017a. Digital vs. conventional full-arch implant impressions: a comparative study. Clin Oral Implants Res 28, 1360–1367. https://doi.org/10.1111/clr.12994

Amin, S., Weber, H.P., Finkelman, M., El Rafie, K., Kudara, Y., Papaspyridakos, P., 2017b. Digital vs. conventional full-arch implant impressions: a comparative study. Clin Oral Implants Res 28, 1360–1367. https://doi.org/10.1111/clr.12994

Aragón, M.L.C., Pontes, L.F., Bichara, L.M., Flores-Mir, C., Normando, D., 2016. Validity and reliability of intraoral scanners compared to conventional gypsum models measurements: a systematic review. The European Journal of Orthodontics 38, 429–434. https://doi.org/10.1093/ejo/cjw033

Arezki, Y., Mehdi-Souzani, C., Anwer, N., Nouira, H., 2018. Reference data simulation for L∞ fitting of aspheres. Procedia CIRP 75, 331–336. https://doi.org/10.1016/j.procir.2018.04.051

Attin, T., Becker, K., Roos, M., Attin, R., Paqué, F., 2009. Impact of storage conditions on profilometry of eroded dental hard tissue. Clin Oral Investig 13, 473–478. https://doi.org/10.1007/s00784-009-0253-9

Attin, T., Wegehaupt, F.J., 2014. Methods for assessment of dental erosion, in: Dental Erosion from Diagnosis to Therapy. Switzerland, pp. 123–142. https://doi.org/10.1159/000360355

Aubreton, O., Bajard, · A, Verney, · B, Truchetet, · F, Bajard, A., Verney, B., Truchetet, F., 2013. Infrared system for 3D scanning of metallic surfaces. Mach Vis Appl 24, 1513–1524. https://doi.org/10.1007/s00138-013-0487-z

Austin, R., 2011. The role of fluoride in erosion, attrition and abrasion of human enamel and dentine in vitro. King's College London.

Austin, R.S., Haji Taha, M., Festy, F., Cook, R., Andiappan, M., Gomez, J., Pretty, I.A., Moazzez, R., 2017. Quantitative Swept-Source Optical Coherence Tomography of Early Enamel Erosion in vivo. Caries Res 51, 410–418. https://doi.org/10.1159/000477098

Austin, R.S., Mullen, F., Bartlett, D.W., 2015. Surface texture measurement for dental wear applications. Surf Topogr 3, 023002. https://doi.org/10.1088/2051-672X/3/2/023002

Autodesk, 2022. STL Export Settings | Revit 2021 | Autodesk Knowledge Network [WWW Document]. URL https://knowledge.autodesk.com/support/revit/learn-explore/caas/CloudHelp/cloudhelp/2021/ENU/Revit-DocumentPresent/files/GUID-01504202-EF80-4815-9675-ADB8802592BD-htm.html (accessed 6.23.22).

Barbour, M.E.E., Rees, J.S.S., 2004. The laboratory assessment of enamel erosion: A review. J Dent 32, 591–602. https://doi.org/10.1016/j.jdent.2004.05.001

Bartlett, D., 2016. A personal perspective and update on erosive tooth wear - 10 years on: Part 1 - Diagnosis and prevention. Br Dent J 221, 167–171. https://doi.org/10.1038/sj.bdj.2016.596

Bartlett, D., Dugmore, C., 2008. Pathological or physiological erosion - Is there a relationship to age? Clin Oral Investig 12, 27–31. https://doi.org/10.1007/s00784-007-0177-1

Bartlett, D., Ganss, C., Lussi, A., 2008. Basic Erosive Wear Examination (BEWE): A new scoring system for scientific and clinical needs. Clin Oral Investig 12, 65–68. https://doi.org/10.1007/s00784-007-0181-5

Bartlett, D.W., 2003. Retrospective long term monitoring of tooth wear using study models. Br Dent J 194, 211–213. https://doi.org/10.1038/sj.bdj.4809914

Bartlett, D.W., Blunt, L., Smith, B.G.N., 1997. Measurement of tooth wear in patients with palatal erosion. British Dental Journal 1997 182:5 182, 179–184. https://doi.org/10.1038/sj.bdj.4809338

Bartlett, D.W., Lussi, A., West, N.X., Bouchard, P., Sanz, M., Bourgeois, D., 2013. Prevalence of tooth wear on buccal and lingual surfaces and possible risk factors in young European adults. J Dent 41, 1007–1013. https://doi.org/10.1016/j.jdent.2013.08.018

Becker, K., Wilmes, B., Grandjean, C., Drescher, D., 2018a. Impact of manual control point selection accuracy on automated surface matching of digital dental models. Clin Oral Investig 22, 801–810. https://doi.org/10.1007/s00784-017-2155-6

Becker, K., Wilmes, B., Grandjean, C., Drescher, D., 2018b. Impact of manual control point selection accuracy on automated surface matching of digital dental models. Clin Oral Investig 22, 801–810. https://doi.org/10.1007/s00784-017-2155-6

Beleidy, M., Ziada, A., 2022. 3D Surface Deviation Wear Analysis of Veneered PEEK Crowns and Its Correlation with Optical Digital Profilometry. Journal of Prosthodontics 1–8. https://doi.org/10.1111/jopr.13490

Beniash, E., Stifler, C.A., Sun, C.Y., Jung, G.S., Qin, Z., Buehler, M.J., Gilbert, P.U.P.A., 2019. The hidden structure of human enamel. Nat Commun 10, 1–13. https://doi.org/10.1038/s41467-019-12185-7

Berkovitz, B.K.B., Holland, G.R., Moxham, B.J., 2009. Oral anatomy, histology and embryology. Mosby Elsevier.

Besl, P.J., McKay, N.D., 1992. A Method for Registration of 3-D Shapes. IEEE Trans Pattern Anal Mach Intell 14, 239–256. https://doi.org/10.1109/34.121791

Bloss, R., 2008. Accordion fringe interferometry: a revolutionary new digital shape-scanning technology. Sensor Review 28, 22–26. https://doi.org/10.1108/02602280810849983

Boeddinghaus, M., Breloer, E.S., Rehmann, P., Wöstmann, B., 2015. Accuracy of single-tooth restorations based on intraoral digital and conventional impressions in patients. Clin Oral Investig 19, 2027–2034. https://doi.org/10.1007/s00784-015-1430-7

Boltryk, P.J., Hill, M., McBride, J.W., 2009. Comparing laser and polychromatic confocal optical displacement sensors for the 3D measurement of cylindrical artefacts containing microscopic grooved structures. Wear 266, 498–501. https://doi.org/10.1016/j.wear.2008.04.082

Boltryk, P.J., Hill, M., McBride, J.W., Nascè, A., 2008. A comparison of precision optical displacement sensors for the 3D measurement of complex surface profiles. Sens Actuators A Phys 142, 2–11. https://doi.org/10.1016/j.sna.2007.03.006

Braian, M., Wennerberg, A., 2019a. Trueness and precision of 5 intraoral scanners for scanning edentulous and dentate complete-arch mandibular casts : A comparative in vitro study. J Prosthet Dent 122, 129-136.e2. https://doi.org/10.1016/j.prosdent.2018.10.007

Braian, M., Wennerberg, A., 2019b. Trueness and precision of 5 intraoral scanners for scanning edentulous and dentate complete-arch mandibular casts: A comparative in vitro study. Journal of Prosthetic Dentistry 122, 129-136.e2. https://doi.org/10.1016/J.PROSDENT.2018.10.007

Brandestini, M., Moermann, W.H., 1989. Method and apparatus for the three-dimensional registration and display of prepared teeth. 4,837,732.

Bronkhorst, H., Bronkhorst, E., Kalaykova, S., van der Meer, W., Huysmans, M.-C., Loomans, B., 2022. Precision of In Vivo Quantitative Tooth Wear Measurement using Intra-Oral Scans. J Vis Exp e63680, 1–17. https://doi.org/10.3791/63680

Burhardt, L., Livas, C., Kerdijk, W., van der Meer, W.J., Ren, Y., 2016. Treatment comfort, time perception, and preference for conventional and digital impression techniques: A comparative study in young patients. American Journal of Orthodontics and Dentofacial Orthopedics 150, 261–267. https://doi.org/10.1016/j.ajodo.2015.12.027

Burian, G., Erdelt, K., Schweiger, J., Keul, C., Edelhoff, D., Güth, J.-F., 2021. In-vivo-wear in composite and ceramic full mouth rehabilitations over 3 years. Sci Rep 11, 14056. https://doi.org/10.1038/s41598-021-93425-z

Burzynski, J.A., Firestone, A.R., Beck, F.M., Fields, H.W., Deguchi, T., 2018. Comparison of digital intraoral scanners and alginate impressions: Time and patient satisfaction. American Journal of Orthodontics and Dentofacial Orthopedics 153, 534–541. https://doi.org/10.1016/J.AJODO.2017.08.017

Camardella, L.T., Breuning, H., de Vasconcellos Vilella, O., 2017a. Accuracy and reproducibility of measurements on plaster models and digital models created using an intraoral scanner. Journal of Orofacial Orthopedics 78, 211–220. https://doi.org/10.1007/s00056-016-0070-0

Camardella, L.T., Breuning, H., Vilella, O. de V., 2017b. Are there differences between comparison methods used to evaluate the accuracy and reliability of digital models? Dental Press J Orthod 22, 65–74. https://doi.org/10.1590/2177-6709.22.1.065-074.oar

Carvalho, T.S., Colon, P., Ganss, C., Huysmans, M.C., Lussi, A., Schlueter3, N., Schmalz, G., Shellis, P., R, T., Wiegand, A., 2015. Consensus report of the European Federation of Conservative Dentistry: erosive tooth wear—diagnosis and management. Clin Oral Investig 19, 1557–1561. https://doi.org/10.1007/s00784-015-1511-7

Chadwick, R.G., Mitchell, H.L., Manton, S.L., Ward, S., Brown, R., 2005. Maxillary incisor palatal erosion: no correlation with dietary variables? J Clin Pediatr Dent 29, 157–164.

Charalambous, P., O'Toole, S., Austin, R., Bartlett, D., 2022. The threshold of an intra oral scanner to measure lesion depth on natural unpolished teeth. Dental Materials 38, 1354–1361. https://doi.org/10.1016/j.dental.2022.06.022

Charalambous, P., Saoirse, O., Thomas, B., Bartlett, D., Austin, R., 2021. The measurement threshold and limitations of an intra-oral scanner on polished human enamel. Dental Materials 1–7. https://doi.org/10.1016/j.dental.2021.01.006

Chen, S., Xue, S., Zhai, D., Tie, G., 2020. Measurement of Freeform Optical Surfaces: Trade-Off between Accuracy and Dynamic Range. https://doi.org/10.1002/lpor.201900365

Cheng, Z.J., Wang, X.M., Cui, F.Z., Ge, J., Yan, J.X., 2009. The enamel softening and loss during early erosion studied by AFM, SEM and nanoindentation. Biomedical Materials 4. https://doi.org/10.1088/1748-6041/4/1/015020

Cheung, K. (German), Baker, S., Kanade, T., 2005. Shape-From-Silhouette Across Time Part I: Theory and Algorithms. Int J Comput Vis 62, 221–247. https://doi.org/10.1007/s11263-005-4881-5

Chiboub, A., Arezki, Y., Vissiere, A., Mehdi-Souzani, C., Anwer, N., Alzahrani, B., Bouazizi, M.L., Nouira, H., 2021. Generation of reference softgauges for minimum zone fitting algorithms: Case of aspherical and freeform surfaces. Nanomaterials 11. https://doi.org/10.3390/nano11123386

Clozza, E., Biasotto, M., Cavalli, F., Moimas, L., Di Lenarda, R., 2012. Three-Dimensional Evaluation of Bone Changes Following Ridge Preservation Procedures. Journal of Oral Maxillofacial Implants 27, 770–775.

Conceição, J.M., Delbem, A.C.B., Danelon, M., da Camara, D.M., Wiegand, A., Pessan, J.P., 2015. Fluoride gel supplemented with sodium hexametaphosphate reduces enamel erosive wear in situ. J Dent 43, 1255–1260. https://doi.org/10.1016/j.jdent.2015.08.006

Corbett, J., 2021. The Battle of File Formats: STL vs OBJ vs PLY [WWW Document]. URL https://blog.medit.com/medit/the-battle-of-file-formats-stl-vs-obj-vs-ply (accessed 5.8.22).

Cui, F.-Z., Ge, J., 2007. New observations of the hierarchical structure of human enamel, from nanoscale to microscale. J Tissue Eng Regen Med 1, 185–191. https://doi.org/10.1002/term.21

Cuy, J.L., Mann, A.B., Livi, K.J., Teaford, M.F., Weihs, T.P., 2002. Nanoindentation mapping of the mechanical properties of human molar tooth enamel. Arch Oral Biol 47, 281–291. https://doi.org/10.1016/S0003-9969(02)00006-7

Daly, S., Seong, J., Parkinson, C., Newcombe, R., Claydon, N., West, N., 2021. A proof of concept study to confirm the suitability of an intra oral scanner to record oral images for the non-invasive assessment of gingival inflammation. J Dent 105, 103579. https://doi.org/10.1016/j.jdent.2020.103579

Darling, C.L., Huynh, G.D., Fried, D., 2006. Light scattering properties of natural and artificially demineralized dental enamel at 1310 nm. J Biomed Opt 11, 034023. https://doi.org/10.1117/1.2204603

de Groot, P., Fitzgerald, D., 2017. Measurement, certification and use of step-height calibration specimens in optical metrology, in: Lehmann, P., Osten, W., Albertazzi Gonçalves, A. (Eds.), Optical Measurement Systems for Industrial Inspection X. SPIE, p. 1032919. https://doi.org/10.1117/12.2269800

Dehurtevent, M., Robberecht, L., Béhin, P., 2015. Influence of dentist experience with scan spray systems used in direct CAD/CAM impressions. J Prosthet Dent 113, 17–21. https://doi.org/10.1016/j.prosdent.2014.07.006

Delize, V., Bouhy, A., Lambert, F., Lamy, M., 2019. Intrasubject comparison of digital vs. conventional workflow for screw-retained single-implant crowns: Prosthodontic and patient-centered outcomes. Clin Oral Implants Res 30, 892–902. https://doi.org/10.1111/CLR.13494

DeLong, R., 2006. Intra-oral restorative materials wear: Rethinking the current approaches: How to measure wear. Dental Materials 22, 702–711. https://doi.org/10.1016/j.dental.2006.02.003

Derceli, J. dos R., Faraoni, J.J., Dias, P.C., Matos, L.L.M. de, Palma-Dibb, R.G., 2020. Effect of gaseous hydrochloric acid on human and bovine enamel. Clinical and Laboratorial Research in Dentistry 1–8. https://doi.org/10.11606/issn.2357-8041.clrd.2020.171222

DigitalMetrology, 2019. Areal Surface Texture Analysis [WWW Document]. URL https://digitalmetrology.com/tutorials/areal-surface-texture-analysis/ (accessed 6.15.22).

DigitalSurf, 2022a. Mountains8 Reference Manual.

DigitalSurf, 2022b. What's New in Mountains® 8? [WWW Document]. URL https://www.digitalsurf.com/news/whats-new-in-mountains-8/ (accessed 6.23.22).

DigitalSurf, 2022c. Software Verification - Surface Metrology Guide - Digital Surf [WWW Document]. URL https://guide.digitalsurf.com/en/guide-software-verification.html (accessed 6.23.22).

Eccles, J.D., 1979. Dental erosion of nonindustrial origin. A clinical survey and classification. J Prosthet Dent 42, 649–53. https://doi.org/10.1016/0022-3913(79)90196-3

Eisenburger, M., Addy, M., 2002. Erosion and attrition of human enamel in vitro Part II: Influence of time and loading. J Dent 30, 349–352. https://doi.org/10.1016/S0300-5712(02)00049-0

Eisenburger, M., Addy, M., Hughes, J.A., Shellis, R.P., 2001. Effect of Time on the Remineralisation of Enamel by Synthetic Saliva after Citric Acid Erosion. Caries Res 35, 211–215. https://doi.org/10.1159/000047458

Ender, A., Attin, T., Mehl, A., 2016a. In vivo precision of conventional and digital methods of obtaining complete-arch dental impressions. J Prosthet Dent 115, 313–20. https://doi.org/10.1016/j.prosdent.2015.09.011

Ender, A., Mehl, A., 2015. In-vitro evaluation of the accuracy of conventional and digital methods of obtaining full-arch dental impressions. Quintessence Int 46, 9–17. https://doi.org/10.3290/j.qi.a32244

Ender, A., Mehl, A., 2013. Accuracy of complete-Arch dental impressions: A new method of measuring trueness and precision. Journal of Prosthetic Dentistry 109, 121–128. https://doi.org/10.1016/S0022-3913(13)60028-1

Ender, A., Zimmermann, M., Attin, T., Mehl, A., 2016b. In vivo precision of conventional and digital methods for obtaining quadrant dental impressions. Clin Oral Investig 20, 1495–504. https://doi.org/10.1007/s00784-015-1641-y

Ender, A., Zimmermann, M., Attin, T., Mehl, A., 2016c. In vivo precision of conventional and digital methods for obtaining quadrant dental impressions. Clin Oral Investig 20, 1495–504. https://doi.org/10.1007/s00784-015-1641-y

Ender, A., Zimmermann, M., Mehl, A., 2019a. Accuracy of complete- and partial-arch impressions of actual intraoral scanning systems in vitro. Int J Comput Dent 22, 11–19.

Ender, A., Zimmermann, M., Mehl, A., 2019b. Accuracy of complete- and partial-arch impressions of actual intraoral scanning systems in vitro. Int J Comput Dent 22, 11–19.

Esquivel-Upshaw, J., Hsu, S.M., Bohórquez, A.C., Abdulhameed, N., Scheiffele, G.W., Kim, M., Neal, D., Chai, J., Ren, F., 2020. Novel methodology for measuring intraoral wear in enamel and dental restorative materials. Clin Exp Dent Res 677–685. https://doi.org/10.1002/cre2.322

Esquivel-Upshaw, J.F., Rose, W.F., Barrett, A.A., Oliveira, E.R., Yang, M.C.K., Clark, A.E., Anusavice, K.J., 2012. Three years in vivo wear: Core-ceramic, veneers, and enamel antagonists. Dental Materials 28, 615–621. https://doi.org/10.1016/J.DENTAL.2012.02.001

Field, J., Waterhouse, P., German, M., 2010. Quantifying and qualifying surface changes on dental hard tissues in vitro. J Dent 38, 182–190. https://doi.org/10.1016/j.jdent.2010.01.002

Flügge, T., Meer, W.J., Gonzalez, B.G., Vach, K., Wismeijer, D., Wang, P., 2018. The accuracy of different dental impression techniques for implant-supported dental prostheses: A systematic review and meta-analysis. Clin Oral Implants Res 29, 374–392. https://doi.org/10.1111/clr.13273

Flügge, T. V., Schlager, S., Nelson, K., Nahles, S., Metzger, M.C., 2013. Precision of intraoral digital dental impressions with iTero and extraoral digitization with the iTero and a model scanner. American Journal of Orthodontics and Dentofacial Orthopedics 144, 471–478. https://doi.org/10.1016/j.ajodo.2013.04.017

Gan, N., Xiong, Y., Jiao, T., 2016. Accuracy of Intraoral Digital Impressions for Whole Upper Jaws, Including Full Dentitions and Palatal Soft Tissues. PLoS One 11, 1–15. https://doi.org/10.1371/journal.pone.0158800

Gangapurwala, P., 2021. Methods of Stereophotogrammetry: A Review. SSRN Electronic Journal. https://doi.org/10.2139/ssrn.3866518

Ganss, C., Klimek, J., Giese, K., 2001. Dental erosion in children and adolescents – a cross-sectional and longitudinal investigation using study models that subjects with erosive lesions in their primary dentition had a signifi. Community Dent Oral Epidemiol 29, 264–71.

Ganss, C., Klimek, J., Schwarz, N., 2000. A comparative profilometric in vitro study of the susceptibility of polished and natural human enamel and dentine surfaces to erosive demineralization. Arch Oral Biol 45, 897–902. https://doi.org/10.1016/S0003-9969(00)00041-8

Ganss, C., Lussi, A., 2014. Diagnosis of Erosive Tooth Wear, in: Monographs in Oral Science. pp. 22–31. https://doi.org/10.1159/000359935

Ganss, C., Lussi, A., Schlueter, N., 2014. The histological features and physical properties of eroded dental hard tissues. Monogr Oral Sci. https://doi.org/10.1159/000359939

Gao, W., Haitjema, H., Fang, F.Z., Leach, R.K., Cheung, C.F., Savio, E., Linares, J.M., 2019. On-machine and in-process surface metrology for precision manufacturing. CIRP Annals 68, 843–866. https://doi.org/10.1016/J.CIRP.2019.05.005

García, V.D.-F., Freire, Y., Fernández, S.D., Murillo, B.T., Sánchez, M.G., 2022a. Application of the Intraoral Scanner in the Diagnosis of Dental Wear: An In Vivo Study of Tooth Wear Analysis. Int J Environ Res Public Health 19, 4481. https://doi.org/10.3390/ijerph19084481

García, V.D.F., Freire, Y., Fernández, S.D., Murillo, B.T., Sánchez, M.G., 2022. Application of the Intraoral Scanner in the Diagnosis of Dental Wear: An In Vivo Study of Tooth Wear Analysis. International Journal of Environmental Research and Public Health 2022, Vol. 19, Page 4481 19, 4481. https://doi.org/10.3390/IJERPH19084481

García, V.D.-F., Freire, Y., Fernández, S.D., Murillo, B.T., Sánchez, M.G., 2022b. Application of the Intraoral Scanner in the Diagnosis of Dental Wear: An In Vivo Study of Tooth Wear Analysis. Int J Environ Res Public Health 19, 4481. https://doi.org/10.3390/ijerph19084481

Ghazal, M., Kern, M., 2009. The influence of antagonistic surface roughness on the wear of human enamel and nanofilled composite resin artificial teeth. J Prosthet Dent 101, 342–349. https://doi.org/10.1016/S0022-3913(09)60068-8

Gjelvold, B., Ramos Chrcanovic, B., Korduner, E.-K., Collin-Bagewitz, I., Kisch, J., BjörnBj, C., SkåneSk, F., 2016. Intraoral Digital Impression Technique Compared to Conventional Impression Technique. A Randomized Clinical Trial. Journal of Prosthodontics 25, 282–287. https://doi.org/10.1111/jopr.12410

Gkantidis, N., Dritsas, K., Ren, Y., Halazonetis, D., Katsaros, C., 2020. An accurate and efficient method for occlusal tooth wear assessment using 3D digital dental models. Sci Rep 10, 10103. https://doi.org/10.1038/s41598-020-66534-4

Gómez-Polo, M., Piedra-Cascón, W., Methani, M.M., Quesada-Olmo, N., Farjas-Abadia, M., Revilla-León, M., 2021. Influence of rescanning mesh holes and stitching procedures on the complete-arch scanning accuracy of an intraoral scanner: An in vitro study. J Dent 110, 103690. https://doi.org/10.1016/j.jdent.2021.103690

Goracci, C., Franchi, L., Vichi, A., Ferrari, M., 2016. Accuracy, reliability, and efficiency of intraoral scanners for full-arch impressions: a systematic review of the clinical evidence. The European Journal of Orthodontics 38, 422–428. https://doi.org/10.1093/ejo/cjv077

Gracia, L.H., Rees, G.D., Brown, A., Fowler, C.E., 2010. An in vitro evaluation of a novel high fluoride daily mouthrinse using a combination of microindentation, 3D profilometry and DSIMS. J Dent 38, S12–S20. https://doi.org/10.1016/S0300-5712(11)70004-5

Grünheid, T., McCarthy, S.D., Larson, B.E., 2014. Clinical use of a direct chairside oral scanner: An assessment of accuracy, time, and patient acceptance. American Journal of Orthodontics and Dentofacial Orthopedics 146, 673–682. https://doi.org/10.1016/j.ajodo.2014.07.023

Güth, J.-F., Edelhoff, D., Schweiger, J., Keul, C., 2016. A new method for the evaluation of the accuracy of full-arch digital impressions in vitro. Clin Oral Investig 20, 1487–1494. https://doi.org/10.1007/s00784-015-1626-x

Güth, J.F., Keul, C., Stimmelmayr, M., Beuer, F., Edelhoff, D., 2013. Accuracy of digital models obtained by direct and indirect data capturing. Clin Oral Investig 17, 1201–1208. https://doi.org/10.1007/s00784-012-0795-0

Güth, J.-F., Runkel, C., Beuer, F., Stimmelmayr, M., Edelhoff, D., Keul, C., 2017a. Accuracy of five intraoral scanners compared to indirect digitalization. Clin Oral Investig 21, 1445–1455. https://doi.org/10.1007/s00784-016-1902-4

Güth, J.-F., Runkel, C., Beuer, F., Stimmelmayr, M., Edelhoff, D., Keul, C., 2017b. Accuracy of five intraoral scanners compared to indirect digitalization. Clin Oral Investig 21, 1445–1455. https://doi.org/10.1007/s00784-016-1902-4

Güth, J.-F.F., Keul, C., Stimmelmayr, M., Beuer, F., Edelhoff, D., 2013. Accuracy of digital models obtained by direct and indirect data capturing. Clin Oral Investig 17, 1201–1208. https://doi.org/10.1007/s00784-012-0795-0

Hack, G.D., Patzelt, S.B.M., 2015. Evaluation of the Accuracy of Six Intraoral Scanning Devices: An in-vitro Investigation. ADA Professional Product Review 10, 1–5.

Haddadi, Y., Ranjkesh, B., Isidor, F., Bahrami, G., 2021. Marginal and internal fit of crowns based on additive or subtractive manufacturing. Biomater Investig Dent 8, 87–91. https://doi.org/10.1080/26415275.2021.1938576

Hara, A.T., Livengood, S. V., Lippert, F., Eckert, G.J., Ungar, P.S., 2016. Dental Surface Texture Characterization Based on Erosive Tooth Wear Processes. J Dent Res 95, 537–542. https://doi.org/10.1177/0022034516629941

Hartkamp, O., Lohbauer, U., Reich, S., 2017a. Antagonist wear by polished zirconia crowns. Int J Comput Dent 20, 263–274.

Hartkamp, O., Peters, F., Bothung, H., Lohbauer, U., Reich, S., 2017b. Optical profilometry versus intraoral (handheld) scanning. Int J Comput Dent 20, 165–176.

Heber, S., 2010. 3D Image Reconstruction Using Active Wavefront Sampling. Graz University of Technology. Graz University of Technology.

Hemmings, K., Truman, A., Shah, S., Chauhan, R., 2018. Tooth wear guidelines for the bsrd part 1: aetiology, diagnosis and prevention. Dent Update 45, 483–495. https://doi.org/10.12968/denu.2018.45.6.483

Heshmati, R.H., Nagy, W.W., Wirth, C.G., Dhuru, V.B., 2002. Delayed linear expansion of improved dental stone. Journal of Prosthetic Dentistry 88, 26–31. https://doi.org/10.1016/S0022-3913(02)00044-6

Hjortsjö, C., Mjølnerød, A., Skaare, A., Jonski, G., Young, A., Ekfeldt, A., 2012. A replica technique for studying the effect of fluoride solutions on enamel erosion. Swed Dent J 36, 169–78.

Holme, B., Hove, L.H., Tveit, A.B., 2005. Using white light interferometry to measure etching of dental enamel. Measurement (Lond) 38, 137–147. https://doi.org/10.1016/j.measurement.2005.04.003

Hughes, J.A., West, N.X., Parker, D.M., Van Den Braak, M.H., Addy, M., 2000. Effects of pH and concentration of citric, malic and lactic acids on enamel, in vitro. J Dent 28, 147–152. https://doi.org/10.1016/S0300-5712(99)00060-3

Imburgia, M., Logozzo, S., Hauschild, U., Veronesi, G., Mangano, C., Mangano, F.G., 2017. Accuracy of four intraoral scanners in oral implantology: A comparative in vitro study. BMC Oral Health 17, 1–13. https://doi.org/10.1186/s12903-017-0383-4

Ionta, F.Q., dos Santos, N.M., Mesquita, I.M., Dionísio, E.J., Cruvinel, T., Honório, H.M., Rios, D., 2019. Is the dentifrice containing calcium silicate, sodium phosphate, and fluoride able to

protect enamel against chemical mechanical wear? An in situ/ex vivo study. Clin Oral Investig 23, 3713–3720. https://doi.org/10.1007/s00784-018-2792-4

ISO, 1994. Accuracy (trueness and precision) of measurement methods and results. Part 1. General principles and definitions.

ISO 17450-1, 2011. Geometrical product specifications (GPS) — General concepts — Part 1: Model for geometrical specification and verification.

JCGM, 2012. International vocabulary of metrology - Basic and general concepts and associated terms (VIM).

Jeong, I.-D., Lee, J.-J., Jeon, J.-H., Kim, J.-H., Kim, H.-Y., Kim, W.-C., 2016. Accuracy of complete-arch model using an intraoral video scanner: An in vitro study. J Prosthet Dent 115, 755–759. https://doi.org/10.1016/j.prosdent.2015.11.007

Jivanescu, A., Faur, A., Rotar, R.N., 2021. Can Dental Office Lighting Intensity Conditions Influence the Accuracy of Intraoral Scanning ? Scanning 2021, 1–10.

Johansson, A.K., Johansson, A., Birkhed, D., Omar, R., Baghdadi, S., Carlsson, G.E., 1996. Dental erosion, soft-drink intake, and oral health in young Saudi men, and the development of a system for assessing erosive anterior tooth wear. Acta Odontol Scand 54, 369–378. https://doi.org/10.3109/00016359609003554

Joshi, M., Joshi, N., Kathariya, R., Angadi, P., Raikar, S., 2016. Techniques to Evaluate Dental Erosion: A Systematic Review of Literature. Journal of Clinical and Diagnostic Research 10, 1–7. https://doi.org/10.7860/jcdr/2016/17996.8634

JYFEL, 2022. Nano Point Scanner NPS - Jyfel Corporation [WWW Document]. URL https://www.jyfel.com/en/produits/nps/ (accessed 6.9.22).

Kaidonis, J.A., 2008. Tooth wear: the view of the anthropologist. Clin Oral Investig 12, 21–26. https://doi.org/10.1007/s00784-007-0154-8

Keul, C., Güth, J.-F., 2020. Accuracy of full-arch digital impressions: an in vitro and in vivo comparison. Clin Oral Investig 24, 735–745. https://doi.org/10.1007/s00784-019-02965-2

Keul, C., Stawarczyk, B., Erdelt, K.-J., Beuer, F., Edelhoff, D., Güth, J.-F., 2014. Fit of 4-unit FDPs made of zirconia and CoCr-alloy after chairside and labside digitalization – A laboratory study. Dental Materials 30, 400–407. https://doi.org/10.1016/j.dental.2014.01.006

Kim, J., Park, J.-M., Kim, Minji, Heo, S.-J., Shin, I.H., Kim, Miae, 2016. Comparison of experience curves between two 3-dimensional intraoral scanners. J Prosthet Dent 116, 221–30. https://doi.org/10.1016/j.prosdent.2015.12.018

Kim, K.-M., Lee, J.-S., Kim, K.-N., Shin, S.-W., 2001. Dimensional changes of dental impression materials by thermal changes. J Biomed Mater Res 58, 217–220. https://doi.org/10.1002/1097-4636(2001)58:3<217::AID-JBM1010>3.0.CO;2-V

Kim, M., Kim, J., Lee, Y., Lim, Y., Lee, S., 2019. The effect of scanning distance on the accuracy of intra-oral scanners used in dentistry. Clinical Anatomy 32, ca.23334. https://doi.org/10.1002/ca.23334

Kim, R.J.Y., Benic, G.I., Park, J.-M., 2021. Trueness of ten intraoral scanners in determining the positions of simulated implant scan bodies. Sci Rep 11, 2606. https://doi.org/10.1038/s41598-021-82218-z

Kontis, P., Güth, J.-F., Keul, C., 2022. Accuracy of full-arch digitalization for partially edentulous jaws — a laboratory study on basis of coordinate-based data analysis. Clin Oral Investig 26, 3651–3662. https://doi.org/10.1007/s00784-021-04335-3

Koseoglu, M., Kahramanoglu, E., Akin, H., 2021. Evaluating the Effect of Ambient and Scanning Lights on the Trueness of the Intraoral Scanner. Journal of Prosthodontics. https://doi.org/10.1111/jopr.13341

Kühne, C., Lohbauer, U., Raith, S., Reich, S., 2021. Measurement of Tooth Wear by Means of Digital Impressions: An In-Vitro Evaluation of Three Intraoral Scanning Systems. Applied Sciences 11, 5161. https://doi.org/10.3390/app11115161

Kuhr, F., Schmidt, A., Rehmann, P., Wöstmann, B., 2016. A new method for assessing the accuracy of full arch impressions in patients. J Dent 55, 68–74. https://doi.org/10.1016/j.jdent.2016.10.002

Kumar, S., Keeling, A., Osnes, C., Bartlett, D., O'Toole, S., 2019. The sensitivity of digital intraoral scanners at measuring early erosive wear. J Dent 81, 39–42. https://doi.org/10.1016/j.jdent.2018.12.005

Kumar, S., Keeling, A., Osnes, C., Bartlett, D., O'Toole, S., 2018. The sensitivity of digital intraoral scanners at measuring early erosive wear. J Dent 81, 39–42. https://doi.org/10.1016/j.jdent.2018.12.005

Kuralt, M., Fidler, A., 2021. Assessment of reference areas for superimposition of serial 3D models of patients with advanced periodontitis for volumetric soft tissue evaluation. J Clin Periodontol 48, 765–773. https://doi.org/10.1111/jcpe.13445

Kwek, S., Mian, M., Hall, C., Xie, Z., Yong, R., Kaidonis, J., Townsend, G., Ranjitkar, S., 2015. Nanoscratch testing for the assessment of enamel demineralization under conditions simulating wine erosion. Aust Dent J 60, 12–17. https://doi.org/10.1111/adj.12277

Lambrechts, P., Braem, M., Vuylsteke-Wauters, M., Vanherle, G., 1989. Quantitative in vivo Wear of Human Enamel. J Dent Res 68, 1752–1754. https://doi.org/10.1177/00220345890680120601

Latham, J., Ludlow, M., Mennito, A., Kelly, A., Evans, Z., Renne, W., 2020. Effect of scan pattern on complete-arch scans with 4 digital scanners. J Prosthet Dent 123, 85–95. https://doi.org/10.1016/j.prosdent.2019.02.008

Leach, R., 2014. Fundamental principles of engineering nanometrology, Fundamental Principles of Engineering Nanometrology. Elsevier. https://doi.org/10.1016/B978-1-4557-7753-2.00011-6

Leach, R., 2013. Characterisation of areal surface texture, Characterisation of Areal Surface Texture. Springer Berlin Heidelberg, Berlin, Heidelberg. https://doi.org/10.1007/978-3-642-36458-7

Leach, R., 2011. Optical Measurement of Surface Topography. Springer Berlin Heidelberg, Berlin, Heidelberg. https://doi.org/10.1007/978-3-642-12012-1

Leach, R., Chetwynd, D., Blunt, L., Haycocks, J., Harris, P., Jackson, K., Oldfield, S., Reilly, S., 2006. Recent advances in traceable nanoscale dimension and force metrology in the UK. Meas Sci Technol 17, 467–476. https://doi.org/10.1088/0957-0233/17/3/S02

Leach, R., de Groot, P., Haitjema, H., 2018. Challenges of high slopes and complex features in the metrology of structured and freeform surfaces. Euspen.

Leach, R., Leigh Brown, X.J., Blunt, R., Mike Conroy, D.M., 2008. A National Measurement Good Practice Guide. Guide for the Measurement of Smooth Surface Topography using Coherence Scanning Interferometry. National Physical Laboratory.

Leach, R., Weckenmann, A., Coupland, J., Hartmann, W., 2014. Interpreting the probe-surface interaction of surface measuring instruments, or what is a surface? Surf Topogr 2. https://doi.org/10.1088/2051-672X/2/3/035001

Leach, R.K., 2015. Is one step height enough? Proceedings - ASPE 2015 Annual Meeting.

Leach, R.K., 2001. The measurement of surface texture using stylus instruments. Measurement Good Practice Guide No. 37 100.

Lee, J.J., Jeong, I. Do, Park, J.Y., Jeon, J.H., Kim, J.H., Kim, W.C., 2017. Accuracy of single-abutment digital cast obtained using intraoral and cast scanners. Journal of Prosthetic Dentistry 117, 253–259. https://doi.org/10.1016/j.prosdent.2016.07.021

Li, H., Lyu, P., Wang, Y., Sun, Y., 2017. Influence of object translucency on the scanning accuracy of a powder-free intraoral scanner: A laboratory study. J Prosthet Dent 117, 93–101. https://doi.org/10.1016/j.prosdent.2016.04.008

Lim, J.H., Park, J.M., Kim, M., Heo, S.J., Myung, J.Y., 2018. Comparison of digital intraoral scanner reproducibility and image trueness considering repetitive experience. Journal of Prosthetic Dentistry 119, 225–232. https://doi.org/10.1016/J.PROSDENT.2017.05.002

Logozzo, S., Zanetti, E.M., Franceschini, G., Kilpelä, A., Mäkynen, A., 2014. Recent advances in dental optics – Part I: 3D intraoral scanners for restorative dentistry. Opt Lasers Eng 54, 203–221. https://doi.org/10.1016/j.optlaseng.2013.07.017

Lopez-Frias, FJ., Castellanos-Cosano, L., Martin-Gonzalez, J., Llamas-Carreras, JM., Segura-Egea, JJ., 2012. Clinical measurement of tooth wear: Tooth Wear Indices. J Clin Exp Dent e48–e53. https://doi.org/10.4317/jced.50592

Lu, E., Zhang, R., Liu, J., Yin, S., Ohmori, H., 2022. Observation of ground surface roughness values obtained by stylus profilometer and white light interferometer for common metal materials. Surface and Interface Analysis 54, 587–599. https://doi.org/10.1002/SIA.7068

Lussi, A., Ganss, C., 2014. Erosive Tooth Wear: From Diagnosis to Therapy, 2nd ed. Karger.

Lussi, A., Schlueter, N., Rakhmatullina, E., Ganss, C., 2011. Dental erosion - An overview with emphasis on chemical and histopathological aspects. Caries Res 45, 2–12. https://doi.org/10.1159/000325915

Maia, A.M.A., Longbottom, C., Gomes, A.S.L., Girkin, J.M., 2014. Enamel erosion and prevention efficacy characterized by confocal laser scanning microscope. Microsc Res Tech 77, 439–445. https://doi.org/10.1002/jemt.22364

Mandelli, F., Gherlone, E., Keeling, A., Gastaldi, G., Ferrari, M., 2018. Full-arch intraoral scanning: Comparison of two different strategies and their accuracy outcomes. Journal of Osseointegration 10, 65–74. https://doi.org/10.23805/JO.2018.10.03.01

Mangano, A., Beretta, M., Luongo, G., Mangano, C., Mangano, F., 2018. Conventional Vs Digital Impressions: Acceptability, Treatment Comfort and Stress Among Young Orthodontic Patients. Open Dent J 12, 118–124. https://doi.org/10.2174/1874210601812010118

Mangano, F., Gandolfi, A., Luongo, G., Logozzo, S., 2017. Intraoral scanners in dentistry: a review of the current literature. BMC Oral Health 17, 149. https://doi.org/10.1186/s12903-017-0442-x

Mann, C., Ranjitkar, S., Lekkas, D., Hall, C., Kaidonis, J.A., Townsend, G.C., Brook, A.H., 2014. Three-dimensional profilometric assessment of early enamel erosion simulating gastric regurgitation. J Dent 42, 1411–1421. https://doi.org/10.1016/j.jdent.2014.06.011

Mansouri, A., 2014. Dental wear surface using 3D profilometry.

Marani, R., Renò, V., Nitti, M., D'Orazio, T., Stella, E., 2016. A Modified Iterative Closest Point Algorithm for 3D Point Cloud Registration. Computer-Aided Civil and Infrastructure Engineering 31, 515–534. https://doi.org/10.1111/mice.12184

Marro, F., De Lat, L., Martens, L., Jacquet, W., Bottenberg, P., 2018a. Monitoring the progression of erosive tooth wear (ETW) using BEWE index in casts and their 3D images: A retrospective longitudinal study. J Dent 73, 70–75. https://doi.org/10.1016/j.jdent.2018.04.008

Marro, F., De Lat, L., Martens, L., Jacquet, W., Bottenberg, P., 2018b. Monitoring the progression of erosive tooth wear (ETW) using BEWE index in casts and their 3D images: A retrospective longitudinal study. J Dent 73, 70–75. https://doi.org/10.1016/j.jdent.2018.04.008

Marro, F., Jacquet, W., Martens, L., Keeling, A., Bartlett, D., O'Toole, S., 2020. Quantifying increased rates of erosive tooth wear progression in the early permanent dentition. J Dent 93, 103282. https://doi.org/10.1016/j.jdent.2020.103282

Marro, F., O'Toole, S., Bernabé, E., Bartlett, D., Aránguiz, V., 2022. Associated risk factors with quantitative erosive tooth wear progression. J Dent 123, 104179. https://doi.org/10.1016/j.jdent.2022.104179

Medina-Sotomayor, P., Pascual-Moscardo, A., Camps A, I., 2019a. Accuracy of 4 digital scanning systems on prepared teeth digitally isolated from a complete dental arch. Journal of Prosthetic Dentistry 121, 811–820. https://doi.org/10.1016/j.prosdent.2018.08.020

Medina-Sotomayor, P., Pascual-Moscardo, A., Camps A, I., 2019b. Accuracy of 4 digital scanning systems on prepared teeth digitally isolated from a complete dental arch. J Prosthet Dent 121, 811–820. https://doi.org/10.1016/j.prosdent.2018.08.020

Medina-Sotomayor, P., Pascual-Moscardo, A., Camps, I., 2018. Relationship between resolution and accuracy of four intraoral scanners in complete-arch impressions. J Clin Exp Dent 10, 0–0. https://doi.org/10.4317/jced.54670

Mehta, S.B., Banerji, S., Millar, B.J., Suarez-Feito, J.-M., 2012. Current concepts on the management of tooth wear: part 1. Assessment, treatment planning and strategies for the prevention and the passive management of tooth wear. Br Dent J 212, 17–27. https://doi.org/10.1038/sj.bdj.2011.1099

Meireles, A.B., Bastos, F.D.S., Cornacchia, T.P., Ferreira, J.A., Las Casas, E.B. De, 2015. Enamel wear characterization based on a skewness and kurtosis surface roughness evaluation. Biotribology 1–2, 35–41. https://doi.org/10.1016/j.biotri.2015.04.001

Meireles, A.B., Vieira, A.W., Corpas, L., Vandenberghe, B., Bastos, F.S., Lambrechts, P., Campos, M.M., Las Casas, E.B. de, 2016a. Dental wear estimation using a digital intra-oral optical scanner and an automated 3D computer vision method. Comput Methods Biomech Biomed Engin 19, 507–514. https://doi.org/10.1080/10255842.2015.1043627

Meireles, A.B., Vieira, A.W., Corpas, L., Vandenberghe, B., Bastos, F.S., Lambrechts, P., Campos, M.M., Las Casas, E.B. de, 2016b. Dental wear estimation using a digital intra-oral optical scanner and an automated 3D computer vision method. Comput Methods Biomech Biomed Engin 19, 507–514. https://doi.org/10.1080/10255842.2015.1043627

Michou, S., Vannahme, C., Ekstrand, K.R., Benetti, A.R., 2020. Detecting early erosive tooth wear using an intraoral scanner system. J Dent 100, 103445. https://doi.org/10.1016/j.jdent.2020.103445

Minetola, P., 2012. The importance of a correct alignment in contactless inspection of additive manufactured parts. International Journal of Precision Engineering and Manufacturing 13, 211–218. https://doi.org/10.1007/s12541-012-0026-2

Mistry, M., 2016. In Vitro Investigation of Tooth Erosion.

Mistry, M., Zhu, S., Moazzez, R., Donaldson, N., Bartlett, D.W., 2015. Effect of model variables on in vitro erosion. Caries Res 49, 508–514. https://doi.org/10.1159/000438725

Mitrirattanakul, S., Neoh, S.P., Chalarmchaichaloenkit, J., Limthanabodi, C., Trerayapiwat, C., Pipatpajong, N., Taechushong, N., Chintavalakorn, R., 2022a. Accuracy of the Intraoral Scanner for Detection of Tooth Wear. Int Dent J. https://doi.org/10.1016/j.identj.2022.06.004

Mitrirattanakul, S., Neoh, S.P., Chalarmchaichaloenkit, J., Limthanabodi, C., Trerayapiwat, C., Pipatpajong, N., Taechushong, N., Chintavalakorn, R., 2022b. Accuracy of the Intraoral Scanner for Detection of Tooth Wear. Int Dent J 0, 1–7. https://doi.org/10.1016/j.identj.2022.06.004

Moretti, M., Gambucci, G., Leach, R.K., Senin, N., 2019. Assessment of surface topography modifications through feature-based registration of areal topography data. Surf Topogr 7. https://doi.org/10.1088/2051-672X/ab152a

Mullan, F, Austin, R.S., Parkinson, C.R., Bartlett, D.W., 2018. An in-situ pilot study to investigate the native clinical resistance of enamel to erosion. J Dent 70, 124–128. https://doi.org/10.1016/j.jdent.2018.01.005

Mullan, Francesca, Austin, R.S., Parkinson, C.R., Hasan, A., Bartlett, D.W., 2017. Measurement of surface roughness changes of unpolished and polished enamel following erosion. PLoS One 12, e0182406. https://doi.org/10.1371/journal.pone.0182406

Mullan, F., Bartlett, D., Austin, R.S., 2017. Measurement uncertainty associated with chromatic confocal profilometry for 3D surface texture characterization of natural human enamel. Dental Materials 33, e273–e281. https://doi.org/10.1016/j.dental.2017.04.004

Mullan, F., Mylonas, P., Parkinson, C., Bartlett, D., Austin, R.S., 2018. Precision of 655 nm Confocal Laser Profilometry for 3D surface texture characterisation of natural human enamel

undergoing dietary acid mediated erosive wear. Dental Materials 34, 531–537. https://doi.org/10.1016/j.dental.2017.12.012

Müller, P., Ender, A., Joda, T., Katsoulis, J., 2016. Impact of digital intraoral scan strategies on the impression accuracy using the TRIOS Pod scanner. Quintessence Int 47, 343–9. https://doi.org/10.3290/j.qi.a35524

Mutahar, M., Carpenter, G., Bartlett, D., German, M., Moazzez, R., 2017. The presence of acquired enamel pellicle changes acid-induced erosion from dissolution to a softening process. Sci Rep 7, 10920. https://doi.org/10.1038/s41598-017-11498-1

Mylonas, P., 2017. Determining the effect of minimal acid exposure on human enamel samples.

Mylonas, P., Austin, R.S., Moazzez, R., Joiner, A., Bartlett, D.W., 2018. In vitro evaluation of the early erosive lesion in polished and natural human enamel. Dental Materials 34, 1391–1400. https://doi.org/10.1016/j.dental.2018.06.018

Mylonas, P., Bull, T., Moazzez, R., Joiner, A., Bartlett, D., 2019. Detection threshold of non-contacting laser profilometry and influence of thermal variation on characterisation of early surface form and textural changes in natural human enamel. Dental Materials 35, e140–e152. https://doi.org/10.1016/j.dental.2019.04.003

NanoFocus, 2022. NanoFocus: µscan technology – Optical profilometry [WWW Document]. URL https://www.nanofocus.com/technology/measurement-principles/uscan-technology/ (accessed 6.9.22).

Nedelcu, R., Olsson, P., Nyström, I., Thor, A., 2018. Finish line distinctness and accuracy in 7 intraoral scanners versus conventional impression: An in vitro descriptive comparison. BMC Oral Health 18, 1–11. https://doi.org/10.1186/s12903-018-0489-3

Nedelcu, R.G., Persson, A.S.K., 2014a. Scanning accuracy and precision in 4 intraoral scanners: An in vitro comparison based on 3-dimensional analysis. J Prosthet Dent 112, 1461–1471. https://doi.org/10.1016/j.prosdent.2014.05.027

Nedelcu, R.G., Persson, A.S.K., 2014b. Scanning accuracy and precision in 4 intraoral scanners: An in vitro comparison based on 3-dimensional analysis. J Prosthet Dent 112, 1461–1471. https://doi.org/10.1016/j.prosdent.2014.05.027

Nouira, H., Salgado, J.A., El-Hayek, N., Ducourtieux, S., Delvallée, A., Anwer, N., 2014. Setup of a high-precision profilometer and comparison of tactile and optical measurements of standards. Meas Sci Technol 25. https://doi.org/10.1088/0957-0233/25/4/044016

Ochsmann, E., Brand, P., Kraus, T., Reich, S., 2020. Ultrafine particles in scanning sprays: a standardized examination of five powders used for dental reconstruction. J Occup Med Toxicol 15, 20. https://doi.org/10.1186/s12995-020-00271-2

O'Toole, S., Bartlett, D.W., Moazzez, R., 2016. Efficacy of sodium and stannous fluoride mouthrinses when used before single and multiple erosive challenges. Aust Dent J 61, 497–501. https://doi.org/10.1111/adj.12418

O'Toole, S., Lau, J.S., Rees, M., Warburton, F., Loomans, B., Bartlett, D., 2020. Quantitative tooth wear analysis of index teeth compared to complete dentition. J Dent 97. https://doi.org/10.1016/j.jdent.2020.103342

O'Toole, S., Mistry, M., Mutahar, M., Moazzez, R., Bartlett, D., 2015. Sequence of stannous and sodium fluoride solutions to prevent enamel erosion. J Dent 43, 1498–503. https://doi.org/10.1016/j.jdent.2015.10.003

O'Toole, S., Mullan, F., 2018. The role of the diet in tooth wear. Br Dent J 224, 379–383. https://doi.org/10.1038/sj.bdj.2018.127

O'Toole, S., Newton, T., Moazzez, R., Hasan, A., Bartlett, D., 2018. Randomised Controlled Clinical Trial Investigating the Impact of Implementation Planning on Behaviour Related to the Diet. Sci Rep 8, 4–9. https://doi.org/10.1038/s41598-018-26418-0

O'Toole, S., Osnes, C., Bartlett, D., Keeling, A., 2019a. Investigation into the accuracy and measurement methods of sequential 3D dental scan alignment. Dental Materials 35, 495–500. https://doi.org/10.1016/j.dental.2019.01.012

O'Toole, S., Osnes, C., Bartlett, D., Keeling, A., 2019b. Investigation into the validity of WearCompare, a purpose-built software to quantify erosive tooth wear progression. Dental Materials 35, 1408–1414. https://doi.org/10.1016/j.dental.2019.07.023

O'Toole, Saoirse, Osnes, C., Bartlett, D., Keeling, A., 2018. Investigation into the accuracy and measurement methods of sequential 3D dental scan alignment. Dental Materials 35, 495–500. https://doi.org/10.1016/j.dental.2019.01.012

Oxford English Dictionary [WWW Document], 2022. URL https://www.oed.com/start?showLogin=false (accessed 6.13.22).

Özkan Karaca, E., Tunar, O.L., 2021. In Vitro Evaluation of Root Surface Roughness in The Use of an Ultrasonic Device with Different Tips Having Different Mechanism of Action: A Profilometric Study. Clinical and Experimental Health Sciences 12, 310–314. https://doi.org/10.33808/clinexphealthsci.1010944

Paepegaey, A.M., Barker, M.L., Bartlett, D.W., Mistry, M., West, N.X., Hellin, N., Brown, L.J., Bellamy, P.G., 2013. Measuring enamel erosion: A comparative study of contact profilometry, non-

contact profilometry and confocal laser scanning microscopy. Dental Materials 29, 1265–1272. https://doi.org/10.1016/j.dental.2013.09.015

Paricio, I., Sanz-Lobera, A., Lozano, F., 2015. Comparative Analysis of Software Measurement Standard According to ISO 5436-2. Procedia Eng 132, 864–871. https://doi.org/10.1016/j.proeng.2015.12.571

Park, G.-H., Son, K., Lee, K.-B., 2019. Feasibility of using an intraoral scanner for a complete-arch digital scan. J Prosthet Dent 121, 803–810. https://doi.org/10.1016/j.prosdent.2018.07.014

Park, G.-H.H., Son, K.B. da, Lee, K.-B.B., 2019. Feasibility of using an intraoral scanner for a complete-arch digital scan. Journal of Prosthetic Dentistry 121, 803–810. https://doi.org/10.1016/j.prosdent.2018.07.014

Patzelt, S.B.M.M., Emmanouilidi, A., Stampf, S., Strub, J.R., Att, W., 2014. Accuracy of full-arch scans using intraoral scanners. Clin Oral Investig 18, 1687–1694. https://doi.org/10.1007/s00784-013-1132-y

Persson, A.S.K., Andersson, M., Odén, A., Sandborgh-Englund, G., 2008. Computer aided analysis of digitized dental stone replicas by dental CAD/CAM technology. Dental Materials 24, 1123–1130. https://doi.org/10.1016/J.DENTAL.2008.01.008

Pintado, M.R., Anderson, G.C., DeLong, R., Douglas, W.H., 1997. Variation in tooth wear in young adults over a two-year period. Journal of Prosthetic Dentistry 77, 313–320. https://doi.org/10.1016/S0022-3913(97)70189-6

Planmeca, 2022. Checking Calibration on a Planmill 50s [WWW Document]. URL https://planmecawiki.com/_media/cadcamoffice/50s_calibration_block.pdf (accessed 10.7.22).

Poggio, C., Lombardini, M., Dagna, A., Chiesa, M., Bianchi, S., 2009. Protective effect on enamel demineralization of a CPP-ACP paste: an AFM in vitro study. J Dent 37, 949–954. https://doi.org/10.1016/j.jdent.2009.07.011

Pottmann, H., Huang, Q.-X., Yang, Y.-L., Hu, S.-M., 2006. Geometry and Convergence Analysis of Algorithms for Registration of 3D Shapes. Int J Comput Vis 67, 277–296. https://doi.org/10.1007/s11263-006-5167-2

Prudente, M.S., Davi, L.R., Nabbout, K.O., Prado, C.J., Pereira, L.M., Zancopé, K., Neves, F.D., 2018. Influence of scanner, powder application, and adjustments on CAD-CAM crown misfit. J Prosthet Dent 119, 377–383. https://doi.org/10.1016/j.prosdent.2017.03.024

Rajshekar, M., Williams, A.-M., Blizzard, L., Walsh, L.J., Wilson, G., Julian, R., Tennant, M., Forrest, A., 2017. The reliability and validity of measurements of human dental casts made by an intra-oral 3D scanner, with conventional hand-held digital callipers as the comparison measure. Forensic Sci Int 278, 198–204. https://doi.org/10.1016/j.forsciint.2017.07.009

Rasaie, V., Abduo, J., Hashemi, S., 2021. Accuracy of Intraoral Scanners for Recording the Denture Bearing Areas: A Systematic Review. Journal of Prosthodontics 30, 520–539. https://doi.org/10.1111/jopr.13345

Raue, L., Gersdorff, N., Rödiger, M., Klein, H., 2012. New insights in prism orientation within human enamel. Arch Oral Biol 57, 271–276. https://doi.org/10.1016/j.archoralbio.2011.08.015

Ren, M.J., Cheung, C.F., Kong, L.B., Jiang, X., 2012. Invariant-feature-pattern-based form characterization for the measurement of ultraprecision freeform surfaces. IEEE Trans Instrum Meas 61, 963–973. https://doi.org/10.1109/TIM.2011.2173047

Renne, W., Ludlow, M., Fryml, J., Schurch, Z., Mennito, A., Kessler, R., Lauer, A., 2017. Evaluation of the accuracy of 7 digital scanners: An in vitro analysis based on 3-dimensional comparisons. Journal of Prosthetic Dentistry 118, 36–42. https://doi.org/10.1016/j.prosdent.2016.09.024

Richert, R., Goujat, A., Venet, L., Viguie, G., Viennot, S., Robinson, P., Farges, J.-C., Fages, M., Ducret, M., 2017. Intraoral Scanner Technologies: A Review to Make a Successful Impression. J Healthc Eng 2017, 1–9. https://doi.org/10.1155/2017/8427595

Rodriguez, J.M., Austin, R.S., Bartlett, D.W., 2012. A method to evaluate profilometric tooth wear measurements. Dental Materials 28, 245–251. https://doi.org/10.1016/j.dental.2011.10.002

Rodriguez, J M, Austin, R.S., Bartlett, D.W., 2012. In vivo measurements of tooth wear over 12 months. Caries Res 46, 9–15. https://doi.org/10.1159/000334786

Rodriguez, J.M., Bartlett, D.W., 2010. A comparison of two-dimensional and three-dimensional measurements of wear in a laboratory investigation. Dent Mater 26, e221-5. https://doi.org/10.1016/j.dental.2010.07.001

Rodriguez, J.M., Curtis, R. V, Bartlett, D.W., 2009. Surface roughness of impression materials and dental stones scanned by non-contacting laser profilometry. Dental Materials 25, 500–505. https://doi.org/10.1016/j.dental.2008.10.003

Ruben, J.L., Roeters, F.J.M., Truin, G.-J., Loomans, B.A.C., Huysmans, M.-C.D.N.J.M., 2019. Cup-Shaped Tooth Wear Defects: More than Erosive Challenges? Caries Res 53, 467–474. https://doi.org/10.1159/000496983

Rudolph, H., Salmen, H., Moldan, M., Kuhn, K., Sichwardt, V., Wöstmann, B., Luthardt, R.G., 2016. Accuracy of intraoral and extraoral digital data acquisition for dental restorations. Journal of Applied Oral Science 24, 85–94. https://doi.org/10.1590/1678-775720150266

Salas, M.M.S., Nascimento, G.G., Huysmans, M.C., Demarco, F.F., 2015. Estimated prevalence of erosive tooth wear in permanent teeth of children and adolescents: An epidemiological systematic review and meta-regression analysis. J Dent 43, 42–50. https://doi.org/10.1016/j.jdent.2014.10.012

Saleeva, L., Kashapov, R., Shakirzyanov, F., Kuznetsov, E., Kashapov, L., Smirnova, V., Kashapov, N., Saleeva, G., Sachenkov, O., Saleev, R., 2022. The Effect of Surface Processing on the Shear Strength of Cobalt-Chromium Dental Alloy and Ceramics. Materials 15, 2987. https://doi.org/10.3390/ma15092987

Sar Sancakli, H., Austin, R., Al-Saqabi, F., Moazzez, R., Bartlett, D., 2015. The influence of varnish and high fluoride on erosion and abrasion in a laboratory investigation. Aust Dent J 60, 38–42. https://doi.org/10.1111/adj.12271

Savio, E., de Chiffre, L., Schmitt, R., 2007. Metrology of freeform shaped parts. CIRP Ann Manuf Technol 56, 810–835. https://doi.org/10.1016/j.cirp.2007.10.008

Schlenz, M.A., Schlenz, M.B., Wöstmann, B., Jungert, A., Ganss, C., 2022. Intraoral scanner-based monitoring of tooth wear in young adults: 12-month results. Clin Oral Investig 26, 1869–1878. https://doi.org/10.1007/s00784-021-04162-6

Schlueter, N., Amaechi, B.T., Bartlett, D., Buzalaf, M.A.R., Carvalho, T.S., Ganss, C., Hara, A.T., Huysmans, M.C.D.N.J.M., Lussi, A., Moazzez, R., Vieira, A.R., West, N.X., Wiegand, A., Young, A., Lippert, F., 2020. Terminology of Erosive Tooth Wear: Consensus Report of a Workshop Organized by the ORCA and the Cariology Research Group of the IADR. Caries Res 54, 2–6. https://doi.org/10.1159/000503308

Schmidt, A., Billig, J.-W., Schlenz, A., Wöstmann, B., 2021. Do different methods of digital data analysis lead to different results? Int J Comput Dent 24, 157–164.

Schmidt, A., Klussmann, L., Wöstmann, B., Schlenz, M.A., 2020. Accuracy of Digital and Conventional Full-Arch Impressions in Patients: An Update. J Clin Med 9, 688. https://doi.org/10.3390/jcm9030688

Scott, P.J., Jiang, X., 2014. Freeform surface characterisation: theory and practice. J Phys Conf Ser 483, 012005. https://doi.org/10.1088/1742-6596/483/1/012005

Sehrawat, S., Kumar, Ajay, Grover, S., Dogra, N., Nindra, J., Rathee, S., Dahiya, M., Kumar, Ashwini, 2022. Study of 3D scanning technologies and scanners in orthodontics. Mater Today Proc. https://doi.org/10.1016/j.matpr.2022.01.064

Sfondrini, M.F., Gandini, P., Malfatto, M., Di Corato, F., Trovati, F., Scribante, A., 2018. Computerized Casts for Orthodontic Purpose Using Powder-Free Intraoral Scanners: Accuracy, Execution Time, and Patient Feedback. Biomed Res Int 2018, 1–8. https://doi.org/10.1155/2018/4103232

Shellis, R.P., Addy, M., 2014. The interactions between attrition, abrasion and erosion in tooth wear. Monogr Oral Sci. https://doi.org/10.1159/000359936

Shellis, R.P., Featherstone, J.D.B., Lussi, A., 2014. Understanding the Chemistry of Dental Erosion, in: Erosive Tooth Wear: From Diagnosis to Therapy. pp. 163–179. https://doi.org/10.1159/000359943

Sim, J.Y., Jang, Y., Kim, W.C., Kim, H.Y., Lee, D.H., Kim, J.H., 2019. Comparing the accuracy (trueness and precision) of models of fixed dental prostheses fabricated by digital and conventional workflows. J Prosthodont Res 63, 25–30. https://doi.org/10.1016/j.jpor.2018.02.002

Smith, B.G., Knight, J.K., 1984. An index for measuring the wear of teeth. Br Dent J. https://doi.org/10.1038/sj.bdj.4805394

Stenhagen, K.R.R., Hove, L.H.H., Holme, B., Taxt-Lamolle, S., Tveit, A.B.B., 2011. Comparing different methods to assess erosive lesion depths and progression in vitro. Caries Res 44, 555–561. https://doi.org/10.1159/000321536

Tapie, L., Lebon, N., Mawussi, B., Fron-Chabouis, H., Duret, F., Attal, J.-P., 2015. Understanding dental CAD/CAM for restorations--accuracy from a mechanical engineering viewpoint. Int J Comput Dent 18, 343–67.

Travassos da Rosa Moreira Bastos, R., Teixeira da Silva, P., Normando, D., 2021a. Reliability of qualitative occlusal tooth wear evaluation using an intraoral scanner: A pilot study. PLoS One 16, e0249119. https://doi.org/10.1371/journal.pone.0249119

Travassos da Rosa Moreira Bastos, R., Teixeira da Silva, P., Normando, D., 2021b. Reliability of qualitative occlusal tooth wear evaluation using an intraoral scanner: A pilot study. PLoS One 16, e0249119. https://doi.org/10.1371/journal.pone.0249119

Van't Spijker, A., Rodriguez, J.M., Kreulen, C.M., Bronkhorst, E.M., Bartlett, D.W., Creugers, N.H.J., 2009. Prevalence of tooth wear in adults. Int J Prosthodont 22, 35–42.

Vasilakos, G., Schilling, R., Halazonetis, D., Gkantidis, N., 2017. Assessment of different techniques for 3D superimposition of serial digital maxillary dental casts on palatal structures. Sci Rep 7, 5838. https://doi.org/10.1038/s41598-017-06013-5

Vieira, A., Jager, D.H.J., Ruben, J.L., Huysmans, M.C.D.N.J.M., 2007. Inhibition of Erosive Wear by Fluoride Varnish. Caries Res 41, 61–67. https://doi.org/10.1159/000096107

Voronets, J., Lussi, A., 2010. Thickness of softened human enamel removed by toothbrush abrasion: An in vitro study. Clin Oral Investig. https://doi.org/10.1007/s00784-009-0288-y

Wesemann, C., Muallah, J., Mah, J., Bumann, A., 2017. Accuracy and efficiency of full-arch digitalization and 3D printing: A comparison between desktop model scanners, an intraoral scanner, a CBCT model scan, and stereolithographic 3D printing. Quintessence Int (Berl) 48, 41–50. https://doi.org/10.3290/j.qi.a37130

West, N.X., Joiner, A., 2014. Enamel mineral loss. J Dent 42, S2–S11. https://doi.org/10.1016/S0300-5712(14)50002-4

West, N.X., Sanz, M., Lussi, A., Bartlett, D., Bouchard, P., Bourgeois, D., 2013. Prevalence of dentine hypersensitivity and study of associated factors: A European population-based cross-sectional study. J Dent 41, 841–851. https://doi.org/10.1016/j.jdent.2013.07.017

White, D.A., Tsakos, G., Pitts, N.B., Fuller, E., Douglas, G.V.A., Murray, J.J., Steele, J.G., 2012. Adult Dental Health Survey 2009: Common oral health conditions and their impact on the population. Br Dent J 213, 567–572. https://doi.org/10.1038/sj.bdj.2012.1088

Whittaker, D.K., 1982. Structural variations in the surface zone of human tooth enamel observed by scanning electron microscopy. Arch Oral Biol 27, 383–92. https://doi.org/10.1016/0003-9969(82)90147-9

Witecy, C., Ganss, C., Wöstmann, B., Schlenz, M.B., Schlenz, M.A., 2021. Monitoring of Erosive Tooth Wear with Intraoral Scanners In vitro. Caries Res 55, 215–224. https://doi.org/10.1159/000514666

Wong, K.Y., Esguerra, R.J., Chia, V.A.P., Tan, Y.H., Tan, K.B.C., 2018. Three-Dimensional Accuracy of Digital Static Interocclusal Registration by Three Intraoral Scanner Systems. Journal of Prosthodontics 27, 120–128. https://doi.org/10.1111/jopr.12714

Wulfman, C., Koenig, V., Mainjot, A.K., 2018. Wear measurement of dental tissues and materials in clinical studies: A systematic review. Dental Materials 34, 825–850. https://doi.org/10.1016/j.dental.2018.03.002

Wulfman, C., Naveau, A., Rignon-Bret, C., 2020. Digital scanning for complete-arch implant-supported restorations: A systematic review. J Prosthet Dent 124, 161–167. https://doi.org/10.1016/j.prosdent.2019.06.014

Yang, X., Lv, P., Liu, Y., Si, W., Feng, H., 2015. Accuracy of Digital Impressions and Fitness of Single Crowns Based on Digital Impressions. Materials 8, 3945–3957. https://doi.org/10.3390/ma8073945

Yip, K., Lam, P.P.Y., Yiu, C.K.Y., 2022. Prevalence and Associated Factors of Erosive Tooth Wear among Preschool Children—A Systematic Review and Meta-Analysis. Healthcare 10, 491. https://doi.org/10.3390/healthcare10030491

Young, A., Tenuta, L.M.A., 2011. Initial erosion models. Caries Res 45, 33–42. https://doi.org/10.1159/000325943

Yuan, T., Liao, W., Dai, N., Cheng, X., Yu, Q., 2010. Single-Tooth Modeling for 3D Dental Model. Int J Biomed Imaging 2010, 1–14. https://doi.org/10.1155/2010/535329

Zarone, F., Ruggiero, G., Ferrari, M., Mangano, F., Joda, T., Sorrentino, R., 2020. Comparison of different intraoral scanning techniques on the completely edentulous maxilla: An in vitro 3-

dimensional comparative analysis. J Prosthet Dent 124, 762.e1-762.e8. https://doi.org/10.1016/j.prosdent.2020.07.017

Zhang, Y., Tian, J., Wei, D., Di, P., Lin, Y., 2019. Quantitative clinical adjustment analysis of posterior single implant crown in a chairside digital workflow: A randomized controlled trial. Clin Oral Implants Res 30, 1059–1066. https://doi.org/10.1111/clr.13519

Zhang, Y.-J., Shi, J.-Y., Qian, S.-J., Qiao, S.-C., Lai, H.-C., 2021. Accuracy of full-arch digital implant impressions taken using intraoral scanners and related variables: A systematic review. Int J Oral Implantol (Berl) 14, 157–179.

Zheng, J., Xiao, F., Qian, L.M., Zhou, Z.R.Ã., 2009. Erosion behavior of human tooth enamel in citric acid solution. Tribiology International 42, 1558–1564. https://doi.org/10.1016/j.triboint.2008.12.008

Zheng, J., Xiao, F., Zheng, L., Qian, L.M., Zhou, Z.R., 2010. Erosion behaviors of human tooth enamel at different depth. Tribol Int 43, 1262–1267. https://doi.org/10.1016/j.triboint.2009.12.008

Zheng, Y., Bashandeh, K., Shakil, A., Jha, S., Polycarpou, A.A., 2022. Review of dental tribology: Current status and challenges. Tribol Int 166, 107354. https://doi.org/10.1016/j.triboint.2021.107354

Zimmermann, M., Mehl, A., Mörmann, W.H., Reich, S., 2015. Intraoral scanning systems - a current overview. Int J Comput Dent 18, 101–29.

Zou, L., Cherukara, G., Hao, P., Seymour, K., Samarawickrama, D., 2009. Geometrics of tooth wear. Wear 266, 605–608. https://doi.org/10.1016/j.wear.2008.04.062

Zygo, 2018. Mx Surface Texture Parameters 28.

Appendix

Search strategy of studies using intraoral scanners for measuring wear

Database: Embase <1974 to 2020 Week 28>

Search Strategy:

1 intra?oral scanner*.mp. (410)

2 digital impression*.mp. (408)

3 digital dental model.mp. (26)

4 three-dimensional digital model*.mp. (129)

5 three-dimensional virtual model*.mp. (66)

6 virtual model*.mp. (1197)

7 digital model*.mp. (1126)

8 digital study model*.mp. (30)

9 digital dental cast*.mp. (45)

10 virtual study model*.mp. (9)

11 virtual dental model*.mp. (19)

12 3-dimensional digital model*.mp. (24)

13 impression-free digital model*.mp. (1)

14 3D digital model*.mp. (191)

15 oral scanner*.mp. (71)

16 intra oral scanning.mp. (14)

17 intraoral digital scanner.mp. (21)

18 1 or 2 or 3 or 4 or 5 or 6 or 7 or 8 or 9 or 10 or 11 or 12 or 13 or 14 or 15 or 16 or 17 (2996)

19 exp accuracy/ or accuracy.mp. or exp diagnostic accuracy/ (851432)

20 measurement.mp. or exp measurement/ or exp measurement precision/ or exp noise measurement/ or exp measurement repeatability/ or exp measurement accuracy/ or exp measurement error/ (2282826)

21 precision.mp. or exp accuracy/ (296868)

22 exp measurement repeatability/ or repeatability.mp. (50550)

23 reproducibility.mp. or exp reproducibility/ (254048)

24 efficiency.mp. (514344)

25 exp reliability/ or reliability.mp. (279085)

26 exp "limit of detection"/ or exp "instrument detection limit"/ (84193)

27 clinical wear.mp. (145)

28 tooth wear.mp. or exp tooth disease/ (212419)

29 dental restoration wear.mp. or exp dental restoration wear/ (240)

30 dental wear.mp. (436)

31 dental wear measurement.mp. (0)

32 enamel wear.mp. (210)

33 exp enamel/ or enamel loss.mp. (21127)

34 in vivo wear.mp. (220)

35 vertical loss.mp. (62)

36 step height.mp. (321)

37 occlusal wear.mp. (323)

38 tooth erosion.mp. (471)

39 tooth attrition.mp. (83)

40 tooth abrasion.mp. (135)

41 19 or 20 or 21 or 22 or 23 or 24 or 25 or 26 or 27 or 28 or 29 or 30 or 31 or 32 or 33 or 34 or 35 or 36 or 37 or 38 or 39 or 40 (3860191)

42 18 and 41 (1423)

****

Material Safety Data Sheet of 3M™High-resolution scanning spray

Material Safety Data Sheet

SECTION 1: PRODUCT AND COMPANY IDENTIFICATION

PRODUCT NAME: 68913COS/68960COS 3M™ ESPE™ LAVA™ C.O.S. POWDER; 68913/68960 3M™ HIGH-RESOLUTION SCANNING SPRAY
MANUFACTURER: 3M
DIVISION: 3M ESPE Dental Products

ADDRESS: 3M Center, St. Paul, MN 55144-1000

EMERGENCY PHONE: 1-800-364-3577 or (651) 737-6501 (24 hours)

Issue Date: 07/12/13
Supercedes Date: 01/27/09

Document Group: 25-6114-0

Product Use:

Intended Use:	Dental Product
Limitations on Use:	For use only by dental professionals.
Specific Use:	Patterning material for use with intra-oral scanner

SECTION 2: INGREDIENTS

Ingredient	C.A.S. No.	% by Wt
TITANIUM DIOXIDE	13463-67-7	50 - 60
ZIRCONIUM OXIDE	1314-23-4	30 - 40
ZINC STEARATE	557-05-1	5 - 10

SECTION 3: HAZARDS IDENTIFICATION

3.1 EMERGENCY OVERVIEW

Specific Physical Form: Powder
Odor, Color, Grade: White, opaque, odorless powder.
General Physical Form: Solid
Immediate health, physical, and environmental hazards: This document has been prepared in accordance with the U.S. OSHA Hazard Communication Standard, which requires the inclusion of all known hazards of the product or ingredients regardless of the potential risk. The risks of the hazards communicated in this document may vary depending on the potential for exposure. No

immediate health, physical, or environmental hazards are expected.

3.2 POTENTIAL HEALTH EFFECTS

Eye Contact:
Mechanical eye irritation: Signs/symptoms may include pain, redness, tearing and corneal abrasion.

Skin Contact:
Mechanical Skin irritation: Signs/symptoms may include abrasion, redness, pain, and itching.

Inhalation:
Respiratory Tract Irritation: Signs/symptoms may include cough, sneezing, nasal discharge, headache, hoarseness, and nose and throat pain.

Prolonged or repeated exposure may cause:
Respiratory Effects: Signs/symptoms may include cough, shortness of breath, chest tightness, wheezing, increased heart rate, bluish colored skin (cyanosis), sputum production, changes in lung function tests, and/or respiratory failure.

Ingestion:
Gastrointestinal Irritation: Signs/symptoms may include abdominal pain, stomach upset, nausea, vomiting and diarrhea.

Carcinogenicity:
Exposures needed to cause the following health effect(s) are not expected during normal, intended use:
Contains a chemical or chemicals which can cause cancer.

Ingredient	C.A.S. No.	Class Description	Regulation
TITANIUM DIOXIDE	13463-67-7	Grp. 2B: Possible human carc.	International Agency for Research on Cancer

SECTION 4: FIRST AID MEASURES

4.1 FIRST AID PROCEDURES

The following first aid recommendations are based on an assumption that appropriate personal and industrial hygiene practices are followed.

Eye Contact: Flush eyes with large amounts of water. If signs/symptoms persist, get medical attention.
Skin Contact: Wash affected area with soap and water. If signs/symptoms develop, get medical attention.
Inhalation: Remove person to fresh air. If signs/symptoms develop, get medical attention.
If Swallowed: Do not induce vomiting unless instructed to do so by medical personnel. Give victim two glasses of water. Never give anything by mouth to an unconscious person. Get medical attention.

SECTION 5: FIRE FIGHTING MEASURES

5.1 FLAMMABLE PROPERTIES

Autoignition temperature	*No Data Available*
Flash Point	No flash point
Flammable Limits(LEL)	*Not Applicable*
Flammable Limits(UEL)	*Not Applicable*

5.2 EXTINGUISHING MEDIA
Ordinary combustible material. Use fire extinguishers with class A extinguishing agents (e.g., water, foam).

5.3 PROTECTION OF FIRE FIGHTERS

Special Fire Fighting Procedures: Wear full protective equipment (Bunker Gear) and a self-contained breathing apparatus (SCBA).

Unusual Fire and Explosion Hazards: No unusual fire or explosion hazards are anticipated.

Note: See STABILITY AND REACTIVITY (SECTION 10) for hazardous combustion and thermal decomposition information.

SECTION 6: ACCIDENTAL RELEASE MEASURES

6.1. Personal precautions, protective equipment and emergency procedures
Evacuate unprotected and untrained personnel from hazard area. The spill should be cleaned up by qualified personnel. Ventilate the area with fresh air.

6.2. Environmental precautions
Place in a closed container approved for transportation by appropriate authorities. Dispose of collected material as soon as possible.

Clean-up methods
Observe precautions from other sections. Call 3M- HELPS line (1-800-364-3577) for more information on handling and managing the spill. Contain spill. Collect as much of the spilled material as possible. Use wet sweeping compound or water to avoid dusting. Sweep up. Clean up residue.

In the event of a release of this material, the user should determine if the release qualifies as reportable according to local, state, and federal regulations.

SECTION 7: HANDLING AND STORAGE

7.1 HANDLING
Do not eat, drink or smoke when using this product. Wash exposed areas thoroughly with soap and water. Avoid eye contact with dust or airborne particles. Avoid breathing of airborne material. Avoid prolonged or repeated skin contact. Wash hands after handling and before eating.

7.2 STORAGE
Store away from heat. Store out of direct sunlight. Store in a cool, dry place.

SECTION 8: EXPOSURE CONTROLS/PERSONAL PROTECTION

8.1 ENGINEERING CONTROLS
Use with appropriate local exhaust ventilation. Use in a well-ventilated area.

8.2 PERSONAL PROTECTIVE EQUIPMENT (PPE)

8.2.1 Eye/Face Protection
Avoid eye contact.

The following eye protection(s) are recommended: Safety Glasses with side shields

.

8.2.2 Skin Protection
Avoid skin contact. Avoid prolonged or repeated skin contact. Gloves not normally required.

8.2.3 Respiratory Protection
Do not breathe dust.

8.2.4 Prevention of Swallowing
Do not eat, drink or smoke when using this product. Wash exposed areas thoroughly with soap and water.

8.3 EXPOSURE GUIDELINES

Ingredient	Authority	Type	Limit	Additional Information
STEARATES	ACGIH	TWA	10 mg/m3	
TITANIUM DIOXIDE	ACGIH	TWA	10 mg/m3	
TITANIUM DIOXIDE	CMRG	TWA, as respirable dust	5 mg/m3	
TITANIUM DIOXIDE	OSHA	TWA, as total dust	15 mg/m3	
ZINC STEARATE	OSHA	TWA, respirable fraction	5 mg/m3	
ZINC STEARATE	OSHA	TWA, as total dust	15 mg/m3	
ZIRCONIUM COMPOUNDS	ACGIH	TWA, as Zr	5 mg/m3	
ZIRCONIUM COMPOUNDS	ACGIH	STEL, as Zr	10 mg/m3	
ZIRCONIUM COMPOUNDS	OSHA	TWA, as Zr	5 mg/m3	

SOURCE OF EXPOSURE LIMIT DATA:
ACGIH: American Conference of Governmental Industrial Hygienists
CMRG: Chemical Manufacturer Recommended Guideline
OSHA: Occupational Safety and Health Administration
AIHA: American Industrial Hygiene Association Workplace Environmental Exposure Level (WEEL)

SECTION 9: PHYSICAL AND CHEMICAL PROPERTIES

Specific Physical Form:	Powder
Odor, Color, Grade:	White, opaque, odorless powder.
General Physical Form:	Solid
Autoignition temperature	*No Data Available*
Flash Point	No flash point
Flammable Limits(LEL)	*Not Applicable*
Flammable Limits(UEL)	*Not Applicable*
Boiling Point	*Not Applicable*
Density	*No Data Available*
Specific Gravity	*No Data Available*
pH	*Not Applicable*
Melting point	*No Data Available*

Solubility in Water	Negligible
Evaporation rate	*No Data Available*
Volatile Organic Compounds	*No Data Available*
Kow - Oct/Water partition coef	*No Data Available*
Percent volatile	*No Data Available*
VOC Less H2O & Exempt Solvents	*No Data Available*
Viscosity	*No Data Available*

SECTION 10: STABILITY AND REACTIVITY

Stability: Stable.

Materials and Conditions to Avoid:
10.1 Conditions to avoid
Heat

10.2 Materials to avoid
Not determined

Hazardous Polymerization: Hazardous polymerization will not occur.

Hazardous Decomposition or By-Products

Substance	Condition
Carbon monoxide	During Combustion
Carbon dioxide	During Combustion

SECTION 11: TOXICOLOGICAL INFORMATION

Please contact the address listed on the first page of the MSDS for Toxicological Information on this material and/or its components.

SECTION 12: ECOLOGICAL INFORMATION

ECOTOXICOLOGICAL INFORMATION

Not determined.

CHEMICAL FATE INFORMATION

Not determined.

SECTION 13: DISPOSAL CONSIDERATIONS

Waste Disposal Method: Dispose of waste product in a sanitary landfill. As a disposal alternative, dispose of waste product in a facility permitted to accept chemical waste.

EPA Hazardous Waste Number (RCRA): Not regulated

Since regulations vary, consult applicable regulations or authorities before disposal.

SECTION 14:TRANSPORT INFORMATION

ID Number(s):
70-2010-5600-2, 70-2010-5761-2

For Transport Information, please visit http://3M.com/Transportinfo or call 1-800-364-3577 or 651-737-6501.

SECTION 15: REGULATORY INFORMATION

US FEDERAL REGULATIONS
Contact 3M for more information.

311/312 Hazard Categories:
Fire Hazard - No Pressure Hazard - No Reactivity Hazard - No Immediate Hazard - Yes Delayed Hazard - Yes

Section 313 Toxic Chemicals subject to the reporting requirements of that section and 40 CFR part 372 (EPCRA):

Ingredient	C.A.S. No	% by Wt
ZINC STEARATE (ZINC COMPOUNDS)	557-05-1	5 - 10

STATE REGULATIONS
Contact 3M for more information.

CHEMICAL INVENTORIES
This material contains one or more substances not listed on the TSCA Inventory. Commercial use of this material is regulated by the FDA.

Contact 3M for more information.

INTERNATIONAL REGULATIONS
Contact 3M for more information.

This MSDS has been prepared to meet the U.S. OSHA Hazard Communication Standard, 29 CFR 1910.1200.

SECTION 16: OTHER INFORMATION

NFPA Hazard Classification
Health: 1 **Flammability:** 1 **Reactivity:** 0 **Special Hazards:** None

National Fire Protection Association (NFPA) hazard ratings are designed for use by emergency response personnel to address the hazards that are presented by short-term, acute exposure to a material under conditions of fire, spill, or similar emergencies. Hazard ratings are primarily based on the inherent physical and toxic properties of the material but also include the toxic properties of combustion or decomposition products that are known to be generated in significant quantities.

Revision Changes:
Section 1: Product name was modified.
Section 1: Product use information was modified.

Section 16: Disclaimer (second paragraph) was modified.
Section 3: Potential effects from inhalation information was modified.
Section 7: Handling information was modified.
Section 7: Storage information was modified.
Section 8: Engineering controls information was modified.
Section 8: Skin protection phrase was modified.
Section 8: Prevention of swallowing information was modified.
Section 10: Hazardous decomposition or by-products table was modified.
Section 8: Eye/face protection information was modified.
Section 14: Transportation legal text was modified.
Page Heading: Product name was modified.
Section 9: Density information was modified.
Section 9: Boiling point information was modified.
Section 5: Flammable limits (UE) information was modified.
Section 5: Flammable limits (LEL) information was modified.
Section 5: Autoignition temperature information was modified.
Section 5: Flash point information was modified.
Section 9: Specific gravity information was modified.
Section 9: pH information was modified.
Section 9: Melting point information was modified.
Section 9: Solubility in water text was modified.
Section 9: Flash point information was modified.
Section 9: Flammable limits (LEL) information was modified.
Section 9: Flammable limits (UEL) information was modified.
Section 9: Autoignition temperature information was modified.
Section 2: Ingredient table was modified.
Section 15: EPCRA 313 information was modified.
Section 8: Exposure guidelines ingredient information was modified.
Section 3: Carcinogenicity phrase was added.
Section 9: Property description for optional properties was added.

Section 3: Carcinogenicity table was added.
Section 3: Carcinogenicity heading was added.
Section 6: 6.2. Environmental precautions heading was added.
Section 6: 6.1. Personal precautions, protective equipment and emergency procedures heading was added.
Section 10.1 Conditions to avoid heading was added.
Section 10.2 Materials to avoid heading was added.
Section 16: Web address was added.
Section 6: Personal precautions information was added.
Section 6: Environmental procedures information was added.
Section 6: Methods for cleaning up information was added.
Section 10: Materials to avoid physical property was added.
Section 10: Conditions to avoid physical property was added.
Section 8: Hand protection information was added.
Section 1: Address was added.
Copyright was added.
Company logo was added.
Section 6: Clean-up methods heading was added.
Telephone header was added.
Company Telephone was added.
Section 1: Emergency phone information was added.
Section 1: Emergency phone information was deleted.
Company Logo was deleted.
Copyright was deleted.
Section 16: Web address heading was deleted.
Section 6: Release measures information was deleted.

Section 6: Release measures heading was deleted.
Section 10: Materials and conditions to avoid physical property was deleted.
Section 1: Address line 1 was deleted.
Section 1: Address line 2 was deleted.
Section 8: Exposure guidelines legend was deleted.

DISCLAIMER: The information in this Material Safety Data Sheet (MSDS) is believed to be correct as of the date issued. 3M MAKES NO WARRANTIES, EXPRESSED OR IMPLIED, INCLUDING, BUT NOT LIMITED TO, ANY IMPLIED WARRANTY OF MERCHANTABILITY OR FITNESS FOR A PARTICULAR PURPOSE OR COURSE OF PERFORMANCE OR USAGE OF TRADE. User is responsible for determining whether the 3M product is fit for a particular purpose and suitable for user's method of use or application. Given the variety of factors that can affect the use and application of a 3M product, some of which are uniquely within the user's knowledge and control, it is essential that the user evaluate the 3M product to determine whether it is fit for a particular purpose and suitable for user's method of use or application.

3M provides information in electronic form as a service to its customers. Due to the remote possibility that electronic transfer may have resulted in errors, omissions or alterations in this information, 3M makes no representations as to its completeness or accuracy. In addition, information obtained from a database may not be as current as the information in the MSDS available directly from 3M

3M USA MSDSs are available at www.3M.com

Patient consent form (tooth collection)

KING'S College LONDON
University of London

Guy's and St Thomas' NHS
NHS Foundation Trust

REC ref: **18/WM/0351**

Consent Form

Title of project: **Investigating erosive tooth wear and its progression**
Name of Chief Investigator: Professor David Bartlett
Name of researcher: Mr Petros Mylonas

Please initial box

1. I have read and understand the volunteer information sheet (Version 4 date 28th November 2019) for the above study and have had the opportunity to ask questions. ☐
2. I have had the opportunity to ask questions and all my questions have been answered to my satisfaction ☐
3. I understand that my participation is voluntary and that I am free to withdraw at any time, without giving any reason, without my medical care or legal rights being affected. ☐
4. I understand that sections of any of my medical notes may be looked at by responsible individuals from regulatory authorities where it is relevant to my taking part in research. I give permission for these individuals to have access to my records. ☐
5. I agree to donate my tooth/teeth for the purposes of this study. ☐

Name of Patient	Signature of patient	Date

Name of Person taking consent	Signature of person taking consent	Date

IRAS – 252842
Version – 4
1 for patient; 1 for researcher; 1 to be kept with notes
Date: 28/11/2018

Patient information leaflet (tooth collection)

Guy's, King's and St Thomas' Dental Institute
Department of Fixed and Removable Prosthodontics
25th Floor, Guy's Tower
Guy's Hospital
London Bridge
London
SE1 9RT
Tel 0207 188 5390
Fax 0207 188 7486

Volunteer information sheet (Version 4) 28/11/2018
Title of project: Investigating erosive toothwear and its progression (donation of extracted tooth)
REC ref: 18/WM/0351
Investigator: Professor David Bartlett
Researcher: Mr Petros Mylonas

If you decide to take part, you will be given a copy of the information sheet and a signed consent form to keep.

Part 1
Invitation
You are being invited to donate your tooth for a research study as part of a PhD conducted by the above named student. Before you decide it is important for you to understand why the research is being done and what it will involve:
Part 1 tells you the purpose of the potential studies and what will happen if you decide to participate.
Part 2 gives you more detailed information about the conduct of the potential studies.

Please take time to read the following information carefully. Ask us if there is anything that is not clear. Talk to others about the research if you wish and the following organization could give you independent advice:
Guy's and St Thomas' Hospital NHS Foundation Trust Patient Advice and Liaison Service Telephone 020 7188 8801 or 020 7188 8803 email: pals@gstt.nhs.uk
Post: Patient information team, Knowledge and information centre, St Thomas' Hospital London, Westminster Bridge Road, SE1 7EH

What is the purpose of the study?
Tooth wear is a condition where the teeth wear away faster than normal and is caused by acid erosion (from acidic foods and drinks and stomach acid), tooth grinding and over brushing. Tooth wear is a common condition that can affect anyone and it appears to be happening more and more nowadays. Severe tooth wear can cause teeth to become very sensitive, as well as causing cosmetic and chewing problems due to shortened teeth and even in severe cases can cause tooth loss. Certain toothpastes and mouth rinses have the potential to prevent and treat tooth wear. However, the scientific evidence for this is lacking and the studies we plan to carry out may provide important information regarding the disease process, progression of the disease and possible prevention of the disease.

Why have I been chosen?
You are suitable for this study because you are a healthy individual who needs a tooth removed.

Guy's, King's and St Thomas' Dental Institute
Department of Fixed and Removable Prosthodontics
25th Floor, Guy's Tower
Guy's Hospital
London Bridge
London
SE1 9RT
Tel 0207 188 5390
Fax 0207 188 7486

Do I have to take part?
No. It is up to you to decide whether or not to take part. If you do, you will be given this information sheet to keep and be asked to sign a consent form. You are still free to withdraw at any time and without giving a reason. A decision to withdraw at any time, or a decision not to take part, **will not** affect the standard of care you receive.

What will happen to me if I decide to take part?
Your treatment by the oral surgeons will continue as normal and **will not** be affected, as it is not related in any way to this research study.

If you choose to donate your tooth/teeth, you will be given a separate research consent form to sign.

At your first visit, when you are consulted about the tooth extraction, you will be invited to join the study by the researcher and will be provided with a consent form to sign confirming that you are happy to donate your tooth/teeth.

After your tooth is extracted it will be transferred to the Biomaterials laboratory at King's College Hospital Dental Institute (Department of Biomaterials, 17th Floor, Guy's Tower, Guy's Hospital, London Bridge SE1 9RT). Once the tooth is extracted your participation in the study is over.

What do I have to do?
Nothing extra to what you will be doing during your current appointment. All you need to do is inform us whether or not you would like to donate your tooth

What is the drug, device or procedure being tested?
Various methods of studying the surface changes of the extracted teeth and the effects of dietary acids, fluorides and other protective agents are being investigated in this study on the extracted teeth.

What are the alternatives for diagnosis or treatment?
The research does not involve any volunteer treatment and you will receive your routine standard treatment as usual.

What are the side effects of any treatment received when taking part?
There are no risks associated with this study, other than the usual risks of a tooth extraction which will be explained to you by the clinical team who are carrying out the treatment.

What are the other possible disadvantages or risks of taking part?
There are no risks associated with this study, other than the usual risks of a tooth extraction which will be explained to you by the clinical team who are carrying out the treatment.

Guy's, King's and St Thomas' Dental Institute
Department of Fixed and Removable Prosthodontics
25th Floor, Guy's Tower
Guy's Hospital
London Bridge
London
SE1 9RT
Tel 0207 188 5390
Fax 0207 188 7488

What are the possible benefits of taking part?
We do not expect that you will receive any benefit from taking part in this study.

What happens when the research study stops?
We aim to publish the results in medical journals.

What if there is a problem? And contact details:
No problems can be foreseen however the contact number for complaints or concerns is for:
Professor David Bartlett 0207 188 5390 or email david.bartlett@kcl.ac.uk

Will my taking part in the study be kept confidential?
We will not be collecting any information about you and your confidentiality is safeguarded during and after the study. Our procedures for handling, processing, storage and destruction of your data are compliant with the Data Protection Act 2018.

General Data Protection Regulation – (GDPR 2018)
Kings College London (KCL) and Guy's and St Thomas' (GSTFT) are the sponsors for this study based in England. The only information we will be collecting from you are your name and signature as per the consent form (version 3), and nothing else. Your consent form will be placed in your clinical records as evidence of your consent to donate your teeth, and a copy will be stored securely in a consent form file. It will not be used for any purpose during our research study. This means that we are responsible for looking after your information and using it properly. Kings College London and Guy's and St Thomas' will keep identifiable information about you for 5 years after the study has finished until 2026.
Your rights to access, change or move your information are limited, as we need to manage your information in specific ways in order for the research to be reliable and accurate. If you withdraw from the study, we will keep the information about you that we have already obtained. To safeguard your rights, we will use the minimum personally-identifiable information possible.
You can find out more about how we use your information [at URL https://www.guysandstthomas.nhs.uk/research/patients/about.aspx for GSTFT and https://www.kcl.ac.uk/terms/privacy.aspx for KCL].

Guy's and St Thomas' (GSTFT) will use your name, and contact details to contact you about the research study, and make sure that relevant information about the study is recorded for your care, and to oversee the quality of the study. Individuals from Kings College London (KCL) and Guy's and St Thomas' (GSTFT) and regulatory organisations may look at your medical and research records to check the accuracy of the research study. Guy's and St Thomas' (GSTFT) will pass these details to Kings College London (KCL) and Guy's and St Thomas' (GSTFT) along with the information collected from you. The people who analyse the information will not be able to identify you and will not be able to find out your name or contact details. Guy's and St Thomas' (GSTFT) will keep identifiable information about you from this study for 5 years after the study has finished until 2026.

Guy's, King's and St Thomas' Dental Institute
Department of Fixed and Removable Prosthodontics
25th Floor, Guy's Tower
Guy's Hospital
London Bridge
London
SE1 9RT
Tel 0207 188 5390
Fax 0207 188 7488

Contact for further information:
Professor David Bartlett 0207 188 5390 or email david.bartlett@kcl.ac.uk

This completes Part 1 of the Information Sheet. If the information sheet in Part 1 has interested you and you are considering participation, please continue to read the additional information in Part 2 before making any decision.

Part 2

What if relevant new information becomes available?
We are a leading establishment in this area of research and if any new information relevant to this study becomes available the researchers will discuss this with you. You are free to withdraw from the study at any time.

What will happen if I don't want to carry on with the study?
You can withdraw from study. Just advise the clinician treating you that you do not want to donate your tooth and your tooth will be disposed of once extracted, or you can keep it to take home.

What if there is a problem?
If you have any concern about any aspect of this study, you should ask to speak with the researchers who will do their best to answer their questions.
Professor David Bartlett 0207 188 5390 or email david.bartlett@kcl.ac.uk

If you remain unhappy and wish to complain formally, you can do this through the NHS complaints procedure. If you are harmed by taking part in this research project there are no special compensation arrangements. If you are harmed due to someone's negligence, then you may have grounds for a legal action but you may have to pay privately for it. Regardless of this, if you wish to complain, or have any concerns about any aspect of the way that you have been approached or treated during the course of this study, the normal NHS complaints mechanisms should be available to you.

Details of how to complain can be obtained from the Volunteer Advice and Liaison Service (PALS)
Guy's and St Thomas' Hospital NHS Foundation Trust Patient Advice and Liaison Service
Telephone 020 7188 8801 or 020 7188 8803 email: pals@gstt.nhs.uk
Post: Patient information team, Knowledge and information centre, St Thomas' Hospital London, Westminster Bridge Road, SE1 7EH

Will my taking part in this study be kept confidential?
We will not be collecting any information about you and your confidentiality is safeguarded during and after the study. Our procedures for handling, processing, storage and destruction of your data are compliant with the Data Protection Act 2018.

IRAS – 252842
Version 4 Date: 28/11/2018

Guy's, King's and St Thomas' Dental Institute
Department of Fixed and Removable Prosthodontics
25th Floor, Guy's Tower
Guy's Hospital
London Bridge
London
SE1 9RT
Tel 0207 188 5390
Fax 0207 188 7488

What will happen to any samples that I give?
After your tooth has been removed, it will be anonymised (i.e. there will be no way of linking the tooth to your personal data or medical records) and then transported to the Biomaterials laboratory at King's College Hospital Dental Institute (Department of Biomaterials, 17th Floor, Guy's Tower, Guy's Hospital, London Bridge SE1 9RT). The tooth will be used in a laboratory study or clinical study investigating erosive tooth wear. The study may be a laboratory experiment which involves simulating erosive wear on the enamel blocks produced using the donated teeth. Measurements of the amount of wear on the tooth surface are taken.

What will happen to the results of the research study?
The results of the study will be published in medical journals. Participants will not be identified in any report or publication. The results will help contribute to the completion of PhD research project.

Who has reviewed the study?
This study has been reviewed by the NHS Health Research Authority, West Midlands – Coventry & Warwickshire Research Ethics Committee
REC reference: 18/WM/0351

Will any genetic tests be done?
No.

Thank you for considering taking part and for taking time to read this sheet – please ask any questions if you need to.

Publications

DENTAL-3713; No. of Pages 7 ARTICLE IN PRESS

DENTAL MATERIALS XXX (2021) XXX–XXX

Available online at www.sciencedirect.com

ScienceDirect

journal homepage: www.intl.elsevierhealth.com/journals/dema

The measurement threshold and limitations of an intra-oral scanner on polished human enamel

Polyvios Charalambous[a], *Saoirse O'Toole*[a], *Thomas Bull*[b], *David Bartlett*[a,*], *Rupert Austin*[a]

[a] *King's College London, Faculty of Dentistry, Oral and Craniofacial Sciences, Guy's Hospital, Tower Wing, London, SE1 9RT, UK*

[b] *University of Southampton, Mechatronics Research Group, Engineering and the Environment, Mechanical Engineering Department, School of Engineering Eustice, Building 5, Highfield Campus, 6 University Rd, Southampton, SO17 1HE, UK*

ARTICLE INFO

Article history:
Received 13 July 2020
Received in revised form
12 January 2021
Accepted 18 January 2021
Available online xxx

Keywords:
Tooth wear
Dental enamel
Dental technology
Diagnostic imaging
Diagnostic equipment

ABSTRACT

Objective. To investigate the measurement threshold of an intra-oral scanner (IOS) on polished human enamel.

Methods. The optical performance of an IOS was compared to a gold-standard non contacting laser profilometer (NCLP), on a painted microscope slide, compared to increasing particle size of silicon-carbide papers (21.8–269.0 μm) and separately on polished human enamel with increasing step-heights. The enamel samples were randomised (n = 80) and scanned using the IOS and NCLP at increasing step-height depths (μm) (1.87–86.46 μm) and quantified according to ISO:5436-1. The measurement threshold of the IOS was determined using a custom designed automated lesion localisation algorithm, corroborated by Gaussian skewness (Ssk) and kurtosis (Sku) analysis, to assess the minimum step-height measured on each enamel sample.

Results. The NCLP showed statistically increased Sq surface roughness for all silicon carbide particle sizes compared to the microscope slide, whereas, the IOS Sq roughness discriminated silicon-carbide particles above 68.0 μm compared to the glass slide ($p \leq 0.02$). On polished enamel, the automated minimum detectable step-height measurable on each sample was 44 μm. No statistically significantly different step-height enamel lesion measurements were observed between NCLP and IOS above this threshold ($p > 0.05$).

Significance. This study revealed the fundamental optical metrological parameters for the IOS, was step-heights above 44 μm and this reflects the data acquisition of the system. These results highlight the limitations of IOS used in this study, mandating further research to optimise the performance of other IOS systems, for measuring wear of materials or tooth wear on human unpolished natural enamel surfaces.

* *Corresponding author.*
E-mail addresses: polyvios.charalambous@kcl.ac.uk (P. Charalambous), saoirse.otoole@kcl.ac.uk (S. O'Toole), T.G.Bull@soton.ac.uk (T. Bull), david.bartlett@kcl.ac.uk (D. Bartlett), rupert.s.austin@kcl.ac.uk (R. Austin).

https://doi.org/10.1016/j.dental.2021.01.006
0109-5641/

Please cite this article in press as: Charalambous P, et al. The measurement threshold and limitations of an intra-oral scanner on polished human enamel. Dent Mater (2021), https://doi.org/10.1016/j.dental.2021.01.006

1. Introduction

Non-contacting laser profilometry (NCLP) is the established gold standard for surface step-height [1,2] and areal (3D) surface roughness [3] measurement of human enamel. NCLP displays ±40 nm accuracy when measuring calibrated submicron step-height standards [3] and ~5 nm precision when measuring 3D surface roughness of highly polished flat human enamel [4]. Intra-oral scanners (IOS), whilst primarily designed for digital production of CAD/CAM restorations, have potential for in vivo quantification of changes to teeth using surface metrological principles. However, IOS have fundamental limitations for optical surface metrology pertaining to the methods by which the surface form is captured using oversampling of digital points of measurement (POM) and then stitching the images to produce a Cartesian point-cloud dataset [5]. Thus, unlike point-measuring profilometers, which scan by traversing an optical stylus, IOS are 'area-devices', detecting optical interactions on the surface via technologies including triangulation, active-waveform-sampling or moiré-fringe patterns which are then converted into surface points [6] with point-spacing varying between ~50–150 μm [7]. Whether IOS can measure surface phenomena at a detection threshold relevant to pathologies, such as material or tooth wear (≤10 μm) [8], has yet to be elucidated.

Surface metrology involves defining surface roughness, waviness and form [9]. Surface roughness consists of the shortest waveform deviations within the surface and is defined using amplitude parameters to quantify the height deviations of a measured surface, the most robust of which is *Sq* (standard deviation of the surface height distribution) for areal (3D) surface roughness measurement. However, quantifying these deviations using IOS is limited by the relatively large point-spacing [10], which may negatively impact characterisation of human enamel micro-spatial surface features. Waviness consists of intermediate wavelengths, whilst form is the macro-shape of the surface topography from which analysis of vertical loss or step-height is calculated [9]. ISO:5436-1 defines a step-height as the difference in height between the mid-third of the lesion and the reference areas on either side and is relatively well established for enamel surface loss measurements [11]. However, to date, no publication has determined the discrimination threshold of IOS for measuring oral features.

Therefore, the primary aim of this study was to determine the discrimination threshold or limits of an IOS, for measuring change on polished human enamel, using a NCLP as a gold standard. The IOS (True Definition™, Midmark Corp., USA) [12] and a non-contacting light profilometer (TaiCaan Technologies™, XYRIS 2000CL, UK), were chosen for the study. The objectives were to assess the IOS's optical performance including limits of agreement and discrimination threshold based on automated image analysis workflows. The null hypothesis was that the IOS, selected for this study, will have a discrimination threshold for measurement which is not inferior to NCLP.

2. Materials and methods

Profilometric scans were conducted using a NCLP (TaiCaan Technologies™, XYRIS 2000CL, UK) with a laser confocal displacement scanner sensor (LT-9010 M, Keyence Corporation, Japan), employing a 655 nm-wavelength laser with spot-diameter Ø 2 μm, 600 μm vertical gauge and 10 nm vertical resolution. Surfaces were scanned using rectilinear grid spacing at 10 μm x, y intervals, according to previously published protocols [2].

The IOS scans (True Definition™, Midmark Corp., USA) were conducted as per manufacturer's instructions by lightly coating the samples with titanium dioxide scanning spray (True Definition™ High-resolution scanning spray, Midmark Corp., USA), via a powder gun (True Definition™ powder gun, Midmark Corp., USA). The IOS used free-form 3D video-scanning based on the principle of Active-Wavefront-Sampling with 6 sensors capturing 60 fps [12]. To optimise scan quality, the enamel surface data were exported with maximal resolution (i.e. 60 μm point-spacing).

A smooth flat (control) surface was created by applying a coating of gloss-black cellulose spray paint (Holts® Mini-mix, Manchester, UK) to a microscope slide optimised for optical scanning. Silicon carbide grinding papers (Versocit, Struers A/S, Copenhagen, Denmark) of increasing roughness (grit grade P800-P60) and increasing average particle size, 21.8, 30.2, 46.2, 68.0, 125.0, 269.0 μm (ISO:6344-2/3), were bonded (UHU stick, GmbH & Co., Bühl, Germany) to microscope slides and each scanned five times by the NCLP and IOS.

All scans' analyses were automated using bespoke algorithms written using surface-metrology software (Mountains® 8, Digitalsurf, France). The *Sq* surface roughness for the smooth flat surface was compared to the silicon carbide papers of increasing particle size, for each scanner over a 4 × 4 mm area following ISO:25178.

Extracted sound permanent human molars were obtained after gaining informed consent for this study (REC ref:12/LO/1836) and buccal-lingual sections used to produce polished enamel samples (n = 80) following previously published protocols [2], achieving flatness tolerance ±0.6 μm. Fiducial markers were geometrically placed on the bis-acrylic surrounding the enamel, using round diamond burs (Hi-Di 520 and 522 Dentsply Sirona, USA), to facilitate enamel sample localisation during analyses. To remove contaminants, enamel samples were ultrasonicated (GP-70, Nusonics, Lakewood, USA) for 15 min and then air-dried for 24 h.

Following sample preparation, a 1 mm-wide window of exposed enamel was created using modelling tape (Model Craft, Shesto Ltd, UK) to provide reference zones surrounding the wear lesion. The samples were randomised into eight groups (n = 10/group), lesions created by exposing each group to 100 ml citric acid solution (0.3%, pH 2.7, titratable acidity 10.2 mL) at increasing total immersion times, ranging from 0 to 150 min., under 62.5 rpm orbital agitation (Stuart mini-Orbital Shaker SST1, Bibby Scientific, England). The samples were washed and left to air-dry for 24 h before tape removal, and then scanned, in randomised order so that the operator was blinded to the depth.

Please cite this article in press as: Charalambous P, et al. The measurement threshold and limitations of an intra-oral scanner on polished human enamel. Dent Mater (2021), https://doi.org/10.1016/j.dental.2021.01.006

DENTAL-3713; No. of Pages 7 ARTICLE IN PRESS
DENTAL MATERIALS XXX (2021) XXX–XXX

Table 1 – Mean (SD) Sq surface roughness (μm) for the gloss-black microscope glass slide (control) and silicon carbide grit surfaces of increasing particle size (21.8–269.0 μm), scanned with NCLP and IOS with statistical significance (* = p < 0.05 and ** p < 0.001) compared to the control.

Surface		Mean (SD) Sq roughness (μm)	
		NCLP	IOS
Gloss-black painted glass slide (control)		1.22 (0.18)	4.11 (0.46)
Silicon carbide grinding paper particle size (μm)	21.8	5.86 (0.05)**	3.29 (0.30)
	30.2	8.06 (0.11)**	3.01 (0.30)
	46.2	11.02 (0.25)**	3.68 (0.89)
	68.0	13.88 (0.06)**	5.40 (0.15)
	125.0	30.79 (0.50)**	7.92 (0.31)**
	269.0	49.13 (2.10)**	14.41 (0.78)**

A bespoke analysis workflow was developed for polished enamel to measure lesion depths as 3D surface step-heights, automatically locate and measure the lesion area (mm^2) and analyse surface skewness and kurtosis. This workflow was applied to 3 × 1 mm areas of polished enamel (with the 1 mm-wide lesion centrally), after removal of outliers or erroneous spikes displayed on the scanned images of the flat surfaces and then mathematically levelling the surface to, excluding the central 1/3rd of the area corresponding to the lesion.

Firstly, the 3D step-height (μm) of the 1 mm-wide central lesion was calculated using a predefined selection of the polished enamel reference areas compared to the central 1/3rd erosion area, based on ISO:5436-1. These predefined areas were programmed to automatically have the same size and location within each NCLP and IOS 3 × 1 mm extracted datasets of each sample.

Secondly, an automated lesion localisation algorithm was used to determine the measurement threshold of the IOS by localising and measuring the x, y lesion area (mm^2) on each scan. This consisted of a 'particle analysis' software function that detected surface points of measurement (POM) with Z-amplitudes below the mean plane of the surface heights according to the histogram of the surface heights distribution, on each 3 × 1 mm dataset. The Z-heights of surface points inside a given lesion would be below the mean plane of surface heights in an otherwise planar surface, resulting in lesion localisation. The surface area (mm^2) of these points was calculated for each IOS scan and was compared to the gold standard NCLP. Based on the standard deviation (SD) of the NCLP lesion area (mm^2) measurements (0.09 mm^2), a <0.18 mm^2 area difference cut-off (2 × SD) was selected as an acceptable margin of error, meaning that a lesion area measured on an IOS scan bigger than this cut-off compared to NCLP would be considered as failure to correctly detect the lesion. The measurement threshold of IOS [13] was defined as the minimum depth that the IOS could achieve ≥80% lesion detection (correct single localisation), according to a priori sample size calculation of 8 samples per group.

Finally, the Gaussian surface height distribution was analysed on each 3 × 1 mm dataset using surface skewness (*Ssk*) and kurtosis (*Sku*) parameters. The surface distribution curve of a nominally flat surface superimposed with a random roughness has a Gaussian distribution symmetrical about the height of the nominal plane which is quantified by *Ssk* equal to zero and *Sku* equal to three. In contrast a surface with a central lesion will display negative skewness and kurtosis less than three [10].

Statistical analysis was conducted using Prism 8 (GraphPad Software Inc, California, USA). Anderson–Darling test was conducted to confirm the normality of data. Two-way ANOVA with post-hoc Sidak's tests ($P < 0.05$ statistically significant) and Bland–Altman (bias and 95% Limits of Agreement, 95%-LOA) analyses were undertaken to compare measurements between the IOS and NCLP. Bias was calculated as the overall mean difference between the IOS minus the NCLP step-height measurements per sample (μm) and 95%-LOA as the variability of these differences (μm).

3. Results

Table 1 shows the mean *Sq* surface roughness (μm) for the smooth flat slide compared to the silicon carbide particles of increasing size for the NCLP and IOS. The NCLP showed consistently statistically significant differences in mean (SD) surface roughness for all grit sizes compared to the control slide ($p < 0.0001$). In contrast, the IOS scans showed statistical differences between the control slide and the sandpaper above 68.0 μm particle size ($p \leq 0.02$). This highlighted the inferior resolution and limitation of IOS in measuring short-wavelength (i.e. below ≈70 μm) surface features.

Fig. 1 shows representative scans for groups of increasing lesion depths (7.21–86.46 μm). For all depths, the NCLP scans clearly defined the lesions with sharp margins. In contrast, the IOS scans displayed lesions with irregular and unclear margins and regions of positive or negative outliers, within and outside the lesions. At increased lesion depths (44.02–86.46 μm), they became clearer; however, the transition was less distinct than the NCLP scans.

Table 2 shows the mean (SD) step-heights (μm) at increasing depth measured by NCLP and IOS, along with automated lesion detection. The mean lesion depth at baseline for the NCLP was 0.01 μm, and this increased from 1.87 μm to 86.46 μm. The IOS could not automatically identify the location and surface area of any lesions shallower than 15.99 μm, while it could detect 20% of lesions in the 18.79 μm group, 90% of lesions in the 44.02 μm group (discrimination threshold) and 100% of lesions in the 86.46 μm group. In contrast, NCLP successfully detected 100% of lesions in all depths from 1.87 μm upwards, as well as returning a 0% detection rate at baseline.

Bland–Altman analysis revealed an overall bias of −0.91 μm for IOS in comparison to NCLP, with relatively large 95%-LOA

Please cite this article in press as: Charalambous P, et al. The measurement threshold and limitations of an intra-oral scanner on polished human enamel. Dent Mater (2021), https://doi.org/10.1016/j.dental.2021.01.006

DENTAL-3713, No. of Pages 7 ARTICLE IN PRESS
4 DENTAL MATERIALS XXX (2021) XXX–XXX

Table 2 – Mean (SD) surface step-height (μm) measured by NCLP and IOS, with the percent of successful automated lesion detection according to location (central 1/3rd) and <0.18 mm² surface area difference cut-off. The measurement threshold of IOS was defined as the minimum depth, measured by NCLP, that the IOS that could achieve ≥80% automated lesion detection.

Mean (SD) 3D surface step-height (μm)		Automated lesion detection (%)	
NCLP	IOS	NCLP	IOS
0.01 (0.13)	1.28 (1.98)	0	0
1.87 (0.50)	−0.32 (3.43)	100	0
7.21 (1.19)	5.57 (2.65)	100	0
10.99 (1.06)	7.27 (2.28)	100	0
15.99 (1.49)	15.98 (3.89)	100	0
18.79 (1.80)	18.04 (5.80)	100	20
44.02 (4.78)	42.24 (6.15)	100	90
86.46 (4.96)	88.00 (7.21)	100	100

of +6.38/−8.20 μm. Therefore, the IOS showed a bias towards slight underestimation of lesion depth, in comparison to NCLP.

Fig. 2 shows the mean (SD) skewness (Ssk) and kurtosis (Sku) of the NCLP and IOS scans for the increasing lesion-depth groups. At baseline, whilst both NCLP and IOS scans produced surface amplitudes which conformed to a Gaussian distribution, representing flat and featureless surfaces, only the NCLP displayed statistically significant reductions in skewness and kurtosis vs. baseline, from the 1.87 μm depth group onwards ($p < 0.0001$), thus indicating the consistent detection of a lesion. On the contrary, IOS did not show any statistically significant reductions vs. baseline until the 10.99 μm lesion-depth group for skewness ($p = 0.0005$) and the 15.99 μm lesion-depth group for kurtosis ($p = 0.0014$), thus suggesting that the IOS did not begin detecting a lesion until these depths were reached.

4. Discussion

This study has quantified the measurement threshold or limits of a commonly reported IOS on polished human enamel surfaces, based on a standardised and validated protocol. This study revealed that 90% of depths at 44.02 μm could be measured using automated localisation and by implication depths greater than this could be confidently detected by the IOS. In contrast, the gold standard NCLP detected 100% of lesions at mean depths from 1.87 μm upwards. Therefore, the null hypothesis was rejected.

A NCLP with a previously reported ±40 nm accuracy [3] and ~5 nm precision [4] was used in this study as a gold standard, to represent the calibrated depths of the enamel wear lesions. This instrument has nanometre-level accuracy and represents instruments of the highest resolution; similar NCLPs have reported comparable accuracies in the order of ~30 nm, measuring V-grooves artefacts with 0.24, 0.75, 2.4, 7.5, 24 and 75 μm depths while using the same surface metrology software as this study (Mountains® 8, Digitalsurf, France) [14]. For this investigation a single IOS was used for convenience. This might be considered a limitation as the resolution of different intra-oral scanners varies. However, the choice of the IOS (True Definition™, Midmark Corp., USA) was deemed suitable as it has been extensively investigated previously and is considered amongst the best performing intra-oral scanners in terms of resolution and accuracy [7,15,16].

Fig. 1 shows limits of IOS in terms of inferior spatial resolution and smoother topography than NCLP. The IOS scans consisted of approximately 466 POM (average x, y point-spacing, 87 μm and 86 μm, respectively) in contrast to 30,401 POM for the NCLP scans, in the same x, y dimensions (Fig. 1). Therefore, the IOS had approximately ×65 lower spatial resolution than the NCLP. Its lower spatial resolution was scrutinized by measuring surface roughness of grit paper surfaces.

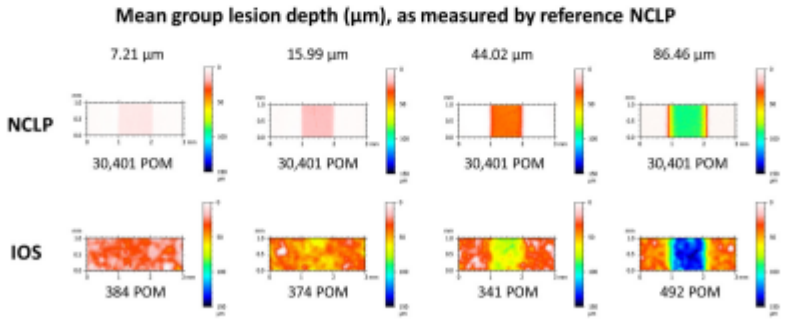

Fig. 1 – Representative pseudo-colour NCLP and IOS scans of wear lesions of increasing depth (7.21–86.46 μm) with the number of points-of-measurement (POM) for each corresponding surface (3 × 1 mm) using surface-metrology software Mountains® 8 (Digitalsurf, France). The digital scans show different colours as a function of z-measurements. The NCLP produced more defined lesions with straight margins. In contrast, IOS often produced lesions with atypical shapes and unclear boundaries. The IOS produced less points of measurement (POM) than the NCLP in the same xy dimensions.

Please cite this article in press as: Charalambous P, et al. The measurement threshold and limitations of an intra-oral scanner on polished human enamel. Dent Mater (2021), https://doi.org/10.1016/j.dental.2021.01.006

DENTAL-3713; No. of Pages 7 ARTICLE IN PRESS
DENTAL MATERIALS XXX (2021) XXX–XXX

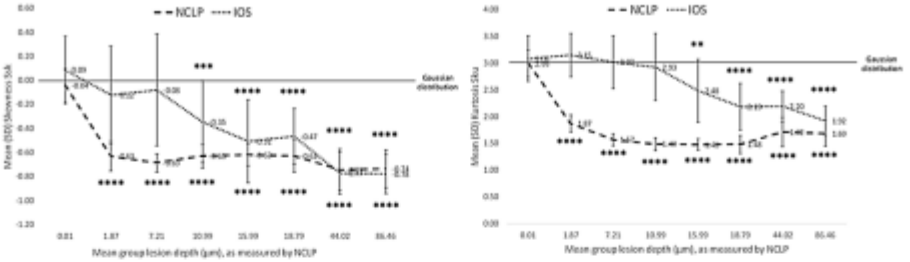

Fig. 2 – Mean (SD) Skewness (Ssk) and Kurtosis (Sku) of the NCLP and IOS scans for increasing lesion-depth groups with horizontal black lines of skewness (Ssk) equal to zero and kurtosis (Sku) equal to three which equate to a Gaussian distribution of the amplitudes of surface POM.

The IOS could detect surface roughness changes with particle sizes on carbide papers above 68 µm compared to the smooth flat surface. This shows that lesions below this are unlikely to be distinguished from random sampling error when scanned with an IOS.

Utilising the ISO:5436-1 step-height measurement technique, no significant differences were observed between the two devices for mean group lesions of 1.87–86.46 µm. This is probably reflective of the large 95%-LOA. The Bland–Altman analysis suggests that IOS measurements for lesions are on average within a micron of profilometry with 95% being within ≈8 µm; however, this is based on a priori knowledge of the lesion location on the sample and therefore potentially leads to the false assumption that IOS can measure wear depths of ≥1.87 µm. For IOS to be useful in measuring features such as depth, area and volume of enamel loss, the surface data needs to be amenable to automated lesion localisation prior to measurement.

The IOS scans demonstrated increased standard deviations which were similarly observed in previous studies [17], as well as relatively large 95%-LOA compared to NCLP. Its scans were nearing normal distribution below 10.99 µm for skewness and 15.99 µm for kurtosis. This can be explained by IOS' lower point-cloud density than NCLP. The IOS data-point interpolation between x, y measurements during surface formation, results in a polygon-mesh, which has a smoothing effect and results in larger triangles and smoother topography, which further limits its resolution. This smoothing effect may not have an impact on the scanner accuracy for larger surfaces but can be apparent when evaluating lesion boundary distinctness, leading to poor depiction of the undulating transition area of the 'step' in a step-height or discrete wear and hence false lesion topography.

Nonetheless, the use of IOS should be balanced against its speed of acquisition, higher automation, clinical application and cost-effectiveness. This study suggests that IOS is a valid technique which may have advantages over profilometry for studies measuring wear ≥44.02 µm, including direct intra-oral measurement. This discrimination threshold is comparable to the reported mean annual vertical wear on molars, 38 µm [8], showing promise for IOS as diagnostic and monitoring tools of erosive tooth wear in vivo.

Previous studies have used wear modelling protocols of questionable clinical relevance involving 37% phosphoric acid [18] or a metal tooth [19], while only one utilised a reference device such as profilometry, in which the lesion depths created were in the order of ≥68 µm [19]. These studies compared sequential scans using iterative-contact-point (ICP) superimposition. Although, this workflow might be more clinically relevant and commonly reported [17,20,21], allowing wear measurements on natural enamel, its analysis performance is more prone to errors as each time-point scan and dataset alignment process introduce an individual set of errors [22]. The quality of ICP-alignment for an optimal fit of two datasets, which is itself dependant on the scanner's accuracy and resolution, affects the accuracy of the measurement [6]. The workflow used in this study was highly controlled and standardised, utilising single post-erosion scans, therefore avoiding introduction of alignment errors.

A key strength of this study was the use of automated algorithms thus eliminating operator bias regarding a priori knowledge of where the lesion is located, which is crucial when discriminating topography changes in the order of microns. The analysis algorithm was not restricted to only measuring vertical tissue loss; instead, additional surface metrology parameters were investigated, namely automated area measurement of the lesion area as well as changes in skewness and kurtosis as the lesion depth progressed. Indeed, if a measurement process cannot automatically localise the lesion, the lesion would be unmeasurable. Therefore, studies purely relying on 3D step-height data measured based on predefined locations using reference or fiducial markers, must be interpreted with caution.

The dimensions of the artificial lesions were 1 mm wide and long whereas only a few microns deep, in an otherwise highly polished surface. These dimensions were designed to overcome the significant handicap of IOS' inferior spatial resolution; however, they represent a limitation of this present study. It is possible that smaller lateral dimensions on naturally complex native tooth surfaces may display a discrimination threshold even greater than 44.02 µm. Established protocols using relatively small flat surfaces are optimised for NCLP step-height measurement. This represents a specific measurement challenge for the IOS, as IOS operate using

Please cite this article in press as: Charalambous P, et al. The measurement threshold and limitations of an intra-oral scanner on polished human enamel. Dent Mater (2021), https://doi.org/10.1016/j.dental.2021.01.006

optical principles which are optimised for freeform shapes. Newer protocols, using complex more biologically appropriate samples, may reduce the disparity in measurements observed between the NCLP and IOS.

In summary, the combination of Active-Wavefront-Sampling IOS and bespoke automated algorithms for localisation on polished human enamel resulted in a measurement threshold of 44.02 μm. Above this, there were no significant differences between NCLP and IOS step-height suggesting that minimal lesions can be consistently quantified using IOS to a level of accuracy that maybe acceptable for clinical monitoring of material or tooth wear. However, caution needs to be applied as the study highlighted fundamental limitations of IOS, necessitating further research.

This study reports on novel optimised imaging algorithms and demonstrated for the first time that enamel lesions can be reliably quantified using automated detection in the order of sub-50 μm, showing promise as a suitable tool for experimental lab-based studies investigating wear. Additionally, it revealed that intra-oral scanning can only detect Sq surface roughness changes of surface features above 68 μm. The limitations of IOS resolution revealed a pressing requirement for further research and technological advancements to optimise the performance of IOS systems for measuring tooth surfaces, especially if below the sub-50 μm detection threshold.

Author contributions

P. Charalambous, contributed to the design, data acquisition, analysis and interpretation, performed all statistical analyses, drafted and critically revised the manuscript; S. O'Toole, contributed to conception, data interpretation and critically revised the manuscript; T. Bull, contributed to conception, design, data interpretation, and critically revised the manuscript; D. Bartlett, contributed to conception, design, data interpretation, and critically revised the manuscript; R. Austin, contributed to conception, design, data analysis and interpretation, and critically revised the manuscript. All authors gave their final approval and agree to be accountable for all aspects of the work.

Funding

This project was funded via a Medical Research Council Industrial Collaborative Award in Science and Engineering (MRC-iCASE) studentship (MR/R015643/1), for which GlaxoSmithKline Consumer Healthcare Oral Health Research & Development was the industrial collaborator. The funding sources were not involved in the collection, analysis and interpretation of data; in the writing of the report; or in the decision to submit the article for publication. They read the manuscript prior to submission.

Acknowledgments

The authors acknowledge technical assistance from Dr. Petros Mylonas in the Faculty of Dentistry, Oral & Craniofacial sciences, King's College London. The authors declare no potential conflicts of interest with respect to the authorship and/or publication of this article.

REFERENCES

[1] Mylonas P, Bull T, Moazzez R, Joiner A, Bartlett D. Detection threshold of non-contacting laser profilometry and influence of thermal variation on characterisation of early surface form and textural changes in natural human enamel. Dent Mater 2019;35:e140–52, http://dx.doi.org/10.1016/j.dental.2019.04.003.

[2] Mylonas P, Austin RS, Moazzez R, Joiner A, Bartlett DW. In vitro evaluation of the early erosive lesion in polished and natural human enamel. Dent Mater 2018;34:1391–400, http://dx.doi.org/10.1016/j.dental.2018.06.018.

[3] Mullan F, Bartlett D, Austin RS. Measurement uncertainty associated with chromatic confocal profilometry for 3D surface texture characterization of natural human enamel. Dent Mater 2017;33:e273–81, http://dx.doi.org/10.1016/j.dental.2017.04.004.

[4] Mullan F, Mylonas P, Parkinson C, Bartlett D, Austin RS. Precision of 655 nm Confocal Laser Profilometry for 3D surface texture characterisation of natural human enamel undergoing dietary acid mediated erosive wear. Dent Mater 2018;34:531–7, http://dx.doi.org/10.1016/j.dental.2017.12.012.

[5] Richert R, Goujat A, Venet L, Viguie G, Viennot S, Robinson P, et al. Intraoral scanner technologies: a review to make a successful impression. J Healthc Eng 2017;2017, http://dx.doi.org/10.1155/2017/8427595.

[6] DeLong R. Intra-oral restorative materials wear: rethinking the current approaches: how to measure wear. Dent Mater 2006;22:702–11, http://dx.doi.org/10.1016/j.dental.2006.02.003.

[7] Medina-Sotomayor P, Pascual-Moscardó A, Camps I. Relationship between resolution and accuracy of four intraoral scanners in complete-arch impressions. J Clin Exp Dent 2018;10:e361–6, http://dx.doi.org/10.4317/jced.54670.

[8] Lambrechts P, Braem M, Vuylsteke-Wauters M, Vanherle G. Quantitative in vivo wear of human enamel. J Dent Res 1989;68:1752–4, http://dx.doi.org/10.1177/00220345890680120601.

[9] Leach R. Fundamental principles of engineering nanometrology; 2014, http://dx.doi.org/10.1016/B978-1-4557-7753-2.00011-6.

[10] Meireles AB, Bastos FDS, Cornacchia TP, Ferreira JA, Las Casas EBDe. Enamel wear characterization based on a skewness and kurtosis surface roughness evaluation. Biotribology 2015;1–2:35–41, http://dx.doi.org/10.1016/j.biotri.2015.04.001.

[11] Austin RS, Giusca CL, Macaulay G, Bartlett DW, Moazzez R. Confocal laser scanning microscopy and area-scale analysis used to quantify enamel surface textural changes from citric acid demineralization and salivary remineralization in vitro. Dent Mater 2016;32:278–84, http://dx.doi.org/10.1016/j.dental.2015.11.016.

[12] Heber S. 3D Image Reconstruction Using Active Wavefront Sampling. Graz University of Tecnology; 2010.

[13] BIPM. JCGM 200:2012 International vocabulary of metrology — basic and general concepts and associated terms (VIM) Vocabulaire international de métrologie — concepts fondamentaux et généraux et termes associés (VIM). Int Organ Stand Geneva 2012;200, http://dx.doi.org/10.1016/0263-2241(85)90006-5 https://www.bipm.org/utils/common/documents/jcgm/JCGM_200_2012.pdf.

Please cite this article in press as: Charalambous P, et al. The measurement threshold and limitations of an intra-oral scanner on polished human enamel. Dent Mater (2021), https://doi.org/10.1016/j.dental.2021.01.006

[14] Nouira H, Salgado JA, El-Hayek N, Ducourtieux S, Delvallée A, Anwer N. Setup of a high-precision profilometer and comparison of tactile and optical measurements of standards. Meas Sci Technol 2014;25, http://dx.doi.org/10.1088/0957-0233/25/4/044016.
[15] Boeddinghaus M, Breloer ES, Rehmann P, Wöstmann B. Accuracy of single-tooth restorations based on intraoral digital and conventional impressions in patients. Clin Oral Investig 2015;19:2027–34, http://dx.doi.org/10.1007/s00784-015-1430-7.
[16] Medina-Sotomayor P, Pascual-Moscardo A, Camps AI. Accuracy of 4 digital scanning systems on prepared teeth digitally isolated from a complete dental arch. J Prosthet Dent 2019;121:811–20, http://dx.doi.org/10.1016/j.prosdent.2018.08.020.
[17] Kumar S, Keeling A, Osnes C, Bartlett D, O'Toole S. The sensitivity of digital intraoral scanners at measuring early erosive wear. J Dent 2018;81:39–42, http://dx.doi.org/10.1016/j.jdent.2018.12.005.
[18] Meireles AB, Vieira AW, Corpas L, Vandenberghe B, Bastos FS, Lambrects P, et al. Dental wear estimation using a digital intra oral optical scanner and an automated 3D computer vision method; 2016.
[19] Hartkamp O, Peters F, Bothung H, Lohbauer U, Reich S. Optical profilometry versus intraoral (handheld) scanning in vitro feasibility study of vertical wear measurement. Int J Comput Dent 2017;20:165–76.
[20] Becker K, Wilmes B, Grandjean C, Drescher D. Impact of manual control point selection accuracy on automated surface matching of digital dental models. Clin Oral Investig 2018;22:801–10, http://dx.doi.org/10.1007/s00784-017-2155-6.
[21] O'Toole S, Osnes C, Bartlett D, Keeling A. Investigation into the accuracy and measurement methods of sequential 3D dental scan alignment. Dent Mater 2019;35:495–500, http://dx.doi.org/10.1016/j.dental.2019.01.012.
[22] Ahmed K, Whitters J, Ju X, Pierce S, MacLeod C, Murray C. A Proposed methodology to assess the accuracy of 3D scanners and casts and monitor tooth wear progression in patients. Int J Prosthodont 2016;29:514–21, http://dx.doi.org/10.11607/ijp.4685.

Please cite this article in press as: Charalambous P, et al. The measurement threshold and limitations of an intra-oral scanner on polished human enamel. Dent Mater (2021), https://doi.org/10.1016/j.dental.2021.01.006

ARTICLE IN PRESS

DENTAL MATERIALS XXX (XXXX) XXX–XXX

Available online at www.sciencedirect.com

ScienceDirect

journal homepage: www.elsevier.com/locate/dental

The threshold of an intra oral scanner to measure lesion depth on natural unpolished teeth

Polyvios Charalambous[a,1], Saoirse O'Toole[a,2], Rupert Austin[a,3], David Bartlett[b,4,*]

[a] King's College London, Faculty of Dentistry, Oral and Craniofacial Sciences, Guy's Hospital, Tower wing, London SE1 9RT, UK

[b] Centre for Oral, Clinical & Translational Sciences, King's College London, Faculty of Dentistry, Oral and Craniofacial Sciences, Guy's Hospital, Tower wing, London SE1 9RT, UK

ARTICLE INFO

Article history:
Received 14 October 2021
Received in revised form 28 April 2022
Accepted 5 June 2022

Keywords:
Tooth wear
Dental enamel
Digital dentistry
Surface registration
Diagnostic imaging
Surface metrology

ABSTRACT

Objectives: To investigate the threshold and accuracy of intraoral scanning in measuring freeform human enamel surfaces.

Methods: Software softgauges, ranging between 20 and 160 µm depth, were used to compare four workflow analysis techniques to measure step height on a freeform surface; with or without reference areas and in combination with surface-subtraction to establish which combination produced the most accurate outcome. Having established the optimum combination, 1.5 mm diameter, individual depths ranging from 11 to 81 µm were created separately on 14 unpolished human enamel samples and then scanned with gold standard laboratory optical profilometry (NCLP, TaiCaan Technologies™, XYRIS2000CL, UK) and a clinical intraoral scanner (TrueDefinition™, Midmark Corp., USA). The sequence of surface registration and subtraction determined from the softgauges was used to measure step height on natural human enamel surfaces. Step heights (µm) were compared using two-way ANOVA with post-hoc Bonferroni ($p < 0.05$) and Bland-Altman analyses.

Results: Software differences were significantly reduced from − 29.7 to − 32.5% without, to − 2.4 to − 3.6% with reference areas ($p < 0.0001$) and the addition of surface-subtraction after registration reduced this further to 0.0 to − 0.3% ($p < 0.0001$). The intraoral scanner had a depth discrimination threshold of 73 µm on unpolished natural enamel and significant differences ($p < 0.05$) were observed compared to NCLP below this level.

* Corresponding author.
E-mail addresses: polyvios.charalambous@kcl.ac.uk (P. Charalambous), saoirse.otoole@kcl.ac.uk (S. O'Toole), rupert.s.austin@kcl.ac.uk (R. Austin), david.bartlett@kcl.ac.uk (D. Bartlett).
[1] ORCID ID: 0000-0003-4289-157X
[2] ORCID ID: 0000-0002-2144-1847
[3] ORCID ID: 0000-0003-2782-1020
[4] ORCID ID: 0000-0001-8599-8401

https://doi.org/10.1016/j.dental.2022.06.022

Significance: The workflow of combining surface-registration and subtraction of surface profiles taken from intraoral scans of freeform unpolished enamel enabled confident measurement of step height above 73 µm. The limits of the scanner is related to data capture and these results provide opportunities for clinical measurement.

1. Introduction

Change on non-flat, freeform surfaces presents challenges for measurement of Z height using profilometry [1]. Freeform surface metrology refers to quantifying specific features on a point cloud mesh produced from optical scans of complex geometrical surfaces, such as seen on teeth. Over the last few years, there have been significant advances in software and hardware of surface metrology which allow 3D digital scans, taken at different epochs, be aligned and compared to quantify vertical or volume surface changes [2–5]. However, there remain errors that impact on reliable quantification of change at the micron scale.

Surface registration refers to merging data files from scanned images which requires reference zones or points independently identified or operator led to create accurate alignment. Best-fit iterative-closest-point (ICP) is commonly utilised to minimise the distance between individual points within two datasets and thus quantify surface change. Its biggest advantage is its automaticity, as the registration process is led by the software's algorithms. However, it is susceptible to errors resulting from erroneous matching of points on sequential digital files of the same surface after change or wear. This error is reduced by employing a reference-based surface registration to register scans using reference (or datum) areas, which is operator led, but finding suitable areas on teeth remains a conundrum [4].

Surface subtraction of sequential datasets has also been described in the literature [6,7]. This refers to the software computation of the difference in a single dimension, between corresponding points from two sequential 3D surfaces producing a residual dataset that represents change and from which measurements can be taken. The residual dataset would contain a 'step' with data from positive or negative Z-axis heights compared to a reference zone and regardless of the original curvature of the surface [8]. Surface-subtraction metrology is particularly useful in industries assessing topographic change such as wear, corrosion, or the degree of similarity between two manufactured parts, in a relatively small area in relation to the entire sample [7]. However, one of its biggest limitations is that subtracted datasets require precise 3D alignment in the XY axes, prior to subtraction, which can introduce error and operator bias. Therefore, an automated method, combining surface-registration and surface-subtraction may offer improvements.

3D digital scans of teeth have been made by digitising stone casts with high-resolution profilometers [4,6,9] or laboratory scanners [10,11], but more recently intraoral scanners has been proposed as a means of directly capturing the geometry of teeth by over sampling and stitching images together[12,13], thus removing the need for any intermediate steps such as impression taking and cast production. Our group reported a depth measurement threshold of 44 µm for a clinical intraoral scanner in measuring wear on polished enamel [12]. However, to date, no study has described a comparable process for unpolished natural surfaces, where finding reference areas either side of a wear scar may not be possible.

Therefore, the aim of this study was to validate a novel workflow combining surface registration and subtraction to investigate the depth discrimination threshold of an intraoral scanner (IOS) on natural unpolished enamel. The null hypothesis stated that the lesion depth measurements from an intra oral scanner and a laboratory based non-contacting profilometer of unpolished freeform enamel surfaces would be the same.

2. Materials and methods

This study firstly assessed, using softgauges, which combinations of software workflow performed to the highest accuracy to measure surface change on freeform surfaces (Fig. 1). Having established the most reliable combinations of surface registration and subtraction we then tested the findings on human enamel samples with increasing depths created with citric acid to determine the threshold/limits of the depth discrimination of an intra oral scanner digital scanner.

A softgauge is a digital measurement standard for testing the numerical correctness of surface metrology software [14]. A point cloud comprising XYZ cartesian coordinates from a previously existing baseline NCLP scan of a single sound natural enamel sample was manipulated in a spreadsheet software (Excel® Microsoft®, version 2008) to digitally create softgauges with known depths of 20, 40, 60, 80, and 160 µm and a consistent diameter of 1.5 mm. Four surface-matching data processing techniques were evaluated for their ability to measure the known lesion depths. Individually, a best-fit surface-registration (BF) and then a reference-based surface-registration (Ref) were tested following which best-fit surface-registration combined with surface-subtraction (BF-SS) and finally, reference-based surface-registration with subtraction (Ref-SS). Each technique was repeated ten times at the varying depths of 20, 40, 60, 80, 160 µm, based on a sample size calculation using GPower freeware, version 3.1.9 (Heinrich Heine, Dusseldorf, Germany), on previous pilot data (α error = 0.05, power = 0.80, effect size 1.30).

For the BF technique, the surface pairs (i.e., the baseline surface and the softgauge with the known lesion) consisting of Cartesian point clouds were loaded into software

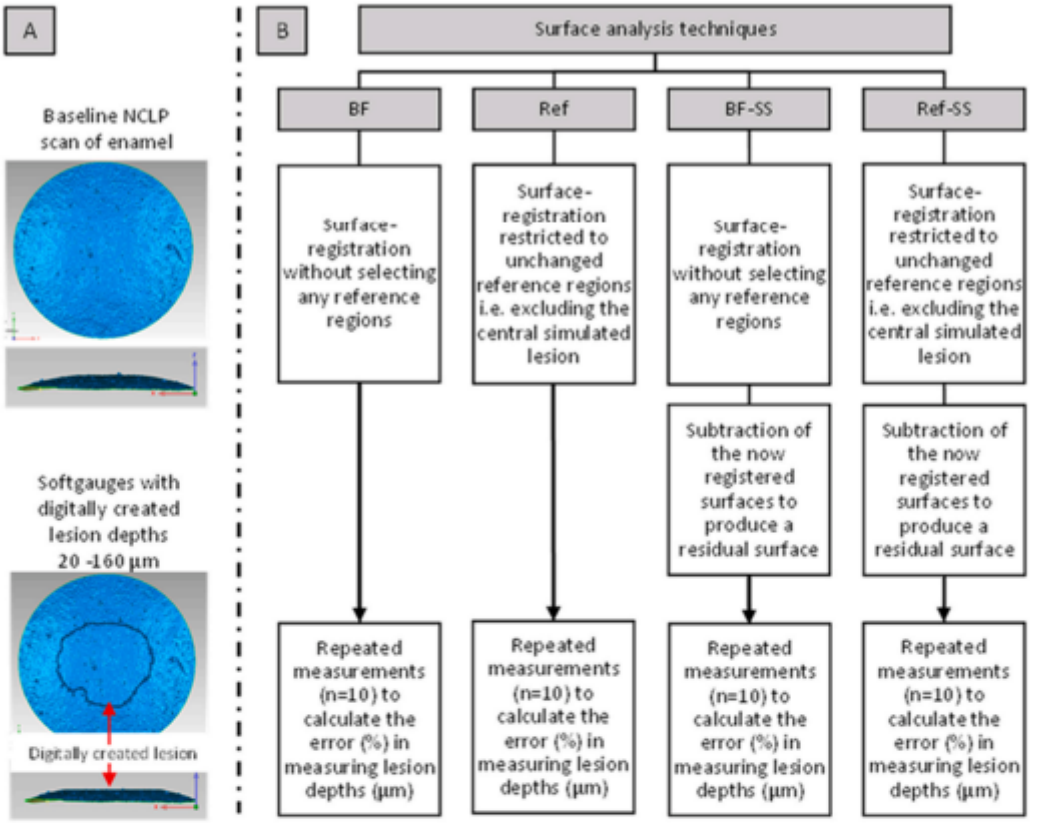

Fig. 1 – a flow diagram to show how the softgauges were used to test the accuracy of the software. The outline of the four surface-matching analysis techniques (BF, Ref, BF-SS, Ref-SS) investigated to calculate the percentage error e%) in measuring the lesions depths (20–160 µm) that were digitally created on the softgauges. BF - Best-fit surface registration, Ref - Reference-based surface-registration, BF-SS - Best-fit surface-registration and surface-subtraction, Ref-SS - Reference-based surface-registration and surface-subtraction.

(Geomagic Control, 3D Systems, Darmstadt, Germany) and transformed into 3D polygon meshes. The ICP algorithm was conducted using 1500 data points to align the two meshes. For the Ref technique, the registration was restricted to unchanged reference regions, excluding the areas where surface change has occurred. For the BF-SS and Ref-SS techniques, the now registered surfaces were loaded into another software package (Mountains® 8, Digitalsurf, Besançon, France) and subtracted to produce a residual surface representing the difference between the two surfaces. Then a levelling process, utilising a best-fit-linear-least-squares plane, excluding the central area was applied. Lesion depths (µm) were reported as the mean mesh-distance (µm) between the two datasets for the BF and Ref techniques and as step-heights (µm) ISO:5436–1 (difference in height between the mid-third of the lesion and the surrounding reference area) for the BF-SS and Ref-SS techniques.

Following determination of the optimal software technique, the Ref-SS technique was used to calculate the discrimination threshold of an intra oral scanner (IOS;True Definition™, Midmark Corp., USA) on freeform surfaces and compared the data to a gold standard laboratory based non-contacting laser profilometer (NCLP;TaiCaan Technologies™, XYRIS 2000CL, UK).

Extracted sound permanent human molars were collected following ethical approval (REC ref:18/WM/0351), disinfected, then the teeth were sectioned to produce buccal/lingual samples, measuring 5 × 5 mm, and each fixed on acrylic blocks (n = 14, one sample per block). The samples were then ultrasonicated to remove contaminants and left to air-dry for 24 h prior to scanning by a single experienced operator.

The NCLP scans were conducted with a confocal displacement sensor (LT-9010 M, Keyence Corporation, Japan), employing a 655 nm-wavelength laser with a spot-diameter

Ø2 µm, 600 µm vertical gauge range and 10 nm vertical resolution. Enamel surfaces were scanned using rectilinear grid-spacing at 10 µm x, y intervals, according to previously published protocols [15]. The IOS scans were conducted, following manufacturer's instructions, after lightly coating the samples with titanium dioxide scanning spray (True Definition™ High-resolution scanning spray, Midmark Corp., USA). The IOS used freeform 3D video-scanning based on the principle of Active-Wavefront-Sampling with 6 sensors capturing 60 fps [16]. To optimise scan quality, the surface data were exported with maximal resolution (i.e., ~60 µm point-spacing).

An electrical polyvinylchloride tape with a 1.5 mm diameter circular hole, made using a punch-biopsy (BP-15 F 1.5 mm KAI Medical, Seki, Japan) was placed over the zenith of each enamel surface to provide a single protected reference region surrounding each central exposed enamel sample. A single lesion of 1.5 mm in diameter was created on each enamel sample, using a citric acid solution (1%, pH 2.2, titratable acidity 31.3 mL) at increasing immersion times, under 62.5 rpm orbital agitation (Stuart mini-Orbital Shaker SST1, Bibby Scientific, England). This resulted in 14 samples each with a single lesion with depths, at 11, 18, 23, 24, 34, 40, 56, 58, 62, 70, 73, 75, 79, and 81 µm, as measured by the gold standard NCLP. The samples were washed and air-dried for 24 h before tape removal, and then scanned again. All samples were scanned five times at baseline (T0) and post-exposure (T1) by NCLP and the IOS to create pairs (T0 + T1). Based on a priori sample size calculation requiring five T0 + T1 scans per depth level (80% power, $\alpha = 0.05$, effect size 2.28 µm for NCLP vs. IOS).

Randomised pairs of scans (T0 + T1) for each sample, from the NCLP and IOS were analysed to produce residual datasets. An automated 3D surface step-height (µm) algorithm was run on all residual datasets to measure lesion depths (µm), which also auto-located and measured the XY lesion surface area (mm^2) for comparison between the NCLP and IOS, following a previously published protocol [12]. The depth discrimination threshold of IOS was determined as the smallest depth (µm) showing no statistically significant difference to profilometry, as well as achieving 100% lesion detection (5 out of 5 analyses) based on the comparison of XY lesion surface areas (mm^2) between IOS and NCLP. A 10% difference in area measurements was selected as an acceptable margin of error based on a previously published protocol [12].

Statistical analyses were conducted using Prism 9 (GraphPad Software Inc, California, USA). Data were checked for normality using Shapiro-Wilk test. A two-way repeated-measures ANOVA with post-hoc Bonferroni tests ($p < 0.05$ statistically significant) was undertaken to compare measurements between the software surface-matching analysis techniques and to compare data between IOS and NCLP measurements. Bland-Altman analysis was also used to calculate the bias and 95% limits of agreement between IOS and NCLP.

3. Results

Table 1 shows the differences (%) in step height from 20 to 160 µm using the softgauges with the four data workflow techniques. These data showed that the largest differences of −29.7 to −32.5%, were observed using BF which reduced to −2.4 to −3.6% in Ref technique ($p < 0.0001$). The combination of surface-registration and subtraction using BF-SS further reduced these differences to −0.1 to −0.3% ($p < 0.0001$) and finally 0.0% with Ref-SS ($p < 0.0001$) compared to BF.

Table 2 shows step height measured by the NCLP and mean (SD) percentage step height and area (mm^2) measurement differences for the IOS compared to NCLP using Ref-SS along with the automated lesion detection (%) of the IOS. The lesion step height ranged from 11 to 81 µm measured by the NCLP. The IOS recorded the same depths and revealed mean (SD) percentage differences in depth measurements from −57 (14) % at the shallower depths improving to −2 (2) % in deeper lesions. Statistically significant differences were observed between the data at depths from 18 µm (−57 (14) %, $p = 0.0002$) to 40 µm (−35 (9) %, $p < 0.0001$), and 56 µm (−17 (7) %, $p = 0.0005$). The mean (SD) percentage difference of IOS ranged from −57 (14) % in shallower lesions to −2(2) % in deeper lesions. The percentage difference of IOS for both depth and XY area measurements dropped below 10% at depths ≥ 62 µm. The automated lesion detection reveaed confidence in the depth measurement from 73 µm. No statistically significant differences were observed between the NCLP and IOS' depth measurements above 73 µm ($p > 0.05$).

Fig. 2 shows a Bland-Altman plot of differences between the NCLP and IOS depth measurements, expressed as percentage of differences (100 x (IOS − NCLP) / average). Due to the high percentage difference between IOS and NCLP at shallower depths, the overall bias was −27% with wide 95%

Table 1 – Mean (SD) percentage depth measuring differences (%), using softgauges at 20, 40, 60, 80 and 160 µm, for BF – Best-fit surface-registration. Ref – Reference-based surface-registration. BF-SS – Best-fit surface-registration and surface-subtraction. Ref-SS – Reference-based surface-registration and surface-subtraction. Statistical significant differences were observed between BF and Ref for all depths and BF and BF-SS and Ref-SS (p = 0.001).

	Mean (SD) depth measurement percentage error (%)			
Softgauage depth of lesion (µm)	BF	Ref	BF-SS	Ref-SS
20	-30.6 (4.8)	-3.4 (0.7)	-0.3 (0.0)	0.0 (0.0)
40	-30.1 (3.6)	-3.3 (1.5)	-0.1 (0.0)	0.0 (0.0)
60	-30.4 (1.7)	-2.4 (0.2)	-0.2 (0.0)	0.0 (0.0)
80	-29.7 (0.9)	-2.7 (0.6)	-0.1(0.0)	0.0 (0.0)
160	-32.5 (0.9)	-3.6 (1.5)	-0.1(0.0)	0.0 (0.0)

Table 2 – Mean (SD) percentage measurement difference (%) of IOS for step height (μm) and area (mm²) compared to the NCLP, with the automated lesion detection (%) of IOS. Statistically significant differences were observed between NCLP and IOS depth measurements are shown (* = $p < 0.05$, ** $p < 0.01$, *** = $p \leq 0.001$ and **** $p \leq 0.0001$). Lesion depth measurements (μm) are correct to the nearest micron.

Sample number	Lesion depth (μm) NCLP	Mean (SD) depth measurement (%) of IOS vs. NCLP	Mean (SD) area measurement difference (%) of IOS vs. NCLP	Automated lesion detection (%) using IOS
1	11	-43 (41)	9 (51)	0
2	18	-57 (14) **	-8 (28)	0
3	23	-41 (33) **	71 (35)	0
4	24	-44 (22) ***	25 (11)	0
5	34	-12 (11)	-3 (26)	0
6	40	-35 (9) ***	3 (15)	0
7	56	-17 (7) **	8 (4)	60
8	58	6 (6)	10 (6)	60
9	62	-6 (5)	-9 (8)	60
10	69	4 (5)	5 (5)	80
11	73	-5 (4)	2 (5)	100
12	75	-6 (3)	-5 (3)	100
13	78	-2 (2)	1 (5)	100
14	81	-4 (1)	-4 (2)	100

Limits of Agreement (LOA), 56 to −109%. However, as the magnitude of lesion depth increased the agreement between the two scanners increased, nearing zero percent above 70 μm lesion depths.= .

4. Discussion

This study demonstrated that the combination of surface-registration and subtraction significantly reduced differences for measurement of change on freeform surfaces using soft gauges. Significant differences between NCLP and IOS measurements were observed and therefore the null hypothesis was rejected. The discrimination threshold for the intraoral scanner was 73 μm above which there was confidence that any measurement was an accurate reflection of depth. These findings, although specific to this intraoral scanner, have broader impact for assessing the confidence and accuracy of any scanner used to record the surface of complex oral structures. As most intraoral scanners utilise similar physics to record the surface of teeth it is reasonable to propose that the limits around 73 μm are probable. Further work would be needed to establish criteria for each scanner, but a broad interpretation would be there are limits on their ability to distinguish varying lesion depths on teeth.

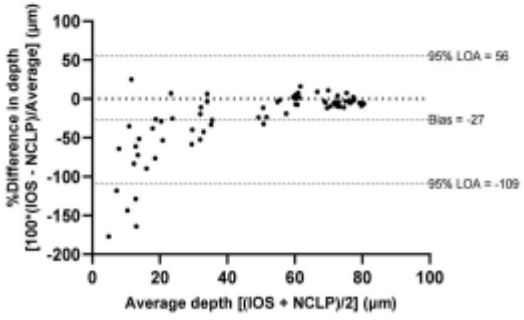

Fig. 2 – Bland-Altman plot of differences between NCLP and IOS depth measurements, expressed as percentage [100 x (IOS – NCLP)/Average)]. The overall bias was – 27% with very wide 95% Limits of Agreement (LOA) 56 to – 109%. At approximately ≥ 70 μm the % difference is near 0.

The value of the softguages was to establish which combination of software/workflow produced the optimum and most accurate results. No significant differences were observed between the two combination techniques (BF-SS and Ref-SS) suggesting that relying on reference regions alone was not necessary when a combination technique is used. This may be because the subtraction of two sequential surfaces that are well-aligned in the XY plane generates a residual 'difference' 3D profile of the same shape no matter the matching error in Z, hence any step height measurement thereafter on this residual surface to quantify change would be very similar. It is relatively straightforward to visualise registration errors in scans in the XY dimension. The additional step of surface subtraction eliminated errors in the Z direction, which are harder to visualise, particularly across a large 3D scan [8]. Finding reference surfaces for alignment which have not undergone changes in the oral cavity remains a significant barrier for erosion [4] and therefore the additional improvement with the surface-subtraction overcomes them. In this study, the surface-registration and subtraction combination was tested using softgauges with digitally created defects of known sizes [17]. However, it only represents differences from the software analysis and does not exclude

those from hardware or operator, which can be significant; and therefore, caution needs to be applied.

Although best-fit surface-registration is relatively more straightforward and automated it has been previously demonstrated by O'Toole et al. (2018) that restricting the alignment of two 3D surfaces to unchanged reference regions minimises measurement errors and improves the accuracy of surface change [4]. However, these previous investigations were limited to techniques involving surface-registration alone, without the additional step of surface subtraction. These authors reported lower volume and vertical depth change errors in reference-based registration compared to best-fit registration and manual alignment of sequential surfaces [4]. This is because standardised best-fit algorithms are forced to draw 3D datasets into the closest mathematical proximity possible, in a way that is not biologically informed of the lesion location, often resulting in inaccurate lesion quantification that limits diagnostic potential. Restricting these algorithms to surfaces that are least likely to have undergone change means they are less susceptible to outliers and results in a more accurate analysis [4,18]. Mylonas et al. (2019) investigated the use of surface-subtraction in characterising early erosion on natural enamel, however, they used a physical positioning jig to ensure repeatable placement of each enamel sample [6], which is a less automated.

Once the combination of surface registration and subtraction was validated, it was applied to sequential scans to show the threshold of the IOS on measuring lesions on unpolished enamel. In contrast to the intraoral scanner, the high-resolution NCLP detected lesions of all simulated depths. Shallow lesion depths were particularly challenging for the IOS to measure accurately. This was highlighted by the wide standard deviations in depth and area measurements, poor automated lesion area detection in shallow lesions, as well as the Bland-Altman plot which showed wide limits of agreement and a clear trend of improved percentage differences between the two devices as the lesion depth increased.

The data showed that as the depth increased the percentage difference compared to the NCLP and the standard deviations reduced. The resolution of the intraoral scanner at the lower values of the lesion depth was insufficient to discriminate an accurate value and both the step height and the area measurement had variation. This was confirmed by the automated lesion detection which is a previously published method to identify the point at which the image seen on the scans taken by the IOS became clear [12]. As the depth increased the difference reduced and the lesion detection followed the same trend. At 73 µm the step height and area had reduced to minimal levels and the lesion detection was 100%. This showed there was high confidence that the intra oral scanner was able to discriminate and so measure the lesion depth.

Unlike point-measuring high-resolution scanners, such as profilometers, which can sharply focus an optical beam onto a surface, intraoral scanners capture surface features and their optical interactions over an area simultaneously. They achieve this by oversampling and averaging multiple points of measurement representing the same area [19]. Although intraoral scanners capture surface topography significantly faster than profilometers, their drawback is lower spatial resolution (lower point cloud density) and point measuring accuracy. The impact of lower spatial resolution results in surfaces with smoother topography and poorer depiction of the margins of the lesion [12]. The addition of surface-subtraction following registration enabled the IOS to reliably quantify surface change on unpolished enamel at 73 µm, a depth that has either not previously been tested nor demonstrated agreement as high as this present study. Though, the underlying constraints associated with the physics of sampling remained and limit the threshold.

A number of in vitro and in vivo studies utilising intraoral scanners for wear quantification have published, most of which do not compare data to a gold standard [20–25]. Any IOS has limitations because of the way the profiles are formed. Recently, quantitative agreement was demonstrated between an intraoral scanner and micro-CT volumetric and depth wear measurements [26]. Hartkamp et al. (2017) were the first to use a profilometer compared to an intraoral scanner to measure vertical wear which suggested an agreement within approximately 20 µm; however, the depths were over 70 µm while lateral measurements of the simulated lesions were not specified [23]. A different intraoral scanner was utilised in this present study to assess surface change as small as 11 µm depth. Furthermore, IOS surface change analysis was not restricted to measuring vertical tissue loss (µm); instead, the XY lesion area measurements (mm^2) were compared against profilometry in order to further scrutinize IOS's performance.

The authors have previously reported the threshold for measuring lesions on polished enamel to be 44 µm using the same IOS [12]. This is lower than the measurement threshold of IOS in this study, 73 µm. This probably reflects that polished enamel has a simpler and flatter morphology, but more importantly, it allows single-scan analysis, utilising reference areas around the lesion to measure tissue loss. Furthermore, simulated lesions on polished enamel have more distinct boundaries which would favour an automated system. The relative performance of the multi-step process required for measuring change on complex freeform surfaces is more prone to measurement uncertainty as each sequential scan introduces an individual set of errors [10] while the alignment process, which is itself dependant on the scanner's accuracy and resolution, is a major contributor of measurement error [4].

Addressing the limitations of the study, a single experienced operator and two software packages tested the different data processing techniques. The impact of other operators and different software needs further investigation, but manipulation of the workflow needs training and experience. Although automation was used whenever possible some degree of operator judgement is still necessary. The software which is used to superimpose and subtract are complex mathematical algorithms and are hidden from the operator. The authors have to rely on the workflows and whilst we did our best to understand and test the conditions these are commercial products. The biggest drawback of the proposed surface-registration and subtraction technique is its time-consuming and cumbersome process, having to use two different software, requiring roughly double the analysis

time than a stand-alone surface-registration technique without the subtraction step. Therefore, further work is needed on automating the workflow and making it more suitable for diagnosis in clinical care.

In conclusion, surface-subtraction after -registration improves the accuracy of measuring surface change on sequential scans. This has potential to improve diagnostics in many fields of dentistry. Using this technique, the intraoral scanner was able to predictably determine changes of 73 µm, a level of accuracy that may be acceptable for future studies and clinical monitoring of surface changes over time such as tooth or material wear.

Funding

This project was funded via a Medical Research Council Industrial Collaborative Award in Science and Engineering (UK MRC-iCASE) studentship (MR/R015643/1), for which Glaxo-SmithKline Consumer Healthcare Oral Health Research & Development was the industrial collaborator. The funding sources were not involved in the collection, analysis, and interpretation of data; in the writing of the report; or in the decision to submit the article for publication. They read the manuscript prior to submission.

CRediT authorship contribution statement

Polyvios Charalambous: Contributed to conception, design, data acquisition, analysis and interpretation, Performed all statistical analyses, Drafted and critically revised the manuscript. **Saoirse O'Toole**: Contributed to conception, Data interpretation and critically revised the manuscript. **Rupert Austin**: Contributed to conception, design, data analysis and interpretation, Critically revised the manuscript. **David Bartlett**: Contributed to conception, design, data interpretation, Critically revised the manuscript. All authors gave their final approval and agree to be accountable for all aspects of the work.

REFERENCES

[1] Chen S., Xue S., Zhai D., Tie G. Measurement of Freeform Optical Surfaces: Trade-Off between Accuracy and Dynamic Range, 2020. https://doi.org/10.1002/lpor.201900365.

[2] Vasilakos G, Schilling R, Halazonetis D, Gkantidis N. Assessment of different techniques for 3D superimposition of serial digital maxillary dental casts on palatal structures. Sci Rep 2017;7:5838. https://doi.org/10.1038/s41598-017-06013-5

[3] Becker K, Wilmes B, Grandjean C, Drescher D. Impact of manual control point selection accuracy on automated surface matching of digital dental models. Clin Oral Invest 2018;22:801–10. https://doi.org/10.1007/s00784-017-2155-6

[4] O'Toole S, Osnes C, Bartlett D, Keeling A. Investigation into the accuracy and measurement methods of sequential 3D dental scan alignment. Dent Mater 2018;35:495–500. https://doi.org/10.1016/j.dental.2019.01.012

[5] Kuralt M, Fidler A. Assessment of reference areas for superimposition of serial 3D models of patients with advanced periodontitis for volumetric soft tissue evaluation. J Clin Periodo 2021;48:765–73. https://doi.org/10.1111/jcpe.13445

[6] Mylonas P, Bull T, Moazzez R, Joiner A, Bartlett D. Detection threshold of non-contacting laser profilometry and influence of thermal variation on characterisation of early surface form and textural changes in natural human enamel. Dent Mater 2019;35:e140–52. https://doi.org/10.1016/j.dental.2019.04.003

[7] Mansouri A. Dental wear surface using 3D profilometry, 2014.

[8] Stenhagen KR, Hove LH, Holme B, Taxt-Lamolle S, Tveit AB. Comparing different methods to assess erosive lesion depths and progression in vitro. Caries Res 2011;44:555–61. https://doi.org/10.1159/000321536

[9] Rodriguez JM, Austin RS, Bartlett DW. A method to evaluate profilometric tooth wear measurements. Dent Mater 2012;28:245–51. https://doi.org/10.1016/j.dental.2011.10.002

[10] Ahmed K, Whitters J, Ju X, Pierce S, MacLeod C, Murray C. A proposed methodology to assess the accuracy of 3d scanners and casts and monitor tooth wear progression in patients. Int J Prosthodont 2016;29:514–21. https://doi.org/10.11607/ijp.4685

[11] Gkantidis N, Dritsas K, Ren Y, Halazonetis D, Katsaros C. An accurate and efficient method for occlusal tooth wear assessment using 3D digital dental models. Sci Rep 2020:10. https://doi.org/10.1038/s41598-020-66534-4

[12] Charalambous P, Saoirse O, Thomas B, Bartlett D, Austin R. The measurement threshold and limitations of an intra-oral scanner on polished human enamel. Dent Mater 2021:1–7. https://doi.org/10.1016/j.dental.2021.01.006

[13] Kühne C, Lohbauer U, Raith S, Reich S. Measurement of Tooth Wear by Means of Digital Impressions: An In-Vitro Evaluation of Three Intraoral Scanning Systems. Appl Sci 2021:11.

[14] Chiboub A, Arezki Y, Vissiere A, Mehdi-Souzani C, Anwer N, Alzahrani B, et al. Generation of reference softgauges for minimum zone fitting algorithms: Case of aspherical and freeform surfaces. Nanomaterials 2021:11. https://doi.org/10.3390/nano11123386

[15] Mylonas P, Austin RS, Moazzez R, Joiner A, Bartlett DW. In vitro evaluation of the early erosive lesion in polished and natural human enamel. Dent Mater 2018;34:1391–400. https://doi.org/10.1016/j.dental.2018.06.018

[16] Heber S. 3D Image Reconstruction Using Active Wavefront Sampling. Graz University of Technology, 2010.

[17] Paricio I, Sanz-Lobera A, Lozano F. Comparative analysis of software measurement standard according to ISO 5436-2. Procedia Eng 2015;132:864–71. https://doi.org/10.1016/j.proeng.2015.12.571

[18] Ren MJ, Cheung CF, Kong LB, Jiang X. Invariant-feature-pattern-based form characterization for the measurement of ultraprecision freeform surfaces. IEEE Trans Instrum Meas 2012;61:963–73. https://doi.org/10.1109/TIM.2011.2173047

[19] Sehrawat S, Kumar A, Grover S, Dogra N, Nindra J, Rathee S, et al. Study of 3D scanning technologies and scanners in orthodontics. Mater Today Proc 2022. https://doi.org/10.1016/j.matpr.2022.01.064

[20] Kumar S, Keeling A, Osnes C, Bartlett D, O'Toole S. The sensitivity of digital intraoral scanners at measuring early erosive wear. J Dent 2018;81:39–42. https://doi.org/10.1016/j.jdent.2018.12.005

[21] Alwadai GS, Roberts G, Ungar PS, González-Cabezas C, Lippert F, Diefenderfer KE, et al. Monitoring of simulated occlusal tooth wear by objective outcome measures. J Dent 2020:102. https://doi.org/10.1016/j.jdent.2020.103467

[22] Marro F, Jacquet W, Martens L, Keeling A, Bartlett D, O'Toole S. Quantifying increased rates of erosive tooth wear progression in the early permanent dentition. J Dent 2020;93:103282https://doi.org/10.1016/j.jdent.2020.103282

[23] Hartkamp O, Peters F, Bothung H, Lohbauer U, Reich S. Optical profilometry versus intraoral (handheld) scanning In vitro feasibility study of vertical wear measurement. Int J Comput Dent 2017;20:165–76.

[24] Michou S, Vannahme C, Ekstrand KR, Benetti AR. Detecting early erosive tooth wear using an intraoral scanner system. J Dent 2020;100:103445https://doi.org/10.1016/j.jdent.2020.103445

[25] O'Toole S, Lau JS, Rees M, Warburton F, Loomans B, Bartlett D. Quantitative tooth wear analysis of index teeth compared to complete dentition. J Dent 2020:97. https://doi.org/10.1016/j.jdent.2020.103342

[26] Esquivel-Upshaw J, Hsu SM, Bohórquez AC, Abdulhameed N, Scheiffele GW, Kim M, et al. Novel methodology for measuring intraoral wear in enamel and dental restorative materials. Clin Exp Dent Res 2020:677–85. https://doi.org/10.1002/cre2.322

Journal of Dentistry 112 (2021) 103738

Contents lists available at ScienceDirect

Journal of Dentistry

journal homepage: www.elsevier.com/locate/jdent

Progress and limitations of current surface registration methods when measuring natural enamel wear

Saoirse O'Toole [a,b,*], Polyvios Charalambous [a], Ali Almatrafi [b], Sandeep Mukar [b], Sherif Elsharkawy [a,b], David Bartlett [a,b]

[a] Centre for Clinical, Oral and Translational Sciences, Faculty for Dental, Oral and Craniofacial Sciences, King's College London, Guy's Hospital, SE1 9RT, UK
[b] Department of Prosthodontics, Faculty for Dental, Oral and Craniofacial Sciences, King's College London, Guy's Hospital, SE1 9RT, UK

ARTICLE INFO

Key words:
Digital dentistry
Tooth wear
Dental erosion
Metrology
Surface measurements

ABSTRACT

Objectives: Our ability to detect dental wear on sequential scans is improving. This experiment aimed to determine if widely used surface registration methods were sufficiently accurate to distinguish differences between intervention groups on early wear lesions.

Methods: Baseline measurements were taken on human molar buccal enamel samples ($n = 96$) with a confocal scanning profilometer (Taicaan, UK). Samples were randomly assigned to subgroups of brushing (30 linear strokes 300 g force) before or after an acid challenge (10 min citric acid 0.3% immersion) for four test dentifrices (medium abrasivity NaF, medium abrasivity SnF_2, low abrasivity NaF and a water control). Post-experimental profilometry was repeated. 3D step height was analysed using WearCompare (www.leedsdigitaldentistry.co.uk/wearcompare, UK). Percentage Sa change was calculated using Boddies (Taicaan Technologies, Southampton, UK). Data were analysed in SPSS (IBM, USA).

Results: The mean 3D step height (SD) observed when samples were brushed before the erosive challenge was −2.33 μm (3.46) and after was −3.5 μm (5.6). No significant differences were observed between timing of toothbrushing or dentifrice used. The mean % Sa change for the low abrasivity group (water control and low abrasivity NaF) was −10.7% (16.8%) and +28.0% (42.0%) for the medium abrasivity group (medium abrasivity NaF and SnF_2).

Conclusions: Detectable wear scars were observed at early stages of wear progression. However standard deviations were high and the experiment was underpowered to detect significant changes. Brushing with a low abrasivity dentifrice or water control produced a smoother surface whereas brushing with a high abrasivity dentifrice produced a rougher surface.

Clinical Significance: The methodology currently used to align sequential scans of teeth and measure change is too imprecise to measure early wear on natural enamel surfaces unless a large sample size is used. Further improvements are required before we can fully assess early wear processes on natural teeth using profilometry.

1. Introduction

The assessment of erosive tooth wear in vivo has been limited by our ability to measure minute amounts of profilometric change on curved and complex surfaces. Erosive tooth wear, recognised as the chemo-mechanical loss of dental hard tissue, is the most difficult condition to detect in early stages. Quantifying profile or volume loss on a reference-free, complex undulating surface with irregular peaks and troughs is not straightforward. For this reason our knowledge on early preventive methods to reduce erosive tooth wear are based upon highly processed, flat, polished enamel surfaces which conform to ISO standards for step height analysis to determine the depth of a wear scar [1]. Measurement metric outcomes are consistent and reliable in the form of 2D and 3D step heights. However, polished enamel surfaces are not representative substrates and react differently to wear challenges, compared to natural enamel surfaces or demineralised lesions [2–5]. Our fundamental laboratory knowledge of how erosive wear challenges interact with saliva, fluoride and other protective compounds may be flawed.

Recently, advancements have been made using 3D imaging and advanced surface registration techniques [6]. Traditionally these have

* Corresponding author at: Floor 17 Tower Wing, Guy's Hospital, London Bridge, SE1 9RT, UK.
E-mail address: Saoirse.otoole@kcl.ac.uk (S. O'Toole).

https://doi.org/10.1016/j.jdent.2021.103738
Received 30 April 2021; Received in revised form 17 June 2021; Accepted 19 June 2021
Available online 25 June 2021

relied upon standardised best fit algorithms which draw two 3D datasets into the closest possible mathematical proximation [7] with negative differences representing wear. However, this closest mathematical proximation does not always result in an accurate data outcome [7]. Underestimation, overestimation or skews in the scan registration can cause errors, sometimes leading to tooth gain, which is biologically implausible, and limits the diagnostic potential [7]. A recent, widely used, method to improve registration with best fit algorithms is registering the data points solely on areas which are hypothesised to have remained stable [7]. This can reduce error, particularly when relatively stable reference areas are identified and can be used for accurate alignment. These successful accurate registrations have been demonstrated in vitro using computer generated defects [7]. However, small differences in scan positioning or microsurface changes influence the accuracy of the registration, even when reference areas are known to exist. This has yet to be tested to date on a natural, unpolished, tooth.

The majority of laboratory based profilometry equipment is accurate to less than a micron [3]. Utilising older best fit methods, without reference areas, the accuracy is nearer to 15–25 microns [8,9]. It is unknown if selective surface registration methods can detect changes in the order of 1–5 microns on a natural teeth, which have a complex shape. Furthermore, the measurement metric is more complex as we cannot rely upon a step height. ISO standards, or profile loss do not apply to the irregular, localised foci of tissue degradation observed in natural surfaces [1] and so volumetric change gives a better indicator of three dimensional change [10]. In order to achieve a reproducible and comparable outcome, volume change needs to be over a standardised area [11]. Volume measured over a standardised 1 × 1 mm^3 area will give you the mathematical equivalent of a 3D step height in microns. This calculation is inherent in WearCompare, a purpose built software to quantify 3D change on dental surfaces. However, it has been untested when looking at very early wear.

The aim of this investigation was to test if selective surface registration is sufficiently accurate to quantify early lesions with minimal tissue loss, on natural enamel surfaces. A secondary aim was to investigate the impact of toothpaste abrasivity on timing of toothbrushing in relation to an acid challenge. The null hypothesis proposes that there will be no difference in volumetric changes between experimental groups using an early wear protocol.

2. Methods

Using mean step height results from a previous study within our group [4], a power calculation was conducted using an effect size of 1.4, at 80% power and 5% alpha error. Ten samples were needed per group. An additional 2 samples were added per group to allow for errors.

Caries-free human molar teeth (n = 96) were collected from consenting patients (REC reference 12/LO/1836) who required extractions in the Oral Surgery Department at Guy's Hospital. The extracted teeth were disinfected with sodium hypochlorite solution and then sectioned using a water-cooled circular saw with a diamond wafer blade using previosuily published protocols [4]. Each surface was scanned, using a 7 μm laser spot-sized white light confocal scanning profilometer (Taicaan, XYRIS 4000, UK) in medium precision mode using a raster scanning pattern at 10 μm intervals. Reference areas using adhesive tape were placed on the enamel surface to create a window approximately 1 mm × 3 mm wide. Samples were stored in dry conditions prior to experimentation.

The samples (n = 96) were randomly allocated to one of four groups, a medium RDA (Relative Dentine Abrasivity) SnF_2 toothpaste (Oral B Pro-Expert toothpaste (Procter & Gamble, Weybridge, UK, RDA 112, n = 24), a medium RDA NaF toothpaste (Colgate Aquafresh, UK RDA 113, n = 24), a low RDA (NaF toothpaste (Pronamel, GSK UK, RDA 34, n = 24) and a water control (n = 24). A total of 640 ml of stimulated whole mouth human saliva were allocated from three healthy volunteers after an absence of food or drinks for one hour prior to donation (Northampton REC, REC ref: 14/EM/0183 using previously published protocols [4]. The samples were fully immersed in 8 ml of whole mouth human saliva for 24 h prior to the erosion cycle. Artificial saliva was prepared according to the protocol used by Eisenburger et al. [12]. Toothpaste slurries were prepared by adding 60 g of toothpaste to 600 ml of artificial saliva in a beaker with a magnetic stirrer at 350 rpm for 5 min according to previously published protocols.

A 0.3% citric acid solution was formulated using previously published protocols [13]. Five manual toothbrushes (Sensodyne Search 3.5, Brentford, Middlesex, England) were set up into an automated toothbrushing machine (DentaGen V.1.50 Syndicad) with the heads aligned parallel to the surfaces of the samples. Samples allocated to sub group 1 (brushing before acid) were immersed in deionised water for 60 s under agitation (Orbital Shaker S05, Stuart Scientific, UK 62.5 rpm) to remove excess saliva and then placed in a toothbrushing machine, (DentaGen V.1.50 Syndicad, Germany) in the toothpaste/artificial saliva slurry brushed using a medium bristled manual toothbrush (Sensodyne® Search 3.5, Brentford, Middlesex, England for 30 linear strokes of abrasion in 30 s, under a constant load of 300 g. They were rinsed for 60 s, in deionised water, under agitation and then exposed to a 100 ml of 0.3% citric acid solution (titratable acidity 41.3 mmol OH/L and pH 3.2) for 10 min again under agitation (62.5 rpm). The samples were then rinsed for 60 s in 100 ml of deionised water under agitation (62.5 rpm) and finally immersed in 100 ml of natural saliva for two hours. This cycle was repeated three times before a final rinse in 100 ml of deionised water for 60 s and being left to air dry overnight prior to analysis. Samples allocated to sub group 2 (brushing after acid), were similarly immersed in deionised water to remove excess saliva. Then were exposed 100 ml of 0.3% citric acid for 10 min, rinsed, and placed in the toothbrushing machine (DentaGen V.1.50 Syndicad, Germany). Samples were brushed using the same protocol, then, rinsed fand the cycle was repeated a total of three times. The adhesive tape was removed resulting in two unaffected reference areas on either side of the experiment area and the surface scanned using the same procedures.

Data were analysed using WearCompare (Leeds Digital Dentistry, UK) [14]. The surfaces were aligned initially, using an iterative closest point (ICP) algorithm with global feature recognition. An operator chose the taped reference areas for the ICP alignment. The mid point central area, over the maximum bulbosity, was selected for measurement. The software used a 3D step height analysis over a standardised 1 mm^2 area to calculate the difference between the baseline and post-experimental scans.

In order to compare it to a conventional method of measurement, surface roughness (Sa) analysis was also performed, blinded to the grouping of the samples using surface metrology software (Boddies®, Taicaan Technologies, Southampton, UK) as per ISO 5436-1 standard protocol. All reference areas were excluded from analysis. A 0.025 mm gaussian filter was applied and Sa measured of the same standardised 1 mm^2 area in the centre of the maximum bulbosity on the surface of each sample before and after the experiment. The percentage Sa Change was calculated by the following formula ((Baseline Sa score-post experiment Sa score) × 100 / Baseline Sa Score).

Data were analysed using SPSS version 26 (IBM Corporation, Armonk, New York) and assessed for normality using normality plots and Shapiro-Wilks tests. Homogeneity were checked using Levene's test. Data were not normally distributed therefore a Kruskal Wallis test was used with dentifrice and timing as the independent variables and % Sa Change and 3D step height change as the dependent variables to assess for group differences. Following this, pairwise assessments with Bonferroni correction was used to assess for individual differences. The level of significance was set at $P \leq 0.05$.

3. Results

The overall mean 3D step height (SD) observed when samples were brushed before the erosive challenge was −2.33 μm (3.46) and after was

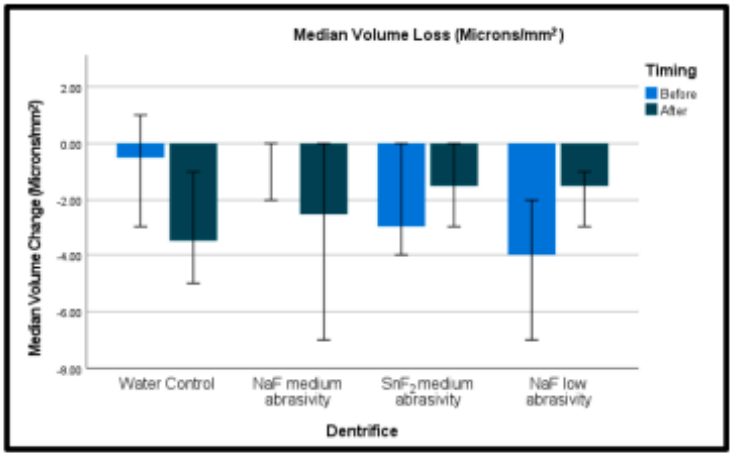

Fig. 1. Loss in enamel height on the samples over a standardised mm^2 section. Note large interquartile ranges but consistent ability to detect loss. No changes were detected between groups irrespective of dentifrice or timing of brushing in relation to the acid challenge.

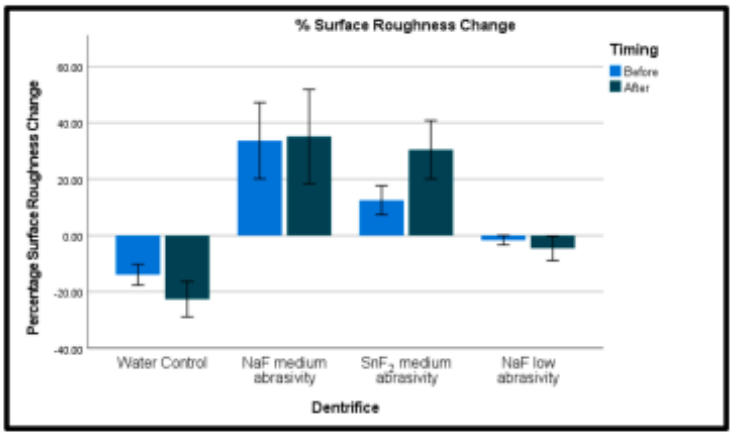

Fig. 2. Percentage change in surface roughness. High abrasivity toothpastes resulted in a significantly rougher enamel surface.

−3.5 μm (5.6). The median 3D step height across the standardised 1 × 1 mm^2 area, as determined in micron loss per mm^2 (IQR) for the water control when brushing was performed before the erosive challenge was 0.5 μm (−3.0, 1.0) and −3.5 μm (−5.75, −0.25) when brushed after. For the, NaF medium RDA group, they were 0.0 μm (−3.5, 0.0) before and −2.5 (−9.3, 0.0) after, for the SnF_2 medium RDA group they were −3.0 (−4.0, 0.0) and −1.5 (−12.0, 7.5) and for NaF low RDA −4.0 (−7.007, −13.0) and −1.5 (−3. 75, −2.5) (Fig. 1.) No statistically significant 3D step height results were observed between dentifrices or the timing of brushing in relation to the acid challenge.

In contrast, surface roughness results produced clearer differences between the groups (Fig. 2). Brushing with a water control resulted in a smoother surface and the median percentage Sa change (IQR) was −11% (−19%,−3%) before and −21% (−37%, −10%) after. Brushing with the NaF medium abrasivity dentifrice before and after was 30% (−7%, 73%) and 19% (3%, 41%), for the SnF_2 dentifrice 3% (0%, 28%) and 17% (0%, 57%) and the NaF low abrasivity dentifrice −1% (−4%, 2%) and −4% (−15%, 2%). No statistical changes were observed between both medium abrasivity dentifrices, however brushing with a water control resulted in a statistically smoother surface compared to the NaF low abrasivity toothpaste ($p = 0.003$) and the medium abrasivity dentifrices ($p < 0.001$). Brushing with a low abrasivity NaF toothpaste resulted in a smoother surface compared to both the medium abrasivity NaF ($p = 0.003$) and the SnF_2 dentifrice ($p = 0.023$). A clear trend was observed between the low and medium abrasivity dentifrices, when grouped together. The mean % Sa change for the low abrasivity group (water control and low abrasivity NaF) was −10.7% (16.8%) and the mean % Sa Change for the medium abrasivity group (medium abrasivity NaF and SnF_2) was +28.0% (42.0%).

4. Discussion

Three dimensional registration analysis of sequential scans were able to detect loss at a micron level. Wear levels demonstrated of 0.5–4 microns of loss and are consistent with step heights we may expect to see on a natural, more resistant enamel surface [4]. However, the surface registration in WearCompare was unable to provide sufficient sensitivity to detect minor differences between sequential scans. This may be

unsurprising given the complexity of the enamel surface and variation on how demineralisation status can impact on wear progression [5]. Previous work from our group has shown that profilometry is accurate to 5 nm for polished enamel and 23 nm for natural enamel [3]. Other subtraction methods, using mountains maps, analysing residual step heights has been shown to detect changes of less than a micron [15]. Our finding here is disappointing as it relies on widely used reference based registration methods but the analysis requires operator input and is technique sensitive. However, it highlights the need for improvement and it is possible that a combination of superimposition and subtraction techniques may accurately quantify tooth wear at this level.

By contrast, the surface roughness data distinguished between the groups. High abrasivity dentifrices produced significantly rougher surfaces. A further novel finding was no difference was observed in Sa surface roughess brushing before or after an erosive challenge. This adds to a growing body of evidence suggesting that the timing of toothbrushing is unimportant when compared to the frequency of acid challenges [16–18]. In vitro studies comparing the difference in fluoride application before or after an acid challenge that observed differences in timing of application, have not included an abrasive component [13, 19]. All studies to date have also been on polished, not natural enamel surfaces which have been observed to react to wear challenges in different manners.

There are several positive aspects to this in vitro study. The sample size, the use of natural surfaces, natural saliva and commercial dentrifices all contributed to a more clinically relevant study design. This study has limitations in that in vitro studies cannot fully replicate the oral environment. A further limitation is our inability to compare readings to a gold standard ISO step height. However, as this methodology is novel, it cannot be compared to a gold standard ISO step height due to the use of curved surfaces. This limits comparison with other trials. Lastly, this study reported RDA only. The dentifrices used in this study had an RDA of 112 which is considered medium to high abrasivity [1]. Unfortunately, most published studies do not refer to the RDA or REA values of dentifrices. Several studies have shown that toothbrush abrasion of eroded enamel and dentine depends on both RDA and REA values [20,21]. Furthermore, the RDA value of toothpastes do not necessarily correlate with the respective REA values. Hence toothpastes with a high RDA value may have a low REA value and vice versa [22]. The majority of studies within the literature report RDA values more frequently when analysing the abrasive potential of dentifrices. Dentifrices with a high REA value (REA > 10) can cause significant wear of enamel due to non-hydrated alumina particles which are harder than enamel [23]. In addition, a highly abrasive dentifrice may reduce the thickness of the acquired pellicle which may reduce enamel protection [24].

In conclusion, current surface registration techniques rely on a reference based best fit alignment to detect wear at a micron level. However the precision is low and given the large standard deviations, we were underpowered to answer our secondary research aim to determine the impact of dentifrice abrasivity on the timing of toothbrushing in relation to an acid challenge. Brushing with stannous fluoride before an acid challenge has been shown in vitro [25–28] and in situ [29,30] to reduce the step height loss compared to a sodium fluoride control. However, the measurements observed in this methodology were not sufficiently precise to determine a change. The focus of future research should concentrate on improving the accuracy of our alignment techniques. This, alongside with improvements to 3D intraoral imaging may mean that we will no longer need to utilise in vitro methods to answer clinical wear questions.

CRediT authorship contribution statement

Saoirse O'Toole: Conceptualization, Data curation, Formal analysis, Investigation, Methodology, Supervision, Writing - original draft, Writing - review & editing. **Polyvios Charalambous:** Data curation, Formal analysis, Investigation, Methodology, Writing - review & editing. **Ali Almatrafi.** Data curation, Formal analysis, Investigation, Methodology, Writing - review & editing. **Sandeep Mukar:** Data curation, Formal analysis, Investigation, Methodology, Writing - review & editing. **Sherif Elsharkawy:** Conceptualization, Supervision, Validation, Writing - review & editing. **David Bartlett:** Conceptualization, Supervision, Validation, Writing - review & editing.

Declaration of Competing Interest

The authors declare that they have no known competing financial interests or personal relationships that could have appeared to influence the work reported in this paper.

References

[1] International Organisation for Standardisation, International standards organisation ISO 11609, Dentistry-toothpastes-requirements, tests methods and marketing, Geneva, 2010.

[2] C. Ganss, J. Klimek, N. Schwarz, A comparative profilometric in vitro study of the susceptibility of polished and natural human enamel and dentine surfaces to erosive demineralization, Arch. Oral Biol. 45 (2000) 897–902, https://doi.org/10.1016/S0003-9969(00)00041-8.

[3] F. Mullan, P. Mylonas, C. Parkinson, D. Bartlett, R.S. Austin, Precision of 655 nm confocal laser profilometry for 3D surface texture characterisation of natural human enamel undergoing dietary acid mediated erosive wear, Dent. Mater. 34 (2018) 531–537, https://doi.org/10.1016/j.dental.2017.12.012.

[4] P. Mylonas, R.S. Austin, R. Moazzez, A. Joiner, D.W. Bartlett, In vitro evaluation of the early erosive lesion in polished and natural human enamel, Dent. Mater. 34 (2018) 1391–1400, https://doi.org/10.1016/j.dental.2018.06.018.

[5] A.M. Kielbassa, L. Gillmann, C. Zantner, H. Meyer-Lueckel, E. Hellwig, J. Schulte-Mönting, Profilometric and microradiographic studies on the effects of toothpaste and acidic gel abrasivity on sound and demineralized bovine dental enamel, Caries Res. 39 (2005) 380–386, https://doi.org/10.1159/000086844.

[6] S. O'Toole, C. Osnes, D. Bartlett, A. Keeling, Investigation into the validity of WearCompare, a purpose-built software to quantify erosive tooth wear progression, Dent. Mater. 35 (2019) 1408–1414, https://doi.org/10.1016/j.dental.2019.07.023.

[7] S. O'Toole, C. Osnes, D. Bartlett, A. Keeling, Investigation into the accuracy and measurement methods of sequential 3D dental scan alignment, Dent. Mater. 35 (2019) 495–500, https://doi.org/10.1016/j.dental.2019.01.012.

[8] J.M. Rodriguez, R.S. Austin, D.W. Bartlett, A method to evaluate profilometric tooth wear measurements, Dent. Mater. 28 (2012) 245–251, https://doi.org/10.1016/j.dental.2011.10.002.

[9] C. Wulfman, V. Koenig, A.K. Mainjot, Wear measurement of dental tissues and materials in clinical studies: a systematic review, Dent. Mater. 34 (2018) 825–850, https://doi.org/10.1016/j.dental.2018.03.002.

[10] G.J.P. Fleming, E. Reilly, A.H. Dowling, O. Addison, Data acquisition variability using profilometry to produce accurate mean total volumetric wear and mean maximum wear depth measurements for the OHSU oral wear simulator, Dent. Mater. (2016) 1–9, https://doi.org/10.1016/j.dental.2016.05.004.

[11] S. O'Toole, J.S. Lau, M. Rees, F. Warburton, B. Loomans, D. Bartlett, Quantitative tooth wear analysis of index teeth compared to complete dentition, J. Dent. 97 (2020), 103342, https://doi.org/10.1016/j.jdent.2020.103342.

[12] M. Eisenburger, M. Addy, J.A. Hughes, R.P. Shellis, Effect of time on the remineralisation of enamel by synthetic saliva after citric acid erosion, Caries Res. 35 (2001) 211–215, https://doi.org/10.1159/000047458.

[13] S. O'Toole, M. Mistry, M. Mutahar, R. Moazzez, D.W. Bartlett, Sequence of stannous and sodium fluoride solutions to prevent enamel erosion, J. Dent. 43 (2015) 1498–1503, https://doi.org/10.1016/j.jdent.2015.10.003.

[14] S. O'Toole, C. Osnes, D. Bartlett, A. Keeling, Investigation into the validity of WearCompare, a purpose-built software to quantify erosive tooth wear progression, Dent. Mater. 35 (2019) 1408–1414, https://doi.org/10.1016/j.dental.2019.07.023.

[15] P. Mylonas, T. Bull, R. Moazzez, A. Joiner, D. Bartlett, Detection threshold of non-contacting laser profilometry and influence of thermal variation on characterisation of early surface form and textural changes in natural human enamel, Dent. Mater. 35 (2019) e140–e152, https://doi.org/10.1016/j.dental.2019.04.003.

[16] S. O'Toole, E. Bernabé, R. Moazzez, D. Bartlett, Timing of dietary acid intake and erosive tooth wear: a case-control study, J. Dent. 56 (2017) 96–104, https://doi.org/10.1016/j.jdent.2016.11.005.

[17] A. Lussi, J. Lussi, T. Carvalho, B. Cvikl, Toothbrushing after an erosive attack: will waiting avoid tooth wear? Eur. J. Oral Sci. 122 (2014) 353–359, https://doi.org/10.1111/eos.12144.

[18] C. Ganss, N. Schlueter, D. Friedrich, J. Klimek, Efficacy of waiting periods and topical fluoride treatment on toothbrush abrasion of eroded enamel in situ, Caries Res. 41 (2007) 146–151, https://doi.org/10.1159/000098049.

[19] A. Wiegand, S. Egert, T. Attin, Toothbrushing before or after an acidic challenge to minimize tooth wear? An in situ/ex vivo study, Am. J. Dent. 21 (2008) 13–16.

[20] S. Hooper, N.X. West, M.J. Pickles, A. Joiner, R.G. Newcombe, M. Addy, Investigation of erosion and abrasion on enamel and dentine: a model in situ using toothpastes of different abrasivity, J. Clin. Periodontol. 30 (2003) 802–808.
[21] A. Wiegand, M. Schwerzmann, B. Sener, A.C. Magalhães, M. Roos, D. Zieholz, T. Imfeld, T. Attin, Impact of toothpaste slurry abrasivity and toothbrush filament stiffness on abrasion of eroded enamel - an in vitro study, Acta Odontol. Scand. 66 (2008) 231–235, https://doi.org/10.1080/00016350802195041.
[22] C.J. Philpotts, E. Weader, A. Joiner, The measurement in vitro of enamel and dentine wear by toothpastes of different abrasivity, Int. Dent. J. 55 (2005) 183–187.
[23] M. Addy, R.P. Shellis, Interaction between attrition, abrasion and erosion in tooth wear. Dent. Eros., KARGER, Basel, 2006, pp. 17–31, https://doi.org/10.1159/000093348.
[24] M. Hannig, The protective nature of the salivary pellicle, Int. Dent. J. 52 (2002) 417–423, https://doi.org/10.1111/j.1875-595X.2002.tb00731.x.
[25] A. Wiegand, D. Bichsel, A.C. Magalhães, K. Becker, T. Attin, Effect of sodium, amine and stannous fluoride at the same concentration and different pH on in vitro erosion, J. Dent. 37 (2009) 591–595, https://doi.org/10.1016/j.jdent.2009.03.020.
[26] N. Schlueter, A. Duran, J. Klimek, C. Ganss, Investigation of the effect of various fluoride compounds and preparations thereof on erosive tissue loss in enamel in vitro, Caries Res. 43 (2009) 10–16, https://doi.org/10.1159/000189702.
[27] N. Schlueter, J. Klimek, C. Ganss, Effect of stannous and fluoride concentration in a mouth rinse on erosive tissue loss in enamel in vitro, Arch. Oral Biol. 54 (2009) 432–436, https://doi.org/10.1016/j.archoralbio.2009.01.019.
[28] C. Ganss, N. Schlueter, M. Hardt, P. Schattenberg, J. Klimek, Effect of fluoride compounds on enamel erosion in vitro: a comparison of amine, sodium and stannous fluoride, Caries Res. 42 (2008) 2–7, https://doi.org/10.1159/000111743.
[29] C. Ganss, J. Klimek, V. Brune, A. Schürmann, Effects of two fluoridation measures on erosion progression in human enamel and dentine in situ, Caries Res. 38 (2004) 561–566, https://doi.org/10.1159/000080587.
[30] K.R. Steinhagen, L.H. Hove, B. Holme, A.B. Tveit, The effect of daily fluoride mouth rinsing on enamel erosive/abrasive wear in situ, Caries Res. 47 (2013) 2–8, https://doi.org/10.1159/000342619.